

USING APTAMERS TO REGULATE ROLLING CIRCLE AMPLIFICATION

USING APTAMERS TO REGULATE ROLLING CIRCLE AMPLIFICATION

By

ROGER MIKOLAJ BIALY, H. B. SC.

A Thesis Submitted to the School of Graduate Studies
in Partial Fulfillment of the Requirements for the Degree
Doctor of Philosophy

McMaster University

© Copyright by Roger M. Bialy, August 2021

DOCTOR OF PHILOSOPHY (2021)

(Chemical Biology)

McMaster University
Hamilton, Ontario

TITLE: Using Aptamers to Regulate Rolling Circle
Amplification

AUTHOR: Roger M. Bialy, H.B.Sc. (University of Toronto)

SUPERVISORS: Dr. John D. Brennan and Dr. Yingfu Li

NUMBER OF
PAGES: xxv, 296

ABSTRACT

The work described in this dissertation focuses on developing simple yet effective assays integrating nucleic acid (NA) aptamers with rolling circle amplification (RCA) for the detection of non-NA biomarkers. The first project, a comprehensive literature review, highlights the current state of the art in functional NA-based RCA applications, and identifies shortcomings in the detection of non-NA targets with RCA. Biosensor design is critically evaluated from four key perspectives: regulation, efficiency, and detection of RCA, and the integration of all three components for point of care (POC) applications. The second project investigates how target-binding to a linear aptamer can be utilized to regulate RCA in a simple and inexpensive format. Phi29 DNA polymerase (DP) exhibits difficulty processing DNA strands that are bound to non-NA materials such as proteins. The work uses this restriction of phi29 DP as a feature by utilizing protein-binding aptamers as primer strands (aptaprimers) for RCA. The simplicity is showcased by adapting the method to a cellulose paper-based device for the real-time detection and quantification of PDGF or thrombin within minutes. As the second project is a turn-off sensor, the third project exploits the inherent 3'-exonuclease activity of phi29 DP to generate a simple turn-on assay instead. As target-bound aptamers were shown to be resistant to exonuclease activity, the phi29 DP preferentially digests target-free aptaprimers instead of target-bound aptaprimers. The target-bound

aptaprimer could be liberated by a circular template (CT) by incorporating toehold-mediated strand displacement (TMSD), and used for RCA. Sensitivity was improved relative to project two, though the dynamic range was narrow owing to difficulty liberating target-bound aptaprimer at high target concentrations. Project four instead used RecJ, which has 5'-exonuclease activity, to modulate aptaprimer availability. Similarly to project three, target-binding conferred protection on the aptaprimer from 5'-exonuclease digestion by RecJ. By including a free 3' terminus on the aptaprimer, inhibition of RCA due to target binding was avoided and CT-mediated TMSD was not needed, simplifying the assay. As well, this approach was generalizable as it was demonstrated using both a protein (thrombin) and a small molecule (ochratoxin A) target. This turn-on method further improved the assay compared to project three with a 100-fold enhancement in sensitivity and a restoration of the dynamic range. In sum, this work contributed multiple simple and sensitive approaches for the real-time fluorescent detection of proteins and small molecules with the RCA of linear aptamers.

ACKNOWLEDGEMENTS

I would like to express my sincerest appreciation to my supervisor, Dr. John D. Brennan, for providing an environment that fostered scientific creativity. Thank you for affording me the independence to see my ideas through while providing me the guidance and support I needed to succeed. I would also like to thank the members of my supervisory committee for your scientific insights and constructive advice. Dr. Yingfu Li – for your honesty when I faltered, and your enthusiasm when I succeeded. Dr. Carlos Filipe – for consistently impressing your positive and optimistic mindset onto me, it meant a lot.

Thank you to all of my colleagues in Dr. Brennan's lab and at the Biointerfaces Institute, both past and present that I have had the pleasure of getting to know throughout the years. Thank you specifically to Carmen Carrasquilla, Christy Hui, Mike Wolfe, and Alexa Mainguy for the good times we shared in the pursuit of (a break from) science. Thanks Alexa for making science during the lockdown a lot more fun and a little more normal. Dawn, Mehdi, and Monsur – thanks for putting up with me!

I would like to thank Dr. Paul Piunno as I never would have considered graduate school if it wasn't for your confidence in me and the opportunities you provided me. Here at McMaster, of course I have to thank Tammy Feher (everyone's guardian angel), the Department of Chemistry &

Chemical Biology, and the team at the Biointerfaces Institute for providing administrative support, and a welcoming and helpful learning environment.

Finally, I would like to thank my family for their love, encouragement, and support throughout my entire academic career. To my mom and dad, dziękuję że zawsze się mną opiekujesz. Kocham was! And to my sister, Klaudia, for always pushing me to be my best self. My loving partner, Andrea Crump, thank you for constantly reminding me that I should have been done by now, and for showing me what a great life we have to look forward to next.

TABLE OF CONTENTS

ABSTRACT	iii
ACKNOWLEDGEMENTS.....	v
TABLE OF CONTENTS.....	vii
LIST OF FIGURES	x
LIST OF TABLES	xxiv
LIST OF ABBREVIATIONS	xxv
CHAPTER 1. INTRODUCTION	1
1.1 Functional Nucleic Acids as Molecular Recognition Elements	1
1.2 Isothermal DNA Amplification.....	3
1.3 Rolling Circle Amplification.....	5
1.4 Combining FNAs and RCA.....	5
1.5 Thesis Goals	6
1.6 References	9
CHAPTER 2. DESIGN STRATEGIES FOR FUNCTIONAL NUCLEIC ACID BIOSENSORS UTILIZING ROLLING CIRCLE AMPLIFICATION	14
2.1 Author's Preface.....	14
2.2 Abstract	15
2.3 Introduction.....	15
2.4 Regulation of RCA by FNA.....	22
2.4.1 Primer Regulation	23
2.4.2 Circle Regulation.....	33
2.5 Amplification Methods	43
2.5.1 Linear amplification	44
2.5.2 <i>Exponential RCA (E-RCA)</i>	47
2.5.3 Pre-amplified RP as MREs.....	54
2.6 RCA Detection Outputs	58
2.6.1 Overview of Detection Methods	58
2.6.2 Generic Detection Methods with Unstructured RPs	60
2.6.3 Detection using Selective Hybridization or Adsorption of Signalling Moieties.....	63

2.6.4	Detection using RPs Incorporating G-Quadruplexes.....	70
2.6.5	Detection using RPs Incorporating DNAzymes	72
2.7	FNA-Based POC Biosensors Utilizing RCA	74
2.7.1	Homogeneous Optical Assays	75
2.7.2	Heterogeneous Assays	88
2.8	Solid-phase Assays	102
2.8.1	Microwell plates and glass slides	103
2.8.1	Microfluidic Devices	109
2.8.3	Paper-based Biosensors	118
2.8.4	Electrochemical Biosensors	130
2.9	Summary and Future Outlook	148
2.9.1	Regulation of RCA by FNAs.....	149
2.9.1	Amplification Methods	150
2.9.3	RCA Detection Outputs	151
2.9.4	Future Outlook	154
2.10	References	158
CHAPTER 3. PROTEIN-MEDIATED SUPPRESSION OF ROLLING CIRCLE AMPLIFICATION FOR BIOSENSING WITH AN APTAMER-CONTAINING DNA PRIMER.....		
174		
3.1	Author's Preface	174
3.2	Abstract	175
3.3	Introduction.....	175
3.4	Results and Discussion	179
3.5	Conclusion.....	193
3.6	Experimental	194
3.7	Acknowledgements	199
3.8	References	200
3.9	Supporting Information	203
CHAPTER 4. TARGET-DEPENDENT PROTECTION OF DNA APTAMERS AGAINST NUCLEOLYTIC DIGESTION ENABLES SIGNAL-ON BIOSENSING WITH TOEHOLD-MEDIATED ROLLING CIRCLE AMPLIFICATION		
216		

4.1 Author's Preface.....	216
4.2 Abstract	217
4.3 Introduction.....	217
4.4 Results and Discussion	220
4.5 Conclusion.....	234
4.6 Acknowledgements	236
4.7 References	236
4.8 Experimental Section	239
4.9 Supporting Information	242
CHAPTER 5. TARGET-MEDIATED 5'-EXONUCLEASE DIGESTION OF DNA APTAMERS WITH RECJ TO MODULATE ROLLING CIRCLE AMPLIFICATION FOR BIOSENSING	259
5.1 Author's Preface.....	259
5.2 Abstract	260
5.3 Introduction.....	260
5.4 Results and Discussion	265
5.5 Conclusion.....	274
5.6 Acknowledgements	275
5.7 References	276
5.8 Experimental Section	279
5.9 Supporting Information	283
CHAPTER 6. CONCLUSIONS	291
6.1 Summary.....	291
6.2 Future Outlooks.....	293
6.3 References	296

LIST OF FIGURES

Chapter 1.

Figure 1.1. Functional Nucleic Acids.

Figure 1.2. Rolling circle amplification.

Figure 1.3. Frequency of publications mentioning RCA and FNAs compared to the frequency of publications mentioning any ITA method and FNAs.

Figure 1.4. Integration of aptamer into circular template for regulation of RCA

Figure 1.5. Integration of aptamer into primer strand for regulation of RCA

Figure 1.6. Tripartite structure-switching aptamer system for regulation of RCA

Chapter 2.

Figure 2.1. Overview of the three overarching ways that rolling circle amplification (RCA) can be manipulated. (A) Regulation, which governs how a non-nucleic acid target can be integrated as a regulator for RCA; (B) Amplification, and the different strategies that determine efficiency of amplicon generation; (C) Detection, which covers the various strategies for optically quantifying the amount of RCA product generated; (D) On paper, which focuses on how all three aspects can be incorporated on a paper-based surface for POC biosensing.

Figure 2.2. RCA-linked FNABs utilizing structure-switching. (A) Traditional structure-switching; (B) Tripartite structure-switching; (C) Structure-switching using reduced graphene oxide material; (D) Target-mediated inhibition of structure-switching.

Figure 2.3. Enzyme-assisted regulation of primer availability. (A)-(C) RCA FNABs incorporating native 3'-exonuclease activity of phi29 DP. (A) Tripartite structure-switching; (B) Supramolecular (split aptamer) variant; (C) Toehold-mediated strand displacement; (D) Hairpin formation via Klenow Fragment.

Figure 2.4. RCA FNABs utilizing RNA-cleaving DNazymes (RCDs). (A) Traditional RCD-mediated cleavage; (B) Tripartite RCD utilizing 3'-exonuclease activity of phi29 DP.

Figure 2.5. RCA-linked FNABs utilizing padlock probes for regulation of circular template. (A) Conformational structure-switching; (B) Structure-switching to release a ligation strand; (C) Structure-switching to release a linearized circular template; (D) Sandwich assay with ligation strand tethered to aptamer; (E) Dual-function DNA acting as aptamer and ligation strand.

Figure 2.6. RCA-linked FNABs utilizing structure-switching for regulation of circular template. (A) Intramolecular structure-switching; (B) Structure-switching using reduced graphene oxide material; (C) Structure-switching using recombinant analyte (GDH); (D) Target-mediated inhibition of structure-switching.

Figure 2.7. RCA FNABs utilizing DNazymes for regulation of circular template. (A) Ligase DNzyme-mediated; (B) Kinase DNzyme-mediated; (C) RCD-mediated with CT ligation step; (D) RCD-mediated utilizing catenane approach and 3'-exonuclease activity of phi29 DP.

Figure 2.8. Schematic illustrations for linear amplification and two methods of exponential amplification. (A) Linear RCA (B) Nicking Endonuclease RCA (C) Circle-to-circle (C2C) RCA (D) Hyperbranched RCA (E) Dendritic RCA (F) DNzyme Feedback Amplification.

Figure 2.9. Examples of methods of detection and signal readouts employed for RCA detection.

Figure 2.10. Homogeneous FNA-RCA assays with optical detection methods. (A) Fluorescence data for proximity extension of circular DNA aptamers with real-time detection of the thrombin target. (B) Visual detection of CEA based on PLP ligation, hyperbranched rolling circle amplification and AuNP aggregation. Figures adapted from references cited in text.

Figure 11. Homogeneous FNA-RCA methods utilizing tripartite structure-switching systems paired with the 3'-exonuclease activity of phi29 DP. (A) Tripartite structure-switching and DNA amplification

of a DNA assembly for detection of PDGF. (B) Tripartite structure switching detection paired with catalytic hairpin assembly for the detection of PDGF. (C) A dual-aptamer approach for ATP detection based on endonuclease-fueled feedback amplification. Figures adapted from references cited in text.

Figure 2.12. Homogeneous FNA-RCA methods where the aptamer and primer are in the same sequence. (A) Digital fluorescence quantification of small molecules using shielding aptamer-triggered RCA. (B) Real-time fluorescence detection of RP using molecular beacons with varying concentrations of thrombin. (C) A signal-on biosensing strategy for PDGF and thrombin enabled by toehold-mediated RCA. Figures adapted from references cited in text.

Figure 2.13. Homogeneous FNA-RCA methods incorporating RCDs. (A) Colorimetric (top) and fluorescent (bottom) detection of a catenane-RCD triggered amplification. (B) A DNAzyme Feedback Amplification (DFA) strategy for fluorescent detection of *E. Coli*. Figures adapted from references cited in text.

Figure 2.14. Heterogeneous FNA-RCA methods where magnetic beads are not used. (A) Colorimetric sensing by using allosteric-DNAzyme-coupled RCA and a PNA–organic dye probe. (B) Fluorescence detection of gastric cancer exosomes based on an aptamer-PLP E-RCA (C) A dual-aptamer PDGF bioassay using the colorimetric detection of PMD-rich RP. Figures adapted from references cited in text.

Figure 2.15. Heterogeneous FNA-RCA methods utilizing magnetic beads. (A) Visualized detection of *Vibrio parahaemolyticus* in food samples using dual-functional aptamers and E-RCA (B) Dual-functional aptamer and CRISPR-Cas12a assisted RCA for the detection of MRSA. (C) Magnetic bead inhibition RCA using quantum dot fluorescent detection of OTA. Figures adapted from references cited in text.

Figure 2.16. Heterogeneous FNA-RCA utilizing magnetic beads. (A) Epitope-specific detection of GDH using circular aptamers and SYBR Gold fluorescence detection of RP. (B) An immunomagnetic strategy for colorimetric pH sensing strategy with GOx for the detection of PDGF. (C) Fluorescence dequenching AuNP biosensing strategy for

the detection of leukemia-derived exosomes. Figures adapted from references cited in text.

Figure 2.17. Microwell plate and glass slide-based FNA-RCA assays with optical detection methods. (A) An aptamer-initiated RCA method for the scanometric detection of VEGF. (B) An inhibitory aptasensor using HRP-mimicking DNAzymes for the reduction of AuNPs and the visual detection of thrombin. (C) Foodborne pathogen RCA-linked aptasensor using colorimetric detection of catalytic HRP action. (D) Quantitation of plasma membrane proteins using an in situ aptasensing approach with fluorometric RP detection. (E) A portable smart-phone infrared-based thermal aptamer-RCA assay for the detection of PSA. Figures adapted from references cited in text.

Figure 2.18. Microfluidic FNA-RCA devices with optical detection methods. (A) A cell culturing microfluidic chip for colorimetric detection of VEGF via RCA (B) A portable thrombin-detecting microchip for visual detection of RCA-generated hemin/G-quadruplexes. (C) A portable pumpless 3D-printed multiarray chip for on-site colorimetric detection of Hg^{2+} . (D) A microfluidic aptasensor for simultaneous detection of kanamycin, aflatoxin M1, and 17β -estradiol based on magnetic tripartite DNA assembly nanostructure probes (E) A ratiometric aptasensor for kanamycin using stir-bar assisted sorptive extraction and RCA. Figures adapted from references cited in text.

Figure 2.19. Paper-based devices with optical detection methods. (A) Hg^{2+} colorimetric dot blot assay utilizing AuNP aggregation with FNA-triggered RP. (B) A simple isothermal RCA-linked FNAB for the fluorometric detection of thrombin. (C) A structure switching aptasensor using pullulan encapsulated RCA-components. Figures adapted from references cited in text.

Figure 2.20. Paper-based devices with optical detection methods. (A) A bridging paper-based device for colorimetric ATP and GDH detection. (B) An origami paper-based RCD-sensor for *E. coli* detection. (C) An aptamer-containing nanoflower device for the colorimetric detection *C. difficile*. Figures adapted from references cited in text.

Figure 2.21. Electrochemical sandwich FNA-RCA assays. (A) Anti-PDGF antibody-aptamer sandwich approach for ALP-enabled

detection of RP. (B) CuNP-reported RCA for ultrasensitive electrochemical detection of PSA. (C) Label-free detection of thrombin using dual-aptamer sandwich MRE and AuNP growth. (D) Split-aptamer-RCA assay for cocaine detection utilizing ALP cDNA. (E) EpCAM-positive tumor cell detection using a dual signal amplification strategy. Figures adapted from references cited in text.

Figure 2.22. Sandwich-free aptamer-based FNA-RCA assays that use electrochemical detection. (A) Structure-switching anti-PDGF aptasensor for electrochemical detection. (B) An ATP detection and regeneration FNA-RCA assay for electrochemical detection of RP-tethered CdS NPs (C) Inhibition-RCA aptasensor for the electrochemical detection of OTA. (D) OTA aptasensor using strand-displacement polymerase reaction. (E) PDGF-triggered and immobilization-free detection on extended-gate field-effect transistor (EGFET)-modified sensor

Figure 2.23. RCD-RCA assays that use electrochemical detection. (A) Electrochemical aptasensor based on Pb^{2+} -DNAzyme cleavage-triggered RCA and quantum dot-tagging. (B) Carbon fiber microelectrode (CFME) detection of a dual Pb^{2+} -DNAzyme assistant feedback amplification strategy. (C) Magnetic bead-bound Pb^{2+} -DNAzyme-RCA assay using pH sensing. Figures adapted from references from text.

Figure 2.24. Frequency of publications mentioning RCA and FNAs compared to the frequency of publications mentioning any ITA method and FNAs as per Web of Science. The total number of publications in 2021 was estimated based on the number of publications as of June 2, 2021.

Chapter 3.

Figure 3.1. (A) Schematic representation of an aptaprimer for target-mediated generation of RCA product by incorporating an intercalating dye such as SYBR Gold or QuantiFluor. Addition of a protein target prevents binding of the aptaprimer to the circular template, inhibiting RCA. (B) Aptaprimer concept: the circle-binding region is embedded within the native aptamer strand on the 3'-end. Polymerization occurs from the 3'-end with ϕ 29DP displacing hybridized aptaprimer to continue elongation of the RP. (C) Sample mixed with aptaprimer and intercalating dye is spotted onto a wax-

contained cellulose well holding pullulan-encapsulated RCA reagents (ϕ 29DP, CT, and dNTPs) allowing for real-time one-step RCA and production of a fluorescence signal.

Figure 3.2. Determination of RCA inhibition mechanism using nPAGE analysis showing the presence of aptaprimer (AP), circular template (CT), AP-CT duplex and aptamer-target (AP-T) complex with and without PDGF using a circular template containing a: (C12) 12 nucleotide binding region; (C18) 18 nucleotide binding region; (C27) 27 nucleotide binding region; (C35) 35 nucleotide binding region. T = target (specifically PDGF). The concentration of reagents used was 0 or 20 nM for AP, 0-40 nM for CT, and 0 or 100 nM for PDGF.

Figure 3.3. Inhibition assay using an anti-PDGF aptaprimer system. (A) Native PAGE (8%) of the species formed when the PDGF aptaprimer is complexed with increasing amounts of PDGF, followed by addition of CT; (B) Denaturing PAGE (10%) of RCA product after treatment with TaqI Restriction Enzyme in the presence of increasing amounts of PDGF. LC denotes the loading control; (C) Denaturing PAGE (10%) of RCA product, denoted as RP, after treatment with TaqI Restriction Enzyme in the absence of protein, and in the presence of 1 μ M of either BSA or PDGF. LC denotes the loading control; (D) Titration curve of RCA product generation in the presence of PDGF monitored in real-time using either SYBR Gold or QuantiFluor as intercalating dyes. All RCA reactions were conducted for 30 minutes.

Figure 3.4. Inhibition assay using an anti-thrombin aptaprimer system. (A) Native PAGE (8%) of the species formed when the thrombin aptaprimer was complexed with increasing amounts of thrombin, followed by addition of CT; (B) Denaturing PAGE (10%) of RCA product after treatment with TaqI Restriction Enzyme in the presence of increasing amounts of thrombin. LC denotes the loading control; (C) Denaturing PAGE (10%) of RCA product, denoted as RP, after treatment with TaqI Restriction Enzyme in the absence of protein, and in the presence of 1 μ M of either BSA or thrombin. LC denotes the loading control; (D) Titration curve of RCA product generation in the presence of thrombin monitored in real-time using either SYBR Gold or QuantiFluor dyes. All RCA reactions conducted for 15 minutes.

Figure 3.5. Inhibition assay on cellulose paper using: (A) the anti-PDGF aptaprimer system titrated with PDGF to generate a fluorescence signal on the cellulose surface after 30 minutes of real-time RCA. Top image shows the observed fluorescence signal of the

paper wells was imaged after real-time RCA using the QuantiFluor dye. Bottom shows the response from the paper-based assay using the QF dye is compared to the solution-based assay using SYBR Gold. (B) the anti-thrombin aptamer system titrated with thrombin to generate a fluorescence signal on the cellulose surface after 15 minutes of real-time RCA. Top image shows the observed fluorescence signal of the paper wells as imaged after real-time RCA using QuantiFluor dye. Bottom shows the response from the paper-based assay using the QF dye is compared to the solution-based assay using SYBR Gold.

Figure S3.1. Ability of anti-PDGF aptamer (AP) to form a duplex in the presence of increasing amounts of a circular template (CT) with an 18 nucleotide primer-binding region (8% nPAGE).

Figure S3.2. Comparison of RCA efficiency using circular templates with varying lengths of primer-binding region. RCA was performed at room temperature and monitored in real-time using SYBR Gold dye. All RCA reactions were conducted for 30 minutes.

Figure S3.3. Inhibition assay using an anti-PDGF aptamer system with preformed AP-CT duplex followed by addition of PDGF target. (A) Native PAGE (8%) of the species formed when the AP-CT duplex was incubated with increasing amounts of PDGF; (B) Denaturing PAGE (10%) of RCA product after treatment with TaqI restriction enzyme in the presence of increasing amounts of PDGF. LC denotes the loading control. (C) Denaturing PAGE (10%) of RCA product, denoted as RP, after treatment with TaqI in the absence of protein, and in the presence of 1 μ M BSA or PDGF. LC denotes the loading control. (D) Titration curve of RCA product generation in the presence of PDGF monitored in real-time using either SYBR Gold or QuantiFluor dyes. All RCA reactions conducted for 30 minutes.

Figure S3.4. Native PAGE analysis showing the ability of the anti-thrombin aptamer (AP) to structure-switch from a complex with 1 μ M thrombin to a duplex in the presence of a circular template (CT) using: (A) a 9 nucleotide primer-binding region (C9); (B) a 15 nucleotide primer-binding region (C15).

Figure S3.5. MST traces of the T-AP-C9 system showing the presence of unbound AP, AP-CT duplex, and AP-T complex species, respectively. AP was complexed with increasing amounts of thrombin, followed by addition of CT.

Figure S3.6. Inhibition Assay using a C15 anti-thrombin aptamer system. (A) Native PAGE (8%) analysis of AP complexed with

increasing amounts of thrombin, followed by addition of CT; (B) Denaturing PAGE (10%) analysis of RCA product after treatment with TaqI in the presence of increasing amounts of thrombin. LC denotes the loading control. (C) Denaturing PAGE (10%) analysis of RCA product, denoted as RP, after treatment with TaqI in the absence of protein, and in the presence of 1 μ M of either BSA or thrombin. LC denotes the loading control. (D) Titration curve of RCA product generation in the presence of thrombin monitored in real-time using SYBR Gold or QuantiFluor dyes. All RCA reactions conducted for 15 minutes.

Figure S3.7. Comparison of dye performance on cellulose paper in the absence or presence of 10 pmol of a 60 nt DNA sequence (linear T-AP-C9) between: (A) SYBR Gold dye and; (B) QuantiFluor dye.

Figure S3.8. Determination of optimal QuantiFluor dye concentration for detection of varying concentrations of a 60 nt DNA sequence (linear T-AP-C9) on a cellulose surface. (A) After 15 minutes of incubation on cellulose at room temperature. (B) After 30 minutes of incubation on cellulose at room temperature.

Figure S3.9. Optimization of aptaprimer concentration on cellulose paper using: (A) the anti-thrombin aptaprimer system with a 15 minute RCA reaction time; (B) the anti-PDGF aptaprimer system with a 30 minute RCA reaction time. The concentrations of thrombin or PDGF, respectively, was 0 μ M for (-) and 1 μ M for (+). Observed fluorescence signal of the paper wells as imaged after real-time RCA using the QuantiFluor dye.

Figure S3.10. Optimization of assay reaction time on cellulose paper using: (A) the anti-thrombin aptaprimer system; (B) the anti-PDGF aptaprimer system. The concentrations of thrombin or PDGF, respectively, was 0 μ M for (-) and 1 μ M for (+). Observed fluorescence signal of the paper wells as imaged after real-time RCA using the QuantiFluor dye.

Figure S3.11. Reagent controls for the inhibition assays on cellulose paper using: (A) an anti-PDGF aptaprimer system after a 30 minute RCA reaction; (B) an anti-thrombin aptaprimer system after a 15 minute RCA reaction. Observed fluorescence signal of the paper wells as imaged after real-time RCA using QuantiFluor dye.

Figure S3.12. Selectivity controls for the inhibition assays on cellulose paper using: (A) an anti-PDGF aptaprimer system after a 30 minute RCA reaction; (B) an anti-thrombin aptaprimer system after a 15 minute RCA reaction. The concentrations of PDGF,

thrombin and BSA were 1 μ M. Observed fluorescence signal of the paper wells as imaged after real-time RCA using QuantiFluor dye.

Chapter 4.

Figure 4.1. Schematic representation of the protein-mediated RCA-based assay. In the absence of a protein target, phi29 DP digests the aptamer prior to addition of a CT, preventing RCA. The binding of a protein protects the aptamer from digestion, allowing the CT to bind a 5' toehold and displace the target, resulting in RCA. The RCA product is detected using a fluorescent intercalating dye.

Figure 4.2. (A) Percentage of P-AP digested in 10 minutes as a function of phi29 DP concentration (U / 10 nM [AP]). (B) Percentage of P-AP digested in 10 minutes using 1.2 U / 10 nM [AP] of phi29 DP followed by heat denaturation at 95 °C for 5 minutes.

Figure 4.3. Optimization of the anti-PDGF aptamer system by the following parameters: (A) Optimal phi29 DP concentration with a digestion time of 10 minutes and a 0.1 CT:AP ratio; (B) Optimal ratio of circular template (CT) to aptamer (AP). RCA product generation monitored in real-time using SYBR Gold intercalating dye. A concentration of either 0 or 10 nM PDGF was used for ratio determination. Results taken after 60 minutes of RCA.

Figure 4.4. Performance of optimized anti-PDGF aptamer system with RCA product generation monitored in real-time using SYBR Gold intercalating dye. (A) Reagent and Selectivity controls, where (+D) denotes exonuclease digestion, and (-D) denotes no exonuclease digestion. BSA, thrombin (Thr), and PDGF concentrations were 10 nM. Inset is the denaturing PAGE of reaction products. (B) Titration curve of RCA product generation in the presence of varying amounts of PDGF. Results taken after 60 minutes of RCA.

Figure 4.5. Ability of the circular template to liberate the aptamer through toehold mediated strand displacement as a function of target concentration. When target concentration is: i) low, the circular template successfully displaces the target, binds to the aptamer, and RCA is activated or; ii) high, the circular template is unable to outcompete the target for aptamer-binding, and RCA is inhibited.

Figure 4.6. Performance of optimized anti-thrombin aptamer system with RCA product generation monitored in real-time using SYBR Gold intercalating dye. (A) Reagent and Selectivity controls, where (+D) denotes exonuclease digestion, and (-D) denotes no exonuclease digestion. BSA, PDGF, and thrombin (Thr)

concentrations were 10 nM each. Inset is the denaturing PAGE of reaction products. (B) Titration curve of RCA product generation in the presence of varying amounts of thrombin. Results taken after 30 minutes of RCA.

Figure 4.7. Performance of optimized anti-PDGF aptamer system in (A) 10% human serum or; (B) 10% human plasma. RCA product generation monitored in real-time using SYBR Gold intercalating dye. Results taken after 60 minutes of RCA.

Figure S4.1. Investigation of the effect of increasing phi29 DP concentration on the 3'-exonuclease digestion of the PDGF aptaprimer (P-AP).

Figure S4.2. Investigation of the effect of increasing reaction time on the 3'-exonuclease digestion of the PDGF aptaprimer (P-AP): (A) Denaturing PAGE and; (B) Digestion as a percentage relative to the 0 minute control condition.

Figure S4.3. Investigation of the effect of increasing PDGF protein concentration on the 3'-exonuclease digestion of the PDGF aptaprimer (P-AP).

Figure S4.4. Observing the degree of liberation of AP from the AP-T complex by increasing the AP-CT binding affinity via elongation of 5'-end of the aptamer in the anti-PDGF aptamer system using native PAGE analysis: T = target (specifically PDGF). Elongation lengths of: (A) 0 nt; (B) 5 nt; (C) 10 nt; (D) 15 nt; (E) 20 nt. Note that the presence of two bands for the CT-AP complex suggests that the complex may adopt two unique conformations.

Figure S4.5. Optimization of digestion time for the anti-PDGF aptamer system using a 0.1 CT:AP ratio. RCA product generation monitored in real-time using SYBR Gold intercalating dye. A concentration of either 0 or 10 nM PDGF was used for ratio determination. Results taken after 60 minutes of RCA.

Figure S4.6. Effect of various heat treatments of protein targets on RP generation for the P-AP system. RCA product generation monitored in real-time using SYBR Gold intercalating dye.

Figure S4.7. Role of toehold length on ability to activate RCA in the anti-PDGF aptamer system. The toehold length increases from left to right: i) no toehold (0 nt); ii) short toehold (5 nt) and; iii) long toehold (15 nt). RCA product generation monitored in real-time using SYBR Gold intercalating dye.

Figure S4.8. Investigation of the effect of increasing various reaction parameters for the anti-thrombin T-AP system: i) concentration of phi29 DP: (A) Denaturing PAGE and; (B) Digestion as a percentage relative to the no phi29 DP control condition. ii) digestion time: (C) Denaturing PAGE and; (D) Digestion as a percentage relative to the 0 minute control condition. iii) concentration of thrombin: (E) Denaturing PAGE and; (F) Digestion as a percentage relative to the no digestion and no target control condition.

Figure S4.9. Observing the degree of liberation of AP from the AP-T complex by increasing the AP-CT binding affinity via elongation of 5'-end of the aptamer in the anti-thrombin aptamer system using native PAGE analysis: T = target (specifically thrombin). Elongation lengths of: (A) 0 nt; (B) 5 nt; (C) 10 nt; (D) 15 nt; (E) 20 nt. The top band indicates an AP-CT duplex whereas the bottom band indicates free AP. Note that the absence of a band for the AP-Target complex is likely the result of rapid on-off rates for the complex.

Figure S4.10. Determination of optimal buffer conditions for the T-AP system. RCA product generation monitored in real-time using SYBR Gold intercalating dye. A concentration of either 0 or 10 nM thrombin was used for ratio determination. Results taken after 30 minutes of RCA.

Figure S4.11. Optimization of the anti-thrombin aptamer system with by the following parameters: (A) Optimal phi29 DP concentration with a digestion time of 60 minutes and a 0.5 CT:AP ratio; (B) Optimal 3'-exonuclease digestion time with a phi29 DP concentration of 0.1 U/ μ L and a 0.5 CT:AP ratio and; (C) Optimal ratio of circular template (CT) to aptamer (AP). RCA product generation monitored in real-time using SYBR Gold intercalating dye. A concentration of either 0 or 10 nM thrombin was used for ratio determination. Results taken after 60 minutes of RCA.

Figure S4.12. Effect of various heat treatments of protein targets on RP generation for the T-AP system. RCA product generation monitored in real-time using SYBR Gold intercalating dye.

Figure S4.13. Effect of complex media on assay performance for P-AP system. (A) 10% human serum or; (B) 10% human plasma. RCA product generation monitored in real-time using SYBR Gold intercalating dye.

Figure S4.14. Determination of optimal digestion time for the P-AP system in either 10% human serum or 10% human plasma. RCA product generation monitored in real-time using SYBR Gold

intercalating dye. A concentration of either 0 or 10 nM PDGF was used for ratio determination. Results taken after 120 minutes of RCA.

Chapter 5.

Figure 5.1. (A) The aptamer strand used for RecJ-mediated RCA. The sequence is comprised of a recognition tail on the 5'-end to promote RecJ recognition, an aptamer region for target recognition, a short spacer, and a primer region on the 3'-end for CT binding. (B) Schematic representation of the target-mediated RCA-based assay. In the absence of a target, RecJ 5'-exonuclease digests the aptamer prior to addition a CT and phi29 DP, preventing RCA. The binding of a target protects the aptamer from digestion, allowing the CT to bind to the protected primer region and permit RCA. The RCA product is detected using a fluorescent intercalating dye.

Figure 5.2. Gel-based optimization of T-AP digestion system: (A) Percentage of T-AP digested in 60 minutes as a function of RecJ 5'-exonuclease concentration (units per reaction). (B) Percentage of T-AP digested as a function of time, using 15 U of RecJ per reaction. (C) Percentage of T-AP digested as a function of thrombin concentration, using 15 U of RecJ per reaction and a digestion time of 60 minutes, followed by heat denaturation at 95 °C for 5 minutes.

Figure 5.3. Real-time RCA-based optimization of T-AP RCA system using the following parameters: (A) Optimal RecJ concentration with a digestion time of 60 minutes; (B) Optimal digestion time with a RecJ concentration of 7.5 U. RCA product generation monitored in real-time using SYBR Gold intercalating dye. A concentration of either 0 or 10 nM thrombin was used for ratio determination. The dark grey bars indicate the selected optimal condition. Results taken after 30 minutes of RCA.

Figure 5.4. Performance of optimized anti-thrombin system with RCA product generation monitored in real-time using SYBR Gold intercalating dye. (A) Reagent and selectivity controls, where (-RecJ) denotes no RecJ-mediated exonuclease digestion. BSA, OTA, and thrombin (Thr) concentrations were 1 μ M. The inset includes the denaturing PAGE gel of the reaction products as well as the intensity ratios between lanes. (B) Concentration-response curve of RCA product generation in the presence of varying amounts of thrombin. Results taken after 30 minutes of RCA.

Figure 5.5. Gel-based optimization of O-AP digestion system: (A) Percentage of O-AP digested in 60 minutes as a function of RecJ 5'-exonuclease concentration (units per reaction). (B) Percentage of O-AP digested as a function of time, using 25 U of RecJ per reaction. (C) Percentage of O-AP digested as a function of OTA concentration, using 25 U of RecJ per reaction and a digestion time of 60 minutes, followed by heat denaturation at 95 °C for 5 minutes.

Figure 5.6. Real-time RCA-based optimization of the O-AP RCA system by varying the following parameters: (A) Optimal RecJ concentration with a digestion time of 60 minutes; (B) Optimal digestion time with a RecJ concentration of 25 U. RCA product generation was monitored in real-time using SYBR Gold intercalating dye. A concentration of either 0 or 1 µM OTA was used for ratio determination. The dark grey bars indicate the selected optimal condition. Results were taken after 30 minutes of RCA.

Figure 5.7. Performance of optimized anti-OTA system with RCA product generation monitored in real-time using SYBR Gold intercalating dye. (A) Reagent and selectivity controls, where (-RecJ) denotes no RecJ-mediated exonuclease digestion. BSA, thrombin (Thr), and OTA concentrations were 1 µM. The inset includes the denaturing PAGE gel of the reaction products as well as the intensity ratios between lanes. (B) Concentration-response curve of RCA product generation in the presence of varying amounts of OTA. Results were taken after 30 minutes of RCA.

Figure S5.1. Investigation of the effect of increasing various reaction parameters for the anti-thrombin T-AP system using 10% denaturing PAGE analysis: (A) concentration of RecJ 5'-exonuclease; (B) digestion time; and, (C) concentration of thrombin.

Figure S5.2. Investigation of the effect of increasing RecJ 5'-exonuclease concentration for the anti-thrombin T-AP system under different reaction conditions using 10% denaturing PAGE analysis: (A) 1x phi29 DP reaction buffer and room temperature; (B) 1x phi29 DP reaction buffer and 37°C; (C) 1x RecJ reaction buffer and room temperature and; (D) 1x RecJ reaction buffer and 37°C.

Figure S5.3. Investigation of the effect of increasing various reaction parameters for the O-AP system using 10% denaturing PAGE analysis: (A) concentration of RecJ 5'-exonuclease; (B) digestion time and; (C) concentration of ochratoxin A (OTA).

Figure S5.4. Investigation of the effect of increasing RecJ 5'-exonuclease concentration for the anti-OTA O-AP system under different reaction conditions using 10% denaturing PAGE analysis: (A) 1x phi29 DP reaction buffer and room temperature; (B) 1x phi29 DP reaction buffer and 37°C; (C) 1x RecJ reaction buffer and room temperature and; (D) 1x RecJ reaction buffer and 37°C.

LIST OF TABLES

Chapter 2.

Table S2.1. Homogeneous solution-based methods.

Table S2.2. Heterogeneous solution-based methods..

Table S2.3. Colorimetric-based solid-phase methods..

Table S2.4. Fluorometric-based solid-phase methods..

Table S2.5. Paper-based methods..

Table S2.6. Electrochemical-based methods..

Chapter 3.

Table S3.1. List of DNA Sequences Used.

Chapter 4.

Table S4.1. List of DNA Sequences Used.

Chapter 5.

Table S5.1. List of DNA Sequences Used.

Table S5.2. Comparison of other RCA-based assays for thrombin detection.

Table S5.3. Comparison of buffer composition.

Table S5.4. Comparison of other RCA-based assays for OTA detection.

LIST OF ABBREVIATIONS

CT	circular template
DNA	deoxyribonucleic acid
DNAzyme	deoxyribozyme
DP	DNA polymerase
EXPAR	exponential amplification reaction
FNA	functional nucleic acid
HDA	helicase-dependent amplification
ITA	isothermal amplification
LAMP	loop-mediated isothermal amplification
MRE	molecular recognition element
NA	nucleic acid
PCR	polymerase chain reaction
POC	point of care
RCA	rolling circle amplification
RNA	ribonucleic acid
RPA	recombinase polymerase amplification
SDA	strand displacement amplification
SELEX	systematic evolution of ligands by exponential enrichment
SNP	single nucleotide polymorphism
TMSD	toehold-mediated strand displacement

CHAPTER 1. INTRODUCTION

1.1 Functional Nucleic Acids as Molecular Recognition Elements

Deoxyribonucleic acids (DNA) have found widespread use as both targets and probes for diagnostic assays.^[1–6] In particular, since the development of polymerase chain reaction (PCR) for amplification of DNA,^[7] the field of molecular diagnostics has grown dramatically, and is now established as a key component of modern clinical diagnostics.^[8–11] In such assays, DNA is used as a molecular recognition element (MRE) to hybridize with a desired nucleic acid (NA) target, and the duplex is then used as the starting point for PCR amplification. Such assays are extremely sensitive (single copy detection limits are possible) and have the precision to detect single nucleotide polymorphisms (SNPs),^[12–14] but are restricted to nucleic acid targets.

Over the past 30 years, a novel class of NAs known as Functional Nucleic Acids (FNAs) have emerged as important class of MREs that have the ability to bind to non-NA targets to allow for their detection.^[15–17] An important FNA is the DNA aptamer, which is able to act as a MRE and selectively binds to an analyte of interest, forming unique secondary and tertiary structures in the process (Figure 1A). Beyond target binding, ribozymes and deoxyribozymes (DNAzymes) are another class of FNAs that operate by undergoing target induced catalytic activity, often with the

ability to cleave nucleic acid substrates to produce signals (Figure 1B).^[18–24]

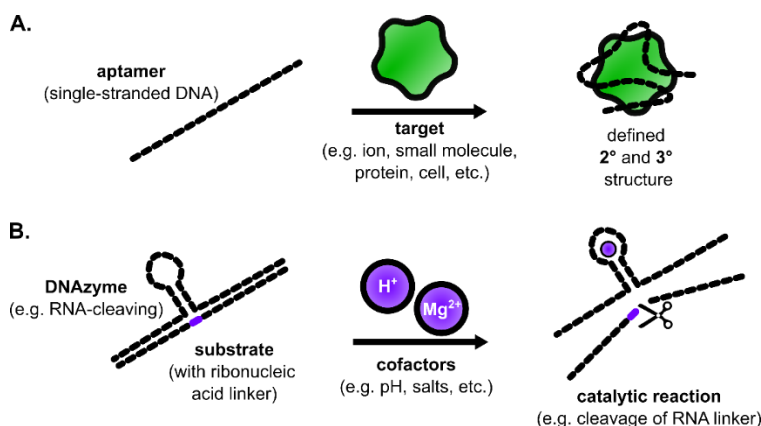


Figure 1. Functional Nucleic Acids: A) Aptamers; B) DNAzymes.

The first reports of DNA aptamers was in 1990, when three research groups independently reported^[25–27] methods for selection of aptamers using a process known as SELEX (Systematic Evolution of Ligands by Exponential Enrichment).^[28] The process typically utilizes a synthetic library of approximately 10^{15} random sequences of single-stranded DNA (or RNA) oligonucleotides. This library undergoes a Darwinian-type process of selection in which the sequences exhibiting the best binding properties to a target analyte are enriched through iterative generations (selection rounds). Using SELEX, or variations of it,^[28–31] aptamers and DNAzymes have been discovered for a variety of targets including ions, small molecules, proteins, viruses, and cells – with picomolar to micromolar binding affinities.^[25,26,32–41] The development of, and advantages of FNAs for detection of such targets are discussed in more detail in Chapter 2.

1.2 Isothermal DNA Amplification

Sensitivity can often be a limiting factor of point of care (POC) biosensors and assays alike.^[15,42,43] In traditional sensors where the sample volumes are on the scale of millilitres, the detection of trace amounts of analytes is relatively trivial as the number of moles of analyte is often quite large. Comparatively, this can be a challenging task for miniaturized assays as the nano- to microlitre scale samples mean that the number of moles of analyte present is orders of magnitude lower than that of traditional millilitre-scale samples. Similar compromises in the analytical properties of an assay can occur when:

- i) assay times are shortened thus reducing the time available to generate detectable signals;
- ii) workflows are simplified or condensed risking a reduction in assay efficiency and yields of the final detectable product or;
- iii) less sensitive detection mechanisms are incorporated thus increasing the threshold number of detectable events required to observe a signal.

As such, many assays incorporate an amplification method to address these compromises with sensitivity. Generally, an amplification step serves to convert a single capture event into multiple detectable events. The most widely known nucleic acid amplification method is PCR.

However, integration of PCR in biosensing applications is challenging as the method requires thermocycling (typically between 66°C and 95°C), which necessitates complex instrumentation and thus limits its utility in resource limited settings.^[14]

There has been a significant amount of work on the development of amplification methods that can operate at a single set temperature (isothermal amplification, or ITA methods) to overcome the need for thermocycling.^[44,45] To date, there are many examples of both enzyme-free and enzyme-based ITA method for both NA and non-NA target detection. Though there are a variety of enzyme-free NA amplification strategies, sensitivity and amplification rates can be limited.^[44] Among enzyme-based ITA methods, the most popular include: Helicase-Dependent Amplification (HDA),^[46] Recombinase Polymerase Amplification (RPA),^[47] Loop-mediated isothermal amplification (LAMP),^[48] Strand Displacement Amplification (SDA),^[49,50] and Exponential Amplification Reaction (EXPAR).^[51] Such methods can be used both for direct amplification of nucleic acids, or can use aptamers to regulate the ITA method.^[52–78] Though effective, these methods all require some combination of elevated temperatures (ranging from 37 °C to as high as 65 °C), additional processing enzymes (such as helicases in HDA, recombinase in RPA, or nicking enzymes in SDA and EXPAR), and multiple reaction steps, making them less effective for biosensing applications.

1.3 Rolling Circle Amplification

As discussed in-depth in Chapter 2, Rolling Circle Amplification (RCA) is an isothermal DNA amplification method that utilizes a circularized DNA strand as the template (circular template, or CT) to amplify a target substrate strand into tens to thousands of concatemeric single stranded DNA copies complementary to the CT (Figure 2).^[19,79–84] RCA requires only a single enzyme (typically ϕ 29 or phi29 DP), a single primer and can be performed at room temperature, making it well suited for biosensor development. The method can also be implemented using either linear or exponential amplification strategies, and is compatible with multiple signal outputs, as described in Chapter 2.

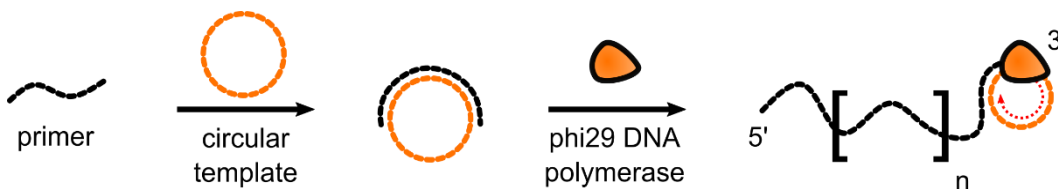


Figure 2. Rolling Circle Amplification.

1.4 Combining FNAs and RCA

The utility of FNAs provides a means to convert non-NA binding events into NA outputs that can be integrated with RCA. Though RCA methods require an initial nucleic acid input to initiate amplification, when combined with FNAs it is possible to use a non-NA target to modulate the amplification steps, drastically expanding the utility of the method for biosensing.^[85–88] Specifically, RCA may be the most prolific ITA method for

non-NA target detection.^[21,22,45] Regulation of RCA can be achieved in a variety of ways by controlling the availability of the primer or the CT, and Chapter 2 extensively reviews the utilization of FNAs for the target-mediated regulation of RCA. However, many of the current methods for RCA regulation by aptamers require either incorporation of the aptamer into the CT,^[89] which can impact native binding affinity,^[90] or develop complicated structure-switching designs to release a linear primer (or the aptamer itself as the primer) to generate homogeneous assays.^[91,92] However, designing such structure-switching systems is not trivial as locking aptamers in such a configuration can have detrimental effects on binding affinity^[93] or lead to high background levels arising from the normal conformational equilibrium observed with such aptamers. Alternative regulation methods can also be used, as described in Chapter 2, however these often require immobilization of the aptamer or multiple separation and washing steps, making them more challenging to implement in simple POC biosensors.^[94] As such, there remains a need for the development of homogeneous RCA regulation methods that utilize linear aptamers without negatively impacting their binding affinities.

1.5 Thesis Goals

Despite many examples of sensitive aptamer-based assays that utilize RCA to enhance analyte detection, many of these have shortcomings and recurring problems. First, and foremost, homogeneous assays are

desirable as they show the most promise for applications at the POC, however almost all homogeneous assays require structure-switching constructs, making it difficult to produce a generalizable assay owing to the risk of reducing the binding affinity of the aptamer. Though RCA applications with circular aptamers provide an avenue to avoid the need to design structure-switching constructs, circular aptamers are limited in availability and can demonstrate reduced binding affinities. Thus, there is a need for systems where an unmodified linear aptamer can simply and effectively be paired with RCA. As such, this thesis focuses on the design of homogeneous assays that utilize linear aptamers for direct regulation of RCA without the need for a structure switching process so as to provide the best balance of sensitivity and simplicity.

The thesis begins with a detailed review of FNA-linked RCA assays and devices (Chapter 2). In this review, four main components are evaluated: i) the input method for non-NA detection; ii) the amplification method; iii) the detection method for quantifying the amount of RCA product created and; iv) the integration of the above three components to produce homogeneous or heterogenous assays with a variety of signalling outputs. By critically reviewing each parameter, we pinpoint current trends, identify strengths, and highlight areas for improvement. As a corollary of this analysis of the field, this review should serve to highlight new approaches for developing the next wave of FNA-linked RCA assays.

The first research project (Chapter 3) serves to evaluate the use of a linear aptamer for direct control of the RCA reaction by using the aptamer as a primer for target-mediated modulation of RCA. In this approach, a primer region is embedded within an aptamer to create an aptaprimer that can quantitatively regulate RCA product generation as a function of target protein concentration. This method takes advantage of the multiple functions of FNAs in their ability to act as DNA-binding NAs, and protein-binding MREs, and evaluates the ability of phi29 DP to read through protein-bound aptaprimers. It is hypothesized that target-bound aptamers should be unable to initiate RCA, and thus increased target should inhibit RCA, producing a turn-off sensor.

In Chapter 4, the ability to utilize the inherent 3' exonuclease activity of phi29 DP is evaluated as a means to modulate the digestion of aptaprimers as a function of target concentration. It was hypothesized that target-bound aptamer should show resistance to nucleolytic activity, while free aptamers would be digested. The ability of the circular template to directly remove the bound target from undigested aptaprimers via toehold-mediated strand displacement (TMSD) was also evaluated to determine if the protected aptaprimer could initiate RCA, which should increase with target concentration, producing a turn-on sensor.

In Chapter 5 an alternative strategy for the exonucleolytic regulation of RCA primer availability was examined using a 5'-exonuclease. In this

case, the binding of target was expected to improve the protection of the aptaprimer from digestion as target concentration increased, but in this case a free 3' terminus was included in the aptaprimer to avoid the need for CT-mediated TMSD, potentially simplifying the assay. Such an approach should not require the need to design a CT to perform target displacement, making the approach more generic. To test this premise, both a protein and small molecule target were evaluated to determine if turn on sensors could be produced for both targets.

Lastly, in Chapter 6 the major achievements and conclusions derived from the research above are summarized and further ways to take advantage of the unique FNA-RCA are described.

1.6 References

- [1] M. Urdea, L. A. Penny, S. S. Olmsted, M. Y. Giovanni, P. Kaspar, A. Shepherd, P. Wilson, C. A. Dahl, S. Buchsbaum, G. Moeller, et al., *Nature* **2006**, *444*, 73–79.
- [2] K. Janssen, K. Knez, D. Spasic, J. Lammertyn, *Sensors* **2013**, *13*, 1353–1384.
- [3] A. Chen, S. Yang, *Biosens. Bioelectron.* **2015**, *71*, 230–242.
- [4] F. Wang, X. Liu, I. Willner, *Angew. Chemie* **2015**, *54*, 1098–1129.
- [5] J. Li, M. Mohammed-Elsabagh, F. Paczkowski, Y. Li, *ChemBioChem* **2020**, *21*, 1547–1566.
- [6] E. M. McConnell, I. Cozma, Q. Mou, J. D. Brennan, Y. Lu, Y. Li, *Chem. Soc. Rev.* **2021**, DOI 10.1039/D1CS00240F.
- [7] K. B. Mullis, F. A. Faloona, in *Methods Enzymol.*, **1987**, pp. 335–350.
- [8] E. Paleček, M. Bartošík, *Chem. Rev.* **2012**, *112*, 3427–3481.
- [9] A. Niemz, T. M. Ferguson, D. S. Boyle, *Trends Biotechnol.* **2011**, *29*, 240–250.
- [10] J. Hu, S. Wang, L. Wang, F. Li, B. Pingguan-Murphy, T. J. Lu, F. Xu, *Biosens. Bioelectron.* **2014**, *54*, 585–597.
- [11] C. C. Pritchard, H. H. Cheng, M. Tewari, *Nat. Rev. Genet.* **2012**, *13*, 358–369.
- [12] C. Batchelor-McAuley, G. G. Wildgoose, R. G. Compton, *Biosens.*

- Bioelectron.* **2009**, *24*, 3183–3190.
- [13] K. Chang, S. Deng, M. Chen, *Biosens. Bioelectron.* **2015**, *66*, 297–307.
- [14] L. Yan, J. Zhou, Y. Zheng, A. S. Gamson, B. T. Roembke, S. Nakayama, H. O. Sintim, *Mol. Biosyst.* **2014**, *10*, 970–1003.
- [15] K. S. Park, *Biosens. Bioelectron.* **2018**, *102*, 179–188.
- [16] H. Zhang, L. Zhou, Z. Zhu, C. Yang, *Chem. Eur. J.* **2016**, *22*, 9886–9900.
- [17] W. Zhou, P. J. Jimmy Huang, J. Ding, J. Liu, *Analyst* **2014**, *139*, 2627–2640.
- [18] S. K. Silverman, *Org. Biomol. Chem.* **2004**, *2*, 2701–2706.
- [19] E. J. Cho, L. Yang, M. Levy, A. D. Ellington, *J. Am. Chem. Soc.* **2005**, *127*, 2022–3.
- [20] Y. Chen, R. M. Corn, *J. Am. Chem. Soc.* **2013**, *135*, 2072–2075.
- [21] W. Zhao, M. M. Ali, M. A. Brook, Y. Li, *Angew. Chemie* **2008**, *47*, 6330–6337.
- [22] M. M. Ali, F. Li, Z. Zhang, K. Zhang, D.-K. Kang, J. A. Ankrum, X. C. Le, W. Zhao, *Chem. Soc. Rev.* **2014**, *43*, 3324.
- [23] K. Tram, P. Kanda, Y. Li, *J. Nucleic Acids* **2012**, *1*, 958683.
- [24] H. Peng, A. M. Newbigging, Z. Wang, J. Tao, W. Deng, X. C. Le, H. Zhang, *Anal. Chem.* **2018**, *90*, 190–207.
- [25] C. Tuerk, L. Gold, *Science* **1990**, *249*, 505–510.
- [26] A. D. Ellington, J. W. Szostak, *Nature* **1990**, *346*, 818–822.
- [27] D. L. Robertson, G. F. Joyce, *Lett. to Nat.* **1990**, *344*, 467–468.
- [28] R. Stoltenburg, C. Reinemann, B. Strehlitz, *Biomol. Eng.* **2007**, *24*, 381–403.
- [29] K. Sefah, D. Shangguan, X. Xiong, M. B. O’Donoghue, W. Tan, M. B. O’Donoghue, W. Tan, *Nat. Protoc.* **2010**, *5*, 1169–1185.
- [30] V.-T. V.-T. Nguyen, Y. S. Kwon, J. H. Kim, M. B. Gu, *Chem. Commun.* **2014**, *50*, 10513–10516.
- [31] L. Martini, A. J. Meyer, J. W. Ellefson, J. N. Milligan, M. Forlin, A. D. Ellington, S. S. Mansy, *ACS Synth. Biol.* **2015**, *4*, 1144–1150.
- [32] A. Sassolas, B. Leca-Bouvier, L. Blum, *Chem. Rev.* **2008**.
- [33] B. Van Dorst, J. Mehta, K. Bekaert, E. Rouah-Martin, W. De Coen, P. Dubruel, R. Blust, J. Robbens, *Biosens. Bioelectron.* **2010**, *26*, 1178–1194.
- [34] S. Tyagi, F. R. Kramer, *Nat. Biotechnol.* **1996**, *14*, 303–308.
- [35] E. Luzi, M. Minunni, S. Tombelli, M. Mascini, *TrAC Trends Anal. Chem.* **2003**, *22*, 810–818.
- [36] D. S. Wilson, J. W. Szostak, *Annu. Rev. Biochem.* **1999**, *68*, 611–647.
- [37] L. S. Green, D. Jellinek, R. Jenison, A. Östman, C. H. Heldin, N. Janjic, *Biochemistry* **1996**, *35*, 14413–14424.
- [38] J. C. Cox, A. D. Ellington, *Bioorganic Med. Chem.* **2001**, *9*, 2525–2531.

- [39] M. Jing, M. T. Bowser, *Anal. Chim. Acta* **2011**, 686, 9–18.
- [40] R. Jenison, S. Gill, A. Pardi, B. Polisky, *Science* **2018**, 263, 1425–1429.
- [41] M. a M. . Cooper, *Nat. Rev. Drug Discov.* **2002**, 1, 515–528.
- [42] P. Craw, W. Balachandran, *Lab Chip* **2012**, 12, 2469–2486.
- [43] T. Tian, Y. Bi, X. Xu, Z. Zhu, C. Yang, *Anal. Methods* **2018**, 10, 3567–3581.
- [44] C. Jung, A. D. Ellington, *Acc. Chem. Res.* **2014**, 47, 1825–1835.
- [45] Y. Zhao, F. Chen, Q. Li, L. Wang, C. Fan, *Chem. Rev.* **2015**, 115, 12491–12545.
- [46] M. Vincent, Y. Xu, H. Kong, *EMBO Rep.* **2004**, 5, 795–800.
- [47] O. Piepenburg, C. H. Williams, D. L. Stemple, N. A. Armes, *PLoS Biol.* **2006**, 4, 1115–1121.
- [48] T. Notomi, *Nucleic Acids Res.* **2000**, 28, 63e – 63.
- [49] G. T. Walker, M. C. Little, J. G. Nadeau, D. D. Shank, *Proc. Natl. Acad. Sci. U. S. A.* **1992**, 89, 392–396.
- [50] G. T. Walker, M. S. Fraiser, J. L. Schram, M. C. Little, J. G. Nadeau, D. P. Malinowski, *Nucleic Acids Res.* **1992**, 20, 1691–1696.
- [51] J. Van Ness, L. K. Van Ness, D. J. Galas, *Proc. Natl. Acad. Sci. U. S. A.* **2003**, 100, 4504–4509.
- [52] S. Barreda-García, R. Miranda-Castro, N. de-los-Santos-Álvarez, A. J. Miranda-Ordieres, M. J. Lobo-Castañón, *Anal. Bioanal. Chem.* **2018**, 410, 679–693.
- [53] Y. Du, D. Liu, M. Wang, F. Guo, J. S. Lin, *Biosens. Bioelectron.* **2021**, 181, 1–8.
- [54] S. Xie, Y. Tang, D. Tang, *Biosens. Bioelectron.* **2018**, 102, 518–524.
- [55] H. Cao, X. Fang, H. H. Li, H. H. Li, J. Kong, *Talanta* **2017**, 164, 588–592.
- [56] Y. M. Wang, J. W. Liu, L. Y. Duan, S. J. Liu, J. H. Jiang, *Microchim. Acta* **2017**, 184, 4183–4188.
- [57] R. Cai, Z. Zhang, H. Chen, Y. Tian, N. Zhou, *Sensors Actuators, B Chem.* **2021**, 326, 128842.
- [58] Y. Li, S. Liu, Z. Zhao, Y. Zheng, Z. Wang, *Talanta* **2017**, 164, 196–200.
- [59] R. Cai, F. Yin, H. Chen, Y. Tian, N. Zhou, *Microchim. Acta* **2020**, 187, DOI 10.1007/s00604-020-04293-9.
- [60] J. Yin, Y. Liu, S. Wang, J. Deng, X. Lin, J. Gao, *Sensors Actuators, B Chem.* **2018**, 256, 573–579.
- [61] C. H. Li, X. Xiao, J. Tao, D. M. Wang, C. Z. Huang, S. J. Zhen, *Biosens. Bioelectron.* **2017**, 91, 149–154.
- [62] Z. Huang, Z. Luo, J. Chen, Y. Xu, Y. Duan, *ACS Sensors* **2018**, 3, 2423–2431.
- [63] W. Wu, M. Zhou, H. He, C. Liu, P. Li, M. Wang, Y. Liu, X. Hao, Z. Fang, *Sensors Actuators, B Chem.* **2018**, 272, 550–558.

- [64] M. Jauset-Rubio, M. Svobodová, T. Mairal, C. McNeil, N. Keegan, M. S. El-Shahawi, A. S. Bashammakh, A. O. Alyoubi, C. K. O'Sullivan, *Anal. Chem.* **2016**, *88*, 10701–10709.
- [65] Y. Zhang, J. Hu, C. Y. Zhang, *Anal. Chem.* **2012**, *84*, 9544–9549.
- [66] W. Tang, T. Zhang, Q. Li, H. Wang, H. Wang, Z. Li, *RSC Adv.* **2016**, *6*, 89888–89894.
- [67] S. Xie, Y. Chai, Y. Yuan, L. Bai, R. Yuan, *Anal. Chim. Acta* **2014**, *832*, 51–57.
- [68] Y. Wang, X. Zhao, M. Zhang, X. Sun, J. Bai, Y. Peng, S. Li, D. Han, S. Ren, J. Wang, et al., *Anal. Chim. Acta* **2020**, *1116*, 1–8.
- [69] J. Chen, Y. Zhang, B. P. Xie, B. Sun, W. J. Duan, M. M. Li, J. X. Chen, Z. Dai, X. Zou, *Talanta* **2021**, *225*, 121980.
- [70] T. Qiu, Y. Wang, J. Yu, S. Liu, H. Wang, Y. Guo, J. Huang, *RSC Adv.* **2016**, *6*, 62031–62037.
- [71] A. M. Liao, W. Pan, J. C. Benson, A. D. Wong, B. J. Rose, G. T. Caltagirone, *Biochemistry* **2018**, *57*, 5117–5126.
- [72] J. F. C. Loo, P. M. Lau, H. P. Ho, S. K. Kong, *Talanta* **2013**, *115*, 159–165.
- [73] F. Shen, E. K. Davydova, W. Du, J. E. Kreutz, O. Piepenburg, R. F. Ismagilov, *Anal. Chem.* **2011**, *83*, 3533–3540.
- [74] Z. A. Crannell, B. Rohrman, R. Richards-Kortum, *Anal. Chem.* **2014**, *86*, 5615–5619.
- [75] B. Rohrman, R. Richards-Kortum, *Anal. Chem.* **2015**, *87*, 1963–1967.
- [76] Y. Yuan, S. Wei, G. Liu, S. Xie, Y. Chai, R. Yuan, *Anal. Chim. Acta* **2014**, *811*, 70–75.
- [77] S. Xie, Y. Chai, Y. Yuan, L. Bai, R. Yuan, *Biosens. Bioelectron.* **2014**, *55*, 324–329.
- [78] J. Feng, Z. Dai, X. Tian, X. Jiang, *Food Control* **2018**, *85*, 443–452.
- [79] P. M. Lizardi, X. Huang, Z. Zhu, P. Bray-Ward, D. C. Thomas, D. C. Ward, *Nat. Genet.* **1998**, *19*, 225–232.
- [80] I. Rodríguez, J. M. Lázaro, L. Blanco, S. Kamtekar, A. J. Berman, J. Wang, M. Vega, T. a Steitz, M. Salas, M. de Vega, et al., *Proc. Natl. Acad. Sci.* **2005**, *102*, 6407–6412.
- [81] A. J. Berman, S. Kamtekar, J. L. Goodman, J. M. Lázaro, M. de Vega, L. Blanco, M. Salas, T. A. Steitz, M. Vega, L. Blanco, et al., *EMBO J.* **2007**, *26*, 3494–3505.
- [82] S. Kamtekar, A. J. Berman, J. Wang, J. M. Lázaro, M. Vega, L. Blanco, T. A. Steitz, M. de Vega, L. Blanco, M. Salas, et al., *EMBO J.* **2006**, *25*, 1335–1343.
- [83] J. Méndez, L. Blanco, M. Salas, *EMBO J.* **1997**, *16*, 2519–2527.
- [84] L. Yang, C. W. Fung, E. J. Cho, A. D. Ellington, *Anal. Chem.* **2007**, *79*, 3320–3329.
- [85] M. Liu, C. Y. Hui, Q. Zhang, J. Gu, B. Kannan, S. Jahanshahi-Anbuhi, C. D. M. M. M. Filipe, J. D. Brennan, Y. Li, C. D. M. M. M. Filipe, et

- al., *Angew. Chemie* **2016**, *55*, 2709–2713.
- [86] C. Y. Hui, M. Liu, Y. Li, J. D. Brennan, *Angew. Chemie* **2018**, *57*, 4549–4553.
- [87] C. Carrasquilla, J. R. L. Little, Y. Li, J. D. Brennan, *Chem. Eur. J.* **2015**, *21*, 7369–7373.
- [88] M. Liu, J. Song, S. Shuang, C. Dong, J. D. Brennan, Y. Li, *ACS Nano* **2014**, *8*, 5564–5573.
- [89] L. Wang, K. Tram, M. M. Ali, B. J. Salena, J. Li, Y. Li, *Chem. Eur. J.* **2014**, *20*, 2420–4.
- [90] M. Liu, Q. Yin, Y. Chang, Q. Zhang, J. D. Brennan, Y. Li, *Angew. Chemie* **2019**, *58*, 8013–8017.
- [91] M. Liu, W. Zhang, Q. Zhang, J. D. Brennan, Y. Li, *Angew. Chemie* **2015**, *54*, 9637–9641.
- [92] X. Liu, F. Yang, D. Li, R. Yuan, Y. Xiang, *Sensors Actuators, B Chem.* **2020**, *305*, 127405.
- [93] R. Nutiu, Y. Li, *J. Am. Chem. Soc.* **2003**, *125*, 4771–4778.
- [94] W. Cheng, L. Ding, Y. Chen, F. Yan, H. Ju, Y. Yin, *Chem. Commun.* **2010**, *46*, 6720–6722.

CHAPTER 2.

DESIGN STRATEGIES FOR FUNCTIONAL NUCLEIC ACID BIOSENSORS UTILIZING ROLLING CIRCLE AMPLIFICATION

2.1 Author's Preface

I was responsible for the review structure, and wrote the first draft of the manuscript. I wrote the content and designed the figures for the Introduction and Regulation sections of the review. I compiled the data and generated the summary tables included in this review.

Alexa Mainguy wrote the content and designed the figures for the Amplification section of the review. Alexa Mainguy, and I both co-wrote the content and co-designed the figures for the remaining sections of the review. Dr. Brennan, Alexa Mainguy, and I provided editorial input for all sections of the review. Dr. Brennan and Dr. Li provided editorial input to generate the final draft of the paper.

2.2 Abstract

Functional nucleic acids (FNA), including DNA aptamers and DNAzymes, are finding increasing use as molecular recognition elements (MRE) for point of care (POC) devices. An ongoing challenge in the development of FNA-based POC sensors is the ability to achieve detection of low levels of analyte without compromising assay time and ease of use. Rolling circle amplification (RCA) is a leading nucleic acid (NA) isothermal amplification (ITA) method which can be coupled with FNAs for the ultrasensitive detection of non-NA targets. Herein we examine the key considerations required when designing FNA-coupled biosensors utilizing RCA. Specifically, we describe methods for using FNAs as inputs to regulate RCA, various modes of RCA amplification, and methods to detect the output of the RCA reaction, along with how these can be combined to allow detection of non-NA targets. Recent progress on development of portable POC devices that incorporate RCA is then described, followed by a summary of key challenges and opportunities in the field.

2.3 Introduction

Modern nucleic acid biosensors (NABs) have found widespread use as they provide many advantages over traditional diagnostic methods.^[1–3] NABs can provide processing times of minutes to hours, are substantially smaller and more affordable relative to traditional instrument-based methods, and are often semi-automated, requiring minimal user training.

These make them excellent candidates for applications at the point of care (POC). A key advantage of NABs is the ability to integrate nucleic acid amplification strategies, which can significantly improve the limit of detection.^[4-6] However, sample preparation remains a major issue for such biosensors, as extraction of NAs (DNA, RNA, or miRNA) from a biological sample is non-trivial and often requires several laborious and time-consuming extraction procedures. Furthermore, many important clinical and environmental sensing applications do not have a relevant NA target. Hence, there has been a significant amount of research devoted to methods that can utilize readily accessible non-NA targets, such as metal ions, small molecules, and proteins, while retaining the advantages offered by NA amplification to lower the detection limit for such species. In this review, we describe methods to utilize functional nucleic acids (FNAs) in combination with isothermal NA amplification via rolling circle amplification (RCA) as a platform for ultrasensitive detection of non-NA targets, with an emphasis on sensors that are suitable for point-of-care (POC) applications.

Functional nucleic acids, which are either NA aptamers or (deoxy)ribozymes (RNAzymes or DNAzymes), have seen widespread use as molecular recognition elements (MREs) for the selective detection of non-NA targets.^[3,7-13] While both RNA aptamers and ribozymes are present in nature, no naturally occurring DNA aptamers or DNAzymes have been

found to date.^[14,15] Hence, all such species have been generated using artificial *in vivo* selection methods.

The first reported selection of a DNA aptamer was in 1990, with three different groups independently reporting the discovery of DNA aptamers using a process known as SELEX (Systematic Evolution of Ligands by Exponential Enrichment).^[16–18] This Darwinian-type process of selection,^[19] and variations of it,^[20] have led to the discovery of aptamers for a variety of targets, including small molecules, proteins, viruses and cells, typically with picomolar to micromolar binding affinities.^[17,18,21–30] These single-stranded NA probes typically undergo substantial conformational changes upon non-covalent target binding, producing a defined tertiary structure based on an induced fit with the target, earning aptamers the nickname “chemical antibodies”.^[17,18,31] Aptamers can be incredibly selective, with the theophylline aptamer able to distinguish between theophylline and caffeine – a single methyl group difference – with 1000-fold selectivity,^[22] and the anti-platelet-derived growth factor (PDGF) aptamer binding the PDGF-BB isoform with 700-fold selectivity over the PDGF-AA isoform.^[21] Even enantiomers can be differentiated with the L-adenosine aptamer showing over 1700-fold chiral discrimination over D-adenosine.^[32]

The first selection of a DNAzyme was conducted in 1994, when Joyce's group reported on the first RNA cleaving DNAzyme, which catalyzed the

transesterification reaction of the phosphodiester bond of RNA.^[33] Since this time, many other DNAzymes have been discovered^[11,34] with various catalytic abilities including nucleic acid ligation,^[35,36] hydrolysis,^[37–39] phosphorylation,^[40] capping,^[41] deglycosylation^[42] and peroxidation.^[43] DNAzymes can either be natively active in the buffer conditions, or an aptamer domain can be incorporated into the DNAzyme as the MRE allosterically activating the catalytic domain upon target binding (often referred to as aptazymes). Many aptazymes such as the ATP aptzyme, are rationally designed to link a target binding event with catalytic activity through a communication module.^[1,44] More recently, aptazymes have been directly selected against bacterial or mammalian cellular media to produce MREs that are selective against desired bacteria or cancer cells.^[45,46] Together, the breadth of DNA aptamers and DNAzymes has made FNAs a particularly useful set of MREs for the development of POC diagnostic tests.^[47–49]

While FNAs represent a novel category of MRE, in many cases their affinity constants are not sufficient to allow detection of trace levels of targets. Indeed, achieving ultrasensitive detection of analytes in a manner that meets the World Health Organization (WHO) ASSURED criteria (Affordable; Sensitive and Specific enough to provide useful information; User-friendly; Rapid and robust; Equipment-free, and; Deliverable to the end-user)^[50–53] remains a major challenge in the field of POC

diagnostics.^[4,6,53,54] To address this issue, binding of a target to a FNA can be coupled to one of several DNA amplification methods to increase sensitivity and drive down detection limits. Though there are non-enzymatic DNA amplification methods, improvements to sensitivity can be limited.^[55] As a result, sensors that utilize FNAs for target recognition commonly incorporate an enzymatic NA amplification method to retain sensitivity that is otherwise lost to miniaturization and simplification.

The most common enzymatic DNA amplification method is the polymerase chain reaction (PCR),^[56] however the need for thermocycling makes this method incompatible with simple point-of-care assays.^[57] Over the past 30 years a number of isothermal amplification (ITA) methods have been developed to overcome this limitation. These include strand displacement amplification (SDA),^[4,6,58,59] recombinase-polymerase amplification (RPA),^[60–62] loop-mediated amplification (LAMP),^[63–66] helicase dependent amplification (HDA),^[67–70] and hybridization chain reaction (HCR).^[55,71,72] While these are powerful amplification methods, and often provide exponential amplification, many of these require multiple enzymes or primers, complicated sequence design, and operate at elevated temperatures (typically 30 – 65 °C) making them difficult to apply in simple POC assays or devices which aim to operate in an equipment-free manner.

Rolling circle amplification (RCA) is another ITA method that has received significant attention for biosensing applications as described in

recent reviews.^[73–79] Replication of DNA around a circular template is a naturally occurring process which normally involves circular plasmids that are typically thousands of nucleotides in length.^[80] However, the CTs used in RCA are often synthesized to be less than one hundred nucleotides long rather than several thousands of nucleotides found in DNA plasmids. In fact, the first literature examples of circular oligonucleotides with open, unpaired structures that showed potential as substrates for polymerases were not reported until 1990,^[81,82] and it was not until 1995 that the Fire group reported on the replication of DNA using short synthetic nucleotide CTs.^[80] Shortly thereafter, Kool *et al.* suggested its possible application in NA amplification.^[83] Since this time, extensive advancements have been made in the use of RCA for detection of nucleic acid targets, including improvements in regulation methods, polymerase selection, amplification methods, and detection strategies. For more extensive information on the history of RCA, readers are referred to early reviews on the field.^[73,80,84]

In contrast to other ITA methods, RCA requires only a single enzyme, a single primer and can be done at room temperature, making it well suited for utilization in simple, equipment-free POC devices. RCA is unique among ITA methods in that it utilizes a circular DNA template (CT) rather than a linear one. In the presence of deoxyribonucleotide triphosphates (dNTPs), and the CT, a DNA polymerase (typically phi29 DNA polymerase (phi29 DP)) amplifies a complementary linear DNA or RNA primer. As the template

is circular, the resultant RCA product (RP) generated is a series of tens to thousands of concatemeric single-stranded DNA copies that are complementary to the CT. As described below in Sections 3 and 4, it is also possible to encode a variety of sequences into the RP to allow subsequent reactions that can improve either amplification efficiency or detection sensitivity, allowing this method to achieve single molecule detection limits.^[85–88]

RCA has been extensively used as an amplification tool for the detection of NA targets,^[73–75] and has the specificity to detect single nucleotide polymorphisms (SNPs).^[87,89–91] However, the use of RCA for the amplified detection of non-NA species requires careful consideration of three main components: 1) molecular recognition in a manner that triggers RCA; 2) the nature of the amplification reaction, and; 3) the method to transduce the RCA output into a measurable signal. While there are examples of RCA reactions that utilize antibodies as MREs,^[92–97] in this review we will focus on FNAs as MREs to trigger RCA, and will describe how the CT sequence can be used to modulate the triggering, amplification efficiency, and output of the RCA reaction (Figure 2.1). We also describe simple POC devices that integrate FNA-based MREs with RCA-enabled amplification and detection systems, with a focus on devices that meet the ASSURED criteria. Particular emphasis is placed on electrochemical and paper-based

biosensing approaches as these devices meet the ASSURED criteria,^[48,53,98,99] and allow for sensitive and robust analyte detection.

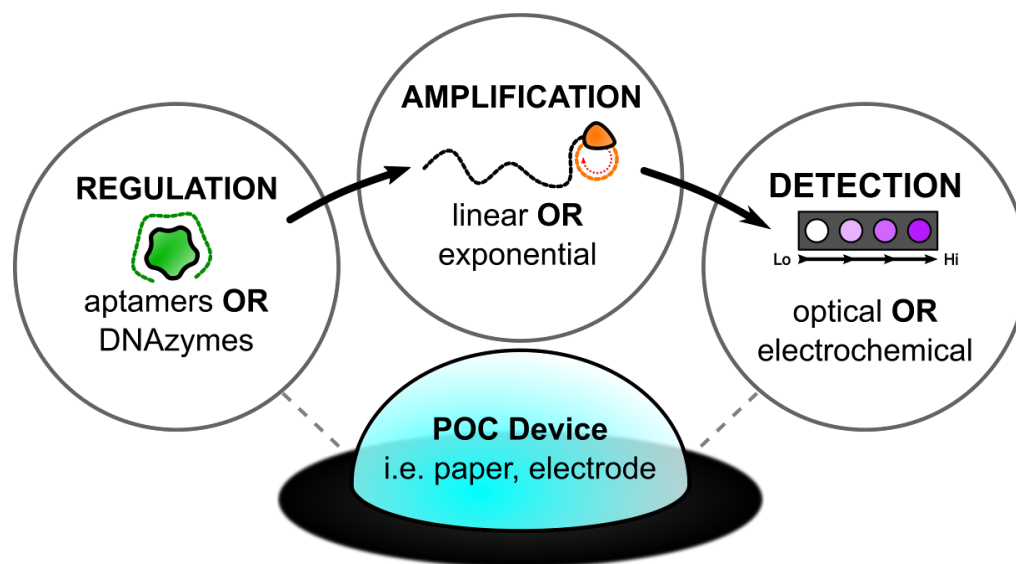


Figure 2.1. Overview of the three overarching ways that rolling circle amplification (RCA) can be manipulated. (A) Regulation, which governs how a non-nucleic acid target can be integrated as a regulator for RCA; (B) Amplification, and the different strategies that determine efficiency of amplicon generation; (C) Detection, which covers the various strategies for optically quantifying the amount of RCA product generated; (D) On paper, which focuses on how all three aspects can be incorporated on a paper-based surface for POC biosensing.

2.4 Regulation of RCA by FNA

Controlling the initiation of the RCA reaction can be achieved by regulating the availability of at least one of the four essential components of RCA: the primer, CT, a DNA polymerase (phi29 DP unless otherwise indicated), or dNTPs. To date, no methods have been reported that involve the modulation of DP or dNTP availability to regulate RCA. Though the

primer and CT are NA strands, FNAs act as a powerful bridge to allow non-NA targets to regulate NA strand availability. Here we will focus on techniques that specifically regulate the availability of either the primer strand or the CT with a focus on methods that best satisfy the ASSURED criteria.

2.4.1 Primer Regulation

The complementary binding of a NA primer to the CT to form a primer-CT complex is a fundamental requirement for RCA. The primer can be as short as six nucleotides in length,^[100] though longer primers will improve selectivity and the efficiency of initiating the RCA process.^[101] Once bound, the phi29 DP will elongate the primer along the CT from the 3' end, eventually displacing the primer after a revolution around the CT. This allows multiple copies of the antisense RP to be generated as identical repeating units. Binding of a target to a FNA can be used to alter that availability of the primer, and thus regulate the initiation of RCA, by three different methods. These include using: i) a target-binding event to trigger the release of a primer strand from a FNA, ii) binding of a target to an aptamer that acts as a primer to control primer-CT hybridization, or, iii) a target-activated RNA cleaving DNzyme (RCD) to liberate an otherwise blocked primer. These methods are described in detail in the following sections.

2.4.1.1 Primer Regulation using Structure-Switching Aptamers

Structure-switching aptamers are designed to switch between a duplex form, which has a short NA strand hybridized across the aptamer domain and a primer extension, and a complex formed between the target and aptamer, which displaces the hybridized NA strand.^[102–105] While often used to directly generate fluorescence signals based on displacement of adjacent quencher- and fluorophore-labelled strands,^[102–105] this method can also be used as a means to initiate RCA by using the displaced NA strand as the RCA primer. For example, Hu *et al.* utilized the thrombin-binding structure switching aptamer to regulate RCA in this manner.^[106] In this case, the aptamer released an RCA primer upon target binding, which was first captured at its 5' end by an immobilized DNA probe (Figure 2.2A). Following a washing step, addition of CT and phi29 DP to the captured primer allowed for target-mediated RP generation from the 3' terminus.

More recently, Liu *et al.* designed a tripartite structure-switching system for the detection of PDGF, which elegantly combined the essential RCA components together in a manner that eliminated the need for washing steps (Figure 2.2B).^[107] The system was comprised of a primer strand with the 5'-end hybridized to a CT and the 3'-end hybridized to an anti-PDGF aptamer. Without target present, the aptamer blocked phi29 DP from initiating RCA on the primer. However, addition of PDGF triggered a structure-switch and released the aptamer. This allowed the 3' end of the

primer to hybridize to the CT to generate a fully complementary primer sequence that could be used to initiate RCA.

A notable drawback of structure-switching aptamers is that hybridizing DNA strands to the aptamer sequence can affect its apparent binding affinity.^[102] For example, Nutiu *et al.* reported that both the anti-thrombin and anti-ATP structure-switching aptamers showed a marked increase in the apparent dissociation constant (60-fold higher for the ATP aptamer). In addition, optimization of such systems requires extensive manipulation of the sequence of the displaced NA to ensure that it is easily released from the aptamer upon target binding, but also has sufficient affinity for the CT to allow facile initiation of RCA.

To overcome this issue, it is possible to perform the structure-switching using graphene oxide (GO) rather than DNA-DNA duplexes (Figure 2.2C). GO exhibits properties that can be tuned to retain single-stranded or double-stranded DNA on its surface.^[108] Structure-switching from GO using an aptamer was first demonstrated by Lu *et al.* in 2009 for the detection of thrombin.^[109] In this case, the adsorbed aptamer is displaced from the GO surface upon binding the target to form a DNA-target complex. Liu *et al.* built upon this initial report by demonstrating GO-linked RCA for the detection of thrombin.^[110] Reduced graphene oxide (rGO) was reported to perform better than its GO counterpart at releasing the thrombin-bound aptamer from the surface while preventing non-specific desorption of the

aptamer. To initiate RCA, the aptamer had a 3' primer extension that could bind to a CT even when the aptamer was bound to its target, allowing the released aptamer to act as the linear primer. This approach has been used to develop RCA-linked assays for a variety of other targets, including PDGF and *C. difficile* glutamate dehydrogenase (GDH).^[110–114] A drawback of this method is the potential for readsorption of the liberated aptamer onto the rGO surface. This necessitates removal of rGO by centrifugation^[110,111] or the use of a paper-based assay to allow migration of the aptamer-target complex away from the immobilized rGO and into a zone containing the CT^[112] (as described in Section 2.7) for regulation of primer availability.

It is also possible to use an unmodified aptamer complexed to a CT to provide a structure switching system that controls RCA. In this method, reported in 2010 by Cheng *et al.* for the colorimetric detection of VEGF,^[115] the VEGF aptamer was covalently immobilized on a glass slide and hybridized to a CT. Addition of the target displaced the CT, which was subsequently washed away. As such, the addition of target lead to the prevention of RCA, producing a “signal-off” sensor.

A simplified one-pot version of the RCA inhibition assay was reported by Bialy *et al.* recently, which removed the need for aptamer immobilization and washing steps. The assay is based on pre-incubation of the target with the aptamer, which forms a complex that blocks the 3' end of the aptamer, preventing it from binding to a subsequently added CT containing the anti-

sense sequence to the aptamer and thus inhibiting RCA (Figure 2.2D).^[101] An important advantage of this method is that the affinity of the aptamer is not affected as is the case for displacement of a hybridized CT. However, the use of an inhibition mechanism results in the signal decreasing as target concentration increases, which leads to a poorer detection limit. In addition, it is important to carefully design the aptamer sequence to avoid background binding of the aptamer-target complex to the CT.

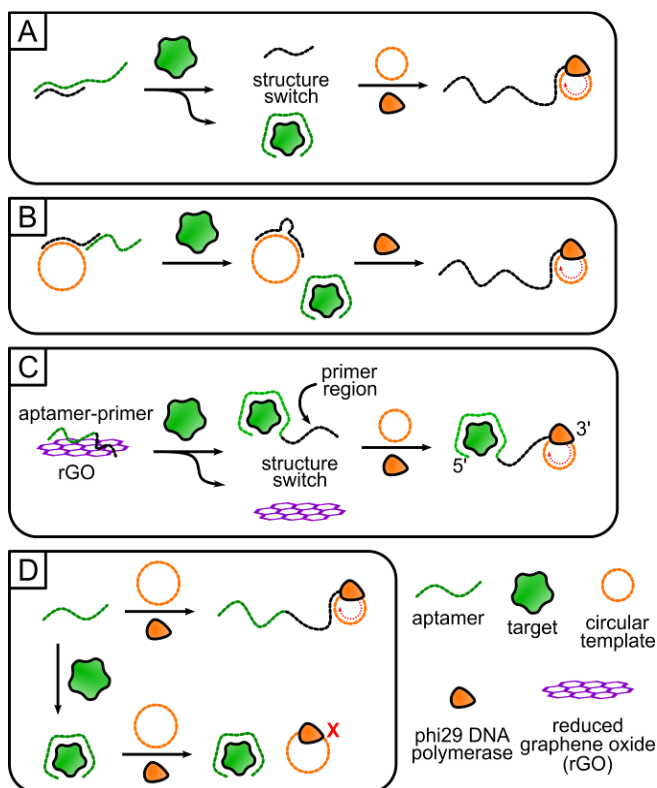


Figure 2.2. RCA-linked FNABs utilizing structure-switching. (A) Traditional structure-switching; (B) Tripartite structure-switching; (C) Structure-switching using reduced graphene oxide material; (D) Target-mediated inhibition of structure-switching.
 2.4.1.2 Integration of native *phi29* DP 3'-exonuclease activity

While phi29 DP is primarily used as a polymerase, the enzyme also has native 3' exonuclease activity as part of its proofreading mechanism. Liu *et al.* made use of this feature to regulate primer availability with a one-pot assay based on the tripartite structure-switching system outlined above (Figure 2.3A).^[116] In this case, RCA was regulated by binding the aptamer partially to the CT and partially to a primer, such that the aptamer blocked the 3' end of the primer. The 3' end of the aptamer was capped with an inverted dT nucleotide to prevent 3'-exonuclease activity on the aptamer itself. In the absence of target, RCA was prevented owing to blocking of the 3' end of the primer. Upon target binding, the aptamer was displaced and the phi29 DP could then trim the 3' overhang of the primer (which was complementary to the aptamer rather than the CT) via 3'-exonuclease digestion to generate a fully complementary primer which could initiate RCA.

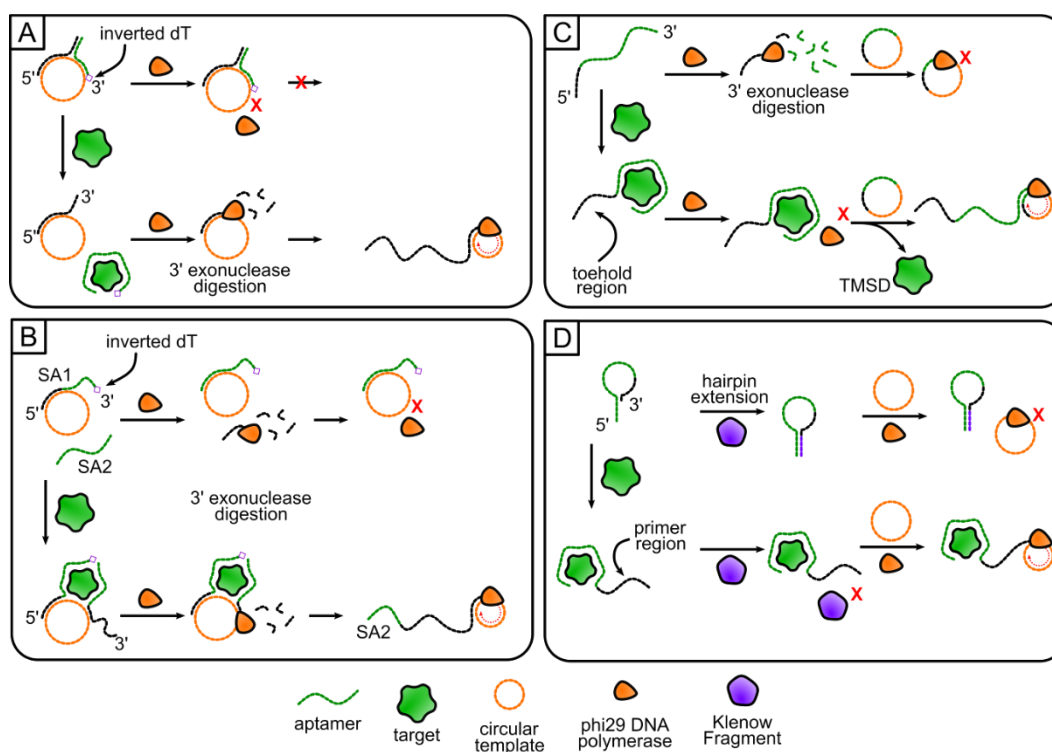
A further example utilized the 3'-exonuclease strategy with a supramolecular aptamer (or split aptamer) for the detection of ATP (Figure 2.3B).^[117] Here, the first subunit (SA1) of the ATP aptamer contains an extended 5'-end region complementary to a CT. The second subunit (SA2) of the ATP aptamer contains the second half of the ATP aptamer on the 5'-end, a short region complementary to the CT in the center of the strand, and a 3'-end that is not complementary to the CT. In this format, SA1 stays hybridized with the circular template, and SA2 is unable to interact with the

duplex. An inverted dT nucleotide on the 3'-end prevents phi29 DP from digesting SA1 and thus no RP can be generated. However, the addition of ATP causes SA1 and SA2 to orient in close proximity and form the ATP aptamer, which brings SA2 close enough to the CT to stabilize the otherwise weak interaction. Addition of phi29 DP allows digestion of the 3'-end of SA2 and initiates the RCA reaction at the middle point of the SA2 strand.

Our group recently reported a simplified approach for utilizing the 3'-exonuclease activity of phi29 DP without requiring inverted dTs or complex structure-switching systems (Figure 2.3C).^[118] In this approach, pre-incubation of the target with an aptamer forms a complex that protects the aptamer from 3'-exonuclease activity. The aptamer contains a toehold extension at its 5'-end, allowing liberation of the aptamer by a CT through toehold-mediated strand displacement (TMSD), which then initiates RCA. In the absence of target, the aptamer is digested and thus RCA does not occur. The method works well for low target concentrations. However, TMSD is not able to displace the target when at high concentrations, leading to blocking of phi29 processing by the target, inhibiting RCA.

Another method to modulate the interaction of a primer with a CT it by using a phi29 nuclease activity to act on a hairpin containing both the aptamer and primer.^[119] In this case, the hairpin contains three regions: an aptamer region on the 5'-end, a primer region in the middle, and a blocking region at the 3'-end that forms a weak hairpin with the aptamer region

(Figure 2.3D). Without target, the blocking region could be extended along the hairpin using Klenow Fragment to strengthen the hairpin and shield the primer from being used for RCA. In the presence of target the hairpin is disrupted and Klenow Fragment cannot extend the hairpin, thereby allowing the primer region to hybridize to the CT. Addition of phi29 DP digests the excess blocking region nucleotides to produce a complementary primer that can initiate RCA.



2.4.1.3 DNAzyme Mediated Primer Regulation

RNA-cleaving DNAzymes (RCD) are another MRE that can be used to modulate RCA via primer regulation, which is achieved through the target-dependent activation of the DNAzyme to allow catalysis of the cleavage reaction involving a DNA substrate containing an embedded ribonucleotide cleavage site. This reaction results in the production of specific cleavage fragments that can be used as primers to control the RCA reaction.

The first example of this method utilized the coupling of an RCD with RCA for the detection of ATP.^[120] The substrate was designed such that the RCA primer region was upstream of the ribonucleic acid linker, so that phi29 DP was unable to access the primer and initiate RCA. Addition of ATP activated DNAzyme catalysis to cleave the ribonucleic acid linker within the substrate (Figure 2.4A), producing a DNA fragment with a free 3' terminus. After treatment with polynucleotide kinase (PNK) to remove the 2,3-cyclic phosphate (a by-product of the RCD cleavage reaction), this primer was able to hybridize with a CT to trigger RCA, allowing for amplified detection of ATP.

In contrast with the first example, it is possible to use a pre-formed tripartite complex to avoid the need for separate addition of the CT (Figure 2.4B). In this case,^[121] a primer was designed such that the 5'-end hybridized to a CT and the 3'-terminal region contained a ribonucleic acid linker bound to an RCD specific for *E. coli*. The presence of *E. coli* activated

the DNAzyme and triggered cleavage of the ribonucleic acid linker. Subsequent 3'-exonuclease digestion by phi29 DP removed the 3'-overhang and allowed RCA to proceed to produce an easily detected reaction product.

In both examples described above, access to the primer strand by phi29 DP specifically required a cleavage reaction to liberate the primer, and thus RCA could not be initiated unless both the DNAzyme and phi29 DP enzymatic functions worked in unison to liberate the primer strand. This is in stark contrast to structure-switching aptamers described above, where access to the primer is typically only gated by one layer of control (DNA-DNA hybridization or DNA-rGO adsorption). As a result, the use of RCDs provides a highly specific approach to primer regulation of RCA activity.

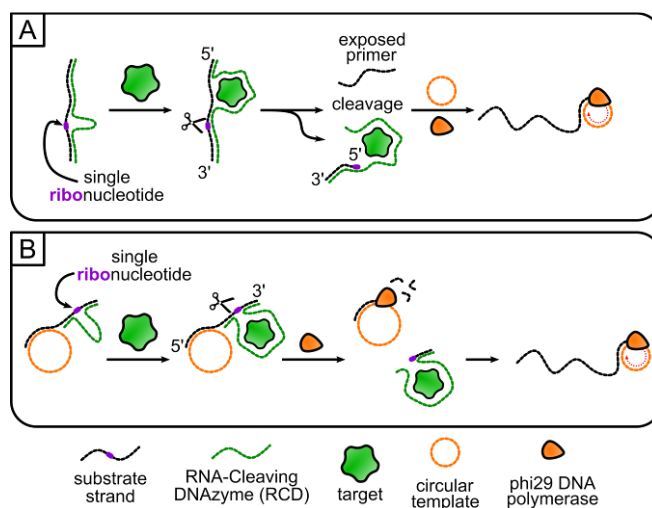


Figure 2.4. RCA FNABs utilizing RNA-cleaving DNAzymes (RCDs). (A) Traditional RCD-mediated cleavage; (B) Tripartite RCD utilizing 3'-exonuclease activity of phi29 DP.

2.4.2 Circle Regulation

FNAs can also be used to regulate the availability of the CT instead of the primer. RCA requires the presence of a circularized template to generate long, concatemeric reaction products, as only trace amounts of monomeric RP can be generated when using phi29 DP with a linear template.^[122,123] The three primary strategies for regulating CT availability involve: 1) using a FNA to control the formation of a circularized template from a linear DNA precursor strand; 2) integrating the aptamer directly into the CT to modulate the ability of phi29 DP to generate RP, or; 3) enabling access to the CT through the use of an RCD.

2.4.2.1 Circle ligation method

In 1994, Nilsson *et al.* reported on the concept of using a ligase to circularize a linear NA strand in the presence of a target NA that hybridizes to the linear strand to guide ligation, denoted as the padlock probe (PLP) method.^[124] This ligation reaction can only occur in the presence of a ligation strand which has segments that are complementary to the 5'-end and 3'-end of the linearized padlock probe, ensuring high selectivity. Lizardi *et al.* built on this work in 1998 by utilizing the ligated padlock probe as a CT for RCA, creating the first CT-regulated RCA system.^[85] Since then, PLP-linked RCA has developed into the most common method for CT regulation of the reaction, providing for ultrasensitive^[85–88] and selective^[85,87,89–91] NA detection. The method has also been utilized using

aptamers as ligation strands to allow detection of non-NA targets.^[125–141] Below, the key advances in aptamer-linked, PLP-regulated RCA are described.

PLP-linked RCA modulated by an aptamer was first demonstrated by Yang *et al.* in 2007 for the detection of PDGF.^[125] Here, the PDGF aptamer was elongated at both the 3' and 5' ends to include carefully designed sequences that only permitted the formation of a ligation junction in the presence of PDGF (Figure 2.5A). Without PDGF, the terminal ends were hybridized to the aptamer domain, and thus unavailable to bind to the linearized CT. The addition of PDGF caused a conformational switch in the aptamer that released the terminal ends, allowing formation of a junction that could be ligated in the presence of T4 DNA ligase. Addition of a separate primer strand then initiated RCA.

An alternative approach is to use a structure-switching aptamer where target binding leads to the release of a ligation strand which doubles as the primer (Figure 2.5B). Ma *et al.* used this approach for the detection of cocaine.^[135] The cocaine aptamer was immobilized on a magnetic bead and hybridized to a ligation strand. Addition of cocaine lead to the liberation of the ligation strand. After magnetic separation to remove the unreacted duplexes, a linear template and T4 DNA ligase was added to form a CT for subsequent amplification. A similar approach was used by Tong *et al.* except that the structure-switching aptamer (in this case for ochratoxin A)

was reacted with its target in solution to liberate a linear template (Figure 2.5C), while the ligation strand was immobilized on a magnetic bead with the 3' end at the distal end. In this way, the ligation strand could act as a primer to allow the RCA reaction to be run directly on the bead and allow RP to be easily extracted from solution.

The ligation strand (and primer) can also be integrated within the aptamer.^[130–132] Jiang *et al.* tethered a ligation strand to the 3'-end of an aptamer in a sandwich assay for the detection of *E. coli*.^[130] In this approach, *E. coli* cells were captured on a PDMS surface with a dendrimer and the modified aptamer was introduced to form a sandwich complex (Figure 2.5D). Addition of a linear CT precursor and T4 DNA ligase allowed for CT formation and subsequent RCA elongation from the 3'-end of the aptamer. The aptamer strand can also be designed to act as the ligation strand without any 3' modifications (Figure 2.5E).^[132] To demonstrate this approach, gastric cancer exosomes were incubated with the aptamer and a filter membrane was used to discard unbound aptamer. Next, the aptamer-exosome complex was heat denatured to release the aptamer. The liberated aptamer subsequently served as the ligation strand for CT formation and as the primer for RP generation.

A potential drawback of current aptamer-modulated PLP methods include the requirement of an additional enzyme, and the need for additional separation or washing steps to remove unreacted ligation templates. In

addition, many examples perform the ligation and amplification reactions separately rather than in one-pot, limiting their use in simple POC devices.

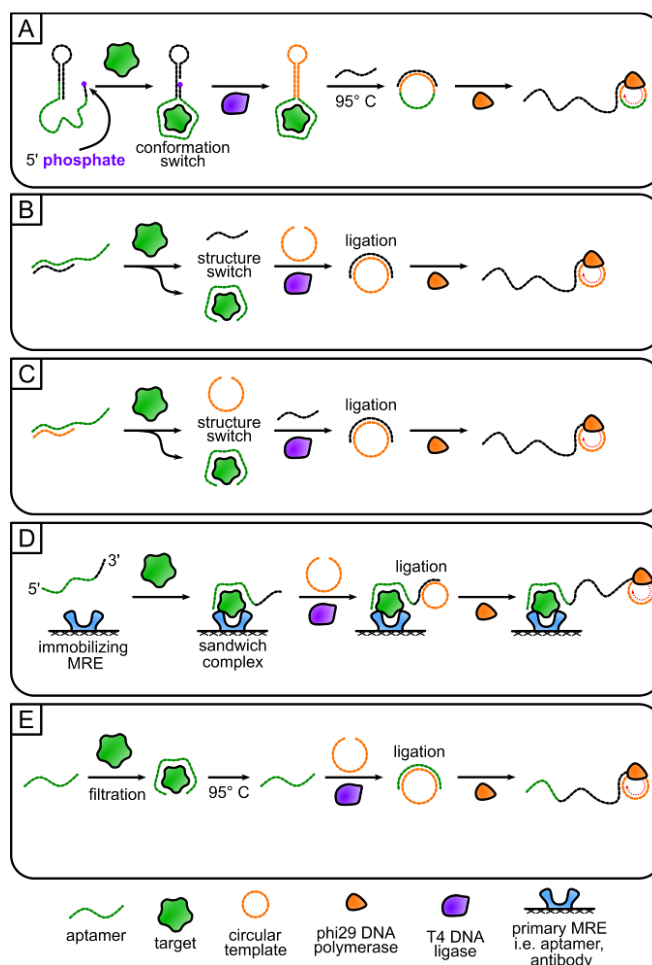


Figure 2.5. RCA-linked FNABs utilizing padlock probes for regulation of circular template. (A) Conformational structure-switching; (B) Structure-switching to release a ligation strand; (C) Structure-switching to release a linearized circular template; (D) Sandwich assay with ligation strand tethered to aptamer; (E) Dual-function DNA acting as aptamer and ligation strand.

2.4.2.2 Circular Aptamers

An emerging method to modulate the CT is to incorporate the sequence of the FNA, and specifically an aptamer, directly into the CT sequence to

regulate the RCA reaction. As noted below, most circularized aptamers were initially generated as linear species, since most SELEX methods used to find novel aptamers utilize linear NA libraries.^[113] Importantly, the linear aptamer sequence can simply be inserted into the CT, while retaining any primer binding or detection sequences encoded within the circle. As the circle lacks both 3' and 5' ends, circularized aptamers (denoted as captamers) are resistant to exonuclease degradation, making them particularly suitable for applications involving biological samples.^[113,142]

The first example of using captamers to regulate RCA was demonstrated by Di Giusto *et al.* for the detection of thrombin in a proximity extension assay.^[143] In this approach, two aptamers were used, one of which had a 3' extension to act as a primer for RCA, and another that was embedded into a CT with a region that was complementary to the primer. As both aptamers could bind to different regions of thrombin, target binding brought the aptamer and captamer together, initiating RCA. To prevent non-specific amplification in the absence of thrombin, the complementary region was 6 base pairs, which is sufficiently short to prevent non-specific hybridization.

The circular nature of captamers allows also for their incorporation into intramolecular structure-switching strategies for RP regulation. Zhao *et al.* converted a linear aptamer for lipopolysaccharides (LPS) into a captamer by embedding the aptamer, along with a primer-binding region, within a CT (Figure 2.6A).^[144] In the absence of target, the captamer formed a dumbbell

shape through intramolecular hybridization, limiting access to the primer-binding region. Upon addition of LPS, the captamer adopted an extended conformation that exposed the primer-binding region, allowing for subsequent binding to a primer and RP generation.

The Liu group demonstrated the ability to use captamers to develop a structure-switching system, where PDGF binding could cause displacement of the circularized PDGF aptamer from rGO (Figure 2.6B).^[114] Once displaced, the complex between the captamer and PDGF was removed from the rGO through centrifugation, and then the supernatant containing the liberated captamer was mixed with primer, allowing for RP generation. Though this method required a centrifugation step to isolate the liberated CT, it should also be amenable to paper-based spatial separation from rGO, as has been demonstrated with linear aptamers (see Section 2.7 for more details).^[112]

While circularizing linear aptamers into CTs is relatively straightforward, the CT sequences must be carefully designed to prevent altering the native activity of the aptamer and its ability to switch between duplex and complex conformations. Recently, our group successfully conducted a SELEX experiment using a circular library and isolated a novel glutamate dehydrogenase (GDH) captamer which was only active in the circular form.^[113] Importantly, this captamer showed lower affinity for recombinant GDH (rGDH) relative to native GDH (nGDH), a key target for *C. difficile*

detection (Figure 2.6C). This allowed the development of a competitive assay wherein the GDH captamer was first incubated with rGDH-coated magnetic beads to form a captamer-rGDH complex. Addition of nGDH caused release of the captamer from the bead, and after removal of MBs, the liberated captamers were able to bind to an added primer to allow for nGDH-mediated RCA.

As was the case for PLP-mediated RCA, most of the examples above required a separation step, making them challenging to implement in POC tests. To overcome this issue, a method was developed using a CT-integrated aptamer to modulate the RCA reaction upon target binding by blocking the ability of phi29 DP to read through the CT (Figure 2.6D). A PDGF aptamer was incorporated within a CT and it was observed that phi29 DP was unable to displace the bound protein and thus read through the aptamer sequence, thereby inhibiting the RCA reaction when the protein was bound.^[145] In this instance, and also with a thrombin-targeting system^[145,146], no modifications of the PDGF or thrombin aptamers were required, thus making the method generalizable. In addition, no separation steps were required, making the assay much simpler. On the other hand, the assay operates as a “turn-off” signalling system, which generally tends to have poorer detection limits relative to “turn-on” systems.

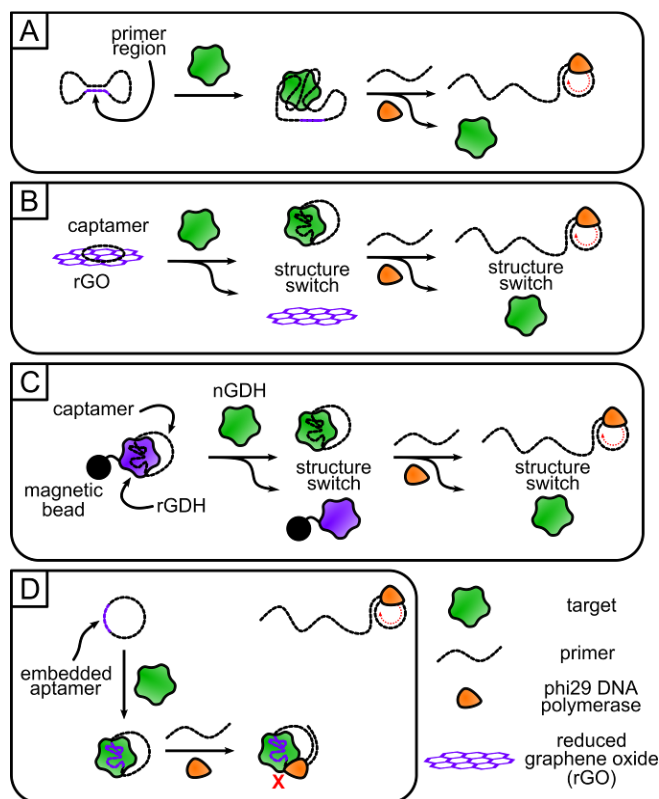


Figure 2.6. RCA-linked FNABs utilizing structure-switching for regulation of circular template. (A) Intramolecular structure-switching; (B) Structure-switching using reduced graphene oxide material; (C) Structure-switching using recombinant analyte (GDH); (D) Target-mediated inhibition of structure-switching.

2.4.2.3 DNAzyme Regulation of CTs

The use of DNAzymes to modulate the formation or accessibility of a CT is less prevalent than CT modulation by aptamers, however, there have been some interesting approaches, as noted below. The first example used a DNAzyme with ligase activity to regulate the formation of a CT from a linear DNA sequence (Figure 2.7A).^[147] Similar to a PLP ligation approach, the Ellington group used a ligase DNAzyme that formed a hairpin loop when bound to ATP. The ends of the hairpin mimicked a ligation strand, bringing

the two ends of the linearized CT together such that DNAzyme catalyzed ligation could occur. This DNAzyme ligase approach did not require an additional protein enzyme, as the linearized form of the CT was functionalized with a 3'-phosphorothioate and 5'-iodine residue.

Another approach to regulate CT formation utilized a DNAzyme with kinase activity, denoted as Dk2, to facilitate the ligation of a circular template in the presence of GTP (Figure 2.7B).^[148] In this strategy, the DNAzyme was used as the linearized form of the CT. In the presence of GTP, the DNAzyme catalyzed a self-phosphorylation reaction wherein GTP transferred a phosphate to the 3' end of the DNAzyme. Circular ligation was carried out using T4 DNA ligase and a splint oligonucleotide complementary to the 5' and 3' ends of Dk2. The splint oligonucleotide also acted as a primer to allow RCA to proceed around the newly formed CT, allowing for sensitive detection of GTP as a target.

An issue with the use of DNAzymes to perform CT ligation is the poor diversity of targets that can activate such DNAzymes (generally NTPs such as ATP or GTP), and thus act as targets for sensing, thereby limiting the potential of this method for biosensing. An alternative strategy is to use a DNAzyme to modulate the accessibility of a CT, usually by liberating it from a constrained configuration. As an example, a Pb^{2+} -specific RCD was used to liberate a NA that served as a ligation strand for PLP ligation (Figure 2.7C).^[149] The ribonucleotide-containing substrate strand was first

hybridized to the DNAzyme. The presence of Pb^{2+} activated the DNAzyme, and cleaved the ribonucleotide junction in the substrate strand, with the cleaved fragment dissociating from the DNAzyme and acting as a ligation template to allow T4 ligase catalyzed ligation to form a circular template suitable for RP generation. Importantly, the diversity of RCDs makes this a more versatile method for sensing, as there are numerous targets that can activate RCDs.^[1,150]

In addition to ligation methods, it is also possible to use RCDs to modulate the accessibility of a preformed CT. Liu *et al.* showed that it was possible to produce a circularized ribonucleotide-containing substrate that was strongly interlocked with the CT by using the CT as the ligation strand to circularize the substrate. By including a sufficiently long section that could hybridize to the CT, phi29 DP was prevented from reading through the hybridized section, and thus neither circle could be used to initiate RCA (Figure 2.7D).^[151] In the presence of the RCD, the addition of the target (in this case *E. coli*) activated the RCD, which could cleave the ribonucleotide junction, linearizing the substrate strand. The phi29 DP was then able to trim the free 3' end of the substrate strand, which could then serve as a primer for RP generation.

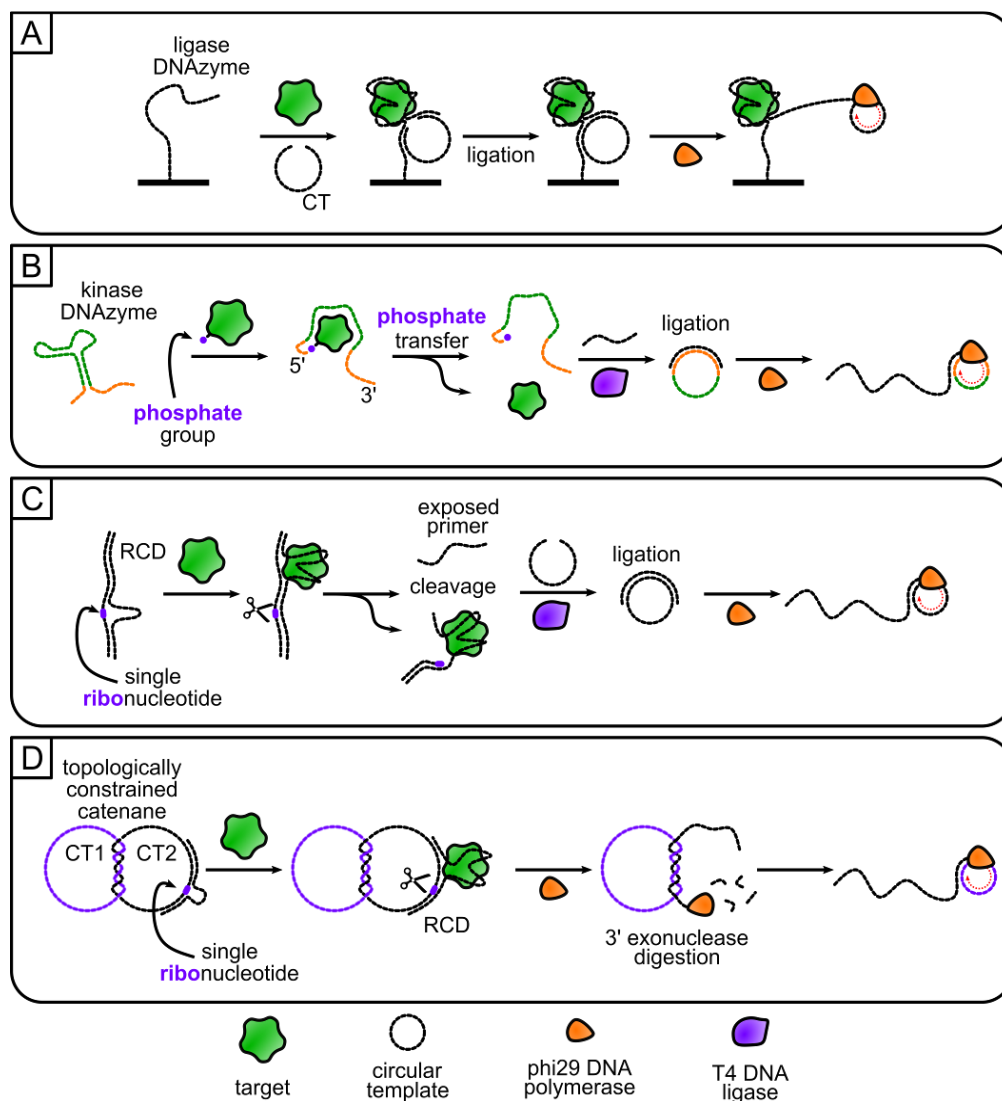


Figure 2.7. RCA FNABs utilizing DNAzymes for regulation of circular template. (A) Ligase DNAzyme-mediated; (B) Kinase DNAzyme-mediated; (C) RCD-mediated with CT ligation step; (D) RCD-mediated utilizing catenane approach and 3'-exonuclease activity of phi29 DP.

2.5 Amplification Methods

The heart of the RCA process is the ability to produce long concatenated DNA products by round-by-round amplification around a CT. Since its introduction in 1995, several groups have investigated the effects of different polymerases and CTs on RCA efficiency. As noted below,

optimization of the polymerase and the CT sequence can improve the rate of RP production by up to an order of magnitude. However, more recent improvements have incorporated various feedback processes to produce exponential RCA, which can improve the rate of RCA by several orders of magnitude relative to linear RCA, depending on the specific method used. Below, we provide an overview of both linear and exponential RCA methods, with a focus on their performance, ease of use, and utility for point-of-care sensing.

2.5.1 Linear amplification

The earliest examples of RCA as an amplification method involved a polymerase simply extending the primer around the CT to produce long, concatenated reaction products that increased linearly in concentration with time (Figure 2.8A). Early work aimed at evaluating the effect of polymerases on RCA efficiency have demonstrated that several replicating polymerases can be used to drive RCA, including *Bst* DNA polymerase and Klenow Fragment (-exo), though phi29 DP has emerged as the preferred polymerase owing to several key features.^[152,153] For example while most polymerases require accessory proteins to assist with clamping the enzyme to DNA,^[154,155] phi29 DP requires no assistance.^[156,157] Phi29 DP also possesses the highest reported processivity of a polymerase, at greater than 70 kilobases in 40 minutes,^[122,156] and excellent proof-reading ability,^[158,159] with an error rate of only 1 in 10^4 to 10^6 bases.^[160] In addition,

as noted above, phi29 DP displays 3' to 5' exonuclease activity for single-stranded DNA,^[161,162] providing an alternative avenue for designing input strategies. Phi29 DP also does not require the help of any helicase proteins as it exhibits excellent strand displacement properties.^[123] Finally, and perhaps most importantly for POC testing, phi29 DP can operate at room temperature, unlike *Bst* DNA polymerase and Klenow Fragment (KF), both of which require elevated temperatures to operate. These factors have helped make phi29 DP a powerful polymerase for simple and effective RCA applications, particularly those that are amenable to POC sensing applications.^[73,74,152,153]

Optimization of the circular template (CT) length and sequence can also be used to improve the efficiency and rate of RCA. Li *et al.* showed that DNA coding strategies can be employed to design optimal circular DNA templates generated through *in vitro* selection.^[111] Amplification efficiency was maximized for certain CT nucleobase compositions, with a strong bias towards adenosine and cytosine-rich CT sequences, which comprised 85.4% of the nucleotides in the top 10 most efficient sequences. The optimized CT yielded detection limits that were an order of magnitude better than obtained with unoptimized CTs, producing the lowest reported LOD for aptameric thrombin detection at 1 pM. CT length may also be modified to impact amplification efficiency when care is taken to modulate the conformational strain in the CT.^[163] Joffroy *et al.* observed that RCA

amplification efficiency was maximized when a CT contained an odd number of helical half turns instead of an even number (~10.3 base pairs per turn) and the conformational strain was maximized. Simulations showed that sequences with maximized CT strain outperformed minimized sequences, amplifying up to 6-fold better. Amplification efficiency was also improved as the overall size of the CT was decreased, stressing the importance of minimizing overall CT length.

In addition to optimizing the polymerase and CT, there are additional modifications that can be made to improve the rate of linear RCA. For example, incorporating multiple primer regions to facilitate multiply primed RCA can increase amplification more than three-fold in some applications^[152]. Multiply primed RCA uses several primers complementary to different unique regions along the CT, allowing each to initiate RCA concurrently. Incorporation of PEG 4000 at concentrations from 10 - 20% can also improve RP generation and uniformity, particularly when RCA is performed on a solid surface.^[164] Liu *et al.* observed that generating RCA on a nitrocellulose surface also led to improved RCA efficiency.^[98] In each case, the authors attributed the improvement in RCA rates to a molecular crowding effect, which increased local concentrations of RCA reagents.

The final method to increase RP concentration, and hence decrease limits of detection when using linear RCA, is to increase reaction time, though this can be a challenge for rapid monitoring applications. Hence,

even when optimized, linear RCA methods can provide at most 1000-fold amplification within 1 h.^[85] Even so, this amplification factor may be adequate in cases where only moderate improvements in LOD are needed relative to unamplified assays. Hui *et al.*'s paper-based ATP and GDH aptasensors achieved sensitive fluorogenic detection in stool samples without any amplification.^[112] To allow for equivalent detection sensitivity using equipment-free detection, the assay incorporated RCA to allow for colorimetric detection, which was as sensitive as the unamplified fluorogenic assay when using an amplification time of 1 hour.

2.5.2 Exponential RCA (E-RCA)

Although many assays can be achieved using linear RCA methods, in cases where ultrasensitive detection or more rapid generation of detectable RP concentrations is required it is necessary to implement exponential methods of RCA (E-RCA). Examples include detection of pathogens of both bacterial and viral origin,^[165] where detection of as low as 1 organism is required,^[166] and early detection of disease biomarkers, which are present at low concentrations.^[167] Monitoring of the response to targeted therapies,^[168] which is a cornerstone of precision medicine,^[169,170] can also make use of these ultrasensitive approaches. In many cases, it is necessary to detect the analytes in complex biological samples, including blood, faeces, saliva or sputum, which may require sample dilution to reduce the effects of interferants within the matrix, further reducing analyte

concentration.^[171] In such cases amplification levels of 10^6 to 10^9 may be required, which requires exponential amplification systems to be achieved in a timely fashion.

In the case of RCA, exponential amplification is achieved through the use of various feedback processes which allow for cross-amplification. This is typically accomplished by incorporating some means to generate additional primers after the initial linear amplification step begins. Specific methods to produce E-RCA are described below, with emphasis on specific design considerations and their potential for use in simple POC sensors.

2.5.2.1 Enzyme-Assisted Exponential Amplification

Several exponential RCA methods utilize a secondary enzyme in addition to phi29 DP to process the RCA product in a manner that can generate new primers to allow cross-amplification. Examples include nicking RCA and circle-to-circle (C2C) amplification (Figure 2.8B and 2.8C, respectively), both of which employ additional enzymes to achieve E-RCA. Nicking RCA, also known as primer-generation RCA, uses nicking endonucleases to monomerize the long concatemeric RP, thereby generating new monomeric primers to initiate amplification on other CTs. The nicking site is engineered in the CT so that the nicking enzyme can cleave along the complementary RCA product.^[172] Nicking RCA can also incorporate multiple antisense nicking sites into the CT to yield different unique monomers, as shown by Li *et al.* in their exonucleolytic digestion-assisted E-RCA strategy.^[173] By

incorporating two nicking sites, one complementary repeat of the CT can be cleaved into two linear pieces. The first acts as a primer to initiate exponential amplification, and the second forms a G-quadruplex structure that can be probed fluorescently (see Section 2.6). Incorporation of the exponential primer feedback can improve the LOD of targets by as much as five orders of magnitude relative to unamplified detection, and 2-4 orders of magnitude better than for linear RCA.^[83,116,173]

C2C amplification is another multi-enzyme E-RCA method, first reported by Nilsson *et al.* as an extension of their work on padlock probes.^[90] C2C amplification consists of two primary steps. First, linear RCA proceeds in the presence of a primer to generate a long RCA concatemer. This RCA concatemer is then monomerized by a restriction enzyme, and then following heat inactivation of the restriction enzyme, each monomer is circularized using T4 ligase to act as a new CT. In this work, Nilsson and co-workers showed a sensitivity improvement of nine orders of magnitude in under an hour in comparison to the analogous linear RCA reaction, though the multi-step process and need for heating make the method difficult to implement in simple POC assays.

It is also possible to integrate non-RCA isothermal amplification methods in combination with RCA to achieve exponential amplification. This approach has been demonstrated with exponential amplification methods including loop-mediated isothermal amplification (LAMP),^[174,175] catalytic

hairpin amplification (CHA)^[176,177] and strand-displacement amplification (SDA).^[178,179] In most cases, linear RCA is used as the primary amplification method, and the concatenated RP is used directly as the input to supply primers for the subsequent exponential ITA scheme. These assays can increase assay sensitivity 1000-fold compared to their original ITA methods^[174] but in most cases these secondary ITA methods require operation at elevated temperatures, making them challenging to integrate into POC sensors. In addition, incorporation of additional enzymes can impact the storage considerations, making NAs a more chemically and thermally robust alternative. These methods also increase the complexity of the assay, as the initial amplification is often performed prior to initiating the second amplification step, requiring significant user intervention to control reaction timing.

2.5.2.2 Hyperbranched RCA (H-RCA)

Hyperbranched RCA (H-RCA), sometimes referred to as ramification amplification,^[180] can produce exponential RCA at room temperature without requiring additional enzymes (Figure 2.8D). First introduced by Lizardi *et al.* to detect point mutations in human genomic DNA,^[85] this has emerged as the most popular method of E-RCA. H-RCA employs two unique primers: one complementary to the CT, and the other complementary to a region of the amplicon. After the first primer is elongated by phi29 DP, the second primer binds to the RP and initiates a

secondary amplification complementary to the RP. This creates a branched system of replication where the linear RP is used as the template for exponential amplification. Some assays opt to use *Bst* DP instead of phi29 DP for H-RCA as this DP shows excellent strand displacement and processivity but does not exhibit 3' exonuclease activity.^[181,182] H-RCA has been paired with a number of FNAs^[116,128,132,181–185] including DNAzymes.^[151] Typically, H-RCA methods can improve amplicon production, and hence detection limits, by as much as 10^4 relative to linear RCA,^[116] with detection limits being several orders of magnitude below the affinity constants for the aptamer MRE. However, attaching such ultrasensitive detection limits can require reaction times of up to 3 h or more.^[116]

H-RCA is also amenable to pairing with nicking enzyme amplification to yield netlike H-RCA (N-RCA) for cubic amplification.^[186] This method can improve sensitivity by more than an order of magnitude compared to H-RCA, and has been used to detect both NA^[187] and protein^[188] targets, but has yet to be paired with FNA-based detection.

For detection methods that benefit from a uniform RP sequence, dendritic RCA can be incorporated as a variation on H-RCA.^[189] A caveat for H-RCA is that the second RP is generated by amplification of the first RP, making two complementary RP strands. In dendritic RCA, an additional hairpin sequence is included which is complementary to both the RP and CT. Upon

RP generation, this hairpin sequence unfolds, exposing the stem region which can subsequently be amplified by the same CT or by a secondary CT (Figure 2.8E).^[190] In contrast to H-RCA, as the RP is exclusively generated using CTs throughout, the length of the RPs are limited by the kinetics of the polymerase rather than the length of the template RP being used.^[85] Importantly, this dendritic RCA method retains the ability to encode the CT to allow generation of various RP outputs for strategic downstream sensing, which is not possible with traditional H-RCA.^[190,191] Dendritic RCA has been used to detect NAs^[189,190] and very recently expanded to the non-NA target PDGF-BB.^[107]

2.5.2.3 DNAzyme Feedback Amplification

DNAzyme Feedback Amplification (DFA) is a recently reported method that utilizes RCA initiated generation of a DNAzyme to achieve E-RCA^[121,192] (Figure 2.8F). The CT encodes a DNAzyme in the RP and is bound to a DNA primer (P2), found in Complex II, that includes a 3' overhang containing a substrate for a RCD, and an inverted 3' dT to prevent phi29 DP from acting as a 3'-exonuclease to trim the overhang. Amplification is initiated when an appropriate primer (P1), found in Complex I, is produced via target-modulated primer generation by the FNA, as described in Section 2.4. The primer can bind to excess free CT to initiate linear amplification, which produces a RCD as a repeating unit in the RP. This RCD then cleaves P2 at the RNA junction, leaving the DNA overhang,

which is acted upon by PNK to produce an unblocked 3' terminus. The exonuclease activity of phi29 DP then trims the overhang and proceeds to generate the mature primer P1 that can initiate RCA to produce more RP, resulting in cross-feedback amplification.

DFA is an interesting case of a multi-enzyme E-RCA method, where the second enzyme is a DNAzyme rather than a protein enzyme. This method specifically highlights the power of RCA assays to produce the secondary enzyme directly, which can be used to achieve exponential amplification through a cross-feedback mechanism.

DFA is versatile in that any RCD for a NA or non-NA target could potentially be incorporated into the assay framework. Thus far, DFA has been used to detect miR-21, an RNA target, by using the miRNA target as a primer and the Mg²⁺-sensitive MgZ as the RCD.^[121] Detection of *Escherichia coli* (*E. coli*) was also achieved by making two alterations to Complex I. First, P1 was redesigned to contain a 3' overhang with a ribonucleotide, like Complex II. Second, the DNAzyme EC1 was added to the system to bind the overhang region and cleave the P1 ribonucleotide only in the presence of *E. coli*, which is a means of FNA-triggered primer generation. The CT still produced the MgZ DNAzyme, which could cleave the substrate on complex II, producing exponential amplification. Such an approach allowed single cell detection limits for *E. coli*. By modifying the substrate in Complex I as was done for *E. coli* detection, DFA has been

extended to the detection of miRNA cancer biomarkers in liquid biopsy samples, with the output linked to a glucose meter (see Section 2.6)^[193] and further modified for Pb^{2+} detection in river water samples using a Pb^{2+} -DNAzyme.^[194] While DFA is a potentially powerful E-RCA method, it should be noted that the ribonucleotide-containing DNA sequences in Complex II are susceptible to nuclease degradation,^[195] potentially making the DFA system less suitable for some POC applications, such as those that use complex samples that may contain ribonucleases.

2.5.3 Pre-amplified RP as MREs

Integrating an amplification step into an assay is not always required to reap some of the benefits of RCA. The production of substantially elevated localized concentrations of DNA has allowed for the visualization of single molecules of long RCA-derived amplicons.^[84,85,196] In several assays, the RP has been used as a pre-amplified sequence not dependent on the presence of target, but instead generated to act as a MRE.^[197–199] Further, using pre-amplified RP eliminates any time restrictions posed on the assay thus sidestepping the need to optimize the amplification efficiency. Other creative uses of RCA amplicons as MREs or as a polymeric biomaterials have been thoroughly discussed in a recent review found here.^[200]

In one example, Gu *et al.* generated a competitive structure-switching assay for the detection of okadaic acid (OA) where the pre-amplified RP is introduced to the reaction, using the aptamer region as an anchor.^[201]

The competitive binding assay with the OA aptamer causes a structure-switch and releases the RP from the surface which could be extracted from the supernatant and detected downstream. Achieving a LOD of 1 pg/mL (1.24 pM), the authors observed that incorporation of this pre-amplified RCA improved the LOD 50-fold compared to an unamplified capture strand.

Aptameric RP was used by Zhao *et al.* to create a 3D-DNA network of RP capable of binding to target surface proteins on potentially cancerous cells for capture and quantification.^[199] This approach engineered 2 functional sites into the CT used to generate the DNA network, giving it two roles within the assay. First functional site, the target aptamer antisense sequence was incorporated into the CT. Generated aptameric RP is then capable of binding to the protein PTK-7, a cancer marker. The second, an encoded restriction site, allowing for release of captured cells upon addition of the restriction enzyme. The authors note that in theory, by incorporating different restriction sites, cells could theoretically be analysed sequentially upon each RE addition to the 3D network. These two functional sites enable both target recognition as well as detection.

Li *et al.* investigated the degree of amplification required to maximize the surface capture potential of aptamer-containing RPs for *E. coli* detection.^[202] Here, the authors compared functionalizing a PDMS surface using dendrimers coated with either single unit aptamers, or with RPs generated at varying amplification times. Interestingly, they observed that maximum

retention of *E. coli* was achieved after 2 hours of RCA as higher degrees of amplification led to decreased capture capacity which the authors attribute to non-specific intramolecular interactions within the RP. Further, not only was capturing efficiency lost but specificity was adversely affected too with amplification times at 12 hours showing poor target capture and little to no specificity.

In a contrasting approach, Carrasquilla *et al.* used an inkjet printer to deposit RP directly on cellulose to generate a localized scaffold of highly concentrated DNA for enhanced analyte detection.^[197] This printed RP “bioink” acted in the same way as a long-chained aptamer might, with each repeat unit capable of aptamer binding. When printed onto the paper surface, the authors found the bioink was too large to migrate across a cellulose surface but could still retain aptameric function in the presence of analyte. In contrast, monomeric aptamers were not able to perform due to their propensity to be displaced from the cellulose surface during sample addition. Inkjet printing can be a convenient form of assay development, as it allows for the incorporation of internal references and multiplexed detection.

Liu and co-workers compared the analytical performance of an immobilized monomeric aptamer (1D) relative to a concatemer of aptamer strands (2D), or a superstructure known as a DNA nanoflower (NF)^[203] comprised of several concatemers of aptamer strands (3D).^[198] The surface

density of the aptamers within the 3D amplicon was 4.6 to 8.1-fold higher than the 1D and 1.9 to 3.1-fold higher than the 2D variants. This enhanced localization of aptameric units improved the signal-to-noise ratio of the thrombin-binding system of the 3D construct by over four-fold relative to the 1D construct. Further, the 3D variant showed notable resistance to nuclease degradation and prevented non-specific protein adsorption onto the nitrocellulose surface – both key considerations for paper-based biosensors (see Section 2.8.3).

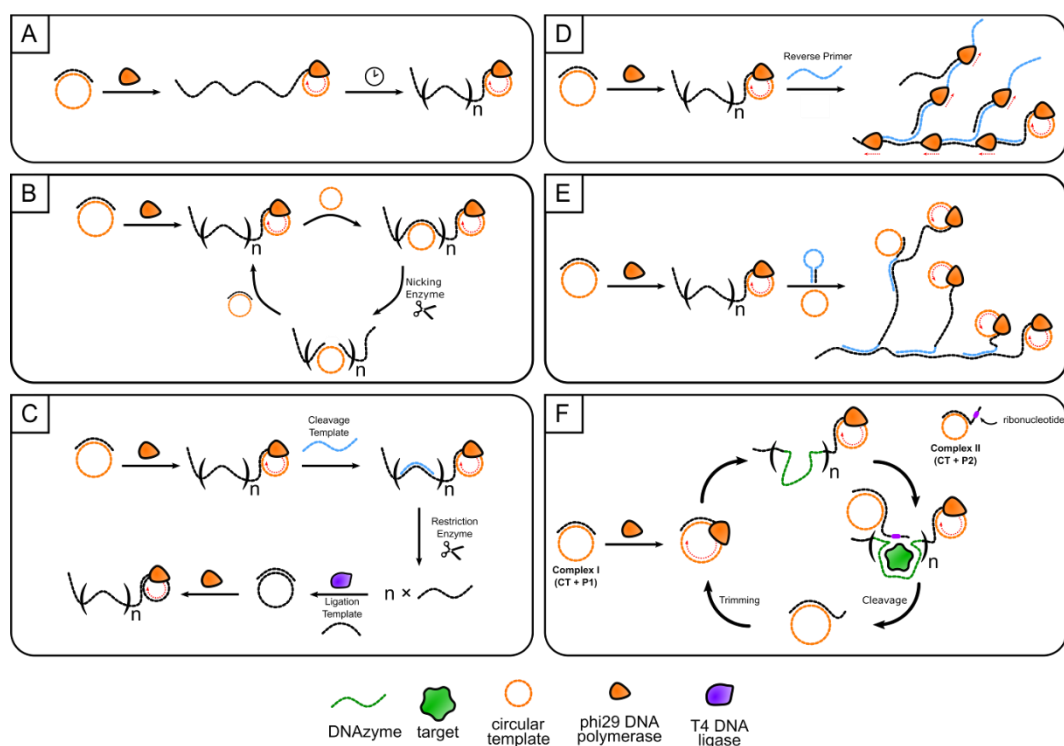


Figure 2.8. Schematic illustrations for linear amplification and two methods of exponential amplification. (A) Linear RCA (B) Nicking Endonuclease RCA (C) Circle-to-circle (C2C) RCA (D) Hyperbranched RCA (E) Dendritic RCA (F) DNAzyme Feedback Amplification.

2.6 RCA Detection Outputs

2.6.1 Overview of Detection Methods

Several different approaches can be used to detect RCA reaction products, some of which are independent of the specific RP sequence, and others which require encoding a specific sequence into the CT to generate an antisense sequence in the RP that is used specifically as part of the detection system. In general, the detection methods are independent of the input methods outlined in Section 2.4, though as noted below, there are very specific requirements for the design of CTs to allow compatibility with some exponential RCA methods such as H-RCA.

Detection of RP can be divided into four broad categories: 1) detection of RCA reaction by-products (i.e., protons, inorganic phosphate, labelled dNTPs); 2) intercalation or adsorption of signalling moieties into or onto the RP; 3) hybridization of DNA carrying a detection moiety to the intact or monomerized RP or; 4) production of a G-quadruplex or DNAzyme output (PMD or RCD). The first two methods are compatible with any output sequence, while the latter two methods require specific CT sequences to generate outputs that allow signal generation. These outputs can generally be used to produce colorimetric, fluorescent, or electrochemical outputs, as shown in Figure 9. We have chosen to focus on these outputs owing to their compatibility with POC devices, and in particular due to the availability

of simple and portable readers to meet the ASSURED criteria and allow use in low-resource settings.^[204–206]

We note that in addition to these three signalling methods, there are several other sensitive instrument-based detection methods for direct detection of RPs.^[73,74,207] These include methods such as surface plasmon resonance (SPR) to measure changes in optical mass of growing RPs^[141,208–210], surface-enhanced Raman spectroscopy (SERS) to measure vibrational bands within RPs,^[211–213] and detection of RP mass using quartz crystal microbalance (QCM) measurements.^[141,214,215] However, such methods are not currently possible using simple and portable instrumentation, and will not be covered here as they are not compatible with the ASSURED criteria.

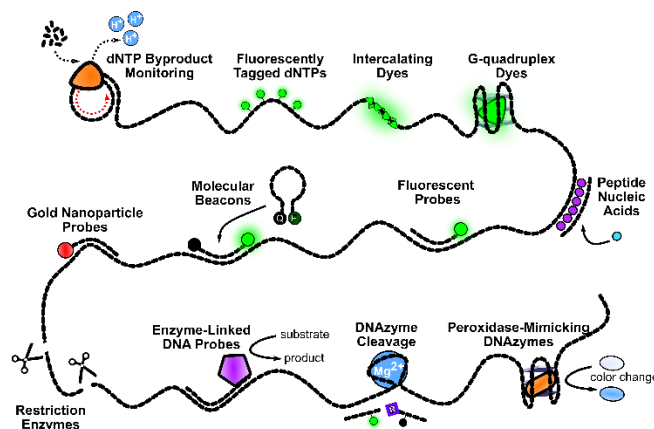


Figure 2.9. Examples of methods of detection and signal readouts employed for RCA detection.

2.6.2 Generic Detection Methods with Unstructured RPs

2.6.2.1 Monitoring RCA by-products

The simplest strategy for the detection of RP involves monitoring the by-products of amplification. In addition to the concatenated DNA strand, the RCA reaction also produces a proton (H^+) and pyrophosphate (PPi) for each dNTP added to the RCA product,^[216] which can be probed to indirectly assess RP generation. Detection of RCA-mediated pH changes can be achieved by using pH indicator dyes^[217], and pH paper^[187], for colorimetric detection. To date, no RCA examples utilizing fluorescent pH indicator dyes have been reported. Likewise, though pH meters are common in electrochemistry, no method has been reported for RCA by-product monitoring. Accounting for the variability in pH of real samples poses a challenge to these styles of assay, especially in POC scenarios. While monitoring of pH is simple and cost-effective, it should be noted that indicator dyes are sensitive over a relatively narrow pH range, requiring careful control of initial solution pH. Solutions with low buffer capacity are generally required to achieve adequate changes in pH, which can require significant sample processing prior to RCA to obtain good sensitivity.^[218,219]

The detection of PPi is typically achieved by monitoring the chelation of PPi with Mg^{2+} in the reaction buffer, which depletes the amount of free Mg^{2+} and causes a color change.^[220] The hydroxy naphthol blue (HNB) metal indicator dye from turns from violet (Mg-HNB) to sky blue (free HNB) as the

concentration of free Mg^{2+} decreases. It was reported however, that the violet-to-blue color change may not be easily observed by eye, requiring a plate reader. Fluorometric monitoring of PPI as an RCA by-product has been reported, where a terpyridine-Zn(II) complex ($ZnCl_2L$) specifically binds to the PPI by-product and triggers fluorescence.^[91,221] In this case the $ZnCl_2L$ is fluorogenic, and will only fluoresce when bound to PPI, avoiding the need for a washing step to remove unbound reagent.

2.6.2.2 Incorporation of Labelled dNTPs

An alternative method to monitor RCA reaction products is to incorporate labelled dNTPs directly into the reagent pool used to generate the RCA product. This is most commonly done using fluorescently-tagged dNTPs, where either the consumption of free dNTPs or generation of the fluorescent RP can be monitored.^[196,222–224] While the detection of labelled dNTPs is highly specific, the used of labelled dNTPs can cause a reduction in the rate of RP production as these species have a lower rate of incorporation. Additionally, unincorporated nucleotides must be removed using a washing step to eliminate background fluorescence. A significant drawback of using labelled dNTPs is the assay cost, as large numbers of relatively expensive labelled dNTPs must be incorporated into the RP to provide good detection limits. To this issue, Linck *et al.* reported that a novel dye was able to reduce costs by one-sixth relative to a Cy3-labelled dUTP.^[222] The authors noted that direct addition of the dNTPs into the RP also avoided the need for

subsequent processing steps, as the signal is generated during the polymerization reaction rather than during a subsequent reagent addition step.

2.6.2.3 Intercalating Species

As RCA generates a substantial amount of DNA, fluorescent DNA intercalating dyes offer a general method to detect RP without the need to encode specific outputs into the CT. The dyes are often fluorogenic cyanine or rhodamine derivatives and undergo conformational changes upon binding to single- or double-stranded DNA sequences, resulting in large increases in their quantum yield (up to 1000-fold), and hence their high emission intensity.^[225] The background emission from such dyes is typically very low, avoiding the need for a washing step to remove unbound dye. Intercalating dyes are also able to monitor RP formation in real-time, which make assays based on dynamic signal changes possible. Taken together, this makes intercalating dyes well suited for POC applications using RCA. It is important to note that these dyes can also bind directly to the CT, and hence can potentially affect the thermodynamics and kinetics of the polymerase reaction,^[226] and can produce high background signals that can impact detection of low levels of RP.

A large number of studies have utilized intercalating dyes for both solution and solid-phase assays (see sections 5 and 6), with typical dyes including SYBR Green I, SYBR Green II, Eva Green, SYBR Gold, and

QuantiFluor.^[101,113,116,119,125,132,143,181,199,227–229] These dyes offer a wide range of properties, including various excitation/emission wavelengths, selectivity for certain DNA sequences over others, different affinities for DNA relative to RNA, or different affinities for single- or double-stranded DNA. Hence, it may be necessary to evaluate several dyes to optimize a given RCA based assay.

2.6.3 Detection using Selective Hybridization or Adsorption of Signalling Moieties

While the examples above could utilize any RP sequence and hence did not require any encoding of outputs into the CT, such methods can suffer from background signals if there are endogenous NAs that can bind to intercalating dyes or affect detection of reaction by-products. To increase detection selectivity it is possible to encode specific sequences into the CT so that the multiple repeats of the antisense sequence appear in the RP. Among the most common methods for detection of RCA products is the hybridization of specific NA sequences to complementary sequences on the RP, which can produce a variety of detection outputs. A summary of these methods is provided below.

2.6.3.1 Hybridization of Peptide Nucleic Acids

For colorimetric outputs, a typical approach is to hybridize peptide nucleic acids (PNA) to the RP, followed by aggregation of specific dyes into the PNA-DNA complex. DisC2 (3,3'-diethylthiadicarbo-cyanine) is a common

dye that aggregates to the PNA-DNA duplex,^[230,231] causing a blue-to-purple color change. This method can reduce background signal generation as PNA is not native to biological samples and is not vulnerable to nucleases,^[232] though the color change can be difficult to determine by eye. This assay can also be relatively slow at room temperature, and thus may require a heating step to increase the rate of the color change.^[120]

2.6.3.2 Hybridization of AuNP-Labelled DNA

Complementary DNA sequences directly labelled with reporter molecules can also be used to bind to the repeating units in the RP. For colorimetric detection, the most common reporter is gold nanoparticles (AuNPs),^[98,115,233] which have found widespread use for colorimetric biosensing owing to their distinctive red color and large molar absorptivities relative to other organic dyes.^[234,235] The high absorptivity is due to the presence of localized surface plasmon resonance (LSPR) in the AuNP, which causes absorbance of light that is in resonance with the surface plasmon. The wavelength absorbed is highly dependent on nanoparticle size, shape, and immediate environment,^[234] making AuNPs highly tuneable for biosensing applications.^[236] AuNPs are also easily modified with thiolated DNA through the well-known sulfur-gold interaction,^[237,238] allowing AuNPs to be modified with specific DNA sequences (AuNP-DNA) that can hybridize to repeating segments of RPs. It is important to note that AuNPs are relatively large (diameter of 5 – 20 nm or more) and carry

multiple DNA strands per particle, and hence can bind across multiple regions of RPs, or to multiple RPs, which can increase overall binding affinity but may also promote aggregation. Examples of assays using AuNPs will be covered in Sections 2.7 (solution assays) and 2.8 (solid-phase assays).

2.6.3.3 Hybridization of DNA Labelled with Fluorophores or Redox Probes

DNA sequences can also be modified with small molecules, and unlike AuNPs, the hybridization sequences typically contain one signalling moiety per strand. A common detection approach involves the hybridization of DNA with covalently bound fluorescent probes (F-DNA) to the RP.^[136,239–246] Under optimized conditions, this method can be applied successfully for single molecule detection using RCA.^[85–87] Although this method normally requires a washing step to remove unbound F-DNA, it is possible to implement methods such as dipstick-based strategies to directly separate bound and unbound probes.^[239] Unlike intercalating dyes, hybridization of F-DNA is selective for the output sequence in the RP, thus minimizing interactions with background NAs. Most commonly, F-DNA is a DNA strand modified with a fluorescent linker such as a fluorescein or cyanine derivative. However, less common fluorophores such as quantum dots can also be used.^[245]

For electrochemical detection, hybridization probes are modified with electrochemically active reporter molecules. Various reporter labels can be

attached to single stranded hybridization probes, including those that otherwise would have no affinity for DNA. These can include methylene blue,^[281] ferrocene,^[125] AuNPs,^[125] or quantum dots.^[137] In these cases, the mediator binds to RP that is tethered to an electrode surface. Gold nanoparticles themselves can play a large role in signal amplification because they can assist in electron transfer along the long surface area of bound RP.^[141,210,247] The presence of the redox mediator along the RP allows for generation of a current based on oxidation or reduction of mediators that are in close proximity to the electrode surface. As with fluorescently-labelled hybridization probes, it is necessary to employ a washing step to remove unbound probes that could contribute to background current.

2.6.3.4 Hybridization of Molecular Beacons

An interesting method to overcome the need for a washing step is the use of molecular beacons (MBs) as hybridization probes. These single-stranded DNA sequences form a hairpin loop structure with the termini modified with a fluorophore-quencher pair, a conformation that quenches the fluorophore.^[248] Upon hybridizing to the RP, the MB adopts an extended conformation that separates the fluorophore and quencher ends, resulting in a 15- to 20-fold increase in fluorescence emission intensity. Given the ability to avoid a washing step and the selective binding to the RP, multiple groups have utilized this approach for sensitive detection of

RCA products generated from both FNA initiated and nucleic acid initiated RCA.^[110,111,135,249–253] Careful design of the CT is required to maximize signal generation with MBs as intermolecular quenching of neighboring fluorophores present in the concatemeric monolith can occur when quencher arms are not hybridized to the RP.^[254] It has been observed that RPs that fully bind to the Q-labelled arm, but not the F-labelled arm, led to the best signal contrast. In addition, it is necessary to protect the 3' end of the MB using species such as 2'-O-Me-RNA to prevent exonucleolytic digestion of the MB by the phi29 DP.

An advantage of MBs (and also hybridization of F-DNA species) is the ability to use fluorophores with different excitation/emission wavelengths bound to different DNA sequences to allow one-pot multiplexed detection of RPs generated by two distinct targets initiating RCA with distinct CTs, or to incorporate a control CT as an internal reference for normalizing variability in assay conditions.^[254]

2.6.3.5 Hybridization of DNA-modified Enzymes

To improve signalling levels, it is possible to bind an enzyme to a DNA sequence that hybridizes to the RP, which provides a second level of amplification and can dramatically improve detection limits. The attachment of the enzyme is typically done by first binding biotinylated DNA to the RP, followed by the addition of streptavidin-modified recombinant enzymes. This approach has been widely used for colorimetric detection, using

enzymes such as glucose oxidase (GOx) to produce pH changes upon formation of gluconic acid,^[184] which can be detected using pH indicator dyes. Avoiding buffer capacity issues with monitoring pH changes, horseradish peroxidase (HRP) can reduce chromogenic substrates such as 3,3',5,5'-tetramethylbenzidine (TMB)^[255–258] in the presence of peroxide to generate colorimetric or electrochemical outputs for RCA-based assays. Importantly, the RCA reaction must reach completion before colorimetric detection can occur as the peroxide can denature the DP.

Redox active enzymes can also be hybridized to RPs to generate RCA-linked electrochemical assays. A commonly used enzyme is alkaline phosphatase (ALP),^[96,259] which is used to convert ascorbic acid 2-phosphate into ascorbic acid, subsequently reducing silver ions which are deposited on the electrode and monitored by linear sweep voltammetry. Alternatively, streptavidin-tagged GOx can be added to a biotinylated probe on an immobilized RP for subsequent redox monitoring of pH changes associated with the oxidation of glucose,^[260,261] though these methods suffer similar drawbacks to other pH based detection strategies such as the need for careful control of buffer capacity and initial pH. It is also possible to hybridize DNA carrying an invertase enzyme, which is used sucrose into fructose and glucose.^[193,262–264] The latter product can be detected directly using a personal glucose meter (PGM), which can allow for operation in complex biological media (see Section 2.8).

2.6.3.6 Dequenching of Hybridized Sequences using Nicking Enzymes

Alternatively, nicking enzymes can be used to generate a fluorescence signal through site-directed cleavage of a hybridized DNA strand carrying a fluorophore quencher pair. The DNA can be hybridized to repeating units of the RP with a nicking site placed between the fluorophore and quencher with subsequent nicking causing release of the F-DNA from the quencher (Q-DNA) and a corresponding increase in fluorescence intensity. This approach may be more sensitive than traditional MBs as the nicking enzyme can cleave multiple probes per monomeric unit, whereas MBs only produce one signal once per RP monomer. The released cleavage products (F-DNA or Q-DNA) can also be used as a secondary primer to provide an exponential RCA output due to their inherent complementarity to the CT.^[252] Similarly, the use of AuNP as an alternative quencher has also been explored.^[265]

2.6.3.7 Nanoparticle Adsorption to RPs

Adapting the CT to produce long stretches of either adenine or thymine bases in the RP can allow for signalling based on nanoparticle adsorption to the RP, which is typically detected using an electrochemical method that takes advantage of the conductive nature of metallic nanoparticles.^[266] Given that many nanoparticles can adsorb to a RP, these moieties can play a large role in signal amplification because they can assist in electron transfer along the surface of bound RP.^[141,210,247] The two most common

systems involve the adsorption of preformed AuNPs to polyadenosine DNA sequences in the RP^[267] and production of copper nanoparticles (CuNP) along a RP via reduction of Cu²⁺ onto polythymine-rich RPs in the presence of ascorbate.^[260] In the latter case the CuNP can either be detected by monitoring the oxidation current for subsequent production of Cu²⁺ or by monitoring the oxidation of a redox probe during the initial reduction of Cu²⁺ to form the CuNP.^[280]

2.6.4 Detection using RPs Incorporating G-Quadruplexes

It is also possible to encode G-rich output sequences into the RP that can fold into highly structured moieties such as G-quadruplexes,^[268] which are present as a specific repeating component of RPs. These guanine-rich sequences can fold into several different four-stranded topologies formed via intermolecular or intramolecular association induced by Hoogsteen interactions between guanine bases.^[269] There are several G-quadruplex specific fluorescent dyes,^[270–272] however RP detection has thus far been demonstrated only with Thioflavin T (ThT),^[173,190,273–275] N-methyl mesoporphyrin IX (NMM),^[117,191,276–278] and protoporphyrin IX (PPIX)^[279–281] using either FNA-initiated or NA-initiated RCA. These dyes are similarly sensitive with detection limits ranging from picomolar to as low as attomolar^[273] when exponential RCA is used. However, while both ThT and NMM dyes have been used for real-time monitoring of amplification signal, PPIX has not yet been used for real-time monitoring of RCA.

An advantage of detection based on dye-binding to G-quadruplexes is the specificity of the binding interaction, which can reduce nonspecific background signals from interfering with NA species. This can be an issue for general intercalating dyes that bind unstructured single- or double-stranded DNA. A disadvantage of the use of G-quadruplexes is the lower overall signal enhancement upon binding (typically 10- to 20-fold enhancements in emission intensity upon G-quadruplex binding versus up to a 1000-fold enhancement for SYBR Gold binding to DNA), which can result in higher background signal levels. For this reason, strategies using fluorescent G-quadruplex binding dyes commonly incorporate nicking enzymes for exponential RCA to generate sufficient G-quadruplex binding regions. Often these enzymes require elevated temperatures for optimal activity thus potentially limiting its utility as a POC approach.

G-quadruplex outputs can also be used to selectively intercalate redox probes. Subsequent reduction or oxidation of these probes changes the overall chemical environment which can be readily monitored via changes in current or impedance. Common redox probes include methylene blue,^[126,138,194,282–287] molybdate-^[288–291] and ruthenium-based^[292,293] DNA intercalating complexes. There are two common formats for the use of intercalating redox probes. In the first, the RP is immobilized on an electrode and with the intercalation of the mediator with the RP brings the mediator in close proximity of the electrode, thus increasing the measured

signal.^[282] Alternatively, RCA reactions can be carried out free in solution to produce RP rich in G-quadruplex subunits. Free mediator in solution intercalates with the RP, thus reducing its availability at the electrode surface and hence decreasing the current.^[285]

2.6.5 Detection using RPs Incorporating DNAzymes

An alternative to hybridizing enzyme-DNA conjugates to RP is to produce RP that contain repeating DNAzymes units that catalyze reactions that can be detected by optical or electrochemical methods. This is commonly achieved by incorporating a peroxidase-mimicking DNAzyme (PMD) into the RP, which will contain hundreds to thousands of PMDs per RCA reaction. Reported nearly 3 decades ago,^[43] the PMD is a specific G-quadruplex that can form a complex with hemin, resulting in HRP-mimicking peroxidase activity.^[294] These G-quadruplex sequences enhance the natural peroxidase activity of hemin upon binding and therefore can be utilized with common optical and electrochemical peroxidase assays, making them attractive as reporter elements for biosensing.^[295] Importantly, the direct formation of the PMD in the RP overcomes the need to hybridize an external enzyme and remove excess unhybridized enzyme with a washing step, making it more compatible with POC diagnostics. There are many examples of RCA-based assays that use PMDs to produce colorimetric outputs based on oxidation of 2,2'-azino-bis(3-ethylbenzothiazoline-6-sulfonic acid (ABTS)),^[112,131,140,151,296–300] or

TMB,^[98,112,114,255] which will be covered in detail in Sections 5 and 6. It must be noted, however, that as is the case for HRP-based assays, long-term peroxide stability becomes a challenge for operation in a POC setting.

PMDs can also be used for fluorescence-based sensing, based on the quenching of fluorescent quantum dot (QD) probes via a peroxidase-mediated photoinduced electron transfer system.^[129,301] In this approach a PMD-containing RP is first generated by RCA followed by hybridization of a fluorescent QD-DNA probe. The proximity of the PMD to the QD causes fluorescence quenching owing to QD-to-hemin electron transfer, resulting in a decrease in signal intensity in the presence of RP.

The catalytic action of PMDs can also be monitored electrochemically by measuring the current related to the reduction of H₂O₂. This method has been extensively utilized for monitoring of RCA reactions (see Section 6) and is compatible with opaque samples that may not be amenable to colorimetric or fluorometric outputs.^{[302][303]} It is also possible to use the PMD to produce an electrochemiluminescence signal wherein the PMD catalyses the oxidation of luminol in the presence of hydrogen peroxide generation of a luminescence output.^[304]

Alternatively, RCA can be used to produce an RNA-cleaving DNAzyme as a component of the RP. When repeating RCD units are incorporated within the RP, they can be used to cleave fluorogenic DNA-RNA substrates to generate a fluorescence output.^[148,189] These substrates have a specific

DNA sequence that contains a single ribonucleotide cleavage site flanked by a fluorophore and quencher, which leads to low fluorescence background. The RP contains many RCDs which can cleave multiple substrates per repeat unit, producing substantial fluorescence enhancements.^[148] The cleavage reaction is performed at room temperature and secondary enzymes do not need to be added following completion of the RCA reaction, making this approach more amenable to POC applications. However, it is important to stabilize the RNA-containing substrate to avoid the potential for self-cleavage which can increase the fluorescence background signal.^[195]

2.7 FNA-Based POC Biosensors Utilizing RCA

The development of a final FNA-enabled RCA assay requires the integration of input, amplification, and detection methods in a manner that produces optimal performance in terms of selectivity, sensitivity, and limits of detection, while ideally meeting all the ASSURED criteria. In many cases, the development of a POC biosensor begins with the optimization of assay parameters using solution-based assays, and it is important to note that the emergence of simple commercially available handheld colorimetric and fluorometric readers (i.e. the Nix Pro Color Sensor™, or the ANDalyze AND1100 Fluorimeter) makes it possible to perform solution-based assays at the point-of-care. For this reason, we first consider simple solution-based RCA assays utilizing DNA aptamers or DNAzymes as MREs and producing

optical outputs, and then describe how these assays are integrated into simple POC devices to produce portable sensors that better meet the ASSURED criteria. We then move on to consider heterogeneous optical assays utilizing solid supports such as beads or microwell plates. Optical assays that utilize fluidic systems based on glass, plastic or paper systems to enable multistep assays without user intervention are then discussed. We then conclude this section with a discussion of RCA-based electrochemical biosensors.

2.7.1 Homogeneous Optical Assays

Homogeneous assays are designed to operate without the inclusion of separation or washing steps, making them one of the simplest POC formats. These assays are generally done in solution (i.e., microwell plates or tubes) and comprise the majority of RCA-enabled sensing strategies as noted in several reviews.^[305,306] Herein, we describe homogeneous assays that are amenable to use of simple optical readers, and highlight the advantages and disadvantages of such methods relative to various heterogeneous RCA-enabled assays. We consider both one-step and multi-step homogeneous assays, though in general it is best to minimize user steps to avoid the potential for user error and minimize assay time. A full list of homogeneous assays is provided in Table 2.1. Below we highlight some of the seminal works in the field.

An early example of an RCA-based homogenous assay was reported by Di Giusto *et al.* in 2005, who described a thrombin-targeting assay that was able to fluorometrically detect thrombin in real-time within 30 minutes in a one-step, one-pot assay.^[143] In this case both a linear and circular thrombin aptamer were employed for a proximity extension assay (see Section 2.4.2.2), with the RCA reaction product detected using SYBR Green I with a detection limit of 30 pM (Figure 2.10A). A drawback of this method is the low number of targets having two or more distinct aptamers that bind to different epitopes, and the need to circularize one of the aptamers, which could have detrimental effects on the native binding affinity of the aptamer.^[113]

Many homogenous FNA-enabled RCA assays utilize structure-switching aptamers to generate inputs to the RCA reaction and fluorescence outputs for detection. Several variations on this approach are described below. One of the initial reports on use of structure switching aptamers to modulate RCA was by Zhu *et al.* who developed a simple method for thrombin detection that operated by aptamer-based inhibition of a PLP reaction, with RP being detected with SYBR Green I (see Section 2.4.2.1).^[181] Without thrombin, the aptamer is able to hybridize to the ligation strand, preventing the formation of a CT and blocking RCA by Bst DP. Thrombin causes switching of the aptamer off the ligation strand, allowing CT formation

followed by linear RCA, producing a detection limit of 1 pM, or hyperbranched RCA to achieve a 2 fM detection limit in 3 hrs.

Yang *et al.* also used a structure switching approach linked to PLP inhibition for PDGF detection (see Section 2.4.2.1, Figure 2.5A).^[125] In this approach, target binding caused a structural change in the aptamer to release the terminal ends, which permitted ligation to convert the aptamer into a CT for real-time monitoring of linear RCA with SYBR Green I. A drawback was that the assay required four steps, including a heating step, and also required 3 hours to produce a detection limit of 0.3 nM of PDGF. However, the assay was also shown to be amenable to detection of PDGF in cell lysate with a comparable LOD of 0.4 nM.

Simple structure-switching systems have also been developed using colorimetric outputs. For example, Liang *et al.* combined structure-switching aptamers to control RCA with the adsorption of unfunctionalized AuNPs onto the RP to detect carcinoembryonic antigen (CEA).^[139] Once again, target binding to an aptamer modulated a PLP reaction (see Section 2.4.2.1), with target binding permitting ligation and amplification. The final LOD was 2 pM using H-RCA, based on a red-to-blue colour transition upon AuNP adsorption to the RP (Figure 2.10B), which is a particularly good LOD for a colorimetric assay. The assay was also highly selective with 10000-fold concentrations of various interferents having no effect on the signal.

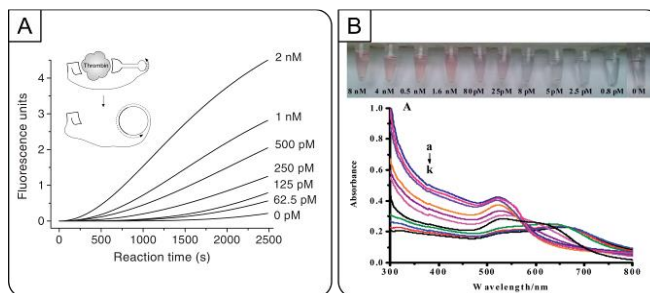


Figure 2.10. Homogeneous FNA-RCA assays with optical detection methods. (A) Fluorescence data for proximity extension of circular DNA aptamers with real-time detection of the thrombin target. (B) Visual detection of CEA based on PLP ligation, hyperbranched rolling circle amplification and AuNP aggregation. Figures adapted from references cited in text.

More complicated structure switching systems can be developed by integrating the aptamer into a tripartite system comprising the aptamer, a pre-primer and a CT (see Section 2.4.1.2, Figure 2.3A), as was demonstrated for PDGF-mediated activation of H-RCA.^[116] In this case, the target removes the aptamer, which acts as a control element to prevent priming of the RCA reaction. Upon removal, phi29 DP mediated exonucleolytic digestion of a pre-primer produces a mature primer to initiate H-RCA, with the RP generation monitored in real-time by EvaGreen (Figure 2.11A, top). This method could detect 100 fM of PDGF after 15 minutes of amplification, and 1 fM of PDGF using an RCA time to 2 hours (Figure 2.11A, bottom). Wang *et al.* used the same tripartite regulation method to initiate an initial catalytic hairpin assembly approach that was then coupled with exponential RCA, providing a detection limit of 0.2 pg/mL of OTA in 90 min (Figure 2.11B).^[191] In addition, a split aptamer variation was reported

that utilizing a similar 3'-exonuclease regulation method paired with an endonuclease-assisted feedback system (Section 2.4.1.2, Figure 2.3B) for the detection of ATP (LOD of 0.09 nM).^[117] Both systems were successfully tested against samples of red wine for OTA and human serum for ATP (see Figure 2.11C), respectively, with the fluorogenic probe NMM binding to G-quadruplexes present in the RP.

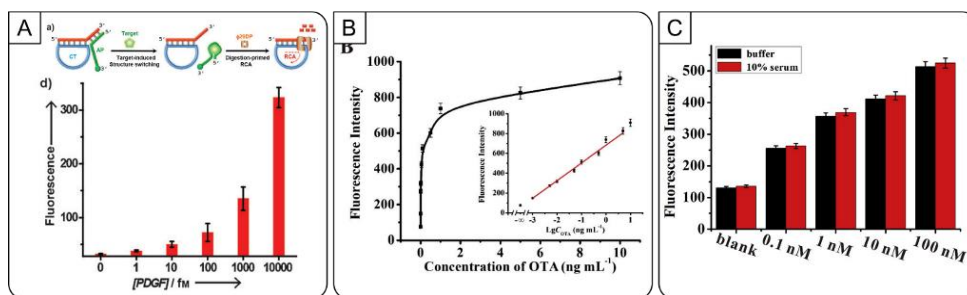


Figure 11. Homogeneous FNA-RCA methods utilizing tripartite structure-switching systems paired with the 3'-exonuclease activity of phi29 DP. (A) Tripartite structure-switching and DNA amplification of a DNA assembly for detection of PDGF. (B) Tripartite structure switching detection paired with catalytic hairpin assembly for the detection of PDGF. (C) A dual-aptamer approach for ATP detection based on endonuclease-fueled feedback amplification Figures adapted from references cited in text.

Recently, Liu et al. reported on a simplified variation of the tripartite structure-switching assay system that removed the need for inverted dT protecting groups on the 3'-end of the pre-primer, as phi29 digestion was not used (Section 2.4.1.1, Figure 2.2B).^[107] This approach used a dendritic RCA method for exponential amplification and PMDs as the output, resulting in the colorimetric detection of PDGF via oxidation of TMB, providing a LOD of 1.96 fM in diluted serum samples. Though very sensitive

for a colorimetric assay, the method required over 3 h to perform and required addition of peroxide and TMB following the RCA reaction, adding complexity to the assay and preventing real-time signal generation.

It is also possible to use an internal structure switching system based on aptamers that can form hairpin structures. Here, a weak hairpin is initially present, which can be extended with Klenow fragment (KF) to produce a strong hairpin, denoted as a shielded aptamer, that is unable to bind target or initiate RCA. Addition of target prior to KF opens the hairpin and prevents hairpin extension by KF, thus allowing a primer extension on the aptamer to initiate RCA (Section 2.4.1.2, Figure 2.3D).^[119] The aptaprimer approach was used for detection of three small molecules, with linear RCA providing one-pot, three-step detection of OTA (LOD of 38.8 fM), kanamycin (LOD of 8.9 fM), or L-tyrosinamide (LOD of 47.5 pM) with a 3 hour assay time (Figure 12A), and was amenable to detection of these targets in spiked serum (kanamycin and L-tyrosinamide) or red wine (OTA).

Control of RCA can also be accomplished by having aptaprimers switch off a reduced graphene oxide surface (Section 2.4.1.1, Figure 2.2C).^[110] This approach has been reported for detection of several types of targets, including thrombin (protein), ATP (small molecule), and HCV-1 DNA (NA). Here, the aptamer was modified with a primer extension, producing an aptaprimer that could initiate RCA. When bound to rGO, the aptaprimer was prevented from binding to a CT. However, release of the aptaprimer

upon target binding freed the primer to bind the CT and initiate RCA, with the RP being detected by binding of a molecular beacon (Figure 2.12B). The authors reported detection limits of 10 pM for thrombin, 60 nM for ATP, and 0.8 pM for HCV-1 DNA each with a total assay time of under 3 hours with linear amplification. The thrombin-targeting assay was also shown to be amenable to detection in 50-fold diluted human serum, with a LOD of 10 pM. In a follow-up paper, Mao *et al.* further optimized the CT with stronger binding to the released aptaprimer to further drive the detection limit down and improved the LOD of the thrombin system 10-fold from 10 pM to 1 pM.^[111]

An alternative method to structure-switching is to use an aptaprimer that can either be blocked from priming RCA upon binding of target (Section 2.4.1.1, Figure 2.2D) to produce a turn-off assay,^[101] or used in combination with the inherent 3'-exonuclease activity of phi29 DP to produce a turn-on assay (Section 2.4.1.2, Figure 2.3C) (Figure 2.12C, top).^[118] In the first case, the binding of either thrombin or PDGF to their respective aptamers resulted in a reduction in RCA product formation, leading to a detection limit of 10 nM for PDGF and 100 pM for thrombin within 1 hour.^[101] By incorporating the digestion step along with CT mediated strand displacement, an activation assay was produced with detection limits of 100 pM for both PDGF and thrombin using real-time monitoring of linear RCA with SYBR Gold within 2 hours.^[118] Notably however, the activation assay

showed signal inhibition at higher concentrations of target (above 10 nM) independent of toehold length (Figure 2.12C, middle) which was ascribed to the inability of the toehold system to displace the target when the target was in large excess. With clinically relevant levels of PDGF and thrombin often falling within only one or two orders of magnitude, the assay could still be applicable at the POC. As well, the assay was optimized for detection of PDGF in human plasma or serum (Figure 2.12C, bottom). As target binding confers protection onto the aptamer from nuclease activity, this approach may be particularly well suited for nuclease-containing samples.

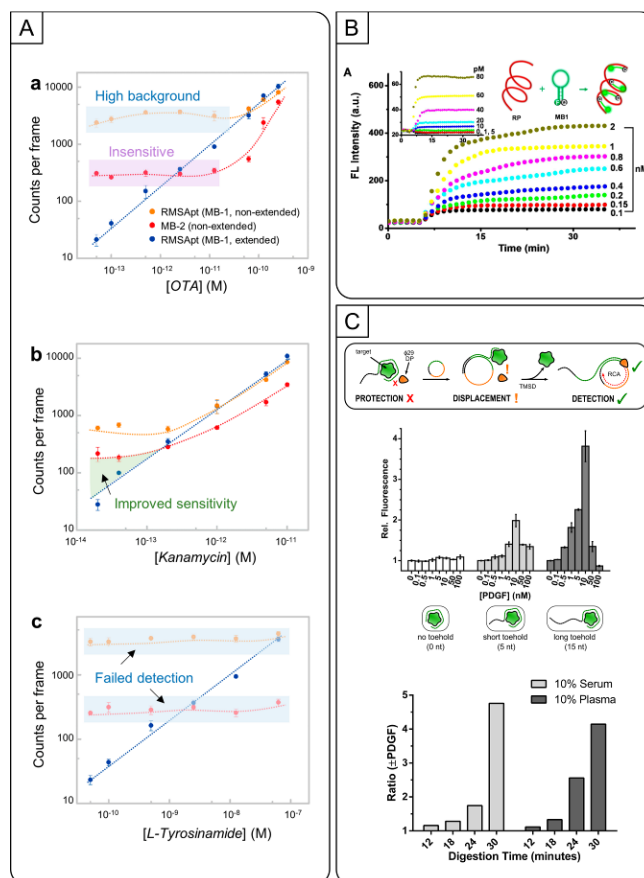


Figure 2.12. Homogeneous FNA-RCA methods where the aptamer and primer are in the same sequence. (A) Digital fluorescence quantification of small molecules using shielding aptamer-triggered RCA. (B) Real-time fluorescence detection of RP using molecular beacons with varying concentrations of thrombin. (C) A signal-on biosensing strategy for PDGF and thrombin enabled by toehold-mediated RCA. Figures adapted from references cited in text.

In addition to aptamer-based homogeneous assays, it is also possible to produce such assays under the regulation of DNazymes. Liu et al. pioneered an approach for the detection of *E. coli* by using a DNA catenane to mechanically lock the system in place until cleaved by the RCD (Section

2.4.2.3, Figure 2.7D) (Figure 2.13A, top).^[151] Topologically constrained nanostructures that are regulated by the use of DNAzymes can increase the specificity of the interaction between the target and FNAs. Amplification at the RNA cleavage site cannot proceed until the base is treated with PNK to remove the 2'3' cyclic phosphate, a common cleavage product for several RCDs.^[307,308] While this was an individual 30-minute step in this assay, the same group has shown that the PNK and amplification steps can be combined together.^[309] The authors investigated the integration of a PMD into the CT for colorimetric linear RCA (Figure 2.13A, middle) and compared it to fluorometric hyperbranched RCA (Figure 2.13A, bottom). The linear PMD approach (LOD of 1000 cells per mL) required six steps and a 3 h assay time, but could be read by eye. The LOD attained with H-RCA (10 cells per mL), was far better, and the assay required only three steps and 2.5 hours, though quantification required a reader.

Another example of DNAzyme-mediated RCA is the use of DFA to achieve exponential signal enhancement when using RCDs as the recognition element, as demonstrated by Liu et al. for the real-time detection of *E. coli*.^[121] Primary amplification through the cleavage of the unique tripartite system (Section 2.4.1.3, Figure 2.4B) allowed for the autonomous generation of primers and secondary amplification products (Section 2.5.2.3). The two-step isothermal amplification incorporated both cleavage and PNK treatment simultaneously and could provide detection of 10 copies

per mL of *E. coli* within one hour (Figure 2.13B). Notably, DFA improved detection limits by 1000-fold relative to the unamplified RCD, requiring just a single additional step. Though it has only been demonstrated for mi-RNA and RCD-mediated (*E. coli*) targets, the authors indicate that the assay should be amenable to many other analytes so long as generation of complex I can be regulated through a molecular recognition event.

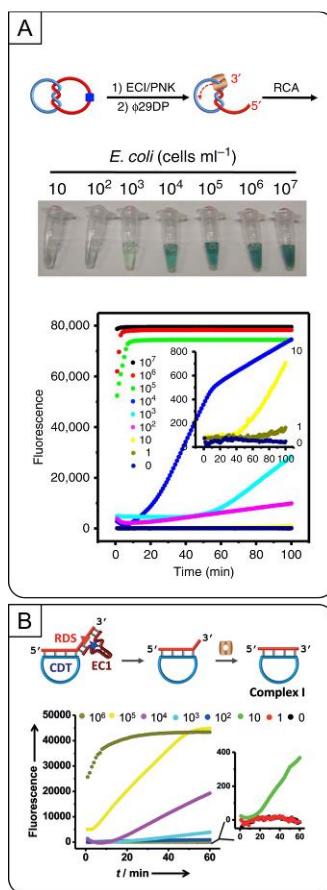


Figure 2.13. Homogeneous FNA-RCA methods incorporating RCDs. (A) Colorimetric (top) and fluorescent (bottom) detection of a catenane-RCD triggered amplification. (B) A DNAzyme Feedback Amplification (DFA) strategy for fluorescent detection of *E. Coli*. Figures adapted from references cited in text.

Table 2.1. Homogeneous solution-based methods.

Detection Method	RCA Method	MRE Type	Regulation Method	Target	LOD	# Steps	Temperature	Assay Time	Ref.
Colorimetric Detection									
AuNP	hyperbranched	aptamer	structure-switching ^[PLP]	CEA	2 pM	many ^[P]	multiple	≥ 2 hrs	[139]
PMD	linear	DNAzyme	RCD	<i>E. coli</i> ^[CM]	1000 cells / mL	many ^[P]	multiple	≥ 2 hrs	[151]
PMD	dendritic	aptamer	structure-switching	PDGF ^[CM]	1.96 fM	many ^[P]	multiple	≥ 3 hrs	[107]
intercalating dye	linear	captamer	inhibition RCA	thrombin	15 nM	many ^[P]	multiple	≥ 1 hr	[145]
Fluorometric detection									
cDNA (fluorophore)	linear	aptamer	inhibition RCA ^[PLP]	aflatoxin M1 ^[CM]	0.0194 pg/mL	many	37 °C	≥ 3 hrs	[133]
G-quad dye	enzyme-assisted	aptamer	structure-switching ^[PLP]	ATP ^[CM]	84 nM	many	multiple	≥ 8 hrs	[274]
intercalating dye	hyperbranched	aptamer	structure-switching ^[PLP]	ATP	1 nM	many	multiple	≥ 2 hrs	[183]
intercalating dye	hyperbranched	aptamer	structure-switching ^[PLP]	ATP	ATP in a single HeLa cell	many	multiple	≥ 2 hrs	[183]
cDNA (MB)	linear	aptamer	structure-switching (rGO)	ATP ^[CM]	60 nM	many	multiple	≥ 2 hrs	[110]
G-quad dye	enzyme-assisted	aptamer (split)	structure-switching	ATP ^[CM]	0.09 nM	2	37 °C	≥ 1 hr	[117]
G-quad dye	enzyme-assisted	aptamer	structure-switching ^[PLP]	BPA ^[CM]	54 aM	many	multiple	≥ 5 hrs	[279]
intercalating dye	hyperbranched	DNAzyme	RCD	<i>E. coli</i> ^[CM]	10 cells / mL	many ^[RT]	multiple	≥ 3 hrs	[151]
intercalating dye	DFA	DNAzyme	RCD	<i>E. coli</i>	10 cells / mL	2 ^[RT]	37 °C	≥ 2 hrs	[121]
cDNA (MB, Fr/Q)	linear	DNAzyme	DNAzyme kinase ^[PLP]	GTP	4 μM.	many	multiple	≥ 4 hrs	[148]
intercalating dye	linear	aptamer	structure-switching	kanamycin ^[CM]	8.9 fM, 1	many	multiple	≥ 3 hrs	[119]
intercalating dye	linear	aptamer	structure-switching	L-tyrosinamide ^[CM]	47.5 pM	many	multiple	≥ 3 hrs	[119]
cDNA (QD)	linear	aptamer	structure-switching ^[PLP]	lysozyme ^[CM]	2.6 nM	many	multiple	≥ 3 hrs	[129]
G-quad dye	strand-displacement assisted RCA	aptamer	structure-switching	MUC1 ^[CM]	0.5 pM	3	37 °C	≥ 2 hrs	[281]
intercalating dye	hyperbranched	aptamer	structure-switching ^[PLP]	OTA ^[CM]	1.2 fg/mL	many	multiple	≥ 4 hrs	[182]
intercalating dye	linear	aptamer	structure-switching	OTA ^[CM]	38.8 fM	many	multiple	≥ 3 hrs	[119]

G-quad dye	CHA-assisted	aptamer	structure-switching	OTA ^[CM]	0.0002 ng/mL	2	37 °C	≥ 1 hr	[191]
dNTP monitoring	linear	aptamer	structure-switching ^[PLP]	OTA ^[CM]	0.01 ng/mL	many	multiple	≥ 8 hrs	[224]
intercalating dye	linear	aptamer	inhibition RCA	PDGF	10 nM	2 ^[RT]	r.t.	60 min	[101]
intercalating dye	linear	aptamer	structure-switching ^[PLP]	PDGF ^[CM]	0.3 nM	many ^[RT]	multiple	≥ 3 hrs	[125]
intercalating dye	hyperbranched	aptamer	structure-switching	PDGF	1 fM	1 ^[RT]	30	≥ 2 hrs	[116]
cDNA (MB)	linear	aptamer	structure-switching ^[PLP]	PDGF	6.8 pM	many	multiple	≥ 3 hrs	[249]
G-quad dye	enzyme-assisted	aptamer	structure-switching ^[PLP]	PDGF ^[CM]	0.38 fM	many	multiple	≥ 8 hrs	[276]
G-quad dye	HCR-assisted	aptamer	structure-switching ^[PLP]	PTK7	0.3 fM	many	multiple	≥ 7 hrs	[278]
G-quad dye	HCR-assisted	aptamer	structure-switching ^[PLP]	PTK7	10 CCRF-CEM cells	many	multiple	≥ 7 hrs	[278]
G-quad dye	HCR-assisted	aptamer	structure-switching ^[PLP]	PTK7	20 HeLa cells	many	multiple	≥ 7 hrs	[278]
intercalating dye	linear	aptamer	inhibition RCA	thrombin	100 pM	2 ^[RT]	r.t.	30 min	[101]
intercalating dye	linear	aptamer	inhibition of PLP ^[PLP]	thrombin	1 pM	many	37 °C	≥ 3 hrs	[181]
intercalating dye	hyperbranched	aptamer	inhibition of PLP ^[PLP]	thrombin	2 fM	many	37 °C	≥ 3 hrs	[181]
cDNA (MB)	linear	aptamer	structure-switching (rGO)	thrombin ^[CM]	10 pM	many	multiple	≥ 2 hrs	[110]
intercalating dye	linear	aptamer	sandwich (apt 2x)	thrombin	30 pM	1 ^[RT]	37 °C	30 min	[143]

[a] Table Footnote. [b] ... ^[RT] denotes that detection was done with real-time monitoring; ^[PLP] denotes that the assay used a padlock probe ligation reaction; ^[CM] denotes that the assay was tested with complex media; "many" denotes any assay that required 4 or more steps; r.t. denotes that room temperature was used.

2.7.2 Heterogeneous Assays

Heterogeneous assays employ some form of separation step to physically separate assay components. While this increases the assay complexity and number of steps, it gives researchers more control over the reaction buffer, which may require strict conditions for subsequent reactions including RCA. Heterogeneous solution-based assays are summarized in Table 2.2. As well, it aids in the removal of unreacted components that may adversely affect downstream steps. For example, FNA-based heterogeneous assays may employ ethanol precipitation as a means of separating NA species during the assay, though this method is intensive and less applicable at the POC. In this approach, Ali and Li used an RCD for the detection of ATP (Section 2.4.1.3, Figure 2.4A) where The linearly amplified output RP was hybridized with PNA probes in solution.^[120] Physical separation using ethanol precipitation was used to isolate the RP and reconstitute it in a hybridization buffer designed to maximize PNA probe hybridization to RP and intercalation of the colorimetric indicator, DisC2. This method can reduce background signal generation as PNA is not native to biological samples and they are not vulnerable to nucleases,^[232] though the blue-to-purple color change can be difficult to determine by eye (Figure 2.14A, top). Notably, the assay was relatively slow at room temperature, and thus required a heating step to increase the rate of the color change otherwise several minutes of incubation at room temperature was required.

The assay achieved a detection limit of 100 μM of ATP in over 4 hours (Figure 2.14A, bottom).

Huang et al. demonstrated a more practical method of separation by using a membrane filter to separate unbound aptamers for gastric cancer exosome detection.^[132] The authors incubated anti-MUC1 aptamers with gastric cancer exosomes allowing the aptamers to hybridize with the MUC1 cell surface protein, which is overexpressed in gastric cancers (Section 2.4.2.1, Figure 2.5E). A 22 nm pore size membrane then filtered the solution to separate free and bound aptamers, removing the large cell-aptamers complexes (Figure 14B, top). The aptamer was liberated from the cell surface by heat treatment and subsequently circularized by PLP reaction only if the unbound aptamer remains in the filtered solution. Finally, they monitored H-RCA in real-time using SYBR Green I (Figure 2.14B, bottom) for detection of as low as 4.27×10^4 exosomes per mL. Though filtration is faster and less labor-intensive than ethanol precipitation, the added processing steps, including heat denaturation, make this approach challenging for POC applications.

Several strategies have been suggested for the physical separation of RP from its endogenous solution, including those tethered to a bulk solid surface (i.e. microwell plates, glass slides, discussed in 2.8.2.2) or their particulate equivalents (i.e. agarose beads, or magnetic beads). These particulates, sometimes called beads, may be used to tether sandwich-style

MREs as Tang *et al.* demonstrated in their dual-aptamer assay for PDGF detection (Section 2.4.2.1, Figure 2.5D).^[310] The centrifugation step was key to this approach as it physically separated any avidin beads with biotin-aptamer-target complexes formed on the bead surface from solution (Figure 2.14C, left). As opposed to ethanol precipitation and membrane filtration, bead-based centrifugation can be performed quickly and with ease where equipment is available. The sandwich formation acted to tether a primer-CT duplex to the bead surface, forgoing any PLP step and allowing for the linear amplification of PMD-rich RP for colorimetric detection (Figure 2.14C, top right). Avidin beads have great utility as the target-binding stage occurred in a volume of 100 μL whereas the centrifuged beads were resuspended in only 10 μL of buffer, effectively concentrating the solution ten-fold. This pre-concentration effect is a typical advantage of bead-based assays and may be a substantial factor in achieving the reported detection limit of 7.1 fM of PDGF (Figure 2.14C, bottom right).

Several classes of particulates used in these homogeneous assays have characteristics that can be exploited to increase assay sensitivity. Gold nanoparticles, specifically, can be used as a surface for target immobilization and for their redox capabilities. Abnous *et al.* made use of these features in their aptasensor to detect the small molecule aflatoxin M1.^[311] This approach regulates the digestion of single-stranded DNA by a CRISPR-Cas12a system, a version of circular ligation regulation (Section

2.4.2.1). CRISPR-Cas12a regulates the availability of a ligation strand for a PLP reaction. In the presence of unbound aptamer, CRISPR-Cas12a is activated and digests the ligation strand, thus blocking RCA. Centrifugation is used in several steps, including one for the removal of unbound aptamers and padlock probes. Target-triggered amplification results in an accumulation of RP on the AuNP surface which limits its ability to reduce endogenous yellow 4-nitrophenol to the colorless 4-aminophenol, giving clear colorimetric indication of amplification. Though this approach utilized a ligation step, it achieved a detection limit of 0.05 ng/L. With sensitive detection achieved in spiked milk samples as well (0.15 ng/L), this approach rivalled several electrochemical alternatives.

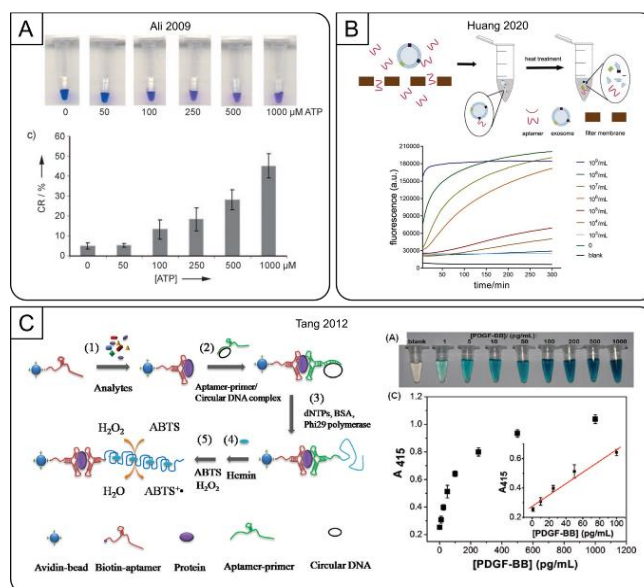


Figure 2.14. Heterogeneous FNA-RCA methods where magnetic beads are not used. (A) Colorimetric sensing by using allosteric-DNAzyme-coupled RCA and a PNA–organic dye probe. (B) Fluorescence detection of gastric cancer exosomes based on an aptamer-PLP E-RCA (C) A dual-aptamer PDGF bioassay using the colorimetric detection of PMD-rich RP. Figures adapted from references cited in text.

2.7.2.1 Magnetic Beads

Magnetic beads are another class of particulates used in homogeneous assays that can replace centrifugation-based bead strategies where centrifugation is not practical, as may be the case with portable POC devices. As implied, a magnetic force applied to the beads allows for simple separation of bead-bound and unbound compounds. This allows researchers to retain the separation powers of the technique while minimizing the infrastructure required to achieve it. Song *et al.* used

magnetic beads for the aptameric detection of the bacteria *V. parahaemolyticus* (Figure 2.15A, top).^[299] This method used a dual-aptamer approach with the addition of a biotinylated anchoring aptamer and a detecting aptamer into a target sample. Next, streptavidin-coated magnetic beads were added and used to extract the pathogenic bacteria. The detecting aptamer could be converted into a CT through a PLP step for amplification with nicking-assisted RCA. With PMDs integrated into the RP, the addition of hemin and ABTS allowed for the colorimetric generation of a green solution in the presence of the target bacteria corresponding to a detection limit of 10 CFU/mL (Figure 2.15A, middle). Monitoring of food-borne pathogens is an ongoing need with *V. parahaemolyticus* being a common pathogen in seafood. Even more so, any colorimetric approaches could be impacted by the composition and opacity of the food product itself. This assay employed magnetic bead-based separation and colorimetrically detected the bacteria in various spiked food samples (oyster, clam, codfish, jellyfish, shrimp, milk, and squid) (Figure 2.15A, bottom). In all, the full assay could be conducted in just 1 h 40 min though it did require several steps including a 95 °C termination step for the PLP reaction.

MRSA cells were reliably enriched using a magnetic bead strategy in Xu *et. al's* assay that used a dual-aptamer sandwich approach to separate the cells using a streptavidin-avidin interaction (Figure 2.15B, top).^[312] Several washing steps liberated the unbound sample components, leaving MRSA

cells tethered to the magnetic bead. A second aptamer was introduced, comprised of a PBP2a-specific structure switching aptamer that released a hybridized blocking sequence after binding to the target protein on the cell surface (Section 2.4.2.1, Figure 2.5B). PLP is only initiated when this second aptamer has MRSA cells to bind to, freeing the blocking strand to act as a ligation template and primer. Together PLP and linear amplification takes approximately 70 minutes. To improve assay sensitivity, instead of using an E-RCA the assay employed CRISPR-Cas12a enzymes whose *trans*-cleavage activity would cleave MBs accumulated on the RP. The wide linear range of this assay (10^2 to 10^6 CFU/mL, Figure 2.15B, bottom) was attributed to the combined powers of RCA and the attached CRISPR-Cas 12a, allowing for bacterial quantification in less than 3 hours. Clinically-obtained serum was spiked to assess the clinical effectiveness of the proposed microwell assay with good success.

Aside from removing assay components from a complex sample matrix, magnetic beads can be advantageous particularly for removing unreacted detection agents, such as fluorescently-tagged cDNA probes. Yao *et al.* utilized magnetic beads to remove unbound fluorescent quantum dot probes, which were then used as an indicator of OTA-triggered RP (Section 2.4.1.1, Figure 2.2D).^[245] In this instance, the magnetic bead was tethered to the 5'-end of the aptamer such that any RP generated would stay immobilized on the magnetic bead (Figure 2.15C, top). As it was an

inhibition RCA regulation approach, only 15 minutes of linear RCA were required with the QD-labelled cDNA probe requiring 30 minutes of incubation with RP, resulting in a total assay time of just over one hour. The resuspension of the beads allowed for high fluorescence with minimal background, achieving a detection limit of 0.13 ppt for OTA (Figure 2.15C, bottom), with validation in red wine samples.

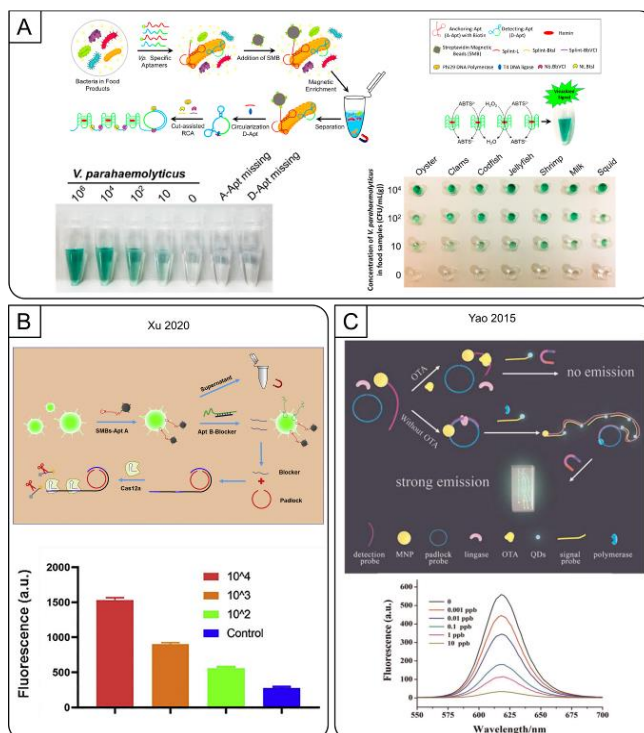


Figure 2.15. Heterogeneous FNA-RCA methods utilizing magnetic beads. (A) Visualized detection of *Vibrio parahaemolyticus* in food samples using dual-functional aptamers and E-RCA (B) Dual-functional aptamer and CRISPR-Cas12a assisted RCA for the detection of MRSA. (C) Magnetic bead inhibition RCA using quantum dot fluorescent detection of OTA. Figures adapted from references cited in text.

Background fluorescence from intercalating dyes can similarly be minimized by ensuring other NA contaminants are removed, as

demonstrated in this assay monitoring real patient faecal samples in real-time using a GDH captamer (Section 2.4.2.2, Figure 2.6C).^[113] After magnetic bead isolation of nGDH-bound captamer in the supernatant, the solution was heated to release the captamer for downstream RP generation at 30 °C (Figure 2.16A, top). Here, the separation step aided in ensuring that there would be minimal interfering NAs that the SYBR Gold could intercalate with, allowing for real-time detection of RP. The authors reported an LOD of 10 pM of GDH in human faeces in just over 1 hour using this strategy (Figure 2.16A, middle), despite employing a linear amplification. More interestingly, this group was able to demonstrate their assay's real-world applicability by testing several real-patient samples (Figure 2.16A, bottom).

Miao *et al.* used immunomagnetic beads to capture and isolate PDGF and used the catalytic power of GOx detection to boost sensitivity (Figure 2.16B, top).^[184] This assay utilized an antibody and aptamer-primer sandwich complex to reduce non-specific target bonding (Section 2.4.2.1, Figure 5D). As there are few targets with aptamers for two unique epitopes to participate in the sandwich, it is very common to see antibody-aptamer (Ab/apt) sandwich interactions.^[288,302,313] Exponential dendritic RP propagates from its sandwich complex anchor, and GOx-labeled primer complexes accumulate within the branched concatemeric RP. The immunomagnetic bead was again magnetically isolated from solution and

resuspended in fresh solution. Next, glucose and bromocresol purple pH indicator were added and the remaining RP-bound GOx drove a color change from purple (basic) to yellow (acidic) (Figure 2.16B, middle), generating a LOD of 0.94 pM of PDGF within 3.5 hours (Figure 2.16B, bottom). Many examples throughout this review have demonstrated the various ways to convert a linear RCA process to exponential for the ultrasensitive detection of analyte. However, this approach combined both exponential RCA with GOx-mediated detection, making for a relatively sensitive dual-exponential approach that could be evaluated by the naked eye. The use of magnetic beads was required to remove background RP as well as to carefully control the buffer capacity in the final detection step, key for the use of the pH indicator.

Huang *et al.*'s assay increased sensitivity by capitalizing on the fluorescence quenching ability of AuNPs. Aptamer-primer binding to nucleolin completed the sandwich assay formation, allowing tethered RCA to occur upon binding to leukaemia-derived exosomes (Section 2.4.2.1, Figure 2.5D).^[265] However, in this case the detection was based on hybridization of F-DNA probes bound to and quenched by a gold nanoparticle in the assay solution (Figure 2.16C, top). These quenched probes would preferentially bind to the target-triggered RP and be cleaved by a nicking endonuclease, separating it from the quenching AuNP and restoring fluorescence. The detection cycle can be repeated multiple times

per AuNP, providing an exponential signal enhancement beyond RCA, limited only by the number of probes immobilized on the AuNP surface (~55 probes per AuNP). This room-temperature approach could detect as few as 10^2 exosomes per μL in slightly more than three hours (Figure 2.16C, bottom). A drawback of this approach was the need to perform the nicking enzyme detection step after the completion of the linear RCA reaction to avoid the possibility of the nicking enzyme cleaving the CT (which must also include the nicking site to produce the complementary sequence), as this would halt RCA entirely.

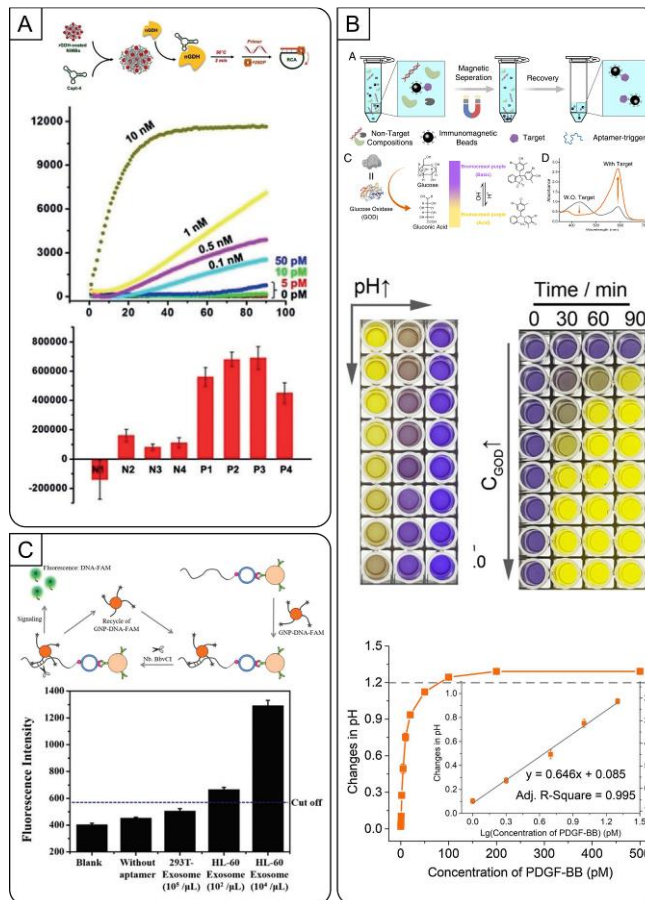


Figure 2.16. Heterogeneous FNA-RCA utilizing magnetic beads. (A) Epitope-specific detection of GDH using circular aptamers and SYBR Gold fluorescence detection of RP. (B) An immunomagnetic strategy for colorimetric pH sensing strategy with GOx for the detection of PDGF. (C) Fluorescence dequenching AuNP biosensing strategy for the detection of leukemia-derived exosomes. Figures adapted from references cited in text.

Table 2.2. Heterogeneous solution-based methods.

Separation Method	Detection Method	RCA Method	MRE Type	Regulation Method	Target	LOD	# Steps	Temperature	Assay Time	Ref.
Colorimetric detection										
centrifugation	4-nitrophenol	linear	aptamer	structure-switching ^[PLP]	aflatoxin M1 ^[CM]	0.05 ng/L	many	multiple	≥ 7 hrs	[311]
ethanol precipitation	intercalating dye	linear	DNAzyme	RCD	ATP	100 μM	many	multiple	≥ 4 hrs	[120]
magnetic bead	PMD	enzyme-assisted	aptamer	structure-switching ^[PLP]	cancer cells (ramos)	81 cells	many	multiple	≥ 6 hrs	[296]
magnetic bead	PMD	enzyme-assisted	aptamer	structure-switching ^[PLP]	lysozyme	7.2 fM	many	multiple	≥ 6 hrs	[296]
magnetic bead	PMD	linear	aptamer	sandwich (apt x2)	OTA ^[CM]	1.09 ng/mL	many	multiple	≥ 5 hrs	[300]
avidin bead	PMD	linear	aptamer	sandwich (apt 2x)	PDGF ^[CM]	~7.1 fM (0.2pg/mL)	2	multiple	≥ 2 hrs	[310]
magnetic bead	pH dye	dendritic	aptamer	sandwich (apt/Ab)	PDGF ^[CM]	0.94 pM	many	37 °C	≥ 3 hrs	[184]
magnetic bead	PMD	enzyme-assisted	aptamer	sandwich (apt x2) ^[PLP]	<i>V. parahaemolyticus</i> ^[CM]	10 cfu/mL	many	multiple	≥ 1 hr	[299]
Fluorometric detection										
magnetic bead	cDNA (MB)	enzyme-assisted	aptamer	structure-switching	17β-Estradiol (E2) ^[CM]	63.09 fM	many	multiple	≥ 3 hrs	[253]
magnetic bead	cDNA (MB)	linear	aptamer	structure-switching ^[PLP]	cocaine	0.48 nM	many	multiple	≥ 3 hrs	[135]
magnetic bead	cDNA (MB)	linear	aptamer	sandwich (apt/Ab)	EpCAM ^[CM]	10 BT474 cells	4	multiple	≥ 7 hrs	[250]
magnetic bead	cDNA (MB, F/Q)	enzyme-assisted	aptamer	sandwich (apt/Ab) ^[PLP]	exosomes ^[CM]	100 particles per μL exosomes	many	r.t.	≥ 3 hrs	[265]
magnetic bead	intercalating dye	linear	captamer	structure-switching (recombinant to native protein)	GDH ^[CM]	10 pM	many ^[RT]	multiple	≥ 1 hr	[113]
magnetic bead	cDNA (MB, F/Q)	linear	aptamer	sandwich (apt x2) ^[PLP]	MRSA ^[CM]	100 CFU/mL	many	multiple	≥ 2 hrs	[312]

centrifugation	intercalating dye	hyperbranched	aptamer	separation by spin-down, no switching ^[PLP]	MUC1 ^[CM]	4.27 x 10 ⁴ exosomes / mL	many ^[RT]	multiple	≥ 5 hrs	[132]
magnetic bead	cDNA (QD)	linear	aptamer	structure-switching ^[PLP]	OTA ^[CM]	0.2 pg/mL	many	multiple	≥ 5 hrs	[136]
magnetic bead	cDNA (QD)	linear	aptamer	inhibition RCA	OTA ^[CM]	0.13 ppt	many	multiple	≥ 1 hr	[245]
magnetic bead	intercalating dye	linear	aptamer	structure-switching ^[PLP]	tetracycline ^[CM]	0.724 pg/mL	3	multiple	≥ 6 hrs	[227]
magnetic bead	intercalating dye	linear	aptamer	sandwich (apt/Ab)	thrombin	2 nM	many ^[RT]	multiple	≥ 2 hrs	[229]
centrifugation	cDNA (MB)	linear	aptamer	structure-switching (rGO)	thrombin	1 pM	many	multiple	≥ 2 hrs	[111]
magnetic bead	intercalating dye	linear	aptamer	sandwich (apt/bead fixation)	Tip60 ^[CM]	220 fM	many	multiple	≥ 3 hrs	[228]

[a] Table Footnote. [b] ... ^[RT] denotes that detection was done with real-time monitoring; ^[PLP] denotes that the assay used a padlock probe ligation reaction; ^[CM] denotes that the assay was tested with complex media; “many” denotes any assay that required 4 or more steps; r.t. denotes that room temperature was used.

2.8 Solid-phase Assays

POC biosensors that utilize the solid-phase in lieu of solution phase are the most likely to be practically applied for real-world applications as many aspects of solid-phase device design intend to simplify user handling steps and increase portability. In solid-phase assays, a portion of the assay components is tethered to a solid surface with the rest free in solution. We focus on solid-phase most often used with POC testing, including the surface of beads (as discussed in S5), glass slides, microwell plates, microfluidic channels, or on paper. With proper care and optimization, FNA-based biosensors that utilize RCA can be integrated into these formats to create powerful, portable devices with an integrated amplification system primed for ultrasensitive detection. Individual POC applications may have unique characteristics and demands that make certain strategies more practical than others. For instance, paper-based biosensing offers a host of advantages compared to using glass or plastic surfaces. Likewise, lateral flow devices allow for simple on-device separations or timed reactions. As such, it is imperative that the assay requirements are well understood such that the best combinations can be selected. In this section, we will focus on these solid-phase mediums that can be detected optically, and the considerations for different surface formats are discussed. A summary of solid-phase examples can be found for colorimetric-based methods in Table 2.3 and fluorometric-based methods in Table 2.4.

2.8.1 Microwell plates and glass slides

Bulk solid immobilization differs from bead immobilization in many ways, and each offers its own advantages and disadvantages compared to their particulate counterparts. While a bulk solid and a particulate solid may have the same volume, their effective surface area differs greatly. The strategies for washing these two different solid surfaces differ, as one is dispersed within solution and the other is submerged within. Commonly these assays will incorporate multiple steps including washing steps, and the use of optical instrumentation to allow for high-throughput analysis. High-throughput analysis is not necessarily applicable at the POC directly, but surely these approaches can simplify, expedite analysis, and decrease costs in those scenarios where basic optical instruments can be maintained. Specifically, microwell plate-based analysis is highly attractive for real-time analysis.

Cheng and co-workers utilized AuNP-DNA to hybridize to RP immobilized on glass slides, further improved by their application of silver enhancement (Figure 2.12A, top).^[115] This scanometric method did not require sophisticated instrumentation but did require washing steps to remove unbound AuNPs that contribute to background signal. The authors covalently immobilized an aptamer-primer and CT on a glass slide, competitively binding with either the target or the CT (Section 2.4.1.1). Any unbound VEGF or displaced CT was removed from solution with a washing step and phi29 DP was added to initiate RCA. Where VEGF had bound to aptamer, no RCA was generated, creating an inhibitory assay. Next, AuNP-DNA was allowed to hybridize with the RP and

was followed by a silver enhancement step to further improve the visibility of the detection probe, which could be visualized with a simple flatbed scanner and quantified. Despite several washing steps, this four-step isothermal (37 °C) approach was able to achieve an ultralow detection limit of 10 fM of VEGF in just over 3 hours (Figure 2.17A, bottom).

Wang *et al.* exploited AuNP's peroxidase activity to develop an ultrasensitive sensor for thrombin detection.^[146] Here, the authors used an inhibition RCA regulation method with a thrombin captamer such that target binding prevents RCA (Section 2.4.2.1, Figure 2.6D) (Figure 2.17B, left). Hydrogen peroxide reduced gold (III) to form well-dispersed AuNPs that are a characteristic red color indicating an absence of thrombin. Conversely, target-triggered RCA generated PMD-rich RP which competes to reduce hydrogen peroxide into water and oxygen gas. A decrease in available hydrogen peroxide slows the kinetics of AuNP growth and results in AuNPs with poor morphology and a tendency to aggregate, leaving a characteristic blue color in solution. This ultrasensitive approach was able to achieve a detection limit of 10 aM for thrombin in just over 4 hours (Figure 17B, right), which is particularly impressive for a colorimetric assay. The PMD strategy is the most widely used colorimetric approach for FNA-linked RCA assays, and typically achieves detection limits in the femto- to picomolar ranges. Here, the same modifications of CT are required but utilizing gold as a redox agent has proved to be very effective relative to the commonly used TMB or ABTS alternatives.

Zhan *et al.* demonstrated an example of colorimetric bacterial detection in food samples using microwell plate detection of *L. monocytogenes* (Figure 2.17C, left).^[256] The authors state their intention to develop a test to compete with the standard ELISA assay, as ELISA been accepted as the gold-standard for antibody-based biosensors, noting their assay's competitive LOD when compared to similar antibody-based tests. This device (and other sandwich-like RCA assays) required several steps and a comparable assay time (over 5 hours) indicating that there is high demand for these tools despite the technical skill required. Structure-switching aptamers were immobilized on the surface, primed to release the aptameric sequence through target binding to *L. monocytogenes* (Section 2.4.1.1), leaving an exposed primer for RCA. Biotinylated DNA and streptavidin-tagged HRP were added to the wells for hybridization to the surface-tethered RP. The HRP converted TMB from colorless to yellow in a target-dependent manner leading to the quantification of *L. monocytogenes* with a detection limit of 460 CFU/mL. This isothermal (37°C) assay successfully detected target in spiked fresh lettuce samples, showing the approach's applicability for food-based detection (Figure 2.17C, right).

In situ RCA analysis allowed Gao *et al.* to distinguish between six cancer cell lines by independently monitoring three different plasma membrane protein (PMP) targets: MUC1, EpCAM, and HER2 (Figure 2.17D, top).^[252] Here, the cells were fixed on glass slides to allow for subsequent washing steps to remove unbound probes. Once immobilized, aptamer-primer sequences bound

available PMPs and the primer end was free to initiate RCA (Section 2.4.2.1). Nicking enzymes nicked bound MB probes, restoring fluorescence for quantification of each target. The authors report they were able to detect as low as 25 copies per cell (or 166 aM) of PMPs based on an analysis of 100 cells. Further, the authors were able to distinguish and identify cell types by running the assay in parallel with different aptamer probes for PMP profiling (Figure 2.17D, bottom), providing a useful multiplexing approach. An important caveat here is that the RCA reaction and amplification must occur consecutively, limiting the ability for real-time RP monitoring. Further, a temperature of 37 °C for 60 min was required to allow optimal function of the nicking enzyme, a common observance for enzyme-assisted amplification strategies

Most FNA-based optical detection platforms using RCA focus on the monitoring of wavelengths in the visible spectrum, either via color or fluorescence. Lv *et al.* showcased a portable smart-phone based infrared-based thermal assay for the sensitive detection of PSA using CuxS, a heat-active nanocrystal, tethered to a DNA strand (CuxS-DNA) as the hybridization probe.^[314] For the assay, an antibody-aptamer sandwich complex was used to perform PLP (Section 2.4.2.1, Figure 2.5D) on a microwell plate in several steps. Linear RCA was generated on the microwell surface and CuxS-DNA was hybridized to the RP (Figure 2.17E, left). Heat from an IR laser was absorbed by CuxS, increasing the solution temperature and with temperature changes monitored using a smartphone with an infrared thermal imager equipped. The

authors reporting a detection limit of 0.2 ng/mL of PSA in just over 5 hours (Figure 2.17E, right) and could potentially be used as an optical detection strategy in otherwise optically challenging mixtures. With the thermal monitoring being conducted at 20°C, we suspect careful calibration of the assay would be required in different environments. Notably, beyond incorporating a smartphone for signal detection, it can also be used for data transmission for interpretation by highly qualified personnel that may not otherwise be present at the POC.^[315]

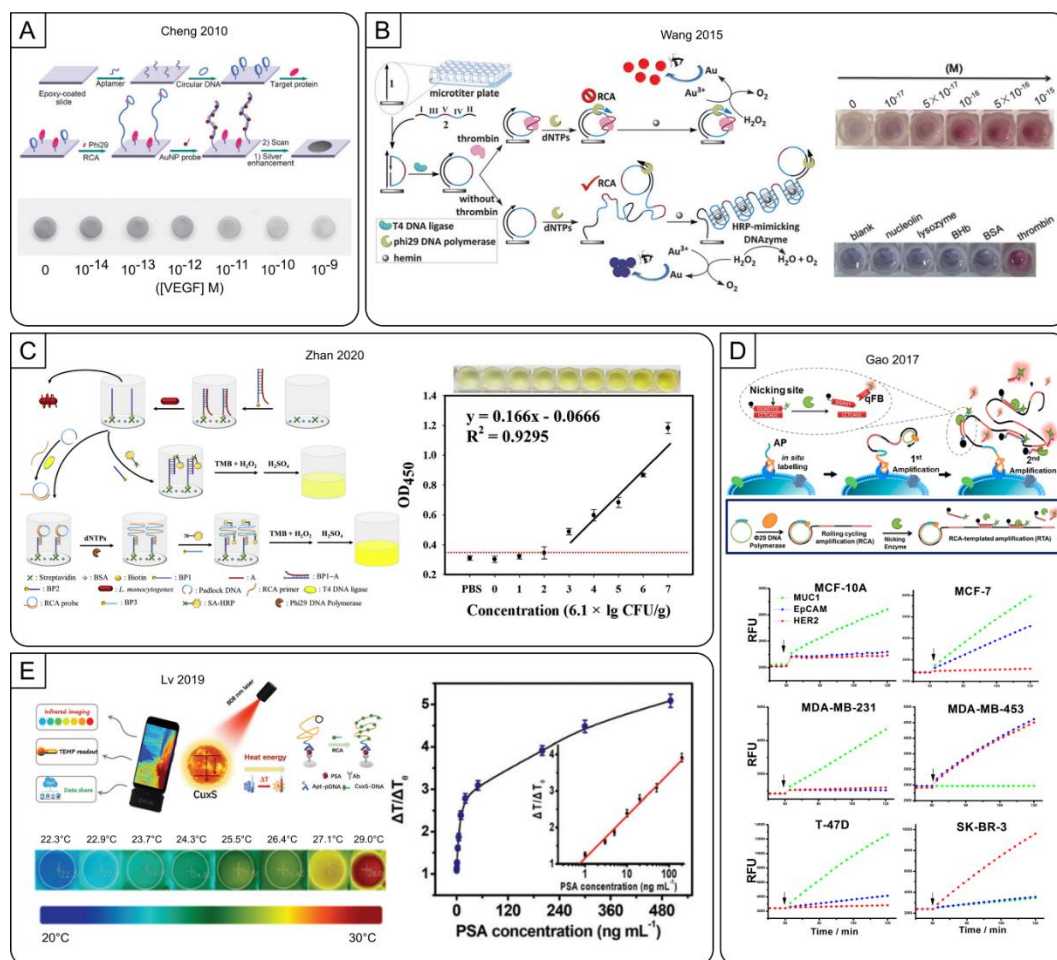


Figure 2.17. Microwell plate and glass slide-based FNA-RCA assays with optical detection methods. (A) An aptamer-initiated RCA method for the scanometric detection of VEGF. (B) An inhibitory aptasensor using HRP-mimicking DNAzymes for the reduction of AuNPs and the visual detection of thrombin. (C) Foodborne pathogen RCA-linked aptasensor using colorimetric detection of catalytic HRP action. (D) Quantitation of plasma membrane proteins using an in situ aptasensing approach with fluorometric RP detection. (E) A portable smart-phone infrared-based thermal aptamer-RCA assay for the detection of PSA. Figures adapted from references cited in text.

2.8.1 Microfluidic Devices

Microfluidic devices operate miniaturized assays that utilize extra low volumes, manipulating liquids in apparatus' on a nanometer to micrometer scale.^[316] Microfluidic devices often prioritize the all-in-one aspect of their design, in that all aspects of the assay proceed without user intervention. Analysis of small volumes in turn requires less reagents, solvents, and assay time, making them an obvious choice for POC designs. Microfluidic devices use comparatively less volume than conventional patient sampling, which may be attractive for invasive and/or frequent sampling measures, such as blood drawing. However, with such small volumes, detection of trace analytes can be a challenge, necessitating on-board amplification strategies. RCA can be paired with microfluidic devices to enhance target signal despite the relative low abundance of target in these small volumes. Another key feature of microfluidic approaches is that the fluidic system can automate sequential steps and direct flow through from one region to another, mimicking separation steps. With such small sample volumes on-board heating elements can be incorporated to rapidly heat solutions to regulate temperature-sensitive reactions or facilitate dissociation of key assay components. The caveat is that this necessitates the use of a power source for the on-board pumps or heaters, complicating its use at the POC.

Feng et al. incorporated a unique open-space microchip for integrating cell culturing with the detection of VEGF that took advantage of fluid flow on

a solid surface.^[317] In this design, the chip was segmented in half by a connecting channel containing an interfacial tension valve that prevented the flow of reagents from one end to the other, specifically enabling sequential reactions. On one end of the chip was the cell culture chamber, and on the other end of the interfacial tension valve was a capture aptamer immobilized on the microchip surface (Figure 2.18A, top) By connecting the two reservoirs, the VEGF excreted into the extracellular matrix flowed to the capture zone and was immobilized (Figure 2.18A, bottom),. The channel was again severed and a signalling aptamer was added to the capture zone to form a sandwich for PLP generation (Section 2.4.2.1, Figure 2.5D). The authors were able to detect as low as 10 pg per mL of VEGF, requiring only 10 μ L of solution and just under 2 hours using fluorescently labelled cDNA. Further, as the chip had on-board cell culturing, inducing a hypoxic cellular microenvironment was confirmed by the measured increased secretion of VEGF into the extracellular matrix.

Microchip devices are designed from the inception with portability in mind, making it logical to pursue detection strategies that can be detected by eye without bulky instrumentation. Integrated devices are well-suited for on-site detection for this reason. The microchip device developed by Lin *et al.* for thrombin detection, a model analyte for protein biomarkers, anticipated the need to dilute their real-blood samples to minimize matrix interferences by incorporating RCA.^[140] The device itself was produced

using soft-lithography technology to design the μm -wide channels. Blocking of the microchannel surface with fetal bovine serum was necessary to prevent the absorption of the protein matrix as unblocked channels lead to high recoveries despite the samples being diluted a thousand-fold. The assay is triggered by aptamer-target binding using dual aptamers (Section 2.4.2.1, Figure 2.5D) resulting in RP immobilization within the microchip. Colorimetric detection is enabled through the accumulation of PMD-rich RP and the redox conversion of TMB to its colorimetric form (Figure 18B, middle). In as little as 45 minutes, this colorimetric device was able to detect thrombin with an LOD of 0.083 pg/mL with only 15 minutes of amplification (Figure 2.18B, bottom). Even more impressively, this was achieved with as little as 25 μL of samples or reagents, as they demonstrated in their assessment of real human serum samples.

3-D printed RCA devices can be tuned for POC testing, as demonstrated by an on-site chip for mercury detection developed by Lim and co-workers.^[297] This turn-off assay demonstrated sensitivity for inorganic mercury through generation of PMD-containing RPs by eye and by portable spectrophotometer. Though there is no aptamer for mercuric ions, they are capable of binding between two thymine residues to stabilize T-T mismatches, as such a twelve nucleotide polyT primer was used for mercuric ion capture. In this inhibition RCA strategy (Section 2.4.1.1, Figure 2.2D), unbound aptamer could be linearly amplified and rapidly heat

denatured by an on-board Peltier heating module. Heating narrow channels and low volumes can be a rapid and energy efficient task. Further, pairing this device with a temperature control module minimizes user error as the temperatures can be better regulated. Here, a fluid pump was required to transfer the RP to a detection reservoir (Figure 2.18C, top), where the RP-PMD sequences reduced ABTS for colorimetric detection by a portable colorimetric reader (Figure 2.18C, middle). This 30-minute assay demonstrated an LOD of 3.6 $\mu\text{g/L}$ in spiked tap water samples, comparable to conventional ICP/MS analysis (Figure 2.18C, bottom). Further, as this microfluidic device is printed rapidly on commercially available 3D printers, it highlights the strengths of 3D printing for accessible POC assays. As well, the same authors recently reported a similar on-site chip for mercury detection without the need for a fluid pump, with fluid transfer being achieved with a commercial 8-well multichannel pipette (LOD of 3.4 $\mu\text{g/L}$ and 4.1 $\mu\text{g/L}$ in simple, and environmental matrices, respectively).^[298]

He *et al.* integrated capillary electrophoresis into a microfluidic chip for the simultaneous detection of kanamycin, AFM1, and E2 in milk samples.^[318] Requiring a total assay time of just over 1 hour using low temperatures ($\leq 30^\circ\text{C}$), the authors were able to achieve multiplexed detection limits of 10 pg/mL for kanamycin, 0.95 pg/mL for AFM1, and 6.8 pg/mL for E2, and were able to do so in spiked milk samples as well. The very short turnaround time and ability to detect multiple targets in tandem

offers tremendous advantage despite the trade-off of requiring magnetic bead washing steps. The authors utilized the tripartite 3'-exonuclease system (Section 2.4.1.1, Figure 2.3A), immobilizing a mixture of three unique tripartite systems (one for each target) onto magnetic beads (Au-Fe₃O₄) to create the probes (Figure 2.18D, left). The sample was incubated with magnetic probes and phi29 DP and incubated at 30°C for 50 minutes, when the RP-labelled magnetic beads were collected and hybridized with unfunctionalized cDNA at room temperature. The recovered supernatant was flowed through a microfluidic device for on-chip capillary electrophoresis using an intercalating dye (Figure 2.18D, right). The remaining unhybridized cDNA probes were inversely proportional to target concentration and could be size separated and quantified after just 3 minutes. For a future iteration, it may be beneficial to integrate all steps into a microfluidic chip, however the multiplexing here provides a clear advantage.

In another example, He et al. developed a ratiometric microfluidic chip that could quantify kanamycin in milk and fish samples.^[319] Here, the authors used a structure-switching aptamer hybridized to an RCA primer, with the aptamer component tethered to a gold stir bar (Section 2.4.1.1, Figure 2.2A) (Figure 2.18E, top). With target addition triggering structure-switching and the subsequent release of the primer, the authors could remove the stir bar to isolate only the liberated primers. Addition of a CT

triggered linear RCA by Bst DP and labelled with SYBR Gold, finally separated by on-chip capillary electrophoresis (Figure 2.18E, middle). By intentionally keeping the amplification time short at 30 minutes, the authors could track the ratio of RP to CT for quantification of kanamycin. As more CTs were activated for RP generation, the proportion of RP-bound CTs to free CTs increased and this ratiometric relationship could be used to quantify the small molecule target. In just over one hour, they could detect as low as 0.3 pg per mL (Figure 2.18E, bottom) with validation in milk and fish samples.

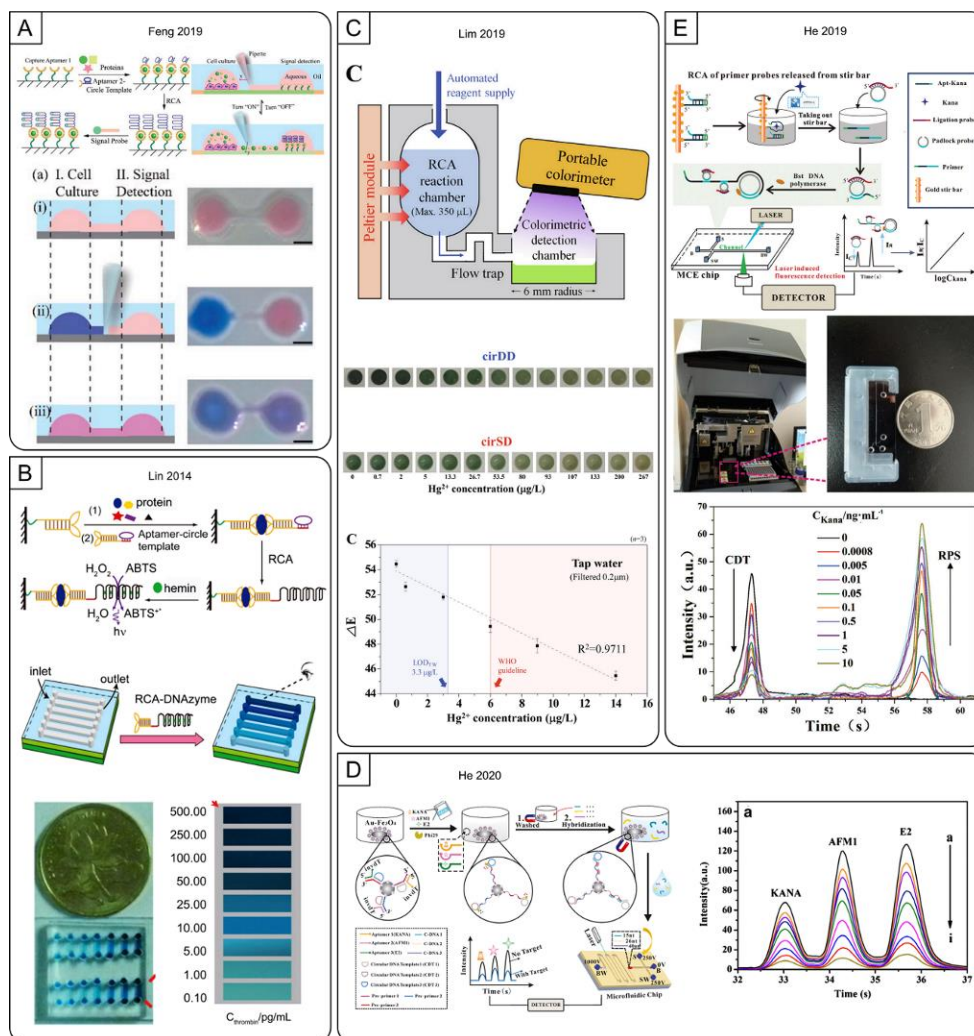


Figure 2.18. Microfluidic FNA-RCA devices with optical detection methods. (A) A cell culturing microfluidic chip for colorimetric detection of VEGF via RCA (B) A portable thrombin-detecting microchip for visual detection of RCA-generated hemin/G-quadruplexes. (C) A portable pumpless 3D-printed multiarray chip for on-site colorimetric detection of Hg^{2+} . (D) A microfluidic aptasensor for simultaneous detection of kanamycin, aflatoxin M1, and 17β -estradiol based on magnetic tripartite DNA assembly nanostructure probes (E) A ratiometric aptasensor for kanamycin using stir-bar assisted sorptive extraction and RCA. Figures adapted from references cited in text.

Table 2.3. Colorimetric-based solid-phase methods.

Surface Type	Detection Method	RCA Method	MRE Type	Regulation Method	Target	LOD	# Steps	Temperature	Assay Time	Ref.
microchip	PMD	linear	aptamer	inhibition RCA	Hg ²⁺ ^[CM]	3.3 µg/L	many	multiple	≥ 1 hr	[297]
microchip	PMD	linear	aptamer	inhibition RCA	Hg ²⁺ ^[CM]	3.4 µg/L	many	multiple	≥ 1 hr	[298]
microwell plate	cDNA (enzyme)	linear	aptamer	structure-switching	Hg ²⁺ ^[CM]	1.6 nM	many	37 °C	≥ 5 hrs	[257]
microwell plate	cDNA (enzyme)	linear	aptamer	structure-switching	<i>L. monocytogenes</i> ^[CM]	460 CFU/mL	many	37 °C	≥ 4 hrs	[256]
glass slide	PMD	linear	aptamer	cell fixation	MCF-7 ^[CM]	10 cells/mL	many	multiple	≥ 2 hrs	[131]
microwell plate	cDNA (enzyme)	linear	aptamer	sandwich (apt/Ab) ^[PLP]	PDGF ^[CM]	3.1 pM	many	37 °C	≥ 5 hrs	[255]
microwell plate	cDNA (enzyme)	thrombin-assisted	aptamer	sandwich (apt/Ab) ^[PLP]	PDGF ^[CM]	31 pM	many	37 °C	≥ 5 hrs	[320]
microchip	PMD	linear	aptamer	sandwich (apt 2x)	thrombin ^[CM]	0.083 pg/mL	many ^[RT]	multiple	45 min	[140]
microwell plate	PMD	linear	captamer	inhibition RCA	thrombin	10 aM	many	multiple	≥ 3 hrs	[146]
glass slide	cDNA (AuNP)	linear	aptamer	inhibition RCA	VEGF ^[CM]	10 fM	many	37 °C	≥ 3 hrs	[115]

[a] Table Footnote. [b] ... ^[RT] denotes that detection was done with real-time monitoring; ^[PLP] denotes that the assay used a padlock probe ligation reaction; ^[CM] denotes that the assay was tested with complex media; “many” denotes any assay that required 4 or more steps; r.t. denotes that room temperature was used.

Table 2.4. Fluorometric-based solid-phase methods.

Surface Type	Detection Method	RCA Method	MRE Type	Regulation Method	Target	LOD	# Steps	Temperature	Assay Time	Ref.
microchip	intercalating dye	linear	aptamer	structure-switching	17 β -Estradiol (E2) ^[CM]	6.8 pg/mL	many	multiple	≥ 1 hr	[318]
microchip	intercalating dye	linear	aptamer	structure-switching	aflatoxin M1 ^[CM]	0.95 pg/mL	many	multiple	≥ 1 hr	[318]
glass slide	cDNA (fluorophore)	linear	DNAzyme	ligase ^[PLP]	ATP	10 μ M	many	multiple	≥ 3 hrs	[147]
microwell plate	cDNA (fluorophore)	linear	aptamer	sandwich (apt/Ab)	cTnI ^[CM]	14.40 pg/mL	many	multiple	≥ 8 hrs	[321]
microchip	cDNA (fluorophore)	linear	aptamer	sandwich (apt/dend) ^[PLP]	E. coli	100 cells/mL	many	multiple	≥ 5 hrs	[130]
microchip	cDNA (fluorophore)	linear	aptamer	sandwich (MRE to capture, FNA to detect) ^[PLP]	E. coli ^[CM]	80 cells/mL	many	multiple	≥ 3 hrs	[246]
glass slide	cDNA (MB)	nicking-assisted	aptamer	cell fixation ^[PLP]	EpCAM	100 cells	many ^[RT]	37	≥ 2 hrs	[252]
glass slide	cDNA (MB)	nicking-assisted	aptamer	cell fixation ^[PLP]	HER2	10 cells	many ^[RT]	37	≥ 2 hrs	[252]
microchip	cDNA (fluorophore)	linear	aptamer	sandwich (apt/Ab)	IL-8 ^[CM]	0.84 pM	many	37	30 min	[322]
microchip	intercalating dye	linear	aptamer	structure-switching	kanamycin ^[CM]	10 pg /mL	many	multiple	≥ 2 hrs	[319]
microchip	intercalating dye	linear	aptamer	structure-switching	kanamycin ^[CM]	0.32 pg/mL	many	multiple	≥ 1 hr	[318]
microchip	cDNA (MB)	linear	aptamer	sandwich (apt x2)	MMP ^[CM]	31.25 ng/mL	many	multiple	30 min	[251]
glass slide	cDNA (MB)	nicking-assisted	aptamer	cell fixation ^[PLP]	MUC1	10 cells	many ^[RT]	37	≥ 2 hrs	[252]
glass slide	intercalating dye	linear	aptamer	structure-switching ^[PLP]	PDGF	8 nM	many	multiple	≥ 4 hrs	[125]
microwell plate	cDNA (CuxS) (thermal)	linear	aptamer	sandwich (apt/Ab) ^[PLP]	PSA	0.2 ng/mL	many	multiple	≥ 5 hrs	[314]
microchip	cDNA (fluorophore)	linear	aptamer	sandwich (apt x2) ^[PLP]	VEGF ^[CM]	10 pg/mL	many	multiple	≥ 1 hr	[317]

[a] Table Footnote. [b] ... ^[RT] denotes that detection was done with real-time monitoring; ^[PLP] denotes that the assay used a padlock probe ligation reaction; ^[CM] denotes that the assay was tested with complex media; “many” denotes any assay that required 4 or more steps; r.t. denotes that room temperature was used.

2.8.3 Paper-based Biosensors

Cellulose-based surfaces are an ultra-low cost option for point of care assays, capitalizing on the natural wicking properties of the paper surface to manipulate liquids. Few modern substrates can be so inexpensive so as to accommodate low-resource areas and to justify their use over the superior technology offered in a lab setting, and paper is simultaneously widely available and cheap. Likewise, the inherent wicking properties of paper to transport material from one location to another without the need for any on-board fluid pumps as is the case with microfluidic-based strategies. A summary of the paper-based methods discussed herein can be found in Table 2.5.

Kim and co-workers elegantly exploited the immobility of RP in a colorimetric dot blot assay for the sensitive detection of mercuric (Hg^{2+}) ions (Figure 2.14A, left).^[233] The authors applied an inhibition RCA method using a polyT DNA sequence for mercury capture or as a primer for RCA (Section 2.4.2.1, Figure 2.2D). After incubation with Hg^{2+} , AuNP-labelled DNA and the reagents to initiate RCA were added. The 30-minute RCA reaction was heat inactivated and the solution was spotted into a nitrocellulose membrane and dried for 20 minutes. Typically, the amplicons generated by RCA are so large that transporting them across a membrane can be challenging (see Section 2.5.3 on RCA as MRE) whereas AuNP-labelled DNA is much smaller, readily wicking across a test strip. In the

absence of RP the small AuNP-labelled DNA migrated and dried in a wide spot with elevated concentration in a concentric ring on the outer edge of the spot (Figure 2.19A, top right). When RP was generated the red color of the AuNPs was localized in the center of the droplet owing to the inability of the large RP to migrate. At just 2 hours, this simple three-step assay allowed for the detection of as low as 21.8 nM of Hg²⁺ in real samples (Figure 2.19A, bottom right), better than the 30 nM allowable limit for mercuric ions in drinking water as outlined by the WHO. Though only the detection step was done on paper, with the recognition and amplification steps conducted in solution, the utility of paper for integrated separation steps is evident as simply spotting the solution on the nitrocellulose surface was sufficient.

Recently we generated a simple isothermal RCA-linked FNAB on a cellulose surface without the need for any blocking steps or immobilization of DNA materials (Section 2.4.1.1, Figure 2.2D) (Figure 2.19B, left).^[101] Similar performance between both SYBR Gold and QuantiFluor dyes was observed in solution, however QuantiFluor alone was found to be compatible with cellulose, maintaining low background fluorescence. We exploited this finding to generate a simple pullulan-coated paper-based RCA assay for the real-time detection of thrombin (the benefits of pullulan-encapsulated reagents are discussed below). Thrombin was incubated with its aptamer for 15 minutes followed by spotting onto cellulose paper

containing pullulan-encapsulated RCA reagents for a 15-minute RCA reaction at room temperature. The presence of thrombin prevented the aptamer from being used as a primer to initiate RCA. With this strategy, rapid real-time detection of picomolar levels of thrombin was achieved within just a two-step 30-minute assay both in solution (100 pM) and on paper (250 pM) without the need for any heating, expensive labelling, surface treatment or blocking steps (Figure 2.19B, right). Here, we demonstrated that in contrast to QuantiFluor, certain dyes such as SYBR Gold, can produce significant background fluorescence upon binding to cellulose, making them unsuitable for paper-based sensor platforms.

RCA-based FNABs have multiple reagents that need to be stabilized to ensure their accuracy over time, an important consideration when considering the long-term storage options for real-world use. This may be especially true in low-resource and remote environments at room temperature. The utility and durability of papers such as cellulose and nitrocellulose has made them an attractive platform for a variety of POC biosensors.^[48,53,323] Our laboratory has worked to expand the applicability of many of our recent biosensors through the use printable pullulan bioink as well as pullulan tablets for storage and application of labile enzymes and substrates.^[324–326] Pullulan, a naturally produced polysaccharide can be used as a simple and inexpensive material for the encapsulation of otherwise labile reagents (Figure 2.19C, top). Pullulan tablets retain high

assay activity for weeks with room temperature storage thanks to the entrapment and immobilization of reagents in a water soluble oxygen impermeable environment.^[324–326] Challenging assays in particular may benefit from use of pullulan by simplifying the assay procedure and stabilizing sensitive reagents (Figure 2.19C, middle).^[219,326,327] At approximately 1 USD per 100 tablets, this method is low cost and well-suited for use in the developing world. Recently, our lab showcased the ability to immobilize a primer on a nitrocellulose surface and initiate RCA (Figure 2.19C, bottom), much like what has been well-established on magnetic beads or microwell plates. As mentioned in S4, improved RCA efficiency was observed owing to a molecular crowding effect causing an increase in local concentrations of RCA reagents.^[98] The same report demonstrated detection of surface-generated RP using a variety of methods including the incorporation of radiolabelled dNTPs, cDNA tagged to gold nanoparticles, the incorporation of PMDs, and the addition of fluorescently tagged cDNA. Several of the recent paper-based assays that utilized RCA have been simplified^[98,101,112,309,328] or long-term stabilized^[98,112] through the use of pullulan encapsulation.

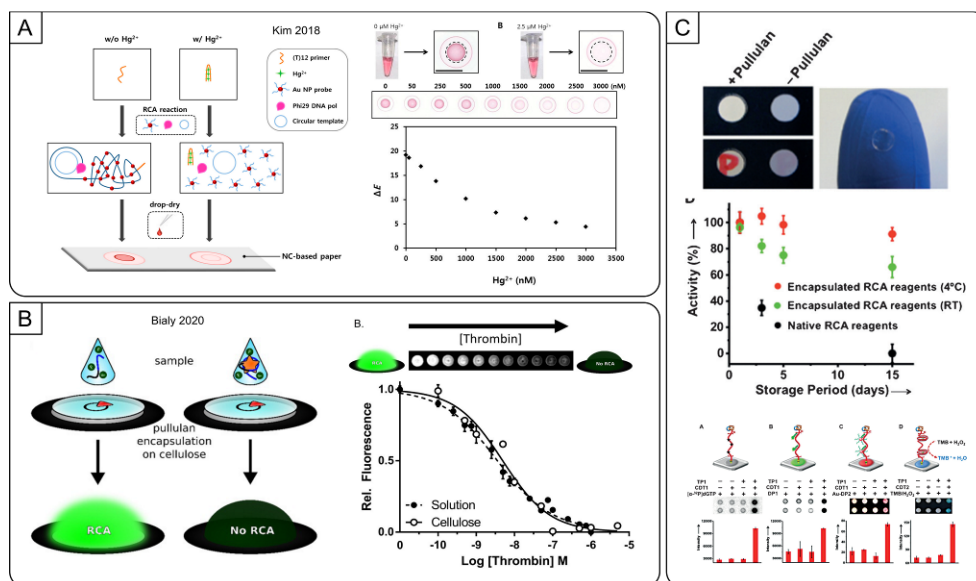


Figure 2.19. Paper-based devices with optical detection methods. (A) Hg^{2+} colorimetric dot blot assay utilizing AuNP aggregation with FNA-triggered RP. (B) A simple isothermal RCA-linked FNAB for the fluorometric detection of thrombin. (C) A structure switching aptasensor using pullulan encapsulated RCA-components. Figures adapted from references cited in text.

G-quadruplex DNAzyme functionality can be incorporated into paper-based assays, especially in FNA-RCA based assays that can act to amplify the colorimetric method's signal with amplification. Li and colleagues reported a paper-based assay^[114] that utilized a captamer (Section 2.4.2.2, Figure 2.6B) for colorimetric detection via the peroxidase-mimicking DNAzyme PW17.^[43,329–333] In solution, the captamer was bound to an rGO surface and was released upon binding to the PDGF target. Rational NA design was paramount in this assay, not only because the CT acted as an aptamer and template for PW17 generation, but also because the CT showed remarkable resistance to nuclease degradation from cell lysates,

an important consideration for POC applications. Once this sample was introduced on paper, RCA was initiated by binding of the captamer to a primer encapsulated within a pullulan-coated paper surface. As the CT also contained the antisense strand for PW17, the RP was capable of converting TMB to colored TMB⁺ for colorimetric detection with a limit of 10 pM for the protein target.

Lateral flow devices (LFDs) are an excellent example of utilizing the inherent wicking properties of paper for integrating sequential steps. Key materials can be immobilized on different sections of the paper and a solution can be wicked across it in a sequential manner. LFDs can be used to incorporate separation of unbound AuNP-DNA without a dedicated washing step. LFDs are a popular test format familiar both to regulatory bodies and the general public due to the popularity of the at-home pregnancy test. This is in part due to their overall simplicity for the end-user, including their operational simplicity. It should be noted that despite the popularity of AuNP-based lateral flow assays, the bulky size of RP can make it difficult for them to move along the LFD membrane. While there are now several examples of NA-based lateral flow detection with RCA,^[334,335] the space remains open for FNA-based contributions.

Nonetheless, there are several FNA-based examples that incorporate natural wicking and paper origami for sequestering reagents and assay timing. Hui *et al.* reported one such paper-based assay utilizing peroxidase-

mimicking DNAzymes for colorimetric detection of both NA and non-NA bacterial markers.^[112] This pullulan-coated device used a bridged paper design to control sample flow (Figure 2.20A, top). This assay was the first aptamer-regulated ITA assay to be accomplished on a paper device. In the first region, the presence of target liberates an aptamer from an rGO surface adsorbed onto nitrocellulose to perform structure-switching primer release (Section 2.4.1.1, Figure 2.2C). The rGO surface acted both as a regulator of primer release, and also protected the aptamer sequences from degradation in the tested clinically relevant matrices. Bridging the paper allowed for the controlled flow of free aptamer to an amplification region where the aptamer could act as a primer for RCA initiation. This bridge used the inherent filtering properties of paper as the sample flowed from sample zone to detection zone, an important advantage in assays with complex matrices. It also prevented unclear colorimetric readout in the detection zone by preventing mixing with coloured matrices like stool. Colorimetric sensing showed similar sensitivity to unamplified fluorescent detection for both ATP and GDH, allowing colorimetric detection of the pathogen by eye. For both fluorescent and colorimetric detection, the LODs for the ATP sensor the GDH sensors were 10 μ M and 3 nM, respectively (Figure 2.20A, middle). In this case, amplification was essential for equipment-free detection, but can also be performed more quickly where the equipment is available by omitting the amplification step. The robustness of each test

was verified by using spiked human blood samples (ATP) and spiked stool samples (GDH) (Figure 2.20A, bottom). Where many of the sensors described in this review used either ABTS or TMD as the colorimetric reagent, the authors observed that combining ABTS and TMB together provided the best balance of rapid color change and maintaining color intensity. This is an important consideration for prolonging the measurement window for accurate analyte quantification. At the POC, personnel may not be immediately available to record the colorimetric readout within a narrow 1-minute range, with any delay possibly causing invalidation of the assay. By stabilizing the color change for a longer time period, the assay becomes functionally more robust for the end-user.

Another advantage to paper-based devices is that creative uses of origami can be incorporated for biosensing. Sun *et al.* demonstrated as much in their origami paper-based sensor for *E. coli* detection.^[309] Here, the authors created a four-panel origami sensor (Figure 2.20B, left). Panel A was an absorbent pad, and panel B contained the dried buffer for cell lysis of *E. coli*. Panel C contains nanoflowers functionalized with *E. coli*-specific RCD. A pullulan solution containing RCA reagents is printed onto panel D. First, cell lysis of *E. coli* occurs on panel B and then panels B, C, and D are folded together. The free bacterial intracellular matrix is able to flow vertically through the cellulose onto panel C where target-dependent cleavage of the substrate strand is achieved (Section 2.4.1.3, Figure 2.4A).

Through the same vertical capillary flow, the cleaved DNA fragment is captured in panel D where it is used as the primer for subsequent linear RCA. As the CT contains the sequence for PMD formation, the resultant RP can be combined with TMB, hemin, and hydrogen peroxide to generate a colorimetric signal proportional to the *E. coli* concentration. With this approach, the authors achieved a detection limit of 100 CFU per mL within only 35 minutes (Figure 2.20B, right), and was validated in juice and milk samples. Impressively, the cell lysis step required only 3 minutes though washing steps were required prior to initiating the cleavage reaction. Though the cleaved substrate strand required PNK treatment, the authors simply added the PNK into the pullulan mixture thus no additional step was required. Likewise, after approximately 30 minutes of cleavage, PNK treatment, and linear RCA, fresh hydrogen peroxide and TMB was added to panel D and colorimetric results were recorded within 1 minute by a digital camera. Here, several reactions were integrated into a single origami paper strip with separation of reagents occurring by the inherent wicking properties of the paper surface. Though rapid, it is important to note that the PMD reaction is time sensitive and quantification efficiency can be adversely impacted by measuring the colorimetric result after 5 or 30 minutes instead of the 1 minute recommended by the author.

In another example utilizing nanoflowers, Liu et al. created a paper device for the detection of toxin B, a *C. difficile* biomarker.^[328] The paper

device consisted of a sensing zone separated by a disconnected bridge to a detection region (Figure 20C, left). The sensing zone had NFs containing repeat sequences of hybridized aptamer-primer complexes (Section 2.4.1.1, Figure 2.2A). The detection and control zones each contained pullulan-encapsulated RCA reagents, though the control zone alone featured a control primer. Upon addition of target to the sensing zone, liberated primers were wicked with the buffer to the detection zone using a connecting paper bridge. This dissolved the pullulan and triggered linear RCA in the test zone proportional to toxin B, and in the control zone independent of toxin B concentration. This colorimetric PMD approach provided a detection limit of 600 pM with an RCA time of 15 minutes and a total assay time of 40 minutes (Figure 2.20C, right). Increasing the RCA time to 30 minutes improved the detection limit ten-fold to 60 pM, and validated in spiked stool samples. As with other PMD-based colorimetric detection methods, fresh TMB and hydrogen peroxide was added and the colorimetric result was recorded within 1 minute.

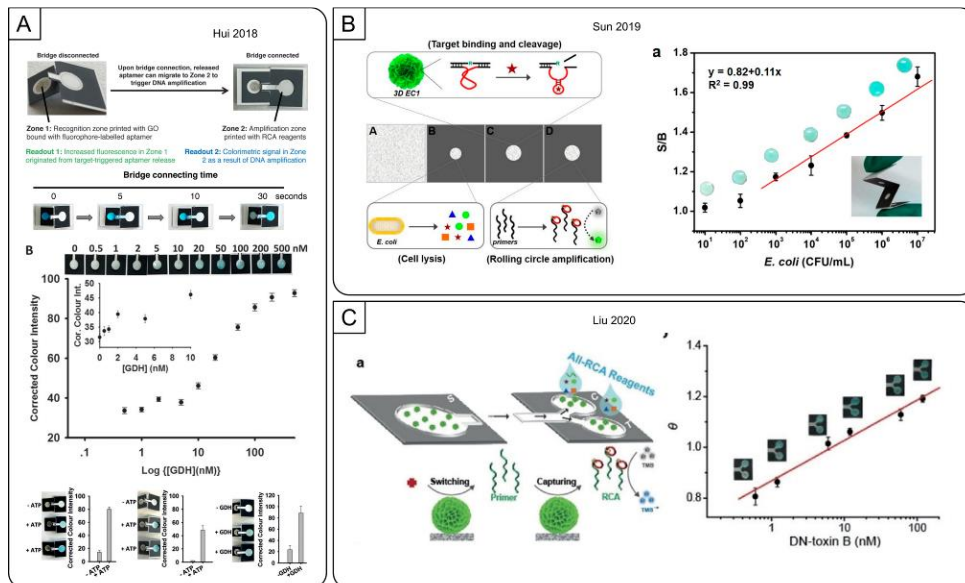


Figure 2.20. Paper-based devices with optical detection methods. (A) A bridging paper-based device for colorimetric ATP and GDH detection. (B) An origami paper-based RCD-sensor for *E. coli* detection. (C) An aptamer-containing nanoflower device for the colorimetric detection *C. difficile*. Figures adapted from references cited in text.

Table 2.5. Paper-based methods

Surface Type	Detection Method	RCA Method	MRE Type	Regulation Method	Target	LOD	# Steps	Temperature	Assay Time	Ref.
Colorimetric										
nitrocellulose	PMD	linear	aptamer	structure-switching (GO)	ATP ^[CM]	10 μ M	3	r.t.	\geq 1 hrs	[112]
cellulose	PMD	linear	DNAzyme	RCD	<i>E. coli</i> ^[CM]	1000 cells / mL	many	r.t.	35 min	[309]
nitrocellulose	PMD	linear	aptamer	structure-switching (GO)	GDH ^[CM]	3 nM	3	r.t.	\geq 1 hrs	[112]
nitrocellulose	cDNA (AuNP)	linear	aptamer	structure-switching	Hg ²⁺ ^[CM]	22.4 nM	3	multiple	\geq 1 hrs	[233]
nitrocellulose	PMD	linear	captamer	structure-switching (GO)	PDGF ^[CM]	100 pM	many	multiple	\geq 1 hrs	[114]
nitrocellulose	PMD	linear	aptamer	structure-switching	toxin B ^[CM]	60 pM	many	r.t.	50 min	[328]
Fluorometric										
cellulose	intercalating dye	linear	aptamer	inhibition RCA	PDGF	6.8 nM	2 ^[RT]	r.t.	45 min	[101]
cellulose	intercalating dye	linear	aptamer	inhibition RCA	thrombin	240 pM	2 ^[RT]	r.t.	30 min	[101]

[a] Table Footnote. [b] ... ^[RT] denotes that detection was done with real-time monitoring; ^[PLP] denotes that the assay used a padlock probe ligation reaction; ^[CM] denotes that the assay was tested with complex media; "many" denotes any assay that required 4 or more steps; r.t. denotes that room temperature was used.

2.8.4 *Electrochemical Biosensors*

Electrochemical methods rely on consumption or accumulation of electroactive species at the surface of an electrode, which are typically monitored as changes in either current, voltage, or impedance, allowing rapid detection of a target species. Though NAs are generally not useful electrochemically in solution at moderate voltages, the electrochemical analysis of NAs has long capitalized on their inherent electrochemical properties,^[336,337] including those that form G-quadruplexes and PMDs.^[338] Electrochemical detection of RCA-generated DNA is possible using several techniques,^[96,339] as electrochemically active species (often denoted as mediators) can be accumulated at electrode surfaces through adsorption or intercalation with DNA, hybridization of labelled DNA species, or generation of electroactive DNAzymes. In many cases, the polymeric RP is generated directly at the electrode surface where it can act as a scaffold to attract redox probes for electrochemical RP detection.^[340–342] Electrochemical assays are most often solid-phase assays due to the nature of the chemical interactions at the electrode, a solid surface. However, it is important to note that electron transfer rates drop exponentially with distance of the redox mediator from the electrode surface.^[343] Thus it is important to ensure that such species bind in close proximity to the electrode surface (within a few nanometers), making it important to avoid generation of very large reaction products that extend far from the electrode surface.^[344] The sensitivity of

the electrode also warrants coating the surface with blocking agents to prevent nonspecific interactions with an assay's components, with washing steps being a common strategy for maintaining low background signals.

The balance between assay complexity and sensitivity is particularly delicate for electrochemical POC assays because instrumentation cannot be avoided. However with care, electrochemical assays can also be some of the most sensitive detection methods that can be paired with ASSURED criteria. Numerous FNA-based RCA electrochemical biosensors have been developed for sensitive target detection in real samples, including for human serum,^[96,106,266,285,286,288,313,340,342,345–350] plasma,^[303] blood,^[290,341] urine,^[351] beverages,^[138,302,352,353] foodstuffs,^[128,282] and environmental samples.^[194,354] Below, we highlight electrochemical methods of RCA detection that are best suited for POC testing in low-resource settings. As well, these methods are summarized in Table 2.6.

2.8.4.1 Sandwich assays

With the many advantages of aptamers and popularity of sandwich-type detection (such as ELISAs, the gold standard in clinical diagnostics for detecting and quantifying protein biomarkers), a large portion of the current generation of FNA with RCA biosensors use dual antibody/aptamer interactions (Section 2.4.2.1, Figure 2.5D) to detect their target,^[184,213,355,356,229,250,255,265,314,320–322] including in electrochemical sensors.^[96,282,288,290,302,303,313,342,352,357] A sandwich-assay utilizing a PDGF

aptamer and RCA was demonstrated as early as 2007 by Zhou *et al.* using alkaline phosphatase (ALP).^[96] Here, an anti-PDGF capture antibody and aptamer formed a sandwich complex with PDGF on a gold electrode surface for subsequent PLP ligation and RCA (Figure 2.21A, top). Biotinylated cDNA probes and streptavidin-tagged ALP were complexed and used to convert ascorbic acid 2-phosphate into ascorbic acid to reduce silver ions deposited on the electrode and monitored by linear sweep voltammetry. As with ELISA, this approach was long (over 5 hours) and required several washing steps and reactants necessitating the immobilization of RP on an electrode. However, this isothermal (37°C) method achieved a detection limit of 30 fM for PDGF, which was a 100-fold improvement over the RCA-free method tested (Figure 2. 21A, bottom).

Rather than incorporating enzymes to generate electroactive species, Zhu *et al.* showed that copper nanoparticles (CuNPs) could be formed along electrode-bound RP to detect PSA.^[342] Interestingly, this electrochemical method was largely predated by fluorometric methods of probing CuNPs, though fluorometric methods were by far less stable, limiting their application for long-term monitoring. Then, the polythymine RP generated in the presence of PSA was used as a template to grow copper nanoparticles from Cu²⁺ ions and ascorbate over 30 minutes. Nitric acid addition dissolves these RP-immobilized CuNPs and the resultant Cu²⁺ ions detected using cyclic voltammetry. One concern with the use of nitric acid

is its storage in POC settings. The authors reported an LOD of 0.02 fg/mL for PSA, including in clinical human serum samples. At just over a 5 hour reaction time, the majority of the assay time was spent forming the sandwich and ligating the CT (3.5 hrs). These long assay times are typical of ELISAs as well.

Shen *et al.* utilized a sandwich-assay for the detection of the breast cancer cell MCF-7 with an impressive LOD of 1 cell per mL, and was used for detection in whole blood samples.^[290] Magnetic beads coated with capture antibodies for EpCAM were used to capture MCF-7 and act as an anchoring point for subsequent addition of a signalling aptamer-primer strand (Figure 2.21B, top). Incorporating a PLP ligation step followed by RCA, this assay used molybdate ($\text{PMo}_{12}\text{O}_4^{3-}$) to generate a quantitative electrochemical current. This ≥ 5 hour approach had a recovery range of 50-77% in spiking experiments of whole blood with no pretreatment, perhaps demonstrating why this electrochemical assay was chosen for the optically challenging matrix (Figure 2.21B, bottom). The challenge with any sandwich assay is that the capture and signalling probes must bind to different epitopes of the target, or the target must be a polymer (dimer, trimer, etc.) to facilitate multiple binding sites.

A dual-aptamer sandwich assay was demonstrated for the electrochemical detection of thrombin by Fan *et al.* and detected by monitoring the accumulation of AuNPs along the RP (Figure 2.21C).^[266]

First, the capture aptamer was immobilized on the glass electrode by the incorporation of a polyA chain at its end, avoiding otherwise expensive or time-consuming surface functionalization. AuNPs have been shown to have a strong binding affinity for polyadenosine DNA sequences,^[267] and the authors also designed the CT to generate a polyadenosine-rich RP which provided an anchor for AuNP adsorption onto the RP.^[358,359] Subsequent electrocatalytic reduction of H₂O₂ by the bound AuNPs was monitored using cyclic voltammetry to detect thrombin. As this method utilizes the high affinity for polyadenosine to facilitate AuNP binding, RP modification was relatively straightforward and the authors reported a detection limit of 35 fM, with demonstrated functionality in spiked human serum.

Split aptamers can be used when multiple aptamers targeting different epitopes are unavailable or if the use of antibodies is not preferred. Shen *et al.* used a split aptamer for the detection of cocaine on a gold electrode (Figure 2.21D).^[351] In separate parts, the split aptamer for cocaine is not effective for target binding, however this can be an advantageous feature for sandwich formation. Where sandwich assays typically separate the capture and signalling steps, the split aptamer offered the advantage of combining both steps simultaneously as cocaine capture could only occur when both split aptamers were present. As the authors had incorporated a biotin onto the signalling split aptamer, they added streptavidin and biotinylated primer-CT duplexes to the sandwich. A complex containing

biotinylated cDNA and streptavidin-tagged alkaline phosphatase annealed to the RP, where the addition of the redox reactive alpha-naphthyl phosphate into solution ultimately led to the detection of as low as 1.3 nM of cocaine in buffer and spiked urine samples. This isothermal (37°C) approach was completed in under 4 hours despite utilizing some more laborious methods for tethering and detecting RCA (anchoring of the primer, hybridization of an enzyme).

In certain instances, unorthodox MREs can be incorporated into the assay. Hashkavayi *et al.* detected EpCAM-positive cells using an EpCAM aptamer as the capture probe and an RCA primer tethered to cholesterol as the signalling probe (Figure 2.21E, left).^[360] As cholesterol is known to interact with binding sites facilitated by membrane proteins, cholesterol could interact with the target cell surface, thus avoiding the need for a secondary aptamer or antibody. After sandwich formation, RCA occurred on the cholesterol-tethered primer, generating multiple PMD units. The PMD-mediated redox reaction of TMB was used to quantify EpCAM positive HT29 cancer cells with a detection limit of 1 cell per mL in solution and in human serum (Figure 2.21E, right).

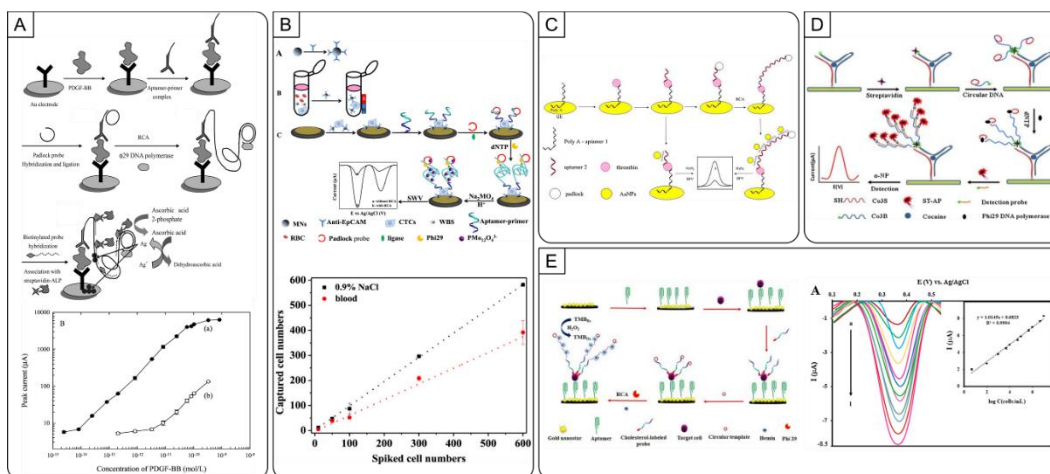


Figure 2.21. Electrochemical sandwich FNA-RCA assays. (A) Anti-PDGF antibody-aptamer sandwich approach for ALP-enabled detection of RP. (B) CuNP-reported RCA for ultrasensitive electrochemical detection of PSA. (C) Label-free detection of thrombin using dual-aptamer sandwich MRE and AuNP growth. (D) Split-aptamer-RCA assay for cocaine detection utilizing ALP cDNA. (E) EpCAM-positive tumor cell detection using a dual signal amplification strategy. Figures adapted from references cited in text.

2.8.4.2 Sandwich-free aptamer-based assays

Moving away from sandwich assays, structure-switching aptamers are still compatible alternatives for electrochemical sensors. In a seminal example in 2010, Wu *et al.* applied a structure-switching aptamer approach for the detection of PDGF where the structure-switching system was combined in one DNA strand such that PDGF-binding led to a conformation switch exposing a region complementary to a ligation probe (Figure 2.22A).^[126] The authors utilized a competitive hybridization approach such that upon undergoing this conformation switch, phi29 DP could elongate the aptamer to form a hairpin, blocking the binding site for the ligation probe. Without this binding site, PLP and RP generation proceeded. In the absence

of PDGF, the hairpin is not formed and the ligation strand instead hybridizes with the aptamer strand, preventing CT formation. PDGF-triggered RP was subsequently captured on a gold electrode and methylene blue was added to enhance the electrochemical signal. This approach had a detection limit of 63 pM.

Guo et al. showcased a structure-switching aptamer assay for the detection of ATP by monitoring the PPI by-product generated during RCA (Section 2.4.2.1, Figure 2.5B).^[361] Here, the ATP aptamer is hybridized to a cDNA which is tethered to a magnetic bead. ATP induces cDNA release and the aptamer forms a complex with ATP (Figure 2.22B). *E. coli* DNA ligase is used with a primer strand to convert the aptamer into a suitable CT for RCA. Amplification byproduct PPI can be converted into ATP by adenosine 5'-phosphosulfate (APS) and ATP sulfurylase, feeding back into the system and triggering the release of more cDNA. Afterwards, a detection DNA probe hybridized to a cadmium sulphate nanoparticle is added to bind to the liberated cDNA. Addition of nitric acid breaks down the nanoparticles, and generates a detectable electrochemical signal providing a detection limit of 100 pM of ATP and could accurately be used for the estimation of ATP in Ramos cells.

Alternatively, one can simply regulate surface-tethered RCA via an inhibition mechanism as shown by Huang *et al.* for the detection of OTA.^[138] Here, a gold electrode was functionalized with capture strands

complementary to an RP (Figure 2.22C). In solution, an OTA aptamer was hybridized to an unligated CT such that subsequent PLP and RCA steps could ligate the CT and permit RCA. However, with OTA present, the ligation failed. In this way, RP was only generated, and tethered onto the electrode surface only occurred in the absence of OTA. Methylene blue was added to intercalate with the RP and enhance the change in surface current. The authors reported a detection limit of 0.065 pg/mL of OTA in just over 2 hours, including successful detection in spiked wine samples as well.

Taghdisi *et al.* offered an interesting approach to converting an inhibition RCA regulation approach into a turn-on assay by using the aptamer sequence as the CT template (Section 2.4.2.1) (Figure 2.22D).^[362] Here, a gold electrode is tethered to a ligation strand hybridized to an anti-OTA aptamer at its terminal ends such that the aptamer can become the CT using DNA ligase. However, in the presence of OTA, the aptamer is liberated from the gold surface, and no CT can be generated. Here, a ferrocyanide redox agent ($\text{Fe}(\text{CN})_6^{3-}$) is unable to interact with the gold electrode inhibiting the redox reaction. This leaves the redox agent is to interact with the gold surface and reduction into $\text{Fe}(\text{CN})_6^{4-}$. With this 4-hour method, the authors reported a detection limit of 5 pM working in clean buffer and in spiked grape juice samples. A similar example was reported for ATP as well.^[363]

The electrochemical response generated by PMDs can be further enhanced by the incorporation of additional redox active probes. Qing *et al.* incorporated both H₂O₂ and NADH as redox reporters into their Pb²⁺ biosensor which generated PMD-rich RP in the presence of the heavy metal ion.^[354] Addition of NADH allowed the acceleration of electron transfer to the electrode surface, and the PMDs act as both a hemin mediated H₂O₂ peroxidase and a NADH oxidase. This bienzyme-type approach nearly doubled the assay response relative to using only H₂O₂ and allowed for monitoring of RP using differential pulse voltammetry pushing the LOD below any other previously reported method at 3.3 fM.

Real-time monitoring of RCA is relatively straightforward in optical devices, however it occurs rarely in electrochemical applications. Lin *et al.* showcased a method for the real-time electrochemical monitoring of RCA on an electrode for the detection of PDGF with a detection limit of 8.8 pM of PDGF (Figure 2.22E, top).^[364] The regulation method was very similar to the seminal paper for real-time protein monitoring by FNA-RCA by the Ellington group (Section 2.4.2.1, Figure 2.5A).^[125] Briefly, binding of PDGF to the aptamer causes a conformational switch, allowing the aptamer to be converted into a CT through a PLP step. With primers immobilized on sensory surface consisting of an extended-gate field-effect transistor (EGFET) surface with a standard complementary metal oxide semiconductor (CMOS) sensor, a format devoid of complex wiring and

amenable to mass-manufacturing. PDGF-triggered RP is bound to and detected by this surface due to the changes in surface charge in real-time as RP is generated (Figure 2.22E, bottom), with the assay yielding a LOD of 8.8 pM.

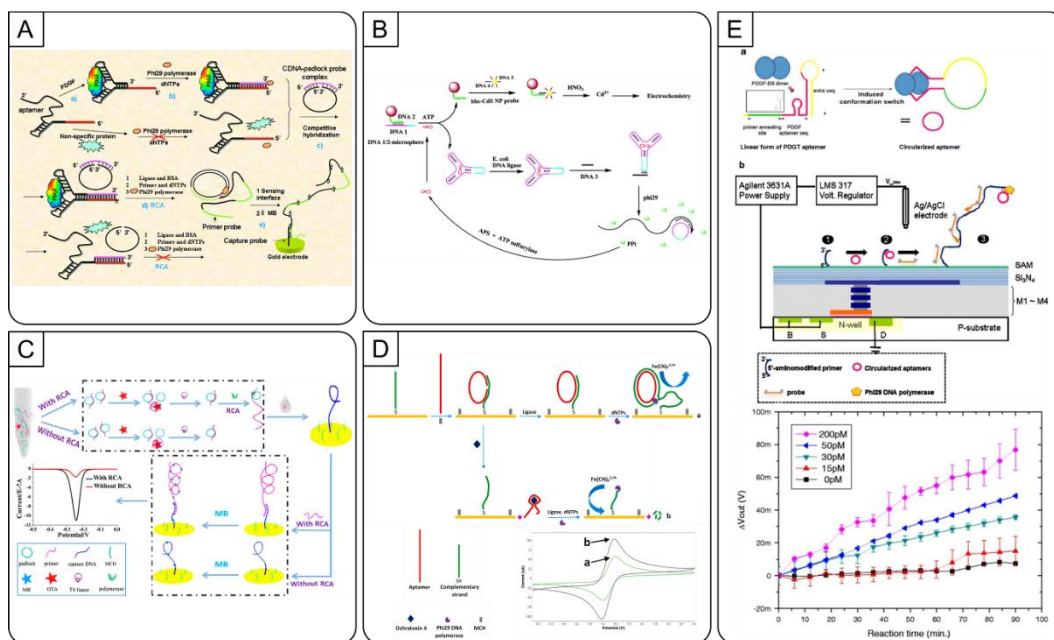


Figure 2.22. Sandwich-free aptamer-based FNA-RCA assays that use electrochemical detection. (A) Structure-switching anti-PDGF aptasensor for electrochemical detection. (B) An ATP detection and regeneration FNA-RCA assay for electrochemical detection of RP-tethered CdS NPs (C) Inhibition-RCA aptasensor for the electrochemical detection of OTA. (D) OTA aptasensor using strand-displacement polymerase reaction. (E) PDGF-triggered and immobilization-free detection on extended-gate field-effect transistor (EGFET)-modified sensor.

2.8.4.3 RNA-cleaving DNazymes as MREs

Where sandwich assays require the gradual addition of binding agents onto a surface, RCDs catalytically remove protective barriers. For example, Tang *et al.* used cadmium sulfide QD-DNA probes with an RCD for the

detection of lead (II).^[149] The lead (II) RCD is often used as a model DNAzyme system. The magnetic beads hosted a Pb^{2+} DNAzyme sequence that cleaved its hybridized strand, allowing multiple cleavage events per bound DNAzyme (Figure 2.23A). Depletion of *trans*-substrate concentration in solution leaves a binding region for an unligated CT to hybridize to the RCD (Section 2.4.2.3, Figure 2.7C). After a PLP and RCA step, QD-tagged cDNA were added and the unbound washed away. Next, the remaining QDs were dissolved using nitric acid, releasing cadmium ions into solution for voltametric detection of lead (II) in buffer as well as in spiked water samples. This approach achieved a detection limit of 7.8 pM of lead (II) and did not need multiple aptamers nor careful design of a split aptamer to be developed.

Tang *et al.* demonstrated that GOx-modified hybridization probes could be used for the detection of lead (II) by monitoring RP generation using a simple pH meter to electrochemically detect the enzymatic conversion of glucose into gluconic acid through change in solution acidity (Figure 2.23B, top).^[261] Free GOx-DNA probes were washed away during magnetic bead separation and washing to properly probe for the immobilization of GOx probes along the RP. Similarly with other pH-monitoring methods, this approach required magnetic separation of RP and was resuspended in a low-capacity buffer for pH monitoring. This portable potentiometric Pb^{2+} assay's LOD was 0.91 nM, operating at room temperature and with spiked

water samples. This approach had a sigmoidal response across three orders of magnitude highlighting the sensitivity of the RCD. The authors also determined assay efficacy after 5 months of reagent storage at 4 °C with the assay retaining 90% activity. The authors verified the performance of the portable reader by comparing signal generation relative to an ICP-MS system with good agreement (Figure 2.23B, bottom). With the growing availability of portable readers, their integration into electrochemical strategies can significantly improve its application at the POC.

Cai *et al.* designed an electrochemical device that used a modified micropipette tip to aid in their detection of Pb^{2+} (Figure 2.23C).^[194] They used a wax-sealed carbon fiber microelectrode (CFME) to sample the solution and probe the changing redox environment instigated by target-recognition and RCA. Dual-DNAzyme feedback amplification was pioneered in this work, using two RCA amplifications simultaneously. This method differentiates itself from DFA by incorporating a second CT to participate in tandem RCA amplification. Both CTs contain an antisense G-quadruplex region. However, the CT1 contains the sequence for the 8-17 DNAzyme (Pb^{2+} DNAzyme), and CT2 contains the antisense sequence for the GR-5DNAzyme (another Pb^{2+} DNAzyme). A third substrate as a pre-primer, was prevented in participating in RCA through protection from polymerase on the 3' end. This pre-primer can bind to either CT because it contains a G-quadruplex, but only CT1 houses an active Pb^{2+} DNAzyme that can cleave

the substrate upon Pb^{2+} binding. Cleavage by CT1 and PNK treatment leaves the liberated primer to be extended complementary to CT2, producing RP containing alternating units of GR-5DNAzyme and G-quadruplex regions. This careful design allows for feedback between these two tandem amplifications, not only producing many DNAzymes but also many G-quadruplex structures. Changes in diffusion were observed with the accumulation of RP and increasing intercalation of free methylene blue in solution with the G-quadruplex-rich RP. This method is completely immobilization-free, which is relatively rare for electrochemical assays especially. Local river samples were analyzed using both this electrochemical device and atomic absorption spectrometry, finding good agreement between the two methods for free Pb^{2+} in the river water. The CFME showed good electrochemical performance and had a renewable electrode surface for multiple uses.

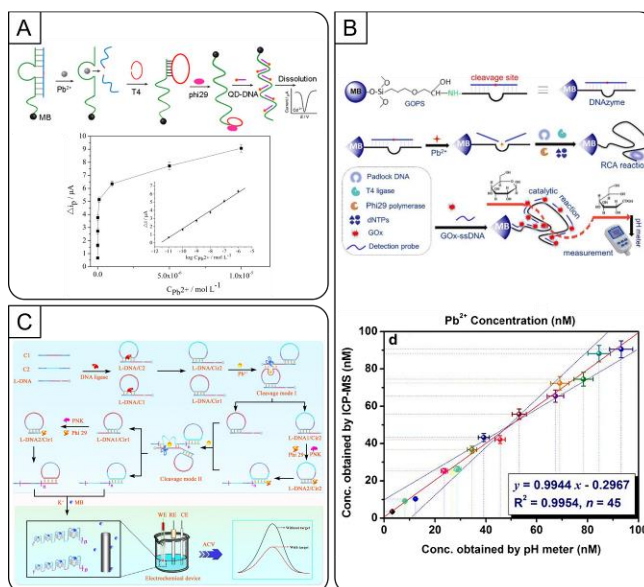


Figure 2.23. RCD-RCA assays that use electrochemical detection. (A) Electrochemical aptasensor based on Pb^{2+} -DNAzyme cleavage-triggered RCA and quantum dot-tagging. (B) Carbon fiber microelectrode (CFME) detection of a dual Pb^{2+} -DNAzyme assistant feedback amplification strategy. (C) Magnetic bead-bound Pb^{2+} -DNAzyme-RCA assay using pH sensing. Figures adapted from references from text.

Table 2.6. Electrochemical-based methods.

Surface Type	Detection Method	RCA Method	MRE Type	Regulation Method	Target	LOD	# Steps	Temperature	Assay Time	Ref.
solution (mag bead)	intercalating dye	enzyme-assisted	aptamer	structure-switching ^[PLP]	adenosine ^[CM]	0.032 nM	many	multiple	≥ 8 hrs	[340]
surface (microwell plate)	PMD	linear	aptamer	sandwich (apt/Ab) ^[PLP]	afatoxin M1 ^[CM]	0.15 ng/mL	many	multiple	≥ 6 hrs	[352]
surface (gold electrode)	PMD	linear	aptamer	structure-switching ^[PLP]	amyloid β oligomers ^[CM]	39 fg/mL	many	37 °C	≥ 5 hrs	[349]
surface	intercalating dye	linear	aptamer	structure-switching ^[PLP]	ATP ^[CM]	320 pM	many	multiple	≥ 8 hrs	[363]
solution	dNTP monitoring	enzyme-assisted	aptamer	structure-switching ^[PLP]	ATP ^[CM]	100 pM	many	multiple	≥ 4 hrs	[361]
surface (gold electrode)	cDNA (AuNP)	linear	aptamer	sandwich (apt 2x) ^[PLP]	CEA	6.7 pg/mL	many	multiple	≥ 6 hrs	[346]
surface (glassy carbon electrode)	intercalating dye	linear	aptamer	sandwich (apt/Ab) ^[PLP]	CEA ^[CM]	0.05 pg/mL	many	multiple	≥ 3 hrs	[288]
solution	G-quad dye	linear	aptamer	inhibition RCA ^[PLP]	CEA ^[CM]	2.6 fg/mL	many	multiple	≥ 5 hrs	[285]
surface (gold electrode)	cDNA (enzyme)	linear	aptamer	sandwich (split aptamer)	cocaine ^[CM]	1.3 nM	many	37 °C	≥ 3 hrs	[351]
surface (electrode)	G-quad dye	linear	aptamer	structure-switching ^[PLP]	C-reactive protein ^[CM]	16 fM	many	multiple	≥ 4 hrs	[348]
surface (gold electrode)	PMD	linear	aptamer	sandwich (apt/Ab)	<i>E. coli</i> ^[CM]	8 cfu / mL	many	37 °C	≥ 4 hrs	[302]
solution	PMD	linear	aptamer	sandwich (apt/Ab)	gastric cancer exosome ^[CM]	954 exosomes/mL	many	multiple	≥ 4 hrs	[303]
surface (glassy carbon electrode)	G-quad dye	linear	aptamer	structure-switching ^[PLP]	Hg ²⁺ ^[CM]	0.684 pM	many	multiple	≥ 8 hrs	[283]
surface (gold electrode)	PMD	linear	aptamer	sandwich (1x apt, 1x cholesterol probe)	HT29 (EpCAM) ^[CM]	1 cell /mL	many	multiple	≥ 5 hrs	[360]
surface (gold electrode)	cDNA (AuNP, CuNP)	linear	aptamer	sandwich (apt 2x) ^[PLP]	LPS ^[CM]	4.8 fg/mL	many	multiple	≥ 4 hrs	[347]
surface (glassy carbon electrode)	PMD	linear	captamer	structure-switching	LPS	0.07 fg/mL	many	37 °C	≥ 3 hrs	[144]

surface (electrode)	cDNA (enzyme)	linear	aptamer	structure-switching ^[PLP]	maltathion ^[CM]	0.68 pg/mL	many	multiple	≥ 4 hrs	[353]
surface (electrode)	intercalating dye	linear	aptamer	sandwich (apt/Ab) ^[PLP]	MCF-7 (cancer cell) ^[CM]	1 cell /mL	many	multiple	≥ 5 hrs	[290]
surface (gold electrode)	GO@Fe3O4@Pt for peroxidase activity	linear	aptamer	sandwich (apt/Ab)	MPT64 ^[CM]	0.34 fg/mL	many	37 °C	≥ 3 hrs	[313]
solution	PMD	enzyme-assisted	aptamer	structure-switching ^[PLP]	MUC1 ^[CM]	0.71 fg/mL	many	multiple	≥ 7 hrs	[304]
solution	G-quad dye	enzyme-assisted	aptamer	inhibition RCA ^[PLP]	NF-κB p50 ^[CM]	3 pM	many	multiple	≥ 3 hrs	[286]
surface (gold electrode)	G-quad dye	linear	aptamer	structure-switching	NF-κB p65 ^[CM]	8.3 fM	many	multiple	≥ 4 hrs	[345]
surface (gold electrode)	intercalating dye	linear	aptamer	inhibition RCA ^[PLP]	OTA ^[CM]	0.065 ppt	many	multiple	≥ 2 hrs	[138]
surface (gold electrode)	intercalating dye	hyperbranched	aptamer	structure-switching ^[PLP]	OTA ^[CM]	0.02 pg/mL	many	multiple	≥ 8 hrs	[128]
surface (gold electrode)	Fe(CN) ₆ ^(3-/4-)	linear	aptamer	inhibition RCA ^[PLP]	OTA ^[CM]	5 pM	many	multiple	≥ 4 hrs	[362]
solution	cDNA (QD)	linear	DNAzyme	RCD ^[PLP]	Pb ²⁺ ^[CM]	7.8 pM	many	multiple	≥ 3 hrs	[149]
solution (mag bead)	cDNA (enzyme)	enzyme-assisted	DNAzyme	RCD ^[PLP]	Pb ²⁺ ^[CM]	0.91 nM	many	r.t.	≥ 4 hrs	[261]
solution	G-quad dye	DFA	DNAzyme	RCD	Pb ²⁺ ^[CM]	48 fM	many	multiple	≥ 2 hrs	[194]
surface (glassy carbon electrode)	PMD	linear	DNAzyme	RCD ^[PLP]	Pb ²⁺ ^[CM]	3.3 fM	many	multiple	≥ 5 hrs	[354]
surface (gold electrode)	non-intercalator	linear	DNAzyme	RCD	Pb ²⁺ ^[CM]	290 fM	many	multiple	≥ 4 hrs	[350]
surface (gold electrode)	cDNA (enzyme)	linear	aptamer	sandwich (apt/Ab) ^[PLP]	PDGF ^[CM]	10 fM	many	37 °C	≥ 5 hrs	[96]
surface (gold electrode)	intercalating dye	linear	aptamer	structure-switching ^[PLP]	PDGF	63 pM	many	multiple	≥ 5 hrs	[126]
surface (gold electrode)	intercalating dye	hyperbranched	aptamer	structure-switching ^[PLP]	PDGF	1.6 fmol/L	many	multiple	≥ 2 hrs	[185]
surface	cDNA (DNA)	linear	aptamer	structure-switching ^[PLP]	PDGF ^[CM]	8.8 pM	many ^[RT]	multiple	≥ 3 hrs	[364]
surface	cDNA (AuNP, CuNP)	linear	aptamer	sandwich (apt/Ab) ^[PLP]	PSA ^[CM]	20 ag/mL	many	multiple	≥ 5 hrs	[342]

solution	PMD	linear	aptamer	sandwich (apt/Ab) ^[PLP]	PSA ^[CM]	16.3 pg/mL	many	37 °C	≥ 7 hrs	[357]
surface (screen printed glass electrode)	G-quad dye (methylene blue)	linear	aptamer	inhibition RCA	PSA ^I	22.3 fM	many	not reported	≥ 8 hrs	[284]
surface (gold electrode)	methylene blue	enzyme-assisted	aptamer	structure-switching	<i>S. aureus</i> ^[CM]	9 CFU/mL	many	multiple	≥ 5 hrs	[287]
surface (gold electrode)	cDNA (enzyme)	linear	aptamer	structure-switching	<i>S. typhimurium</i> ^[CM]	19498 cfu/mL	many	37 °C	≥ 4 hrs	[259]
surface (gold electrode)	intercalating dye	hyperbranched	aptamer	structure-switching ^[PLP]	thrombin ^[CM]	1.2 aM	many	multiple	≥ 7 hrs	[127]
surface (glassy carbon electrode)	intercalating dye	linear	aptamer	structure-switching	thrombin ^[CM]	34.6 fM	many	37 °C	≥ 8 hrs	[106]
surface (gold electrode)	cDNA (AuNP)	linear	aptamer	sandwich (apt x2) ^[PLP]	thrombin ^[CM]	35 fM	many	multiple	≥ 6 hrs	[266]
surface (gold electrode)	cDNA (enzyme)	linear	aptamer	structure-switching ^[PLP]	thrombin ^[CM]	35.3 fM	many	multiple	≥ 7 hrs	[258]
surface (gold electrode)	cDNA (AuNP)	linear	aptamer	sandwich (apt/Ab)	<i>V. parahaemolyticus</i> ^[CM]	2 cfu/mL	many	multiple	≥ 3 hrs	[282]

[a] Table Footnote. [b] ... ^[RT] denotes that detection was done with real-time monitoring; ^[PLP] denotes that the assay used a padlock probe ligation reaction; ^[CM] denotes that the assay was tested with complex media; "many" denotes any assay that required 4 or more steps; r.t. denotes that room temperature was used.

2.9 Summary and Future Outlook

A notable theme with NABs is the interchangeability of the recognition, and detection strategies. This is also evident in RCA-based FNABs as the number of possible variations of regulation, amplification, and detection strategies can be overwhelming. There is no doubt that RCA is the most prolific ITA method. Every week, new variations of FNA-based RCA methods are published, representing as much as 50% of all FNA-based ITA methods (Figure 2.24). The flexibility is a massive boon for rationally designing the most appropriate RCA assay. However, it is because there are so many choices that it is especially important to be thorough and strategic in deciding on the individual components, especially as different POC applications may have unique characteristics and demands that make certain strategies more practical than others. This is particularly true with paper-based biosensing, which comes with a host of advantages under the right conditions. As such, it is imperative that the assay requirements are well understood such that the best combinations can be selected.

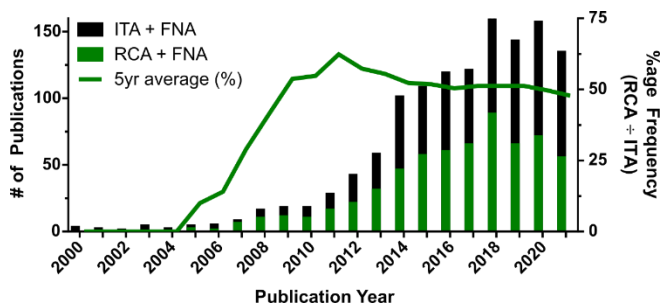


Figure 2.24. Frequency of publications mentioning RCA and FNAs compared to the frequency of publications mentioning any ITA method and FNAs as per Web of Science. The total number of publications in 2021 was estimated based on the number of publications as of June 2, 2021.

2.9.1 Regulation of RCA by FNAs

The first step in selecting the optimal molecular recognition strategy is determining whether to regulate the primer or CT for RCA. If real samples contain a substantial number of exonucleases or potential interferents, regulating the CT would allow one to take advantage of the exonuclease resistance properties accredited to captamers. Conversely, if the sample matrices are relatively simple, integrating a linear aptamer may be most effective as the pool of tested captamers remains limited. Another fundamental consideration is cost limitations. Incorporating rGO can be a powerful alternative to structure-switching aptamers with the added benefit of providing nuclease resistance however the high batch to batch variability may complicate its applications for low-resource.^[108] Likewise, some tripartite structure-switching designs may necessitate DNA functionalization

to protect from nonspecific 3'-exonuclease digestion by phi29 DP. Even the final sensitivity of the assay can be greatly affected by the recognition strategy used. Strategies utilizing target binding to inhibit RCA provide a particularly straightforward assay platform but can limit sensitivity downstream due to practical limitations of inhibitory assays. Using structure-switching aptamers can be a double-edged sword as though many creative strategies exist, poor design of the structure-switching aptamer can hamstring its apparent binding affinity.

As noted above, there are an abundance of methods available for primer regulation, using either aptamers or DNazymes as MREs. Fewer methods exist to modulate the CT, and some of these, such as use of DNazyme ligases or DNazyme kinases, have relatively limited utility. In addition, methods that modulate the CT often require additional components, such as ligase enzymes, or require multiple separation or washing steps, which are challenging to integrate into simple POC devices. Even so, through careful design it is possible to design homogeneous assays using either aptamers or DNazymes as MREs, and modulation of primer or CT availability to initiate RCA.

2.9.1 Amplification Methods

Luckily, any shortcomings in regulation strategies (such as binding affinities) can be mitigated with appropriate amplification strategies. When the application demands particularly sensitive detection, E-RCA techniques

can improve LODs by several orders of magnitude. This can be particularly pertinent when handling complex media such as blood or stool samples which necessitate several dilutions. However, if clinically relevant or actionable amounts of analyte are easily accessible, or the sample inherently has minimal interferences, then careful optimization of the CT combined with linear RCA may be sufficient. For instance, an E-RCA method may provide a working dynamic range for early detection of disease progression, but linear RCA may be better suited for later stages of disease monitoring when the analyte is more abundant. Further, the equipment limitations of the POC setting must be considered. In a laboratory setting where high quality optical readers are abundant, linear RCA can provide sufficient RP for detection. In low-resource settings relying only on the human eye, E-RCA may be required to make the assay readout more definitive.

2.9.3 RCA Detection Outputs

Though the ASSURED criteria promotes POC assays that are accessible in low-resource areas with limited expertise and instrumentation, the selection of a colorimetric, fluorometric, or electrochemical approach is ultimately governed by the resources and requirements of the end-user. Colorimetric assays can be interpreted by eye, making them a popular choice for detection despite often requiring additional washing or handling steps. As colorimetric methods are fundamentally less sensitive than their

fluorometric counterparts, they are best suited for applications where there is a high abundance of RP or where semi-quantitative answers are sufficient. Optical readers may improve assay sensitivity, and technological advances have made access to miniature and portable optical readers increasingly affordable especially with the increasing ubiquity of cell phones which can be used as optical devices.^[205] Where fluorometric readers are available, the assays benefit from increased sensitivity and can incorporate real-time monitoring of RP generation or fluorogenic multiplexing. In the absence of significant sample handling and preparation steps, media such as blood and faecal matter can be difficult to monitor optically due to their opacity. Electrochemical strategies provide an avenue for handling complex samples while maintaining ultrasensitive assay performance with the caveat that these assays often require additional washing or handling steps in addition to readers to allow for complex media analysis. Ultimately, careful consideration of the optimal detection strategy is essential for developing POC devices and can significantly decrease assay complexity.

2.9.3.1 FNA-Based POC Biosensors Utilizing RCA

Whereas the strategies in Chapters 2-4 aimed to guide readers in their considerations for biosensor development, Chapter 5 detailed numerous seminal works and recent publications in the literature that use these strategies to great effect. Though these assays may share many similarities or core schematic components, they differ greatly in assay time,

sensitivities, and ease of use. Colorimetric detection methods are perhaps the most user-friendly POC detection methods for diagnostic tests as it is possible to directly visualize color changes by eye, avoiding the need for an external reader device. Though colorimetric detection is generally less sensitive than either fluorometric or electrochemical methods, its integration with ITA techniques is usually sufficient to allow detection limits in the low picomolar or even femtomolar range. Fluorometric methods require a reader to detect a signal, however, there have been many examples using either smartphones or affordable portable fluorescence readers for detection, making such assays more amenable to use in low-resource settings.^[204–206] While electrochemical detection also requires a reader, there are many portable and inexpensive electrochemical readers that are compatible with the ASSURED criteria, including widely available devices such as the glucose meter.^[365] While many electrochemical methods require longer operation times than other optical strategies, their incredible sensitivity and strengths with handling optically complex sample matrices makes them serious contenders for POC applications. As demonstrated, assay time can be greatly shortened by incorporating alternative assay designs which could improve its application at the POC.

To emphasize the importance of decentralizing these assays from the laboratory, we discuss assays that incorporate solution and solid-phase designs that may be more easily performed at the POC. Solution-phase

assays, whether homogeneous or heterogeneous, may incorporate some amount of liquid manipulation and washing steps. Heterogeneous assays move beyond just the solution phase by incorporate particulate solids, often for MRE immobilization and washing. Solution-phase assays that minimize user interaction, such as those denoted as one-pot, act to minimize this concern central to solution-based POC analysis. Solid-phase biosensors and bioassays like those performed in microwell plates, microfluidic chips, or paper-based devices use the solid interface to manipulate the assay solution. Microfluidic devices and paper-based devices demonstrate that beyond acting as solid supports for MRE, the solid surface can be used to direct and manipulate flow and enable sequential on-device processes independent of user input.

2.9.4 Future Outlook

Using FNA-based strategies for regulating RCA can yield flexible and tunable platforms for biosensing. Though the antibody-antigen interaction continues to constitute the most popular mechanism of biorecognition for many biological assays, NA-based alternatives to traditional antibody-based diagnostics systems have garnered interest in part because of their expanded toolbox of analytes, as well as advantages with synthesis and handling.^[4,7,366] Further, as this review has highlighted, the incorporation of RCA adds a powerful method for ultrasensitive detection of numerous analytes beyond NAs. With the emergence of RCA-linked biosensing in the

late 90s, we have seen over thirty years of advancements in techniques across all stages of the assay process. Though true POC examples remain limited, great strides have been made towards this goal. Here we discuss some of the ongoing challenges facing the diagnostics field, how RCA-linked FNABs can help overcome them and highlight areas we hope to see advance.

A global interest in early disease-state biosensing in preventative healthcare measures grows in the 21st century.^[367] These applications may require extremely sensitive sensing methods as analytes often exist at low concentrations at early stages of disease before clinical symptoms present. Clinical biosensors may reduce the burden on healthcare infrastructure ideally offering fast and accurate results at the POC to guide the appropriate prescription of drugs, reducing frequency and duration of clinic visits, as well as decreasing the workload of medical staff.^[368–371] Perhaps most importantly, assays should strive to validate their assays' proficiency with clinically relevant matrices because despite their utility, many of the RCA methods remain untested with real samples specifically. To our benefit, creative advancements in converting linear RCA into E-RCA gives hope that some sample matrix challenges can be overcome with sample dilution and signal recovery with amplification.

While there is an application, time and place for both laboratory-based assays and POC biosensors, there is increasing interest in biosensors that

compete with conventional multi-day laboratory testing. As well, reaction temperatures are equally critical. As phi29 DP is effectively able to operate at room temperature, it is pertinent to ensure that other steps are equally compatible at the same temperature. Fortunately, solutions exist for equipment-free heating elements that are compatible with POC devices.^[372] These tools can help serve as a compromise as we work toward truly isothermal sensors. On-site biosensors for environmental assessment are especially useful in remote areas with the importance of monitoring water quality an ongoing pursuit. To this end, it is desirable to move POC assays from solution onto paper platforms as they are robust, cheap, and easy to store and transport. Ideally, paper-based assays should provide a procedurally simple, user-friendly, and interpretable test. Despite the many advantages, adopting RCA-based strategies to paper-based detection can be challenging. Though there are several paper-based RCA-linked FNAB examples available, the vast majority are performed in paper-based wells. At this stage, a renewed focus should be on the incorporation of lateral flow strategies to take full advantage of the inherent wicking properties of paper for sample handling.

We believe that optical detection methods, especially those that give easy to interpret real-time results, will make future RCA-based FNABs competitive on a global scale. For assay readouts, colorimetric methods such as hemin/G-quadruplex peroxidase-mimicking DNAzymes are

commonly used to achieve naked-eye detection. However the peroxidase-mimicking reaction requires stringent buffer conditions making real-time monitoring challenging. We look forward to increased innovation in this portion of the field, including incorporation of real-time colorimetric sensing methods. While there are fewer examples of colorimetric detection strategies, there are numerous examples of real-time fluorogenic detection strategies for RCA. Though portable fluorescent readers are becoming increasingly prevalent, the simplicity of a test that can be interpreted by the naked eye should not be understated. As an example, real-time colorimetric monitoring has already been demonstrated for LAMP-linked NABs using crystal violet as an intercalating dye.^[373,374] As DNA probe functionalization can otherwise constitute a large fraction of an assay's cost, migration of alternative real-time colorimetric monitoring techniques of NAs to RCA applications alongside other discoveries could significantly minimize the costs of optical probes.

To our knowledge, there are currently no commercially available RCA biosensors, hence there is clearly a need to produce simpler and faster RCA assays with real-world applications. The advent of the COVID-19 pandemic has put into hyper-focus the need for rapid and reliable POC testing particularly for early disease-state monitoring. This crisis has led to an enormous surge of innovation and novel ideas and we are optimistic that these efforts will propel the field of sensitive POC FNABs forward. We are

confident that advancements in RCA-linked FNABs do not necessitate reinventions of the wheel but rather finding the right vehicle to hitch our templates to.

Keywords: rolling circle amplification • aptamers • DNAzymes • POC biosensors • isothermal amplification

2.10 References

- [1] J. Liu, Z. Cao, Y. Lu, *Chem. Rev.* **2009**, *109*, 1948–1998.
- [2] Y. Krishnan, F. C. Simmel, *Angew. Chemie* **2011**, *50*, 3124–3156.
- [3] Y. Du, S. Dong, *Anal. Chem.* **2017**, *89*, 189–215.
- [4] P. Craw, W. Balachandran, *Lab Chip* **2012**, *12*, 2469–2486.
- [5] K. Janssen, K. Knez, D. Spasic, J. Lammertyn, *Sensors* **2013**, *13*, 1353–1384.
- [6] Y. Zhao, F. Chen, Q. Li, L. Wang, C. Fan, *Chem. Rev.* **2015**, *115*, 12491–12545.
- [7] K. S. Park, *Biosens. Bioelectron.* **2018**, *102*, 179–188.
- [8] A. Dhiman, P. Kalra, V. Bansal, J. G. Bruno, T. K. Sharma, *Sensors Actuators, B Chem.* **2017**, *246*, 535–553.
- [9] M. Chen, S. Bi, X. Jia, P. He, *Anal. Chim. Acta* **2014**, *837*, 44–51.
- [10] C. Teller, I. Willner, *Curr. Opin. Biotechnol.* **2010**, *21*, 376–391.
- [11] S. K. Silverman, *Trends Biochem. Sci.* **2016**, *41*, 595–609.
- [12] I. Willner, B. Shlyahovsky, M. Zayats, B. Willner, *Chem. Soc. Rev.* **2008**, *37*, 1153–1165.
- [13] Y. Lu, J. Liu, *Curr. Opin. Biotechnol.* **2006**, *17*, 580–588.
- [14] W. Winkler, A. Nahvi, R. R. Breaker, *Nature* **2002**, *419*, 952–956.
- [15] R. R. Breaker, *Mol. Cell* **2011**, *43*, 867–879.
- [16] D. L. Robertson, G. F. Joyce, *Lett. to Nat.* **1990**, *344*, 467–468.
- [17] A. D. Ellington, J. W. Szostak, *Nature* **1990**, *346*, 818–822.
- [18] C. Tuerk, L. Gold, *Science* **1990**, *249*, 505–510.
- [19] R. Stoltenburg, C. Reinemann, B. Strehlitz, *Biomol. Eng.* **2007**, *24*, 381–403.
- [20] M. Darmostuk, S. Rimpelova, H. Gbelcova, T. Ruml, *Biotechnol. Adv.* **2014**, *33*, 1141–1161.
- [21] L. S. Green, D. Jellinek, R. Jenison, A. Östman, C. H. Heldin, N. Janjic, *Biochemistry* **1996**, *35*, 14413–14424.
- [22] R. Jenison, S. Gill, A. Pardi, B. Polisky, *Science* **2018**, *263*, 1425–1429.
- [23] S. Tyagi, F. R. Kramer, *Nat. Biotechnol.* **1996**, *14*, 303–308.
- [24] M. a M. . Cooper, *Nat. Rev. Drug Discov.* **2002**, *1*, 515–528.

- [25] B. Van Dorst, J. Mehta, K. Bekaert, E. Rouah-Martin, W. De Coen, P. Dubruel, R. Blust, J. Robbens, *Biosens. Bioelectron.* **2010**, *26*, 1178–1194.
- [26] E. Luzzi, M. Minunni, S. Tombelli, M. Mascini, *TrAC Trends Anal. Chem.* **2003**, *22*, 810–818.
- [27] D. S. Wilson, J. W. Szostak, *Annu. Rev. Biochem.* **1999**, *68*, 611–647.
- [28] J. C. Cox, A. D. Ellington, *Bioorganic Med. Chem.* **2001**, *9*, 2525–2531.
- [29] M. Jing, M. T. Bowser, *Anal. Chim. Acta* **2011**, *686*, 9–18.
- [30] A. Sassolas, B. Leca-Bouvier, L. Blum, *Chem. Rev.* **2008**.
- [31] M. Bauer, M. Strom, D. S. Hammond, S. Shigdar, *Molecules* **2019**, *24*, 4377.
- [32] F. Kleinjung, S. Klussmann, V. A. Erdmann, F. W. Scheller, J. P. Fürste, F. F. Bier, *Anal. Chem.* **1998**, *70*, 328–331.
- [33] R. R. Breaker, G. F. Joyce, *Chem. Biol.* **1994**, *1*, 223–229.
- [34] S. K. Silverman, *Acc. Chem. Res.* **2009**, *42*, 1521–1531.
- [35] D. E. Huizenga, J. W. Szostak, *Biochemistry* **1995**, *34*, 656–665.
- [36] A. Flynn-Charlebois, Y. Wang, T. K. Prior, I. Rashid, K. A. Hoadley, R. L. Coppins, A. C. Wolf, S. K. Silverman, *J. Am. Chem. Soc.* **2003**, *125*, 2444–2454.
- [37] M. Chandra, A. Sachdeva, S. K. Silverman, *Nat. Chem. Biol.* **2009**, *5*, 718–720.
- [38] H. Gu, K. Furukawa, Z. Weinberg, D. F. Berenson, R. R. Breaker, *J. Am. Chem. Soc.* **2013**, *135*, 9121–9129.
- [39] D. J. Parker, Y. Xiao, J. M. Aguilar, S. K. Silverman, *J. Am. Chem. Soc.* **2013**, *135*, 8472–8475.
- [40] Y. Li, R. R. Breaker, *Proc. Natl. Acad. Sci. U. S. A.* **1999**, *96*, 2746–2751.
- [41] Y. Li, Y. Liu, R. R. Breaker, *Biochemistry* **2000**, *39*, 3106–3114.
- [42] T. L. Sheppard, P. Ordoukhanian, G. F. Joyce, *Proc. Natl. Acad. Sci. U. S. A.* **2000**, *97*, 7802–7807.
- [43] P. Travascio, Y. Li, D. Sen, *Chem. Biol.* **1998**, *5*, 505–517.
- [44] M. Famulok, J. S. Hartig, G. Mayer, *Chem. Rev.* **2007**, *107*, 3715–3743.
- [45] M. M. Ali, S. D. Aguirre, H. Lazim, Y. Li, *Angew. Chemie* **2011**, *50*, 3751–3754.
- [46] Z. Shen, Z. Wu, D. Chang, W. Zhang, K. Tram, C. Lee, P. Kim, B. J. Salena, Y. Li, *Angew. Chemie* **2016**, *128*, 2477–2480.
- [47] M. Mauk, J. Song, H. H. Bau, R. Gross, F. D. Bushman, R. G. Collman, C. Liu, *Lab Chip* **2017**, *17*, 382–394.
- [48] J. R. Choi, K. W. Yong, R. Tang, Y. Gong, T. Wen, F. Li, B. Pingguan-Murphy, D. Bai, F. Xu, *TrAC - Trends Anal. Chem.* **2017**, *93*, 37–50.
- [49] E. M. McConnell, I. Cozma, Q. Mou, J. D. Brennan, Y. Lu, Y. Li, *Chem. Soc. Rev.* **2021**, DOI 10.1039/D1CS00240F.

- [50] D. Mabey, R. W. Peeling, A. Ustianowski, M. D. Perkins, *Nat. Rev. Microbiol.* **2004**, *2*, 231–240.
- [51] M. Urdea, L. A. Penny, S. S. Olmsted, M. Y. Giovanni, P. Kaspar, A. Shepherd, P. Wilson, C. A. Dahl, S. Buchsbaum, G. Moeller, et al., *Nature* **2006**, *444*, 73–79.
- [52] P. Yager, G. J. Domingo, J. Gerdes, *Annu. Rev. Biomed. Eng.* **2008**, *10*, 107–144.
- [53] A. W. Martinez, S. T. Phillips, G. M. Whitesides, E. Carrilho, *Anal. Chem.* **2010**, *82*, 3–10.
- [54] W. Zhou, P. J. Jimmy Huang, J. Ding, J. Liu, *Analyst* **2014**, *139*, 2627–2640.
- [55] C. Jung, A. D. Ellington, *Acc. Chem. Res.* **2014**, *47*, 1825–1835.
- [56] K. B. Mullis, F. A. Faloona, in *Methods Enzymol.*, **1987**, pp. 335–350.
- [57] L. Yan, J. Zhou, Y. Zheng, A. S. Gamson, B. T. Roembke, S. Nakayama, H. O. Sintim, *Mol. Biosyst.* **2014**, *10*, 970–1003.
- [58] G. T. Walker, M. S. Fraiser, J. L. Schram, M. C. Little, J. G. Nadeau, D. P. Malinowski, *Nucleic Acids Res.* **1992**, *20*, 1691–1696.
- [59] P. Gill, A. Ghaemi, *Nucleosides. Nucleotides Nucleic Acids* **2008**, *27*, 224–43.
- [60] O. Piepenburg, C. H. Williams, D. L. Stemple, N. A. Armes, *PLoS Biol.* **2006**, *4*, 1115–1121.
- [61] S. Lutz, P. Weber, M. Focke, B. Faltin, J. Hoffmann, C. Müller, D. Mark, G. Roth, P. Munday, N. Armes, et al., *Lab Chip* **2010**, *10*, 887–893.
- [62] R. K. Daher, G. Stewart, M. Boissinot, M. G. Bergeron, *Clin. Chem.* **2016**, *62*, 947–958.
- [63] T. Notomi, *Nucleic Acids Res.* **2000**, *28*, 63e – 63.
- [64] N. Tomita, Y. Mori, H. Kanda, T. Notomi, *Nat. Protoc.* **2008**, *3*, 877–882.
- [65] T. Notomi, Y. Mori, N. Tomita, H. Kanda, *J. Microbiol.* **2015**, *53*, 1–5.
- [66] J. T. Connelly, J. P. Rolland, G. M. Whitesides, *Anal. Chem.* **2015**, *87*, 7595–7601.
- [67] M. Vincent, Y. Xu, H. Kong, *EMBO Rep.* **2004**, *5*, 795–800.
- [68] Y.-J. Jeong, K. Park, D.-E. Kim, *Cell. Mol. Life Sci.* **2009**, *66*, 3325–3336.
- [69] P. J. Asiello, A. J. Baeumner, *Lab Chip* **2011**, *11*, 1420–1430.
- [70] S. Barrera-García, R. Miranda-Castro, N. de-los-Santos-Álvarez, A. J. Miranda-Ordieres, M. J. Lobo-Castañón, *Anal. Bioanal. Chem.* **2018**, *410*, 679–693.
- [71] R. M. Dirks, N. A. Pierce, *Proc. Natl. Acad. Sci. U. S. A.* **2004**, *101*, 15275–15278.
- [72] S. Bi, S. Yue, S. Zhang, *Chem. Soc. Rev.* **2017**, *46*, 4281–4298.
- [73] W. Zhao, M. M. Ali, M. A. Brook, Y. Li, *Angew. Chemie* **2008**, *47*, 6330–6337.

- [74] M. M. Ali, F. Li, Z. Zhang, K. Zhang, D.-K. Kang, J. A. Ankrum, X. C. Le, W. Zhao, *Chem. Soc. Rev.* **2014**, *43*, 3324.
- [75] L. Gu, W. Yan, L. Liu, S. Wang, X. Zhang, M. Lyu, *Pharmaceuticals* **2018**, *11*, 1–19.
- [76] S. Yue, Y. Li, Z. Qiao, W. Song, S. Bi, *Trends Biotechnol.* **2021**, 1–13.
- [77] X. Xu, Y. Su, Y. Zhang, X. Wang, H. Tian, X. Ma, H. Chu, W. Xu, *TrAC - Trends Anal. Chem.* **2021**, *141*, 116293.
- [78] L. Xu, J. Duan, J. Chen, S. Ding, W. Cheng, *Anal. Chim. Acta* **2021**, *1148*, 238187.
- [79] H. Shi, J. Cui, H. Sulemana, W. Wang, L. Gao, *Luminescence* **2021**, *36*, 842–848.
- [80] M. G. Mohsen, E. T. Kool, *Acc. Chem. Res.* **2016**, *49*, 2540–2550.
- [81] E. T. Kool, *J. Am. Chem. Soc.* **1991**, *113*, 6265–6266.
- [82] G. Prakash, E. T. Kool, *J. Chem. Soc. Chem. Commun.* **1991**, 176, 1161.
- [83] D. Liu, S. L. Daubendiek, M. A. Zillman, K. Ryan, E. T. Kool, *J. Am. Chem. Soc.* **1996**, *118*, 1587–1594.
- [84] V. V. Demidov, *Expert Rev. Mol. Diagn.* **2002**, *2*, 542–548.
- [85] P. M. Lizardi, X. Huang, Z. Zhu, P. Bray-Ward, D. C. Thomas, D. C. Ward, *Nat. Genet.* **1998**, *19*, 225–232.
- [86] O. Söderberg, M. Gullberg, M. Jarvius, K. Ridderstråle, K. J. Leuchowius, J. Jarvius, K. Wester, P. Hydbring, F. Bahram, L. G. Larsson, et al., *Nat. Methods* **2006**, *3*, 995–1000.
- [87] J. Jarvius, J. Melin, J. Göransson, J. Stenberg, S. Fredriksson, C. Gonzalez-Rey, S. Bertilsson, M. Nilsson, S. Bertilsson, M. Nilsson, *Nat. Methods* **2006**, *3*, 725–727.
- [88] K. Sato, R. Ishii, N. Sasaki, K. Sato, M. Nilsson, *Anal. Biochem.* **2013**, *437*, 43–45.
- [89] C. Larsson, J. Koch, A. Nygren, G. Janssen, A. K. Raap, U. Landegren, M. Nilsson, *Nat. Methods* **2004**, *1*, 227–232.
- [90] F. Dahl, J. Baner, M. Gullberg, M. Mendel-Hartvig, U. Landegren, M. Nilsson, *Proc. Natl. Acad. Sci.* **2004**, *101*, 4548–4553.
- [91] Q. Ma, Z. Gao, *Anal. Bioanal. Chem.* **2018**, *410*, 3093–3100.
- [92] B. Schweitzer, S. Wiltshire, J. Lambert, S. O'Malley, K. Kukanskis, Z. Zhu, D. C. Ward, S. O'Malley, K. Kukanskis, Z. Zhu, et al., *Proc. Natl. Acad. Sci. U. S. A.* **2000**, *97*, 10113–10119.
- [93] B. Schweitzer, S. Roberts, B. Grimwade, W. Shao, M. Wang, Q. Fu, Q. Shu, I. Laroche, Z. Zhou, V. T. Tchernev, et al., *Nat. Biotechnol.* **2002**, *20*, 359–365.
- [94] M. C. Mullenix, R. Sivakamasundari, W. J. Feaver, R. M. Krishna, M. P. Sorette, H. J. Datta, D. M. Morosan, S. P. Piccoli, *Clin. Chem.* **2002**, *48*, 1855–1858.
- [95] A. Raghunathan, M. P. Sorette, H. R. Ferguson, S. P. Piccoli, *Clin.*

- Chem.* **2002**, *48*, 1853–1855.
- [96] L. Zhou, L.-J. Ou, X. Chu, G.-L. Shen, R.-Q. Yu, *Anal. Chem.* **2007**, *79*, 7492–7500.
- [97] F. Akter, M. Mie, E. Kobatake, *Anal. Biochem.* **2011**, *416*, 174–179.
- [98] M. Liu, C. Y. Hui, Q. Zhang, J. Gu, B. Kannan, S. Jahanshahi-Anbuhi, C. D. M. M. M. Filipe, J. D. Brennan, Y. Li, C. D. M. M. M. Filipe, et al., *Angew. Chemie* **2016**, *55*, 2709–2713.
- [99] A. K. Yetisen, M. S. Akram, C. R. Lowe, *Lab Chip* **2013**, *13*, 2210–2251.
- [100] J. Méndez, L. Blanco, M. Salas, *EMBO J.* **1997**, *16*, 2519–2527.
- [101] R. M. Bialy, M. M. Ali, Y. Li, J. D. Brennan, *Chem. – A Eur. J.* **2020**, *26*, 5085–5092.
- [102] R. Nutiu, Y. Li, *J. Am. Chem. Soc.* **2003**, *125*, 4771–4778.
- [103] R. Nutiu, Y. Li, *Angew. Chemie* **2005**, *44*, 1061–1065.
- [104] P. S. Lau, B. K. Coombes, Y. Li, *Angew. Chemie* **2010**, *49*, 7938–7942.
- [105] P. S. Lau, Y. Li, in *Biosens. Based Aptamers Enzym.*, **2013**, pp. 69–92.
- [106] T. Hu, Y. N. Zheng, M. J. Li, W. B. W. B. Liang, Y. Q. Chai, R. Yuan, *Anal. Chem.* **2018**, *90*, 6096–6101.
- [107] X. Liu, F. Yang, D. Li, R. Yuan, Y. Xiang, *Sensors Actuators, B Chem.* **2020**, *305*, 127405.
- [108] M. Liu, W. Zhang, D. Chang, Q. Zhang, J. D. Brennan, Y. Li, *TrAC - Trends Anal. Chem.* **2015**, *74*, 120–129.
- [109] C. H. Lu, H. H. Yang, C. L. Zhu, X. Chen, G. N. Chen, *Angew. Chemie* **2009**, *48*, 4785–4787.
- [110] M. Liu, J. Song, S. Shuang, C. Dong, J. D. Brennan, Y. Li, *ACS Nano* **2014**, *8*, 5564–5573.
- [111] Y. Mao, M. Liu, K. Tram, J. Gu, B. J. Salena, Y. Jiang, Y. Li, *Chem. Eur. J.* **2015**, *21*, 8069–8074.
- [112] C. Y. Hui, M. Liu, Y. Li, J. D. Brennan, *Angew. Chemie* **2018**, *57*, 4549–4553.
- [113] M. Liu, Q. Yin, Y. Chang, Q. Zhang, J. D. Brennan, Y. Li, *Angew. Chemie* **2019**, *58*, 8013–8017.
- [114] X. Li, X. He, Q. Zhang, Y. Chang, M. Liu, *Anal. Methods* **2019**, *11*, 4328–4333.
- [115] W. Cheng, L. Ding, Y. Chen, F. Yan, H. Ju, Y. Yin, *Chem. Commun.* **2010**, *46*, 6720–6722.
- [116] M. Liu, W. Zhang, Q. Zhang, J. D. Brennan, Y. Li, *Angew. Chemie* **2015**, *54*, 9637–9641.
- [117] J. Wang, Y. Wang, S. Liu, H. Wang, X. Zhang, X. Song, J. Huang, *Anal. Chim. Acta* **2019**, *1060*, 79–87.
- [118] R. M. Bialy, Y. Li, J. D. Brennan, *Chem. Eur. J.* **2021**, (Accepted), 1–7.

- [119] R. Deng, Y. Dong, X. Xia, Y. Dai, K. Zhang, Q. He, W. C. Zeng, X. Ren, J. Li, *Anal. Chem.* **2018**, *90*, 14347–14354.
- [120] M. M. Ali, Y. Li, *Angew. Chemie* **2009**, *48*, 3512–3515.
- [121] M. Liu, Q. Zhang, D. Chang, J. Gu, J. D. Brennan, Y. Li, *Angew. Chemie* **2017**, 1–6.
- [122] L. Blanco, A. Bernad, J. M. Lazaro, G. Martin, C. Garmendia, M. Salas, *J. Biol. Chem.* **1989**, *264*, 8935–8940.
- [123] J. Banér, M. Nilsson, M. Mendel-Hartvig, U. Landegren, *Nucleic Acids Res.* **1998**, *26*, 5073–5078.
- [124] M. Nilsson, H. Malmgren, M. Samiotaki, M. Kwiatkowski, B. Chowdhary, U. Landegren, *Science* **1994**, *265*, 2085–2088.
- [125] L. Yang, C. W. Fung, E. J. Cho, A. D. Ellington, *Anal. Chem.* **2007**, *79*, 3320–3329.
- [126] Z.-S. Wu, H. Zhou, S. Zhang, G. Shen, R. Yu, *Anal. Chem.* **2010**, *82*, 2282–2289.
- [127] G. Jin, C. Wang, L. Yang, X. Li, L. Guo, B. Qiu, G. Chen, Z. Lin, G. Chen, Z. Lin, et al., *Biosens. Bioelectron.* **2015**, *63*, 166–171.
- [128] L. Yang, Y. Zhang, R. Li, C. Lin, L. Guo, B. Qiu, Z. Lin, G. Chen, *Biosens. Bioelectron.* **2015**, *70*, 268–274.
- [129] Z. Qiu, J. Shu, Y. He, Z. Lin, K. Zhang, S. Lv, D. Tang, *Biosens. Bioelectron.* **2017**, *87*, 18–24.
- [130] Y. Jiang, S. Zou, X. Cao, *Sensors Actuators, B Chem.* **2017**, *251*, 976–984.
- [131] L. Xu, Z. Jiang, Y. Mu, Y. Zhang, Q. Zhan, J. Cui, W. Cheng, S. Ding, *Sensors Actuators, B Chem.* **2018**, *259*, 596–603.
- [132] R. Huang, L. He, S. Li, H. Liu, L. Jin, Z. Chen, N. He, Y. Zhao, Z. Li, Y. Deng, et al., *Nanoscale* **2020**, *12*, 2445–2451.
- [133] S. Niazi, I. M. Khan, Y. Yu, I. Pasha, Y. Lv, A. Mohsin, B. S. Mushtaq, Z. Wang, *Sensors Actuators, B Chem.* **2020**, *315*, 1–10.
- [134] S. Bi, L. Li, S. Zhang, *Anal. Chem.* **2010**, *82*, 9447–9454.
- [135] C. Ma, W. Wang, Q. Yang, C. Shi, L. Cao, *Biosens. Bioelectron.* **2011**, *26*, 3309–3312.
- [136] P. Tong, W.-W. W. Zhao, L. Zhang, J.-J. J. Xu, H.-Y. Y. Chen, *Biosens. Bioelectron.* **2012**, *33*, 146–151.
- [137] C. Ding, N. Wang, J. Zhang, Z. Wang, *Biosens. Bioelectron.* **2013**, *42*, 486–491.
- [138] L. Huang, J. Wu, L. Zheng, H. Qian, F. Xue, Y. Wu, D. Pan, S. B. Adeloju, W. Chen, *Anal. Chem.* **2013**, *85*, 10842–10849.
- [139] K. Liang, S. Zhai, Z. Zhang, X. Fu, J. Shao, Z. Lin, B. Qiu, G. N. Chen, B. Qiu, G. N. Chen, *Analyst* **2014**, *139*, 4330–4334.
- [140] X. Lin, Q. Chen, W. Liu, H. Li, J.-M. Lin, *Biosens. Bioelectron.* **2014**, *56*, 71–76.
- [141] P. He, L. Liu, W. Qiao, S. Zhang, *Chem. Commun.* **2014**, *50*, 1481–1484.

- [142] J. Li, M. Mohammed-Elsabagh, F. Paczkowski, Y. Li, *ChemBioChem* **2020**, *21*, 1547–1566.
- [143] D. A. Di Giusto, W. A. Wlassoff, J. J. Gooding, B. A. Messerle, G. C. King, *Nucleic Acids Res.* **2005**, *33*, e64.
- [144] M. Zhao, A. Y. Chen, D. Huang, Y. Q. Chai, Y. Zhuo, R. Yuan, *Anal. Chem.* **2017**, *89*, 8335–8342.
- [145] L. Wang, K. Tram, M. M. Ali, B. J. Salena, J. Li, Y. Li, *Chem. Eur. J.* **2014**, *20*, 2420–4.
- [146] S. Wang, S. Bi, Z. Wang, J. Xia, F. Zhang, M. Yang, R. Gui, Y. Li, Y. Xia, *Chem. Commun.* **2015**, *51*, 7927–7930.
- [147] E. J. Cho, L. Yang, M. Levy, A. D. Ellington, *J. Am. Chem. Soc.* **2005**, *127*, 2022–3.
- [148] S. A. McManus, Y. Li, *J. Am. Chem. Soc.* **2013**, *135*, 7181–7186.
- [149] S. Tang, P. Tong, H. Li, J. Tang, L. Zhang, *Biosens. Bioelectron.* **2013**, *42*, 608–611.
- [150] K. Tram, P. Kanda, Y. Li, *J. Nucleic Acids* **2012**, *1*, 958683.
- [151] M. Liu, Q. Zhang, Z. Li, J. Gu, J. D. Brennan, Y. Li, *Nat. Commun.* **2016**, *7*, 1–7.
- [152] F. B. Dean, *Genome Res.* **2001**, *11*, 1095–1099.
- [153] F. B. Dean, S. Hosono, L. Fang, X. Wu, A. F. Faruqi, P. Bray-Ward, R. S. Lasken, Z. Sun, Q. Zong, Y. Du, et al., *Proc. Natl. Acad. Sci.* **2002**, *99*, 5261–5266.
- [154] S. Tabor, H. E. Huber, C. C. Richardson, *J. Biol. Chem.* **1987**, *262*, 16212–23.
- [155] H. E. Huber, S. Tabor, C. C. Richardson, *J. Biol. Chem.* **1987**, *262*, 16224–16232.
- [156] S. Kamtekar, A. J. Berman, J. Wang, J. M. Lázaro, M. de Vega, L. Blanco, M. Salas, T. . T. a. Steitz, M. Vega, L. Blanco, et al., *Mol. Cell* **2004**, *16*, 609–618.
- [157] A. J. Berman, S. Kamtekar, J. L. Goodman, J. M. Lázaro, M. de Vega, L. Blanco, M. Salas, T. A. Steitz, M. Vega, L. Blanco, et al., *EMBO J.* **2007**, *26*, 3494–3505.
- [158] B. D. Harfe, S. Jinks-Robertson, *Annu. Rev. Genet.* **2000**, *34*, 359–399.
- [159] I. V. Shevelev, U. Hübscher, *Nat. Rev. Mol. Cell Biol.* **2002**, *3*, 364–375.
- [160] I. Rodríguez, J. M. Lázaro, L. Blanco, S. Kamtekar, A. J. Berman, J. Wang, M. Vega, T. a Steitz, M. Salas, M. de Vega, et al., *Proc. Natl. Acad. Sci.* **2005**, *102*, 6407–6412.
- [161] L. Blanco, M. Salas, *Nucleic Acids Res.* **1985**, *13*, 1239–1249.
- [162] V. Khare, K. A. Eckert, *Mutat. Res. Mol. Mech. Mutagen.* **2002**, *510*, 45–54.
- [163] B. Joffroy, Y. O. Uca, D. Prešern, J. P. K. Doye, T. L. Schmidt, *Nucleic Acids Res.* **2018**, *46*, 538–545.

- [164] J. Björkesten, S. Patil, C. Fredolini, P. Lönn, U. Landegren, *Nucleic Acids Res.* **2020**, *48*, DOI 10.1093/nar/gkaa419.
- [165] A. S. Fauci, D. M. Morens, *N. Engl. J. Med.* **2012**, *366*, 454–461.
- [166] O. Lazcka, F. J. Del Campo, F. X. Muñoz, *Biosens. Bioelectron.* **2007**, *22*, 1205–1217.
- [167] M. Mascini, S. Tombelli, *Biomarkers* **2008**, *13*, 637–657.
- [168] K. S. McKeating, A. Aubé, J. F. Masson, *Analyst* **2016**, *141*, 429–449.
- [169] M. U. Ahmed, I. Saaem, P. C. Wu, A. S. Brown, *Crit. Rev. Biotechnol.* **2014**, *34*, 180–196.
- [170] A. P. Dhawan, in *IEEE J. Transl. Eng. Heal. Med.*, Institute Of Electrical And Electronics Engineers Inc., **2016**.
- [171] S. R. Corrie, J. W. Coffey, J. Islam, K. A. Markey, M. A. F. Kendall, *Analyst* **2015**, *140*, 4350–4364.
- [172] T. Murakami, J. Sumaoka, M. Komiyama, *Nucleic Acids Res.* **2009**, *37*, e19–e19.
- [173] X. Y. Li, Y. C. Du, Y. P. Zhang, D. M. Kong, *Sci. Rep.* **2017**, *7*, 6263.
- [174] W. Tian, P. Li, W. He, C. Liu, Z. Li, *Biosens. Bioelectron.* **2019**, *128*, 17–22.
- [175] J. Y. Marciniak, A. C. Kummel, S. C. Esener, M. J. Heller, B. T. Messmer, *Biotechniques* **2008**, *45*, 275–280.
- [176] J. Zhuang, W. Lai, G. Chen, D. Tang, *Chem. Commun.* **2014**, *50*, 2935–2938.
- [177] Q. Li, F. Zeng, N. Lyu, J. Liang, *Analyst* **2018**, *143*, 2304–2309.
- [178] H. Xu, Y. Zhang, S. Zhang, M. Sun, W. Li, Y. Jiang, Z. S. Wu, *Anal. Chim. Acta* **2019**, *1047*, 172–178.
- [179] H. Xu, D. Wu, Y. Zhang, H. Shi, C. Ouyang, F. Li, L. Jia, S. Yu, Z. S. Wu, *Sensors Actuators, B Chem.* **2018**, *258*, 470–477.
- [180] D. Y. Zhang, W. Zhang, X. Li, Y. Konomi, *Gene* **2001**, *274*, 209–216.
- [181] X. Zhu, H. Xu, H. Zheng, G. Yang, Z. Lin, B. Qiu, L. Guo, Y. Chi, G. Chen, L. Guo, et al., *Chem. Commun.* **2013**, *49*, 10115–10117.
- [182] Y. Zhang, L. Yang, C. Lin, L. Guo, B. Qiu, Z. Lin, G. Chen, *Anal. Methods* **2015**, *7*, 6109–6113.
- [183] F. Wu, W. Liu, S. Yang, Q. Yao, Y. Chen, X. Weng, X. Zhou, *J. Photochem. Photobiol. A Chem.* **2018**, *355*, 114–119.
- [184] X. Miao, Z. Zhu, H. Jia, C. Lu, X. Liu, D. Mao, G. Chen, *Sensors Actuators, B Chem.* **2020**, *320*, 128435.
- [185] Q. Wang, H. Zheng, X. Gao, Z. Lin, G. Chen, *Chem. Commun.* **2013**, *49*, 11418–11420.
- [186] X. Zhu, C. Feng, B. Zhang, H. Tong, T. Gao, G. Li, *Analyst* **2015**, *140*, 74–78.
- [187] C. Feng, X. Mao, H. Shi, B. Bo, X. Chen, T. Chen, X. Zhu, G. Li, *Anal. Chem.* **2017**, *89*, 6631–6636.
- [188] C. Feng, B. Bo, X. Mao, H. Shi, X. Zhu, G. Li, *Theranostics* **2017**, *7*, 31–39.

- [189] F. Wang, C. H. Lu, X. Liu, L. Freage, I. Willner, *Anal. Chem.* **2014**, *86*, 1614–1621.
- [190] H. Fujita, Y. Kataoka, S. Tobita, M. Kuwahara, N. Sugimoto, *Anal. Chem.* **2016**, *88*, 7137–7144.
- [191] J. Wang, Y. Wang, S. Liu, H. Wang, X. Zhang, X. Song, J. Yu, J. Huang, *Analyst* **2019**, *144*, 3389–3397.
- [192] M. Liu, Q. Yin, E. M. McConnell, Y. Chang, J. D. Brennan, Y. Li, *Chem. Eur. J.* **2018**, *24*, 4473–4479.
- [193] Y. Gu, T. T. Zhang, Z. F. Huang, S. W. Hu, W. Zhao, J. J. Xu, H. Y. Chen, *Chem. Sci.* **2018**, *9*, 3517–3522.
- [194] W. Cai, S. Xie, J. Zhang, D. Tang, Y. Tang, *Biosens. Bioelectron.* **2018**, *117*, 312–318.
- [195] Y. Li, R. R. Breaker, *J. Am. Chem. Soc.* **1999**, *121*, 5364–5372.
- [196] T. Konry, I. Smolina, J. M. Yarmush, D. Irimia, M. L. Yarmush, *Small* **2011**, *7*, 395–400.
- [197] C. Carrasquilla, J. R. L. L. Little, Y. Li, J. D. Brennan, *Chem. Eur. J.* **2015**, *21*, 7369–7373.
- [198] M. Liu, Q. Zhang, B. Kannan, G. A. Botton, J. Yang, L. Soleymani, J. D. Brennan, Y. Li, *Angew. Chemie* **2018**, *57*, 12440–12443.
- [199] W. Zhao, C. H. Cui, S. Bose, D. Guo, C. Shen, W. P. Wong, K. Halvorsen, O. C. Farokhzad, G. S. L. Teo, J. A. Phillips, et al., *Proc. Natl. Acad. Sci. U. S. A.* **2012**, *109*, 19626–19631.
- [200] J. Li, L. Lin, J. Yu, S. Zhai, G. Liu, L. Tian, *ACS Appl. Bio Mater.* **2019**, *2*, 4106–4120.
- [201] H. Gu, L. Hao, N. Duan, S. Wu, Y. Xia, X. Ma, Z. Wang, *Microchim. Acta* **2017**, *184*, 2893–2899.
- [202] S. Li, Y. Jiang, X. Yang, M. Lin, H. Dan, S. Zou, X. Cao, *Anal. Chim. Acta* **2021**, *1150*, 338229.
- [203] G. Zhu, R. Hu, Z. Zhao, Z. Chen, X. Zhang, W. Tan, *J. Am. Chem. Soc.* **2013**, *135*, 16438–16445.
- [204] E. Petryayeva, W. R. Algar, *RSC Adv.* **2015**, *5*, 22256–22282.
- [205] X. Huang, D. Xu, J. Chen, J. Liu, Y. Li, J. Song, X. Ma, J. Guo, *Analyst* **2018**, *143*, 5339–5351.
- [206] M. Mayer, A. J. Baeumner, *Chem. Rev.* **2019**, *119*, 7996–8027.
- [207] C. Feng, X. Mao, Y. Yang, X. Zhu, Y. Yin, G. Li, *J. Electroanal. Chem.* **2016**, *781*, 223–232.
- [208] R. Lorenzo-Gómez, N. Fernández-Alonso, R. Miranda-Castro, N. de los-Santos-Álvarez, M. J. Lobo-Castañón, *Talanta* **2019**, *197*, 406–412.
- [209] H. Chen, Y. Hou, F. Qi, J. Zhang, K. Koh, Z. Shen, G. Li, *Biosens. Bioelectron.* **2014**, *61*, 83–87.
- [210] P. He, W. Qiao, L. Liu, S. Zhang, *Chem. Commun.* **2014**, *50*, 10718–10721.
- [211] X. Li, L. Wang, C. Li, *Chem. Eur. J.* **2015**, *21*, 6817–6822.

- [212] F. Gao, L. Du, D. Tang, Y. Lu, Y. Zhang, L. Zhang, *Biosens. Bioelectron.* **2015**, *66*, 423–430.
- [213] L. Yao, Y. Ye, J. Teng, F. Xue, D. Pan, B. Li, W. Chen, *Anal. Chem.* **2017**, *89*, 9775–9780.
- [214] X. Zhang, J. Chen, H. Liu, S. Zhang, *Biosens. Bioelectron.* **2015**, *65*, 341–345.
- [215] W. Sun, W. Song, X. Guo, Z. Wang, *Anal. Chim. Acta* **2017**, *978*, 42–47.
- [216] A. J. Berdis, *Chem. Rev.* **2009**, *109*, 2862–2879.
- [217] S. V. Hamidi, J. Perreault, *Talanta* **2019**, *201*, 419–425.
- [218] K. Tram, P. Kanda, B. J. Salena, S. Huan, Y. Li, *Angew. Chemie* **2014**, *53*, 12799–12802.
- [219] M. M. Ali, M. Wolfe, K. Tram, J. Gu, C. D. M. Filipe, Y. Li, J. D. Brennan, *Angew. Chemie* **2019**, *58*, 9907–9911.
- [220] S. V. Hamidi, H. Ghourchian, *Biosens. Bioelectron.* **2015**, *72*, 121–126.
- [221] Q. Ma, P. Li, Z. Gao, S. F. Yau Li, *Sensors Actuators, B Chem.* **2019**, *281*, 424–431.
- [222] L. Linck, E. Reiß, F. Bier, U. Resch-Genger, *Anal. Methods* **2012**, *4*, 1215–1220.
- [223] X. J. Yang, K. Zhang, J. J. Xu, H. Y. Chen, *Anal. Chem.* **2018**, *90*, 6199–6205.
- [224] L. Hao, W. Wang, X. Shen, S. Wang, Q. Li, F. An, S. Wu, *J. Agric. Food Chem.* **2020**, *68*, 369–375.
- [225] A. N. Glazer, H. S. Rye, *Nature* **1992**, *359*, 859–861.
- [226] A. S. Biebricher, I. Heller, R. F. H. Roijmans, T. P. Hoekstra, E. J. G. Peterman, G. J. L. Wuite, *Nat. Commun.* **2015**, *6*, DOI 10.1038/ncomms8304.
- [227] C. Hong, X. Zhang, S. Ye, H. Yang, Z. Huang, D. Yang, R. Cai, W. Tan, *ACS Appl. Mater. Interfaces* **2021**, *13*, 19695–19700.
- [228] S. Jiang, M. Liu, W. Tantai, Q. Xu, X. Zou, F. Ma, C. Y. Zhang, *Chem. Commun.* **2021**, *57*, 2041–2044.
- [229] N. O. Fischer, T. M. Tarasow, J. B. H. H. Tok, *Anal. Biochem.* **2008**, *373*, 121–128.
- [230] M. Wang, I. Dilek, B. A. Armitage, *Langmuir* **2003**, *19*, 6449–6455.
- [231] J. O. Smith, D. A. Olson, B. A. Armitage, *J. Am. Chem. Soc.* **1999**, *121*, 2686–2695.
- [232] V. V. Demidov, V. N. Potaman, M. D. Frank-Kamenetskii, M. Egholm, O. Buchard, S. H. Sönnichsen, P. E. Nielsen, *Biochem. Pharmacol.* **1994**, *48*, 1310–1313.
- [233] T. Y. Kim, M. C. Lim, M. A. Woo, B. H. Jun, *Nanomaterials* **2018**, *8*, 1–13.
- [234] H. Jans, Q. Huo, *Chem. Soc. Rev.* **2012**, *41*, 2849–2866.
- [235] W. Zhou, X. Gao, D. Liu, X. Chen, *Chem. Rev.* **2015**, *115*, 10575–

10636.

- [236] W. Zhao, M. A. Brook, Y. Li, *ChemBioChem* **2008**, *9*, 2363–2371.
- [237] E. Boisselier, D. Astruc, *Chem. Soc. Rev.* **2009**, *38*, 1759–1782.
- [238] R. Elghanian, J. J. Storhoff, R. C. Mucic, R. L. Letsinger, C. A. Mirkin, *Science* **1997**, *277*, 1078–1081.
- [239] M. M. Ali, S. D. Aguirre, Y. Xu, C. D. M. M. Filipe, R. Pelton, Y. Li, *Chem. Commun.* **2009**, 6640–6642.
- [240] C. Hong, A. Baek, S. S. Hah, W. Jung, D. E. Kim, *Anal. Chem.* **2016**, *88*, 2999–3003.
- [241] K. Liang, H. Wang, P. Li, Y. Zhu, J. Liu, B. Tang, *Talanta* **2020**, *207*, 120285.
- [242] X. Sun, Y. Wang, L. Zhang, S. Liu, M. Zhang, J. Wang, B. Ning, Y. Peng, J. He, Y. Hu, et al., *Anal. Chem.* **2020**, *92*, 3032–3041.
- [243] Y. Zhang, L. Chen, K. Hsieh, T. H. Wang, *Anal. Chem.* **2018**, *90*, 12180–12186.
- [244] C. Larsson, I. Grundberg, O. Söderberg, M. Nilsson, *Nat. Methods* **2010**, *7*, 395–397.
- [245] L. Yao, Y. Chen, J. Teng, W. Zheng, J. Wu, S. B. Adeloju, D. Pan, W. Chen, D. Pan, W. Chen, *Biosens. Bioelectron.* **2015**, *74*, 534–538.
- [246] Y. Jiang, Z. Qiu, T. Le, S. Zou, X. Cao, *Anal. Chim. Acta* **2020**, *1127*, 79–88.
- [247] D. Zhu, Y. Yan, P. Lei, B. Shen, W. Cheng, H. Ju, S. Ding, *Anal. Chim. Acta* **2014**, *846*, 44–50.
- [248] S. Tyagi, F. R. Kramer, *Nat. Biotechnol.* **1996**, *14*, 303–308.
- [249] Z.-S. Wu, S. Zhang, H. Zhou, G.-L. Shen, R. Yu, *Anal. Chem.* **2010**, *82*, 2221–2227.
- [250] J. Wang, H. yan H. ya. H. yan Dong, Y. Zhou, L. yu L. y. Han, T. Zhang, M. Lin, C. Wang, H. Xu, Z. S. Wu, L. Jia, et al., *Biosens. Bioelectron.* **2018**, *122*, 239–246.
- [251] N. Li, L. Yi, Z. He, W. Zhang, H. Li, J. M. Lin, *Analyst* **2017**, *142*, 634–640.
- [252] T. Gao, B. Wang, L. Shi, X. Zhu, Y. Xiang, J. I. Anzai, G. Li, *Anal. Chem.* **2017**, *89*, 10776–10782.
- [253] J. Bai, Z. Gao, W. Wang, Y. Peng, J. Wu, M. Zhang, Q. Li, Z. Zhao, M. Liu, J. Wang, et al., *Anal. Chem.* **2021**, *93*, 4488–4496.
- [254] M. Nilsson, M. Gullberg, F. Dahl, K. Szuhai, A. K. Raap, *Nucleic Acids Res.* **2002**, *30*, 66e – 66.
- [255] L. Lv, L. Guo, Q. Zhao, *Anal. Methods* **2015**, *7*, 1855–1859.
- [256] Z. Zhan, H. Li, J. Liu, G. Xie, F. Xiao, X. Wu, Z. P. Aguilar, H. Xu, *Food Control* **2020**, *107*, 106806.
- [257] S. Wu, Q. Yu, C. He, N. Duan, *Spectrochim. Acta - Part A Mol. Biomol. Spectrosc.* **2020**, *224*, 117387.
- [258] Z. W. Wu, X. C. Xie, H. R. Guo, H. Xia, K. J. Huang, *Anal. Bioanal. Chem.* **2020**, *412*, 915–922.

- [259] C. Ge, R. Yuan, L. Yi, J. Yang, H. Zhang, L. Li, G. Yi, W. Nian, G. Yi, *J. Electroanal. Chem.* **2018**, 826, 174–180.
- [260] S. Ciftci, R. Cánovas, F. Neumann, T. Paulraj, M. Nilsson, G. A. Crespo, N. Madaboosi, *Biosens. Bioelectron.* **2020**, 151, DOI 10.1016/j.bios.2019.112002.
- [261] D. Tang, B. Xia, Y. Tang, J. Zhang, Q. Zhou, *Microchim. Acta* **2019**, 186, DOI 10.1007/s00604-019-3454-1.
- [262] Y. Jia, F. Sun, N. Na, J. Ouyang, *Anal. Chim. Acta* **2019**, 1060, 64–70.
- [263] F. Sun, X. Sun, Y. Jia, Z. Hu, S. Xu, L. Li, N. Na, J. Ouyang, *Analyst* **2019**, 144, 6019–6024.
- [264] L. Ge, B. Li, H. Xu, W. Pu, H. F. Kwok, *Biosens. Bioelectron.* **2019**, 132, 210–216.
- [265] L. Huang, D. B. Wang, N. Singh, F. Yang, N. Gu, X. E. Zhang, *Nanoscale* **2018**, 10, 20289–20295.
- [266] T. Fan, Y. Du, Y. Yao, J. Wu, S. Meng, J. Luo, F. Gao, X. Zhang, D. Yang, C. Wang, et al., *Sensors Actuators, B Chem.* **2018**, 266, 9–18.
- [267] G. Yao, H. Pei, J. Li, Y. Zhao, D. Zhu, Y. Zhang, Y. Lin, Q. Huang, C. Fan, *NPG Asia Mater.* **2015**, 7, e159.
- [268] B. T. Roembke, S. Nakayama, H. O. Sintim, *Methods* **2013**, 64, 185–198.
- [269] D. Sen, W. Gilbert, *Nature* **1988**, 334, 364–366.
- [270] B. R. Vummidi, J. Alzeer, N. W. Luedtke, *ChemBioChem* **2013**, 14, 540–558.
- [271] P. Chilka, N. Desai, B. Datta, *Molecules* **2019**, 24, 752.
- [272] Y. Guo, W. Yao, Y. Xie, X. Zhou, J. Hu, R. Pei, *Microchim. Acta* **2016**, 183, 21–34.
- [273] H. X. Jiang, Z. Z. Liang, Y. H. Ma, D. M. Kong, Z. Y. Hong, *Anal. Chim. Acta* **2016**, 943, 114–122.
- [274] X. Xu, H. Wei, W. Jiang, *Analyst* **2017**, 142, 2247–2252.
- [275] I. J. Lee, N. I. Goo, D. E. Kim, *Analyst* **2016**, 141, 6503–6506.
- [276] W. Li, W. Jiang, L. Wang, *Anal. Chim. Acta* **2016**, 940, 1–7.
- [277] X. Zheng, L. Niu, D. Wei, X. Li, S. Zhang, *Sci. Rep.* **2016**, 6, 2–7.
- [278] W. Li, L. Wang, Y. Wang, W. Jiang, *Talanta* **2018**, 189, 383–388.
- [279] X. Li, J. Song, Q. W. Xue, F. H. You, X. Lu, Y. C. Kong, S. Y. Ma, W. Jiang, C. Z. Li, *Nanomaterials* **2016**, 6, 1–10.
- [280] F. Yang, X. Li, J. Li, Y. Xiang, R. Yuan, *Talanta* **2019**, 204, 812–816.
- [281] J. Li, F. Yang, B. Jiang, W. Zhou, Y. Xiang, R. Yuan, *Analyst* **2020**, 145, 7858–7863.
- [282] J. Teng, Y. Ye, L. Yao, C. Yan, K. Cheng, F. Xue, D. Pan, B. Li, W. Chen, *Microchim. Acta* **2017**, 184, 3477–3485.
- [283] J. Lv, S. Xie, W. Cai, J. Zhang, D. Tang, Y. Tang, *Analyst* **2017**, 142, 4708–4714.
- [284] C. Y. Lee, H. T. Fan, Y. Z. Hsieh, *Sensors Actuators, B Chem.* **2018**,

- 255, 341–347.
- [285] T. Liu, D. Sun, M. Gu, X. Wu, G. L. Wang, *Sensors Actuators, B Chem.* **2020**, *317*, 128210.
- [286] M. Gu, D. Sun, T. Liu, X. Wu, G. L. Wang, *Sensors Actuators, B Chem.* **2020**, *324*, 128660.
- [287] R. Cai, S. Zhang, L. Chen, M. Li, Y. Zhang, N. Zhou, *ACS Appl. Mater. Interfaces* **2021**, *13*, 4905–4914.
- [288] W. Jiang, L. Liu, L. Zhang, Q. Guo, Y. Cui, M. Yang, *Microchim. Acta* **2017**, *184*, 4757–4763.
- [289] W. Xiang, G. Wang, S. Cao, Q. Wang, X. Xiao, T. Li, M. Yang, *Microchim. Acta* **2018**, *185*, 335.
- [290] C. Shen, S. Liu, X. Li, M. Yang, *Anal. Chim. Acta* **2019**, *91*, 11614–11619.
- [291] C. Shen, S. Liu, X. Li, D. Zhao, M. Yang, *Microchim. Acta* **2018**, *185*, DOI 10.1007/s00604-018-3086-x.
- [292] Q. Wang, B. Jiang, J. Xie, Y. Xiang, R. Yuan, Y. Chai, *Analyst* **2013**, *138*, 5751–5756.
- [293] P. Miao, L. Ning, X. Li, P. Li, G. Li, *Bioconjug. Chem.* **2012**, *23*, 141–145.
- [294] X. Cheng, X. Liu, T. Bing, Z. Cao, D. Shangguan, *Biochemistry* **2009**, *48*, 7817–7823.
- [295] J. Kosman, B. Juskowiak, *Anal. Chim. Acta* **2011**, *707*, 7–17.
- [296] S. Bi, Y. Cui, Y. Dong, N. Zhang, *Biosens. Bioelectron.* **2014**, *53*, 207–213.
- [297] J. W. Lim, T. Y. Kim, S. W. Choi, M. A. Woo, *Food Chem.* **2019**, *300*, 125177.
- [298] J. W. Lim, T. Y. Kim, M. C. Lim, S. W. Choi, M. A. Woo, *Biochip J.* **2020**, *14*, 169–178.
- [299] S. Song, X. Wang, K. Xu, G. Xia, X. Yang, *J. Agric. Food Chem.* **2019**, *67*, 1244–1253.
- [300] E. Santovito, D. Greco, V. D’Ascanio, S. M. Sanzani, G. Avantaggiato, *Anal. Chim. Acta* **2020**, *1133*, 20–29.
- [301] P. Yan, Y. Hao, Z. Shu, C. Gu, X. Zhou, X. Liu, H. Xiang, *Microchim. Acta* **2018**, *185*, 299.
- [302] Y. Guo, Y. Wang, S. Liu, J. Yu, H. Wang, Y. Wang, J. Huang, *Biosens. Bioelectron.* **2016**, *75*, 315–319.
- [303] R. Huang, L. He, Y. Xia, H. Xu, C. Liu, H. Xie, S. Wang, L. Peng, Y. Y. Y. Liu, Y. Y. Y. Liu, et al., *Small* **2019**, *15*, 1–7.
- [304] S. K. Li, A. Y. Chen, Y. Q. Chai, R. Yuan, Y. Zhuo, *Electrochim. Acta* **2016**, *212*, 767–774.
- [305] F. Li, H. Zhang, Z. Wang, A. M. Newbigging, M. S. Reid, X.-F. Li, X. C. Le, *Anal. Chim. Acta* **2014**, *87*, 274–292.
- [306] H. Zhang, F. Li, B. Dever, X. F. Li, X. C. Le, *Chem. Rev.* **2013**, *113*, 2812–2841.
- [307] M. Liu, D. Chang, Y. Li, *Acc. Chem. Res.* **2017**, *50*, 2273–2283.

- [308] D. Morrison, M. Rothenbroker, Y. Li, *Small Methods* **2018**, *2*, 1700319.
- [309] Y. Sun, Y. Chang, Q. Zhang, M. Liu, *Micromachines* **2019**, *10*, 531.
- [310] L. Tang, Y. Liu, M. M. Ali, D. K. Kang, W. Zhao, J. Li, *Anal. Chem.* **2012**, *84*, 4711–4717.
- [311] K. Abnous, N. M. Danesh, M. Ramezani, M. Alibolandi, M. A. Nameghi, T. S. Zavvar, S. M. Taghdisi, *Anal. Chim. Acta* **2021**, *1165*, 338549.
- [312] L. Xu, Q. Dai, Z. Shi, X. Liu, L. Gao, Z. Wang, X. Zhu, Z. Li, *J. Microbiol. Methods* **2020**, *173*, 105917.
- [313] D. Gou, G. Xie, Y. Li, X. Zhang, H. Chen, *Microchim. Acta* **2018**, *185*, 436.
- [314] S. Lv, K. Zhang, D. Tang, *Analyst* **2019**, *144*, 3716–3720.
- [315] S. M. Russell, R. De La Rica, *ACS Sensors* **2018**, *3*, 1059–1068.
- [316] N. Convery, N. Gadegaard, *Micro Nano Eng.* **2019**, *2*, 76–91.
- [317] S. Feng, S. Mao, J. Dou, W. Li, H. Li, J. M. Lin, *Chem. Sci.* **2019**, *10*, 8571–8576.
- [318] L. He, Z. Shen, J. Wang, J. Zeng, W. Wang, H. Wu, Q. Wang, N. Gan, *Microchim. Acta* **2020**, *187*, 176.
- [319] L. He, Z. Shen, Y. Cao, T. Li, D. Wu, Y. Dong, N. Gan, *Analyst* **2019**, *144*, 2755–2764.
- [320] L. Guo, L. Hao, Q. Zhao, *Anal. Bioanal. Chem.* **2016**, *408*, 4715–4722.
- [321] Y. Li, W. Dai, X. Lv, Y. Deng, *Anal. Methods* **2018**, *10*, 1767–1773.
- [322] W. Zhang, Z. He, L. Yi, S. Mao, H. Li, J. M. Lin, *Biosens. Bioelectron.* **2018**, *102*, 652–660.
- [323] J. Credou, T. Berthelot, *J. Mater. Chem. B* **2014**, *2*, 4767–4788.
- [324] S. Jahanshahi-Anbuhi, K. Pennings, V. Leung, M. Liu, C. Carrasquilla, B. Kannan, Y. Li, R. Pelton, J. D. Brennan, C. D. M. Filipe, *Angew. Chemie* **2014**, *53*, 6155–6158.
- [325] B. Kannan, S. Jahanshahi-Anbuhi, R. H. Pelton, Y. Li, C. D. M. Filipe, J. D. Brennan, *Anal. Chem.* **2015**, *87*, 9288–9293.
- [326] S. Jahanshahi-Anbuhi, B. Kannan, V. Leung, K. Pennings, M. Liu, C. Carrasquilla, D. White, Y. Li, R. H. Pelton, J. D. Brennan, et al., *Chem. Sci.* **2016**, *7*, 2342–2346.
- [327] M. M. Ali, C. L. Brown, S. Jahanshahi-Anbuhi, B. Kannan, Y. Li, C. D. M. Filipe, J. D. Brennan, *Sci. Rep.* **2017**, *7*, 1–10.
- [328] M. Liu, J. Wang, Y. Chang, Q. Zhang, D. Chang, C. Y. Hui, J. D. Brennan, Y. Li, *Angew. Chemie* **2020**, *59*, 7706–7710.
- [329] W. Chiuman, Y. Li, *PLoS One* **2007**, *2*, e1224.
- [330] Y. Li, D. Sen, *Nat. Struct. Mol. Biol.* **1996**, *3*, 743–747.
- [331] P. Travascio, P. K. Witting, A. G. Mauk, D. Sen, *J. Am. Chem. Soc.* **2001**, *123*, 1337–1348.
- [332] Z. Cheglakov, Y. Weizmann, B. Basnar, I. Willner, *Org. Biomol.*

- Chem.* **2007**, *5*, 223–225.
- [333] Y. Tian, Y. He, C. Mao, *Chembiochem* **2006**, *7*, 1862–4.
- [334] M. Yao, X. Lv, Y. Deng, M. Rasheed, *Anal. Chim. Acta* **2019**, *1055*, 115–125.
- [335] A. R. Pavankumar, A. Engström, J. Liu, D. Herthnek, M. Nilsson, *Anal. Chem.* **2016**, *88*, 4277–4284.
- [336] E. Paleček, M. Bartošík, *Chem. Rev.* **2012**, *112*, 3427–3481.
- [337] E. Paleček, F. Jelen, *Crit. Rev. Anal. Chem.* **2002**, *32*, 261–270.
- [338] A.-M. Chiorcea-Paquim, R. Eritja, A. M. Oliveira-Brett, *J. Nucleic Acids* **2018**, *2018*, 1–20.
- [339] T. Goda, M. Tabata, Y. Miyahara, *Front. Bioeng. Biotechnol.* **2015**, *3*, 29.
- [340] J. Shen, H. Wang, C. Li, Y. Zhao, X. Yu, X. Luo, *Biosens. Bioelectron.* **2017**, *90*, 356–362.
- [341] D. Sun, J. Lu, Z. Luo, L. Zhang, P. Liu, Z. Chen, *Biosens. Bioelectron.* **2018**, *120*, 8–14.
- [342] Y. Zhu, H. Wang, L. Wang, J. Zhu, W. Jiang, *ACS Appl. Mater. Interfaces* **2016**, *8*, 2573–2581.
- [343] R. A. Marcus, *Annu. Rev. Phys. Chem.* **1964**, *15*, 155–196.
- [344] D. Li, S. Song, C. Fan, *Acc. Chem. Res.* **2010**, *43*, 631–641.
- [345] K. Deng, C. Li, H. Huang, X. Li, *Sensors Actuators, B Chem.* **2017**, *238*, 1302–1308.
- [346] S. Lv, K. Zhang, Q. Zhou, D. Tang, *Sensors Actuators, B Chem.* **2020**, *310*, 127874.
- [347] S. Xie, J. Zhang, L. Teng, W. Yuan, Y. Tang, Q. Peng, Q. Tang, *Sensors Actuators, B Chem.* **2019**, *301*, 127072.
- [348] M. J. Li, H. J. Wang, R. Yuan, Y. Q. Chai, *Chem. Commun.* **2019**, *55*, 10772–10775.
- [349] X. Liao, C. Zhang, Z. Shi, H. Shi, Y. Qian, F. Gao, *J. Electroanal. Chem.* **2020**, *878*, 114604.
- [350] Y. Peng, L. Li, X. Yi, L. Guo, *Biosens. Bioelectron.* **2014**, *59*, 314–320.
- [351] B. Shen, J. Li, W. Cheng, Y. Yan, R. Tang, Y. Li, H. Ju, S. Ding, *Microchim. Acta* **2015**, *182*, 361–367.
- [352] Y. H. Pang, L. L. Guo, X. F. Shen, N. C. Yang, C. Yang, *Electrochim. Acta* **2020**, *341*, 136055.
- [353] J. Tang, J. Li, P. Xiong, Y. Sun, Z. Zeng, X. Tian, D. Tang, *Microchim. Acta* **2020**, *187*, 450.
- [354] M. Qing, Y. Yuan, W. Cai, S. Xie, Y. Tang, R. Yuan, J. Zhang, *Sensors Actuators B Chem.* **2018**, *263*, 469–475.
- [355] L. Y. Yao, X. Q. Yu, Y. J. Zhao, A. P. Fan, *Anal. Methods* **2015**, *7*, 8786–8792.
- [356] J. Zhang, J. Shi, H. Zhang, Y. Zhu, W. Liu, K. Zhang, Z. Zhang, *J. Extracell. Vesicles* **2020**, *10*, DOI 10.1002/jev2.12025.

- [357] K. Zhang, S. Lv, M. Lu, D. Tang, *Biosens. Bioelectron.* **2018**, *117*, 590–596.
- [358] H. Pei, F. Li, Y. Wan, M. Wei, H. Liu, Y. Su, N. Chen, Q. Huang, C. Fan, *J. Am. Chem. Soc.* **2012**, *134*, 11876–11879.
- [359] D. Zhu, P. Song, J. Shen, S. Su, J. Chao, A. Aldalbahi, Z. Zhou, S. Song, C. Fan, X. Zuo, et al., *Anal. Chem.* **2016**, *88*, 4949–4954.
- [360] A. Bagheri Hashkavayi, B. S. Cha, S. H. Hwang, J. Kim, K. S. Park, *Sensors Actuators, B Chem.* **2021**, *343*, 130087.
- [361] Y. Guo, X. Sun, G. Yang, J. Liu, *Chem. Commun.* **2014**, *50*, 7659–7662.
- [362] S. M. Taghdisi, N. M. Danesh, M. Ramezani, M. Alibolandi, M. A. Nameghi, G. Gerayelou, K. Abnous, *Talanta* **2021**, *223*, 121705.
- [363] X. Yi, L. Li, Y. Peng, L. Guo, *Biosens. Bioelectron.* **2014**, *57*, 103–109.
- [364] M. Y. Lin, W. Y. Hsu, Y. S. Yang, J. W. Huang, Y. L. Chung, H. Chen, *Anal. Bioanal. Chem.* **2016**, *408*, 4785–4797.
- [365] J. Wang, *TrAC - Trends Anal. Chem.* **2002**, *21*, 226–232.
- [366] A. Chen, S. Yang, *Biosens. Bioelectron.* **2015**, *71*, 230–242.
- [367] A. Leaf, *JAMA J. Am. Med. Assoc.* **1993**, *269*, 616–618.
- [368] A. P. Dhawan, W. J. Heetderks, M. Pavel, S. Acharya, M. Akay, A. Mairal, B. Wheeler, C. C. Dacso, T. Sunder, N. Lovell, et al., *IEEE J. Transl. Eng. Heal. Med.* **2015**, *3*, 1–10.
- [369] D. A. Giljohann, C. A. Mirkin, *Nature* **2009**, *462*, 461–464.
- [370] C. P. Price, *BMJ* **2001**, *322*, 1285–1288.
- [371] C. P. Price, *Clin. Chem. Lab. Med.* **2002**, *40*, 246–251.
- [372] B. Udugama, P. Kadhiresan, W. C. W. Chan, *Proc. Natl. Acad. Sci. U. S. A.* **2020**, *117*, 4632–4641.
- [373] S. Miyamoto, S. Sano, K. Takahashi, T. Jikihara, *Anal. Biochem.* **2015**, *473*, 28–33.
- [374] S. Roy, N. F. Mohd-Naim, M. Safavieh, M. U. Ahmed, *ACS Sensors* **2017**, *2*, 1713–1720.

CHAPTER 3.

PROTEIN-MEDIATED SUPPRESSION OF ROLLING CIRCLE AMPLIFICATION FOR BIOSENSING WITH AN APTAMER- CONTAINING DNA PRIMER

3.1 Author's Preface

The following chapter was published in *Chemistry – A European Journal* under the citation:

Roger M. Bialy, Monsur M. Ali, Yingfu Li, and John D. Brennan.
Protein-Mediated Suppression of Rolling Circle Amplification for
Biosensing with an Aptamer-Containing DNA Primer. *Chem. Eur. J.*
2020 26(20): 5085-5092, DOI: 10.1002/chem.20200245

I was responsible for all experimental design, execution and analysis included in this chapter. Dr. Ali provided insight into sensor troubleshooting. I wrote the first draft of the manuscript. Dr. Brennan and Dr. Li provided editorial input to generate the final draft of the paper. This article has been reprinted with permission from John Wiley and Sons ©.

3.2 Abstract

We report a method to detect proteins via suppression of rolling circle amplification (RCA) by using an appropriate aptamer as the linear primer (denoted as an aptaprimer) to initiate RCA. In the absence of a protein target, the aptaprimer is free to initiate RCA, which can produce long DNA products that are detected via binding of a fluorescent intercalating dye. Introduction of a target causes the primer region within the aptamer to become unavailable for binding to the circular template, inhibiting RCA. Using SYBR Gold or QuantiFluor dyes as fluorescent probes to bind to the RCA reaction product, it is possible to produce a generic protein-modulated RCA assay system that does not require fluorophore- or biotin-modified DNA species, substantially reducing complexity and cost of reagents. Based on this modulation of RCA, we demonstrate the ability to produce both solution and paper-based assays for rapid and quantitative detection of proteins including platelet derived growth factor and thrombin.

3.3 Introduction

DNA amplification is a widely used technique in many fields, and has particular utility in the area of molecular diagnostics. While early work focussed on DNA amplification via the polymerase chain reaction (PCR), more recent studies have focused on isothermal DNA amplification methods, such as strand displacement amplification (SDA),¹⁻³ recombinase-polymerase amplification (RPA),¹ loop-mediated amplification

(LAMP),^{1,2,4} helicase dependent amplification (HDA),^{1,2,4,5} hybridization chain reaction (HCR)^{1,6} and rolling circle amplification (RCA).⁷⁻⁹ These methods are easier to perform and have the power to deliver ultrasensitive detection of nucleic acid species.

Over the past decade there has been increasing interest in utilizing DNA amplification methods for the detection of non-nucleic acid targets. Common strategies involve the use of nucleic acid modified antibodies (i.e., immuno-RCA^{10,11} and immuno-HCR^{12,13}), antibody-directed proximity ligation assays¹⁴⁻¹⁶ and target binding to a DNA aptamer or DNA enzyme (DNAzyme) as a means to modulate the degree of amplification achieved by a given isothermal amplification (ITA) system. In the latter case, examples include: the use of a proximity extension assay involving both a linear and circular aptamer that combine to perform RCA;¹⁷ circle ligation-RCA¹⁸ involving aptamers switching conformation upon protein binding to allow ligation into a circle to initiate RCA; nicking enzyme-assisted recycling using aptamer hairpin switches;¹⁹⁻²² exonuclease-assisted amplification assays;²³⁻²⁶ and aptamer-mediated SDA systems wherein the aptamer-protein complex modulates SDA.²⁷⁻³⁰ While these methods provide the ability to detect proteins at low levels, there are several drawbacks, including the need for specially modified antibodies and separation steps for immuno-coupled ITA methods, requirements for specially modified nucleic acids (i.e., carrying optical or electrochemical labels) and multiple

primers or processing enzymes for most of the aptamer-coupled ITA methods, or a requirement for operation of ITA reactions at elevated temperatures, which makes it difficult to adapt such assays to simple point-of-care devices, such as lateral flow tests or paper analytical devices, to allow use at the point of care (POC).

With regard to POC tests, RCA has several advantages over other ITA methods. It can be performed at room temperature, requires minimal reagents (a linear and circular primer and one processing enzyme) and is compatible with many types of assay outputs.^{31–35} Our groups have reported on several methods to modulate RCA using a protein target, including: integration of a protein-binding aptamer into a circular template to modulate rolling circle amplification (RCA);³⁶ binding of a protein to release an aptamer-primer conjugate from reduced graphene oxide (rGO) to initiate RCA;^{32,34} using an aptamer to inhibit a linear primer from being extended along a circular template until target binds to release the aptamer;³⁷ and use of protein-binding DNAzymes that can release a DNA primer upon catalytic cleavage of an embedded ribonucleic acid to initiate RCA.³⁸ While such systems could often be integrated into paper-based POC devices, the assays still required multiple steps and expensive reagents such as rGO or doubly-labelled DNAzyme species, or addition of labile reagents such as hemin or peroxide to generate a signal.

Herein, we describe a simplified method to couple protein-binding aptamers to isothermal amplification, which can be performed as a one-pot reaction without using any labelled or otherwise modified DNA species, and can be easily adapted to a paper-based POC device. The assay (Fig. 3.1) utilizes a protein-binding aptamer that can also act as the linear primer to initiate RCA (denoted as an aptaprimer). In the absence of target, the aptaprimer (AP) can bind a complementary circular template (CT) and initiate RCA in the presence of phi29 DNA polymerase (ϕ 29DP) and dNTPs to produce a long DNA reaction product (RP) that is able to bind to fluorescent dyes such as SYBR Gold™ or QuantiFluor™ to generate a fluorescence signal (Fig. 3.1A). Addition of a protein target causes the aptaprimer to form an aptamer-protein complex, which prevents binding of the aptaprimer to the CT, inhibiting RCA and modulating the fluorescence signal. In the AP, the primer-binding region is embedded within the native aptamer at the 3'-end. Polymerization of the AP strand occurs on the 3'-end with displacement of hybridized AP by ϕ 29DP as it reads through the CT (Fig. 3.1B). We demonstrate the assay system for detection of two proteins, platelet derived growth factor (PDGF) and thrombin, and highlight the ability to couple protein-mediated isothermal DNA amplification to an output signal in a simple one-step assay format that can be utilized both in solution or as part of a paper-based POC test (Fig. 3.1C).

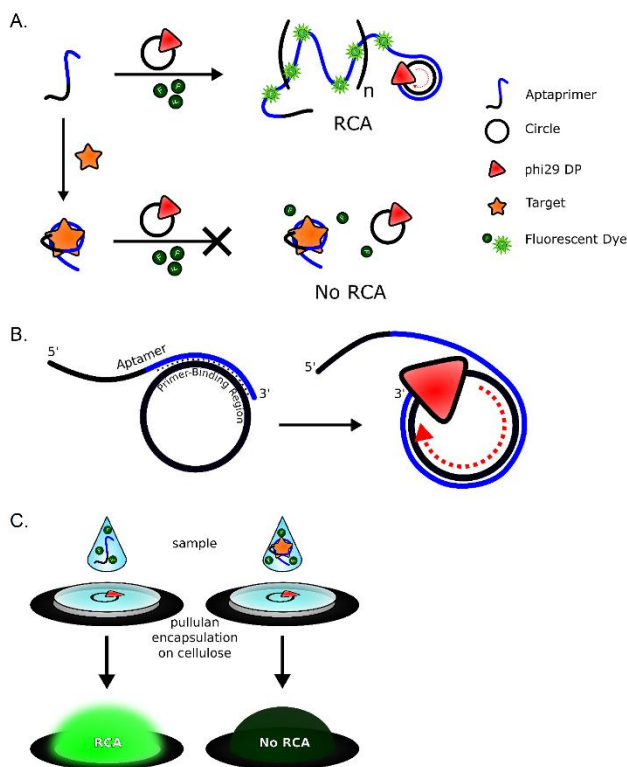


Figure 3.1. (A) Schematic representation of an aptamer for target-mediated generation of RCA product by incorporating an intercalating dye such as SYBR Gold or QuantiFluor. Addition of a protein target prevents binding of the aptamer to the circular template, inhibiting RCA. (B) Aptamer concept: the circle-binding region is embedded within the native aptamer strand on the 3'-end. Polymerization occurs from the 3'-end with ϕ 29DP displacing hybridized aptamer to continue elongation of the RP. (C) Sample mixed with aptamer and intercalating dye is spotted onto a wax-contained cellulose well holding pullulan-encapsulated RCA reagents (ϕ 29DP, CT, and dNTPs) allowing for real-time one-step RCA and production of a fluorescence signal.

3.4 Results and Discussion

As noted above, our groups have previously investigated the inhibition of RCA based on binding of protein targets to aptamers present within the circular template.³⁶ In this case, RCA was inhibited due to the inability of ϕ 29DP to read through the bound protein and extend the primer. However,

this approach requires that linear aptamers be ligated to form circular aptamers, which can severely alter performance,^{39,40} or that circular aptamers be selected directly from circularized pools of DNA.⁴¹ Given that the vast majority of aptamers are linear, we were interested in determining whether a protein-aptamer complex that was partially complementary to a circular template (i.e., an aptaprimer) would prevent RCA owing to an inability to bind the circular template, as such an approach should be amenable to any linear aptamer and thus be more versatile.

Our initial studies utilized the anti-PDGF aptamer as the linear aptaprimer, along with a circular template containing a variable number of complementary nucleotides so as to modulate the binding affinity of the CT to the anti-PDGF aptamer.^{42,43} This optimization is analogous to that used for developing structure-switching aptamers.^{44–46} The number of complementary nucleotides was varied from as short as 9 nt up to the full length of the AP (35 nt). Complementary regions shorter than 9 nt were not investigated, as significantly shortened primers can reduce the extent of amplification due to a hindered rate of RCA initiation.⁴⁷

Figure 3.2 shows native polyacrylamide gel electrophoresis (nPAGE) data to evaluate the binding between the PDGF aptaprimer (P-AP) and the CT, with and without PDGF, using 12 (Fig. 3.2A), 18 (Fig. 3.2B), 27 (Fig. 3.2C) and 35 (Fig. 3.2D) complementary nucleotides in the CT. A pairing sequence of 12 nt did not result in duplex formation between the CT and AP

under any conditions (Fig. 3.2A; this was also observed for a CT with 9 complementary nucleotides, data not shown) and thus was not investigated further. As shown in Figure 3.2B, use of an 18 nt complementary region allowed duplex formation between the CT and AP in the absence of PDGF, though some unbound CT and AP was still present. Addition of PDGF to the AP prior to the addition of CT caused the formation of an AP-target (AP-T) complex, and importantly, no AP-CT duplex band was observed, even at elevated levels of CT (2:1 mole ratio of CT:AP). In addition, no AP-CT-T triplex was observed. This suggested that binding of PDGF to the AP prevented binding of the CT to the same AP, which should thus prevent RCA (see below).

Increasing the primer-binding region to 27 nt (Fig. 3.2C) showed improved duplex formation in the absence of PDGF with less free AP and CT present in the gel. However, a faint band corresponding to the AP-CT complex can be observed at higher CT:AP mole ratios, which could potentially lead to background RCA. In addition, the CT showed a secondary band in the nPAGE, which may have resulted from the CT adopting an intramolecular secondary structure with an altered mobility on the gel.⁴⁸ Increasing the primer-binding region to the full length of the PDGF aptamer (35 nt, Fig. 3.2D) led to strong duplex formation in the absence of PDGF, with no visible band corresponding to free AP. However, even in the presence of PDGF, clear formation of an AP-CT duplex band was

detected by nPAGE (as well as a primary and secondary CT band, as was observed for the 27 nt CT), which would be expected to produce significant background RCA, and potentially require significantly higher concentrations of PDGF to initiate the inhibition reaction. Based on the results above, a CT with an 18 nt complementary region was selected for further studies. A mole ratio of 1:1 CT:AP was chosen based on titration of CT into AP (Fig. 3.2B) and titration of AP into CT (Fig. S3.1), both of which showed a high level of AP-CT duplex at a 1:1 ratio in the absence of PDGF.

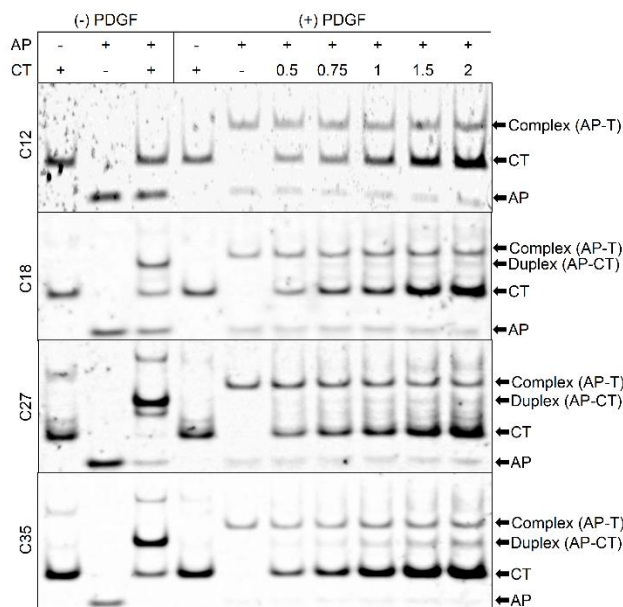


Figure 3.2. Determination of RCA inhibition mechanism using nPAGE analysis showing the presence of aptaprimer (AP), circular template (CT), AP-CT duplex and aptamer-target (AP-T) complex with and without PDGF using a circular template containing a: (C12) 12 nucleotide binding region; (C18) 18 nucleotide binding region; (C27) 27 nucleotide binding region; (C35) 35 nucleotide binding region. T = target (specifically PDGF). The concentration of reagents used was 0 or 20 nM for AP, 0-40 nM for CT, and 0 or 100 nM for PDGF.

We next examined the effect of varying the concentration of PDGF on the formation of the AP-CT duplex and AP-T complex using the 18 nt complementary region (Fig. 3.3A), as well as the effect of PDGF concentration on RCA efficiency (Figs. 3B-D). nPAGE data demonstrated that increased concentrations of PDGF caused a loss of the AP-CT duplex band and a corresponding increase in the AP-T complex band. More importantly, denaturing PAGE demonstrated that in the absence of PDGF, the AP-CT system was able to initiate the RCA reaction (Fig. 3.3B), producing substantial reaction product (RP band in the gel, note that all RP bands are measured relative to a loading control, LC). RCA efficiency was also tested with CTs with complementary regions of 12, 27 and 35 nts; however, the 18 nt system was determined to produce the highest degree of amplification (Fig. S3.2). Increased concentrations of PDGF were observed to produce a decrease in the intensity of the band for the RP (Fig. 3.3B), confirming that the formation of the AP-T complex prevented the AP from binding to the CT, in agreement with Figure 3.3A, and thus was able to inhibit the RCA reaction. As a control, BSA was used in place of PDGF, and was observed to be unable to inhibit the RCA reaction, indicating that the inhibition was caused specifically by the presence of PDGF (Fig. 3.3C).

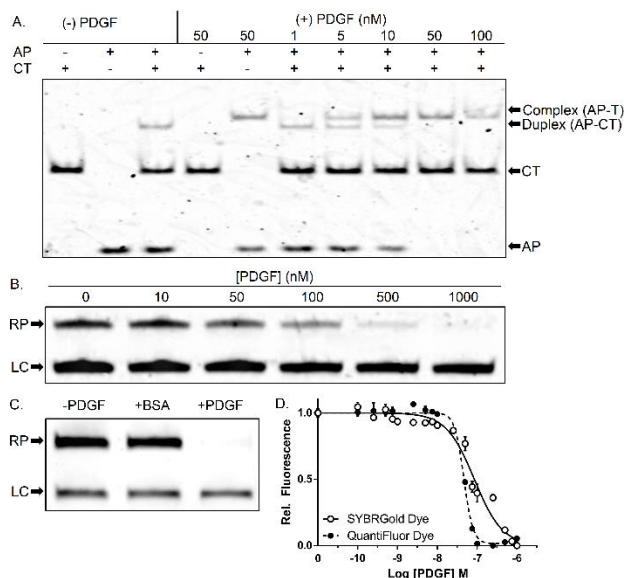


Figure 3.3. Inhibition assay using an anti-PDGF aptamer system. (A) Native PAGE (8%) of the species formed when the PDGF aptamer is complexed with increasing amounts of PDGF, followed by addition of CT; (B) Denaturing PAGE (10%) of RCA product after treatment with TaqI Restriction Enzyme in the presence of increasing amounts of PDGF. LC denotes the loading control; (C) Denaturing PAGE (10%) of RCA product, denoted as RP, after treatment with TaqI Restriction Enzyme in the absence of protein, and in the presence of 1 μ M of either BSA or PDGF. LC denotes the loading control; (D) Titration curve of RCA product generation in the presence of PDGF monitored in real-time using either SYBR Gold or QuantiFluor as intercalating dyes. All RCA reactions were conducted for 30 minutes.

To monitor this inhibition of the RCA reaction in real-time, two intercalating dyes (SYBR Gold and QuantiFluor) were used to quantify the amount of RP produced as a function of PDGF concentration (Fig. 3.3D). In both cases, the fluorescence response was determined to be dependent on PDGF concentration, with the SYBR Gold dye providing a limit of detection (LOD) of 10 nM (3σ) using a RCA reaction time of 30 minutes at

room temperature, and the QuantiFluor dye providing an LOD of 25 nM (3σ) with a somewhat narrower dynamic range under identical reaction conditions. These values are an order of magnitude higher than those reported for non-amplified assays of PDGF (0.1 – 1 nM),^{18,43,49} but significantly higher than previously reported PDGF assays utilizing RCA (1 – 10 fM).^{37,50} The poorer performance is likely a result of the use of an inhibition assay, where it is more difficult to see a small change in signal on a high background.

We note that it is also possible to form the AP-CT duplex prior to the addition of PDGF, in which case the added PDGF can bind to the AP when present in a duplex and either displace the AP from the CT or form a tripartite AP-CT-T complex, both of which can inhibit RCA (Fig. S3.3). However, this method requires both a longer incubation time (1 h) to allow displacement of the AP from the CT, and an additional step involving later addition of phi29DP, as the presence of the enzyme when PDGF is added will lead to high background RCA. As shown in Fig S3, this procedure also leads to higher variability in the data, with more scatter and higher error bars.

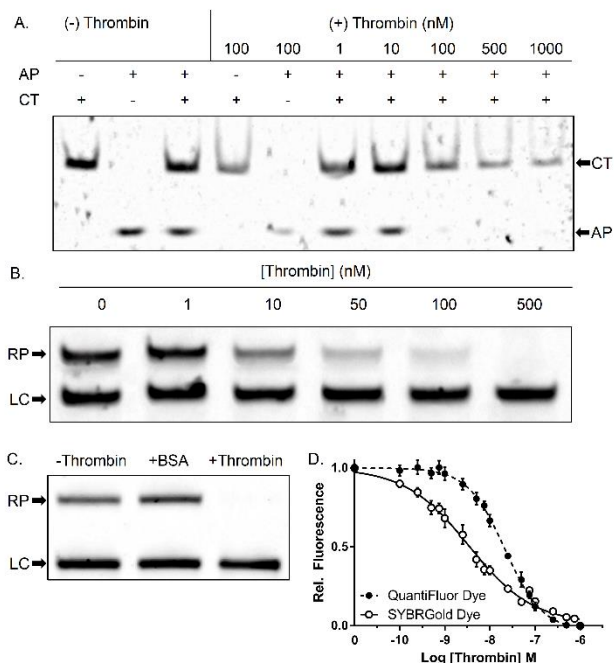


Figure 3.4. Inhibition assay using an anti-thrombin aptamer system. (A) Native PAGE (8%) of the species formed when the thrombin aptamer was complexed with increasing amounts of thrombin, followed by addition of CT; (B) Denaturing PAGE (10%) of RCA product after treatment with TaqI Restriction Enzyme in the presence of increasing amounts of thrombin. LC denotes the loading control; (C) Denaturing PAGE (10%) of RCA product, denoted as RP, after treatment with TaqI Restriction Enzyme in the absence of protein, and in the presence of 1 μ M of either BSA or thrombin. LC denotes the loading control; (D) Titration curve of RCA product generation in the presence of thrombin monitored in real-time using either SYBR Gold or Quantifluor dyes. All RCA reactions conducted for 15 minutes.

To investigate the versatility of this approach, the anti-thrombin aptamer (T-AP) system was also investigated, in this case using the 15-nt thrombin aptamer.⁵¹ As T-AP is much shorter than P-AP, tuning of the binding-region length within the CT is limited. Primer-binding regions of 9 nt (T-AP-C9) or 15 nt (T-AP-C15) were evaluated, using the addition of thrombin to the aptamer, followed by addition of the CT. As shown in

Figure S3.4, T-AP-C15 system produced the expected AP-CT duplex in the absence of thrombin, and formed an AP-CT-T complex in the presence of thrombin. The T-AP-C9 system did not show any obvious formation of an AP-CT duplex, but did appear to show formation of an AP-CT-T complex at high levels of CT. It should be noted that the weak binding between the T-AP-C9 and CT may allow dissociation during electrophoresis, and thus the lack of a band for the AP-T complex may not reliably reflect the ability of this complex to form.

To confirm the presence of an AP-CT band for the T-AP-C9 system, we utilized microscale thermophoresis (MST) using a Cy5 labelled T-AP aptamer to evaluate the formation of the AP-CT complex (Fig. S3.5). This method is based on the thermophoretic mobility and solvent induced fluorescence quenching of a labelled species upon local heating, with larger species typically showing less mobility and higher quenching, and hence a lower decrease in fluorescence.^{52,53} Predicting the thermophoretic mobility of a species is complicated as it is reliant on changes in conformation, particle size, surface charge, and hydration entropy. For example, it has been observed that DNA with G-quadruplex properties can be found in G-hairpin or G-triplex intermediates which have higher thermophoretic mobility than G-quadruplex structures.⁵⁴ As shown in Figure S3.5, the AP-CT duplex showed the most rapid fluorescence decrease. Binding between the AP and CT disrupts the G-quadruplex structure of the aptamer, which has

a more pronounced effect on the thermophoretic mobility than the added size of the CT. In contrast, the G-quadruplex structure of AP is unperturbed upon binding to thrombin, and the AP-T complex shows a slower change in fluorescence, consistent with the larger size. Unbound AP shows an intermediate fluorescence decrease as there is no thrombin to impede the mobility nor is the G-quadruplex structure disrupted to accelerate the mobility, thus confirming the presence of each species.

We then assessed the effect of varying thrombin concentration on the performance of both the T-AP-C9 (Fig. 3.4) and T-AP-C15 (Fig. S3.6) aptaprimer systems. For T-AP-C15, increased levels of thrombin resulted in an obvious decrease in the concentration of the AP-CT band, and an increase in the CT band (Fig. S3.5A); once again the T-AP-C9 electropherogram did not show formation of the AP-CT band (Fig. 3.4A), owing to dissociation of the weak complex during electrophoresis, as noted above. Interestingly, both the T-AP-C9 (Fig. 3.4B-D) and the T-AP-C15 (Figs. S6B-D) systems showed a concentration-dependent production of RP, with increasing concentrations of thrombin showing a decrease in the amount of RP generated (Fig. 3.4B, Fig. S3.5B), as well as substantial signal inhibition in the presence of thrombin relative to the buffer or the non-target protein BSA (Fig. 3.4C, Fig. S3.6C).

Real-time fluorescence monitoring of RCA reaction in solution showed that both the T-AP-C9 (Fig. 3.4D) and T-AP-C15 (Fig. S3.6D) system

produced concentration dependent fluorescence changes. In the case of the T-AP-C9 system, the limit (LOD) using SYBR gold was 100 pM (3σ) after just 15 minutes of amplification, while the QuantiFluor dye produced a detection limit of 2.5 nM (3σ) and a narrower dynamic range under identical conditions. The T-AP-C15 system produced a LOD of 500 pM for SYBR gold and 1 nM for QuantiFluor, and in each case produced a narrower dynamic range than was obtained using the T-AP-C9 system. The data show that the T-AP-C9 and T-AP-C15 systems are very similar, although the best LOD is obtained using the T-AP-C9 system with SYBR Gold.

The detection limits for this assay were somewhat poorer than was reported in a previous study involving release of the thrombin aptamer from rGO to initiate RCA³⁴ where a LOD of 10 pM was obtained using molecular beacons to report the RP. However, this assay required expensive reagents (reduced graphene oxide, molecular beacons), had multiple steps and utilized a longer amplification time (1 h) and a higher reaction temperature (30 °C).^[33] On the other hand, the LOD was observed to be up to 100-fold better than was reported for fluorescence assays that did not incorporate a RCA amplification step, such as the thrombin structure-switching assay which achieved an LOD of 10 nM.⁴⁴

An interesting point to note is that the anti-PDGF aptamer system exhibited a higher detection limit than the anti-thrombin aptamer system, even though the anti-PDGF aptamer had a higher target-binding affinity

than the anti-thrombin aptamer. We suspect that the performance of RCA the assay is governed by several factors, including: (i) the binding affinity of the aptamer to its target; (ii) the stability of the secondary and tertiary structures of the aptamer and; (iii) the accessibility of the ϕ 29DP and CT to the target-bound aptaprimer. Though the anti-PDGF aptamer has a higher affinity for its target, its secondary structure is primarily composed of several stem-loop base pairing regions, whereas the anti-thrombin aptamer is shorter and only has a simple G-quadruplex secondary structure, which may be easier to read though as a primer and thus allowed more facile initiation of RCA and a better LOD for the thrombin system.

The integration of ITA techniques^{1,55,56} onto paper-based platforms^{31,32,57–59} provides a method to simplify and miniaturize assays while maintaining sensitivity. Previously, our lab has demonstrated the ability to perform RCA on paper using both aptamers and DNAzymes that liberate a DNA sequence upon target binding, which then acts as a primer to activate RCA in a zone that contains phi29DP, an appropriate CT and dNTPs.^{31,32,60} However, as noted above, these methods were time-intensive and required costly reagents and multiple steps. Thus, we wanted to investigate the performance of the RCA inhibition assay on paper as a simpler and less expensive biosensor platform. To do so, a wax pattern was printed onto Whatman No. 1 cellulose paper and heated to create circular wells with a wax barrier. The CT (with complementary regions of

18 nt for P-AP and 9 nt for T-AP), ϕ 29DP, and dNTPs were mixed with pullulan (a stabilizing agent^{31,61}), pipetted onto the cellulose surface and allowed to dry. A second mixture contained the aptamer and fluorescent intercalating dye. The target was added to this mixture, incubated for 15 minutes, and then spotted onto the circular well to initiate RCA for a further 15-30 minutes, accompanied by real-time fluorescent intensity measurements.

Initial studies using both SYBR Gold and QuantiFluor to detect RP in the cellulose wells demonstrated that SYBR Gold interacted with the cellulose surface (Fig. S3.7A), generating significant background fluorescence even in the absence of DNA, while QuantiFluor exhibited minimal background fluorescence (Fig. S3.7B). We next optimized the concentration of dye to obtain the greatest change in signal as a function of DNA concentration, which was evaluated at two different RCA reaction times. As shown in Figure S3.8, the optimal conditions involved use of 0.1 \times concentration of QF dye. Next, the concentration of aptamer used for paper-based RCA was also optimized. As shown in Fig. S3.9, the optimal concentration of the thrombin aptamer was 100 fmol (in a volume of 15 μ L, corresponding to 66.7 nM), which showed the best fluorescence intensity ratio between samples with no thrombin and 1 μ M thrombin (Fig. S3.9A). Higher levels of aptamer (500-1000 fmol) showed elevated background signals. In the case of PDGF (Fig. S3.9B), the optimal concentration was 1 pmol (667 nM),

which showed both a higher absolute fluorescence signal (not shown) and a better fluorescence intensity ratio between samples with no PDGF and those with 1 μM of PDGF. Lastly, RCA times of 15 minutes for thrombin assays and 30 minutes for PDGF assays showed the best compromise between minimizing background and assay time while avoiding signal saturation (Fig. S3.10).

Using the optimized values, the paper-based RCA inhibition assay was performed for both PDGF (Fig. 3.5A) and thrombin (Fig. 3.5B). In both cases, increased levels of target led to concentration dependent decreases in emission intensity, with the paper-based response curves closely matching those obtained from solution-based assays. In the case of PDGF, the paper-based assay provided a LOD of 6.8 nM (3σ), which was approximately 3-fold better than was obtained in solution. In the case of thrombin, the LOD was 240 pM (3σ) after just 15 minutes of amplification, which is slightly worse than the value obtained in solution (100 pM). As expected, no signals were obtained for either target when specific assay components were excluded (Fig. S3.11), and no inhibition was observed when a non-target protein was utilized (Fig. S3.12). Importantly, for both PDGF and thrombin the fluorescence was monitored in real-time immediately after addition of the mixture containing the aptamer, target and dye to the paper well, without the need for any washing or drying steps,

demonstrating the simplicity of assay relative to previously reported RCA assays on paper.^{31,32,60}

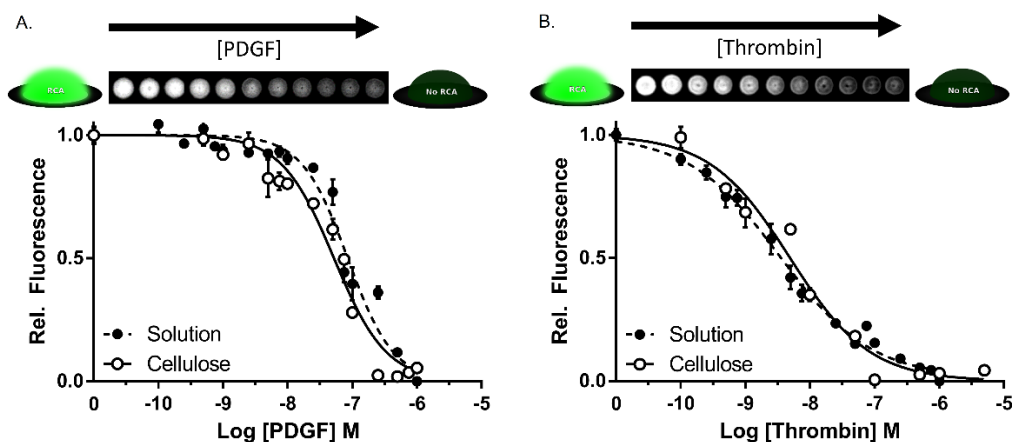


Figure 3.5. Inhibition assay on cellulose paper using: (A) the anti-PDGF aptamer system titrated with PDGF to generate a fluorescence signal on the cellulose surface after 30 minutes of real-time RCA. Top image shows the observed fluorescence signal of the paper wells was imaged after real-time RCA using the QuantiFluor dye. Bottom shows the response from the paper-based assay using the QF dye is compared to the solution-based assay using SYBR Gold. (B) the anti-thrombin aptamer system titrated with thrombin to generate a fluorescence signal on the cellulose surface after 15 minutes of real-time RCA. Top image shows the observed fluorescence signal of the paper wells as imaged after real-time RCA using QuantiFluor dye. Bottom shows the response from the paper-based assay using the QF dye is compared to the solution-based assay using SYBR Gold.

3.5 Conclusion

Utilizing an aptamer as the linear primer for an RCA reaction, it is possible to modulate the amplification reaction by using a protein target to control the ability of the aptamer to bind a circular template to initiate RCA. In this

manner, increased concentrations of a target lead to inhibition of RCA, which can be easily detected by using an intercalating dye that binds to the product of the RCA reaction. This method is both simple and rapid, and should allow for detection of any aptamer-binding target. Furthermore, the method avoids the need for expensive fluorophore- or biotin-modified DNA species. The assay can be performed both in solution and on paper, potentially making the assay amenable to use in resource limited settings if integrated with a portable smartphone-based fluorescence reader.^{62–64}

3.6 Experimental

Oligonucleotides and Other Materials. All DNA oligonucleotides (Table S1) were obtained from Integrated DNA Technologies (IDT), and purified by standard 10% denaturing (8 M urea) polyacrylamide gel electrophoresis (dPAGE) or high-performance liquid chromatography (HPLC). SYBR Gold, T4 DNA ligase, T4 polynucleotide kinase (PNK), phi29 DNA polymerase (ϕ 29DP), FastDigest TaqI restriction enzyme, and deoxyribonucleoside 5'-triphosphate mixture (dNTP) were purchased from Thermo Fisher (USA). QuantiFluor ssDNA dye was purchased from Promega (USA). Bovine Serum Albumin (BSA) was purchased from Millipore Sigma (Oakville, ON). Human thrombin was purchased from Haematologic Technologies Inc (Essex Jct., VT). Recombinant Human PDGF was purchased from Cedarlane Labs (Burlington, ON). Pullulan (molecular weight of ~200,000 Daltons) was obtained from Polysciences Inc. Whatman No. 1 cellulose

paper was purchased from Millipore Sigma (Oakville, ON). Water was purified with a Milli-Q Synthesis A10 water purification system. All other chemicals and solvents were of analytical grade and were used as received.

Instruments. Cellulose paper was laminated using a Scotch Thermal Laminator (3M) with 3 mm thick pouches for standard (8.5' x 11") paper. Wax barriers were printed onto cellulose using a ColorQube 8580 Printer (Xerox). The fluorescent images of gels and cellulose paper micro-well plates were obtained using a Chemidoc MP imager (Biorad), analyzed using ImageLab software (Biorad) and processed using ImageJ. Real-time fluorescence monitoring of the in-solution RCA assay was performed using an Infinite M1000 Plate Reader (Tecan). The MicroScale Thermophoresis traces were obtained using a Monolith NT.115 Pico (NanoTemper Technologies).

Preparation of Circular Templates. Circular DNAs were prepared from 5'-phosphorylated linear DNA oligonucleotides through template-assisted ligation with T4 DNA ligase. Phosphorylation of linear DNA oligonucleotides was done as follows: a 50 μ L reaction mixture containing 8 μ M linear circular template DNA (AP-C), 1 μ L of 0.2 unit/ μ L PNK, 1 \times PNK buffer A (50 mM Tris-HCl, pH 7.6 at 25 $^{\circ}$ C, 10 mM MgCl₂, 5 mM DTT, 0.1 mM spermidine), and 2 mM ATP. The mixture was incubated at 37 $^{\circ}$ C for 1 hour, followed by heating at 90 $^{\circ}$ C for 5 minutes. The circularization reaction

was performed in a volume of 100 μL , produced by adding 34 μL of H_2O , 5 μL of ligation strand DNA (AP-L) (100 μM) and 10 μL of 10 \times T4 DNA ligase buffer (400 mM Tris-HCl, 100 mM MgCl_2 , 100 mM DTT, 5 mM ATP, pH 7.8 at 25 $^\circ\text{C}$). After heating at 90 $^\circ\text{C}$ for 2 minutes and cooling down to room temperature for 10 minutes, 1 μL of T4 DNA ligase (10 u/ μL) was added. The mixture was incubated at room temperature for 2 hours, followed by heating at 90 $^\circ\text{C}$ for 5 minute. The reaction mixtures were ethanol precipitated followed by purification of the DNA circles by dPAGE and storage at -20 $^\circ\text{C}$ until use.

Aptaprimer Binding Mechanism. Each binding reaction was conducted in a final volume of 20 μL . First, a 10 μL solution was prepared containing 1 μL of 10 \times RCA buffer (330 mM Tris acetate, pH 7.9 at 37 $^\circ\text{C}$, 100 mM magnesium acetate, 660 mM potassium acetate, 1% (v/v) Tween 20, 10 mM DTT), 0 or 20 nM of aptaprimer (P-AP-P), and 0 or 100 nM of PDGF and incubated at room temperature for 15 minutes. Next, 10 μL of 1 \times RCA buffer containing 0 - 40 nM of circular template (P-AP-C12, -C18, -C27, or -C35, respectively) was added and incubated at room temperature for 15 minutes. Each reaction mixture was mixed with 20 μL of a 2 \times native PAGE Loading Buffer solution and loaded for native PAGE (8%) analysis.

Binding Reaction in Solution prior to RCA. Each binding reaction was conducted in a final volume of 20 μL . First, a 10 μL solution was prepared

containing 1 μL of 10 \times RCA buffer, 0 or 20 nM of aptamer (P-AP-P), and varying concentrations of PDGF, and incubated at room temperature for 15 minutes. Next, 10 μL of 1 \times RCA buffer containing 20 nM of circular template (P-AP-C18) was added and incubated at room temperature for 15 minutes. Each reaction mixture was mixed with 20 μL of a 2 \times native PAGE Loading Buffer solution and loaded for native PAGE (8%) analysis. For the anti-thrombin aptamer assay, T-AP-P, thrombin, and T-AP-C9 were used instead of P-AP-P, PDGF, and P-AP-C18, respectively.

RCA Reaction in Solution. Each RCA reaction was conducted in a final volume of 50 μL . First, a 20 μL solution was prepared containing 2 μL of 10 \times RCA buffer, 2 μL of dNTPs (10 mM), 0.5 μL of aptamer (P-AP-P or T-AP-P) (100 nM), 5 μL of 10 \times intercalating dye (SYBR Gold or QuantiFluor) and 10.5 μL of H_2O . Next, 10 μL of 1 \times RCA buffer containing the protein of interest was added and incubated at room temperature for 15 minutes. Finally, a 20 μL solution of 1 \times RCA buffer containing 0.5 μL of ligated circle (P-AP-C18 or T-AP-C9) (100 nM), and 0.5 μL of phi29 DNA polymerase (10U/ μL) was added to produce the final 50 μL mixture. This was incubated at room temperature for 30 minutes (for P-AP) or 15 minutes (for T-AP), and then heated at 90 $^\circ\text{C}$ for 5 minutes to stop the reaction. A 5 μL aliquot of the RCA reaction was used for the Restriction Digestion assay below.

RCA Product Restriction Digestion. A 3 μL solution containing 5 μM of digestion template DNA (AP-D), and 1 μL of 1 \times FastDigest Buffer was added to a 5 μL aliquot of the RCA reaction mixture above. The mixture was heated at 90 $^{\circ}\text{C}$ for 2 minutes and cooled at RT for 5 minutes followed by the addition of 2 μL of FastDigest TaqI Restriction Enzyme. This mixture was incubated at 65 $^{\circ}\text{C}$ for 24 hr to ensure complete digestion. Each digest was mixed with 10 μL of a 2 \times PAGE Loading Buffer solution containing 25 nM of a 50 bp DNA strand as a loading control. The solution was heated to 90 $^{\circ}\text{C}$ for 2 minutes, cooled to RT and loaded for denaturing PAGE (10%) analysis.

Preparation of Bioactive Paper. Whatman No. 1 filter paper was laminated on one side to create a plastic backing. A pattern resembling a 96-well plate was printed onto the cellulose paper using a ColorQube 8580 wax printer with well diameters of 4 mm wide. The patterned paper was placed in a 120 $^{\circ}\text{C}$ oven for 5 minutes to melt the wax through the thickness of the paper to form a hydrophobic barrier. The paper was allowed to cool to room temperature and spotted with pullulan-encapsulated RCA reagents as described below.

Preparation of Pullulan-Encapsulated RCA Reagents on Cellulose Paper. For each paper micro-well, 0.1 μL of 1 μM circular template, 1 μL of 10 mM dNTPs, 0.5 μL of ϕ29DP (10 U/ μL), 2.4 μL of H_2O and 6 μL of 10%

(w/v) pullulan were mixed together. The mixtures were pipetted onto the paper micro-wells and allowed to dry overnight.

RCA Reaction on Paper. Each RCA reaction was conducted in a final volume of 15 μL . A 15 μL solution of 1.5 μL of 10 \times RCA buffer, 1.5 μL of 1 \times QuantiFluor dye, 1 μL of aptaprimer (1 μM for P-AP-P, 0.1 μM for T-AP-P), various concentrations of target analyte, and H_2O was added to the test zone and incubated at room temperature for 30 minutes (for P-AP) or 15 minutes (for T-AP). The patterned paper was scanned in real-time using the ChemiDoc MP Imager.

Image Processing for Cellulose Paper Micro-wells. Images were processed using ImageJ using the “Subtract Background” function to subtract the inherent background fluorescence of the cellulose paper at time 0.

3.7 Acknowledgements

Funding for this work was provided by the Natural Sciences and Engineering Research Council of Canada (NSERC) via Discovery Grants to YL and JDB, the Canadian Foundation for Innovation (CFI) and the Ontario Ministry for Research and Innovation (ORF-RE; Grant No. RE07-045). JDB holds the Canada Research Chair in Point-of-Care Diagnostics.

3.8 References

- (1) Yan, L.; Zhou, J.; Zheng, Y.; Gamson, A. S.; Roembke, B. T.; Nakayama, S.; Sintim, H. O. *Mol. Biosyst.* **2014**, *10*, 970–1003.
- (2) Asiello, P. J.; Baeumner, A. J. *Lab Chip* **2011**, *11*, 1420–1430.
- (3) Stougaard, M.; Juul, S.; Andersen, F. F.; Knudsen, B. R. *Integr. Biol.* **2011**, *3*, 982–992.
- (4) Gill, P.; Ghaemi, A. *Nucleosides. Nucleotides Nucleic Acids* **2008**, *27*, 224–243.
- (5) Jeong, Y.-J.; Park, K.; Kim, D.-E. *Cell. Mol. Life Sci.* **2009**, *66*, 3325–3336.
- (6) Jung, C.; Ellington, A. D. *Acc. Chem. Res.* **2014**, *47*, 1825–1835.
- (7) Ali, M. M.; Li, F.; Zhang, Z.; Zhang, K.; Kang, D.-K.; Ankrum, J. A.; Le, X. C.; Zhao, W. *Chem. Soc. Rev.* **2014**, *43*, 3324.
- (8) Zhao, W.; Ali, M. M.; Brook, M. A.; Li, Y. *Angew. Chemie* **2008**, *47*, 6330–6337.
- (9) Gao, H.; Zhang, K.; Teng, X.; Li, J. *TrAC - Trends Anal. Chem.* **2019**, *121*, 115700.
- (10) Zhou, L.; Ou, L.-J.; Chu, X.; Shen, G.-L.; Yu, R.-Q. *Anal. Chem.* **2007**, *79*, 7492–7500.
- (11) Akter, F.; Mie, M.; Kobatake, E. *Anal. Biochem.* **2011**, *416*, 174–179.
- (12) Zhang, B.; Liu, B.; Tang, D.; Niessner, R.; Chen, G.; Knopp, D. *Anal. Chem.* **2012**, *84*, 5392–5399.
- (13) Hou, L.; Wu, X.; Chen, G.; Yang, H.; Lu, M.; Tang, D. *Biosens. Bioelectron.* **2015**, *68*, 487–493.
- (14) Frei, A. P.; Bava, F. A.; Zunder, E. R.; Hsieh, E. W. Y. Y. Y.; Chen, S. Y.; Nolan, G. P.; Gherardini, P. F. *Nat. Methods* **2016**, *13*, 269–275.
- (15) Gullberg, M.; Gustafsdottir, S. M.; Schallmeiner, E.; Jarvius, J.; Bjarnegard, M.; Betsholtz, C.; Landegren, U.; Fredriksson, S. *Proc. Natl. Acad. Sci.* **2004**, *101*, 8420–8424.
- (16) Schallmeiner, E.; Oksanen, E.; Ericsson, O.; Spångberg, L.; Eriksson, S.; Stenman, U. H.; Pettersson, K.; Landegren, U. *Nat. Methods* **2007**, *4*, 135–137.
- (17) Di Giusto, D. A.; Wlassoff, W. A.; Gooding, J. J.; Messerle, B. A.; King, G. C. *Nucleic Acids Res.* **2005**, *33*, e64.
- (18) Yang, L.; Fung, C. W.; Cho, E. J.; Ellington, A. D. *Anal. Chem.* **2007**, *79*, 3320–3329.
- (19) Xue, L.; Zhou, X.; Xing, D. *Anal. Chem.* **2012**, *84*, 3507–3513.
- (20) Feng, K.; Kong, R.; Wang, H.; Zhang, S.; Qu, F. *Biosens. Bioelectron.* **2012**, *38*, 121–125.
- (21) Xue, L.; Zhou, X.; Xing, D. *Chem. Commun.* **2010**, *46*, 7373–7375.
- (22) Jie, G.; Yuan, J. *Anal. Chem.* **2012**, *84*, 2811–2817.
- (23) Gao, T.; Ning, L.; Li, C.; Wang, H.; Li, G. *Anal. Chim. Acta* **2013**, *788*, 171–176.

- (24) Chen, C.; Zhao, J.; Jiang, J.; Yu, R. *Talanta* **2012**, *101*, 357–361.
- (25) Yi, H.; Xu, W.; Yuan, Y.; Wu, Y.; Chai, Y.; Yuan, R. *Biosens. Bioelectron.* **2013**, *47*, 368–372.
- (26) Zhao, J.; Hu, S.; Zhong, W.; Wu, J.; Shen, Z.; Chen, Z.; Li, G. *ACS Appl. Mater. Interfaces* **2014**, *6*, 7070–7075.
- (27) Ren, R.; Yu, Z.; Zou, Y.; Zhang, S. *Chem. Eur. J.* **2012**, *18*, 14201–14209.
- (28) Ye, S.; Xiao, J.; Guo, Y.; Zhang, S. *Chem. Eur. J.* **2013**, *19*, 8111–8116.
- (29) Li, Y.; Lei, C.; Zeng, Y.; Ji, X.; Zhang, S. *Chem. Commun.* **2012**, *48*, 10892–10894.
- (30) Zhu, C.; Wen, Y.; Li, D.; Wang, L.; Song, S.; Fan, C.; Willner, I. *Chem. Eur. J.* **2009**, *15*, 11898–11903.
- (31) Liu, M.; Hui, C. Y.; Zhang, Q.; Gu, J.; Kannan, B.; Jahanshahi-Anbuhi, S.; Filipe, C. D. M. M. M.; Brennan, J. D.; Li, Y.; Filipe, C. D. M. M. M.; Brennan, J. D.; Li, Y. *Angew. Chemie* **2016**, *55*, 2709–2713.
- (32) Hui, C. Y.; Liu, M.; Li, Y.; Brennan, J. D. *Angew. Chemie* **2018**, *57*, 4549–4553.
- (33) Carrasquilla, C.; Little, J. R. L. L.; Li, Y.; Brennan, J. D. *Chem. Eur. J.* **2015**, *21*, 7369–7373.
- (34) Liu, M.; Song, J.; Shuang, S.; Dong, C.; Brennan, J. D.; Li, Y. *ACS Nano* **2014**, *8*, 5564–5573.
- (35) Deng, R.; Zhang, K.; Wang, L.; Ren, X.; Sun, Y.; Li, J. *Chem* **2018**, *4*, 1373–1386.
- (36) Wang, L.; Tram, K.; Ali, M. M.; Salena, B. J.; Li, J.; Li, Y. *Chem. Eur. J.* **2014**, *20*, 2420–2424.
- (37) Liu, M.; Zhang, W.; Zhang, Q.; Brennan, J. D.; Li, Y. *Angew. Chemie* **2015**, *54*, 9637–9641.
- (38) Ali, M. M.; Li, Y. *Angew. Chemie* **2009**, *48*, 3512–3515.
- (39) Di Giusto, D. A.; Knox, S. M.; Lai, Y.; Tyrelle, G. D.; Aung, M. T.; King, G. C. *ChemBioChem* **2006**, *7*, 535–544.
- (40) Di Giusto, D. A.; King, G. C. *J. Biol. Chem.* **2004**, *279*, 46483–46489.
- (41) Liu, M.; Yin, Q.; Chang, Y.; Zhang, Q.; Brennan, J. D.; Li, Y. *Angew. Chemie* **2019**, *58*, 8013–8017.
- (42) Green, L. S.; Jellinek, D.; Jenison, R.; Östman, A.; Heldin, C. H.; Janjic, N. *Biochemistry* **1996**, *35*, 14413–14424.
- (43) Zhao, W.; Schafer, S.; Choi, J.; Yamanaka, Y. J.; Lombardi, M. L.; Bose, S.; Carlson, A. L.; Phillips, J. a.; Teo, W.; Droujinine, I. a.; Cui, C. H.; Jain, R. K.; Lammerding, J.; Love, J. C.; Lin, C. P.; Sarkar, D.; Karnik, R.; Karp, J. M. *Nat. Nanotechnol.* **2011**, *6*, 524–531.
- (44) Nutiu, R.; Li, Y. *J. Am. Chem. Soc.* **2003**, *125*, 4771–4778.
- (45) Achenbach, J. C.; Nutiu, R.; Li, Y. *Anal. Chim. Acta* **2005**, *534*, 41–51.
- (46) Lau, P. S.; Coombes, B. K.; Li, Y. *Angew. Chemie* **2010**, *49*, 7938–

7942.

- (47) Méndez, J.; Blanco, L.; Salas, M. *EMBO J.* **1997**, *16*, 2519–2527.
- (48) Vicens, M. C.; Sen, A.; Vanderlaan, A.; Drake, T. J.; Tan, W. *ChemBioChem* **2005**, *6*, 900–907.
- (49) Fang, X.; Sen, A.; Vicens, M.; Tan, W. *ChemBioChem* **2003**, *4*, 829–834.
- (50) Tang, L.; Liu, Y.; Ali, M. M.; Kang, D. K.; Zhao, W.; Li, J. *Anal. Chem.* **2012**, *84*, 4711–4717.
- (51) Bock, L. C.; Griffin, L. C.; Latham, J. A.; Vermaas, E. H.; Toole, J. J. *Nature* **1992**, *355*, 564–566.
- (52) Baaske, P.; Wienken, C. J.; Reineck, P.; Duhr, S.; Braun, D. *Angew. Chemie* **2010**, *49*, 2238–2241.
- (53) Jerabek-Willemsen, M.; André, T.; Wanner, R.; Roth, H. M.; Duhr, S.; Baaske, P.; Breitsprecher, D. *J. Mol. Struct.* **2014**, *1077*, 101–113.
- (54) Zhang, M.-L. L.; Xu, Y.-P. P.; Kumar, A.; Zhang, Y.; Wu, W.-Q. Q. *Biochemistry* **2019**, *58*, 3955–3959.
- (55) Janssen, K.; Knez, K.; Spasic, D.; Lammertyn, J. *Sensors* **2013**, *13*, 1353–1384.
- (56) Li, J.; Macdonald, J. *Biosens. Bioelectron.* **2015**, *64*, 196–211.
- (57) Zanolli, L. M.; Spoto, G. *Biosensors* **2012**, *3*, 18–43.
- (58) Niemz, A.; Ferguson, T. M.; Boyle, D. S. *Trends Biotechnol.* **2011**, *29*, 240–250.
- (59) Craw, P.; Balachandran, W. *Lab Chip* **2012**, *12*, 2469–2486.
- (60) Liu, M.; Zhang, Q.; Kannan, B.; Botton, G. A.; Yang, J.; Soleymani, L.; Brennan, J. D.; Li, Y. *Angew. Chemie* **2018**, *57*, 12440–12443.
- (61) Jahanshahi-Anbuhi, S.; Pennings, K.; Leung, V.; Liu, M.; Carrasquilla, C.; Kannan, B.; Li, Y.; Pelton, R.; Brennan, J. D.; Filipe, C. D. M. *Angew. Chemie* **2014**, *53*, 6155–6158.
- (62) Gordon, P.; Venancio, V. P.; Mertens-Talcott, S. U.; Côté, G. *J. Biomed. Opt.* **2019**, *24*, 1.
- (63) Knowlton, S.; Joshi, A.; Syrrist, P.; Coskun, A. F.; Tasoglu, S. *Lab Chip* **2017**, *17*, 2839–2851.
- (64) Priye, A.; Bird, S. W.; Light, Y. K.; Ball, C. S.; Negrete, O. A.; Meagher, R. J. *Sci. Rep.* **2017**, *7*, 44778.

3.9 Supporting Information

Table S3.1. List of DNA Sequences Used.

Name of DNA oligonucleotide	Sequence (5'-3')
Linear precursor of PDGF system (P-AP)	
P-AP-C12 (60 nt, 12-nt binding region)	CGAACAACAT CAGGATCATG GTAAAGCCCA TACTAATCAA AGCCCATACT ACAACAACCTT
P-AP-C18 (60 nt, 18-nt binding region)	CGAACAACAT CAGGATCATG GTGATGCTCA TACTAATCAA AGCCCATACT ACAACAACCTT
P-AP-C27 (60 nt, 27-nt binding region)	CGAACAACAT CAGGATCATG GTGATGCTCT ACGTGCCCAA AGCCCATACT ACAACAACCTT
P-AP-C35 (60 nt, 35-nt binding region)	CGAACAACAT CAGGATCATG GTGATGCTCT ACGTGCCGTA GCCTGATACT ACAACAACCTT
Linear precursor of thrombin system (T-AP)	
T-AP-C9 (60 nt, 9-nt binding region)	CGAACAACAT CCAACCACAA TCAAAGCCCA TACTAATCAA AGCCCATACT ACAACAACCTT
T-AP-C15 (60 nt, 15-nt binding region)	CGAACAACAT CCAACCACAC CAACCGCCCA TACTAATCAA AGCCCATACT ACAACAACCTT
DNA aptaprimers	
P-AP-P (35 nt)	AAGGCTACGG CACGTAGAGC ATCACCATGA TCCTG
T-AP-P (15 nt)	GGTTGGTGTG GTTGG
T-AP-P-Cy5 (15 nt)	/5Cy5/ GGTTGGTGTG GTTGG
DNA ligation strand	
AP-L (20 nt)	ATGTTGTTTCG AAGTTGTTGT
DNA template for digestion	
AP-D (20 nt)	ACAACAACCTT CGAACAACAT
Loading control DNA	
LC (50 nt)	ATCATTCTTT GAAAGCAGAC ATCCTACAAC AACTACAACA TGACTIONCGAT

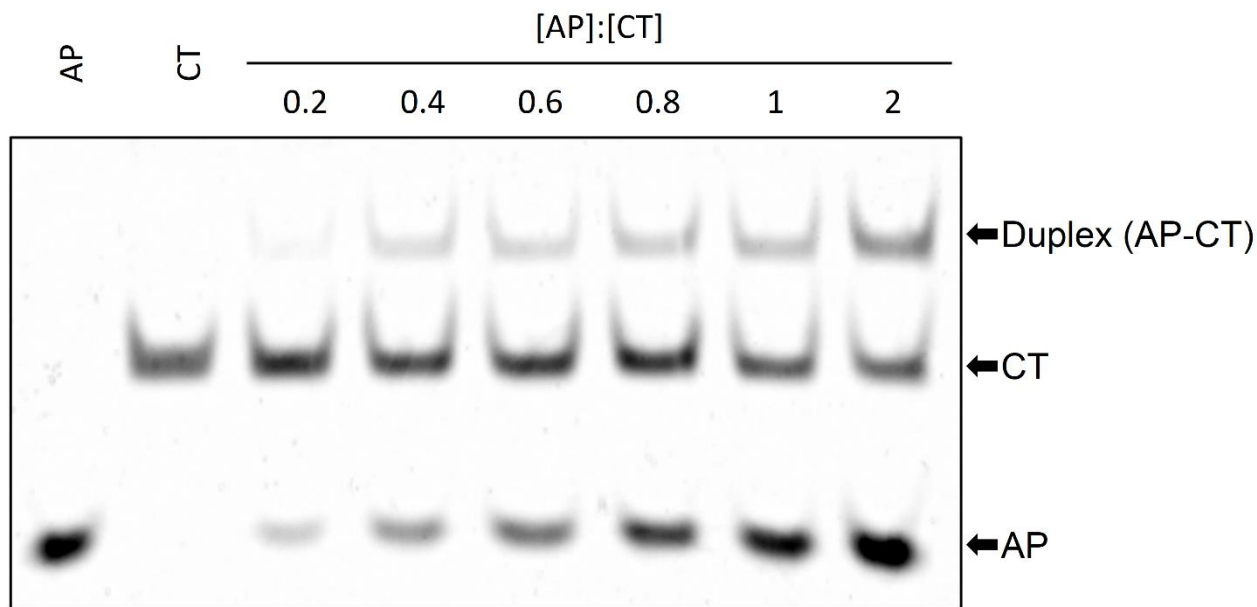


Figure S3.1. Ability of anti-PDGF aptamer (AP) to form a duplex in the presence of increasing amounts of a circular template (CT) with an 18 nucleotide primer-binding region (8% nPAGE).

Experimental Details: A 20 μL solution containing 2 μL of 10 \times RCA buffer, 0-10 nM of circular template (P-AP-C18), and 0-20 nM of aptamer (P-AP-P) was incubated together at room temperature for 20 minutes, mixed with 2 \times native loading buffer and separated using 8% polyacrylamide gel electrophoresis (PAGE) under native conditions.

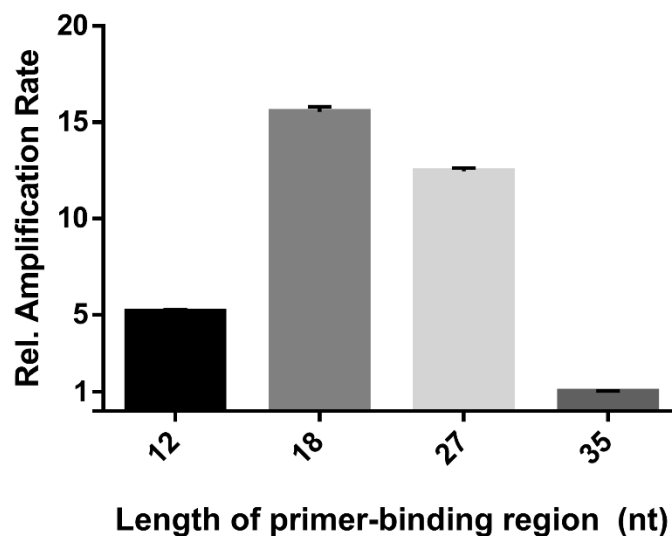


Figure S3.2. Comparison of RCA efficiency using circular templates with varying lengths of primer-binding region. RCA was performed at room temperature and monitored in real-time using SYBR Gold dye. All RCA reactions were conducted for 30 minutes.

Experimental Details: The protocol was similar to the “RCA Reaction in Solution” described in the **Experimental Section**, however, no PDGF was added and the CT used was either P-AP-C12, -C18, -C27, or -C35.

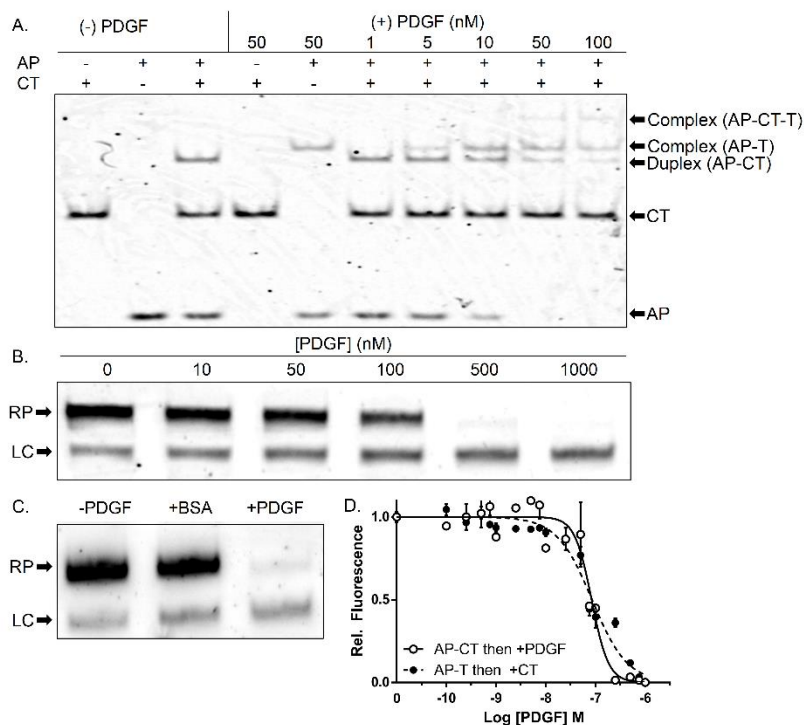


Figure S3.3. Inhibition assay using an anti-PDGF aptaprimer system with preformed AP-CT duplex followed by addition of PDGF target. (A) Native PAGE (8%) of the species formed when the AP-CT duplex was incubated with increasing amounts of PDGF; (B) Denaturing PAGE (10%) of RCA product after treatment with TaqI restriction enzyme in the presence of increasing amounts of PDGF. LC denotes the loading control. (C) Denaturing PAGE (10%) of RCA product, denoted as RP, after treatment with TaqI in the absence of protein, and in the presence of 1 μ M BSA or PDGF. LC denotes the loading control. (D) Titration curve of RCA product generation in the presence of PDGF monitored in real-time using either SYBR Gold or QuantiFluor dyes. All RCA reactions conducted for 30 minutes.

Experimental Details: The protocol for (A) was similar to that used for “Aptaprimer Binding Mechanism” except that PDGF was added to a preformed AP-CT duplex. The protocol for (B) was similar to the “Binding Reaction in Solution Prior to RCA”. The protocol for (C) and (D) was similar to the “RCA Reaction in Solution” described in the **Experimental Section**, however, AP was initially mixed with CT first and incubated for 30 minutes, and then PDGF was added afterwards and incubated for 30 minutes.

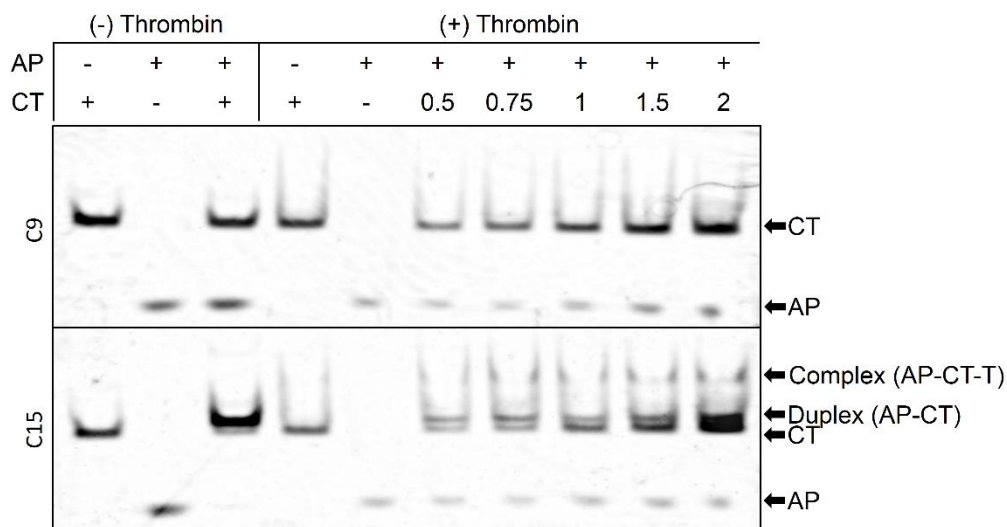


Figure S3.4. Native PAGE analysis showing the ability of the anti-thrombin aptamer (AP) to structure-switch from a complex with 1 μ M thrombin to a duplex in the presence of a circular template (CT) using: (A) a 9 nucleotide primer-binding region (C9); (B) a 15 nucleotide primer-binding region (C15).

Experimental Details: The protocol was similar to the “Aptamer Binding Mechanism” described in the **Experimental Section**, however, T-AP-P, thrombin, and T-AP-C9 or -C15 were used instead of P-AP-P, PDGF, and P-AP-C12, -C18, -C27 or -C35, respectively.

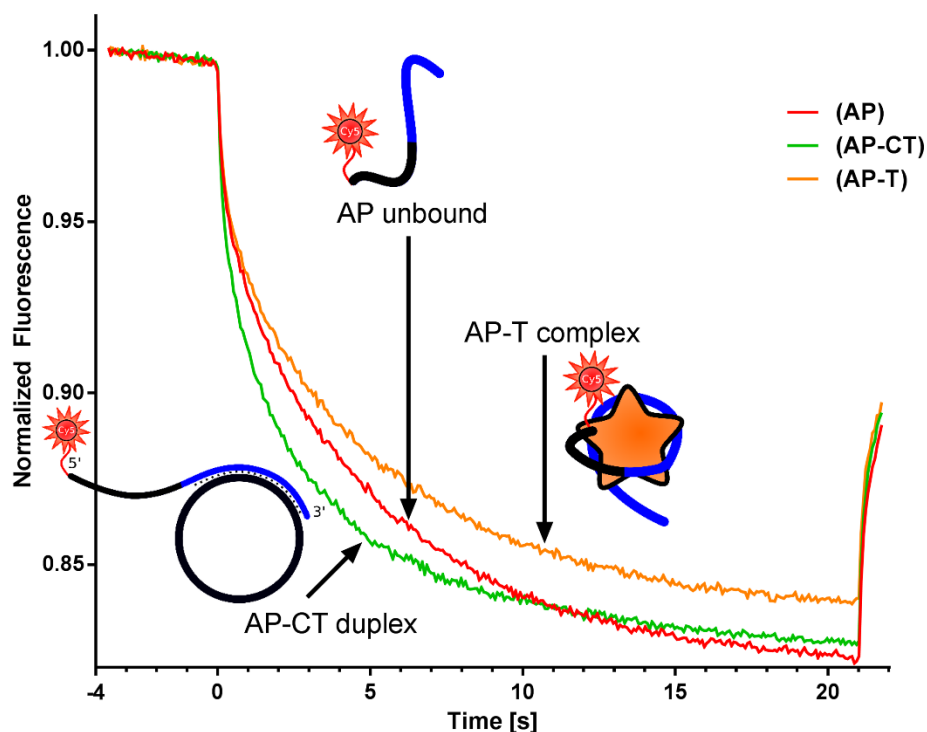


Figure S3.5. MST traces of the T-AP-C9 system showing the presence of unbound AP, AP-CT duplex, and AP-T complex species, respectively. AP was complexed with increasing amounts of thrombin, followed by addition of CT.

Experimental Details: Each binding reaction was conducted in a final volume of 20 μL . First, a 10 μL solution was prepared containing 1 μL of 10 \times RCA buffer, and 20 nM of aptamer (T-AP-P-Cy5). Next, 10 μL of 1 \times RCA buffer containing 20 nM of circular template (T-AP-C9) or 1 μM of thrombin protein was added and incubated at room temperature for 15 minutes. Each reaction mixture was diluted in buffer by a factor of 5 to a final volume of 100 μL and 10 μL aliquots were loaded into microcapillary tubes and scanned using MicroScale Thermophoresis (MST). MST traces were obtained using a Monolith NT.115 Pico (NanoTemper Technologies).

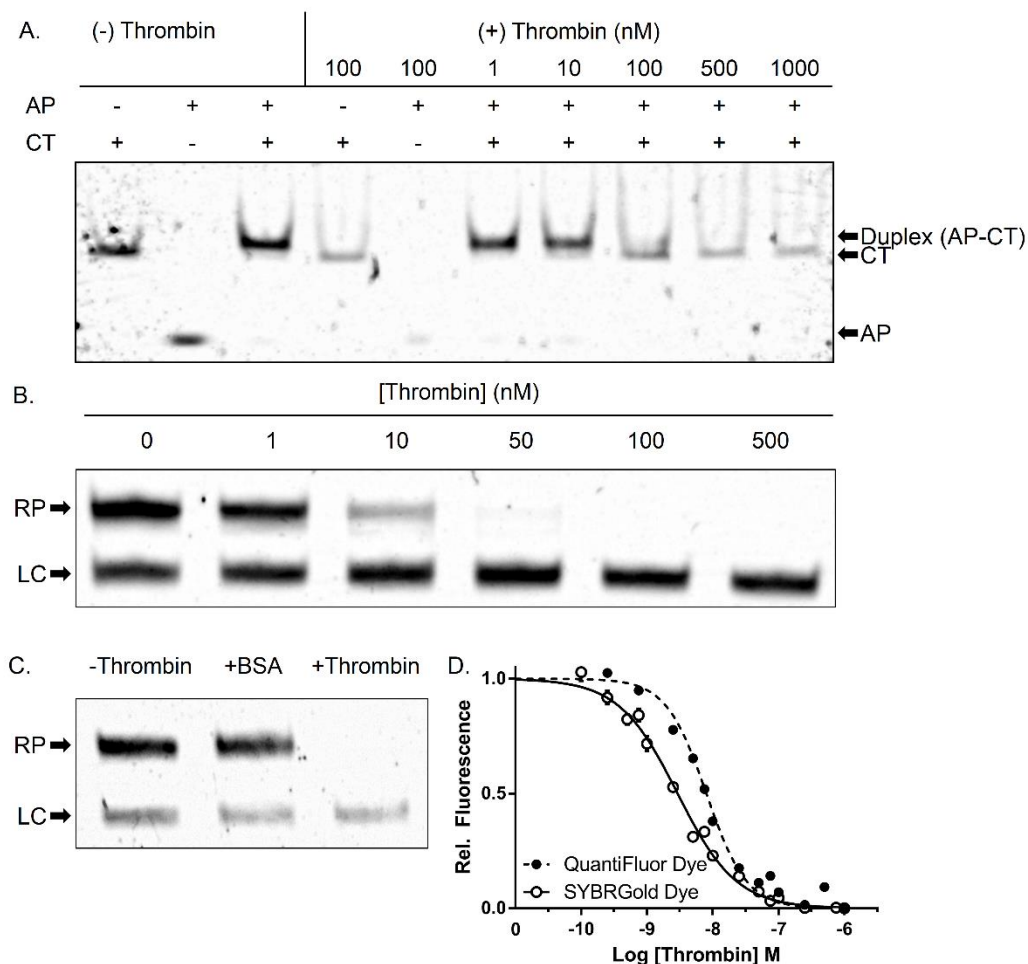


Figure S3.6. Inhibition Assay using a C15 anti-thrombin aptamer system. (A) Native PAGE (8%) analysis of AP complexed with increasing amounts of thrombin, followed by addition of CT; (B) Denaturing PAGE (10%) analysis of RCA product after treatment with TaqI in the presence of increasing amounts of thrombin. LC denotes the loading control. (C) Denaturing PAGE (10%) analysis of RCA product, denoted as RP, after treatment with TaqI in the absence of protein, and in the presence of 1 μ M of either BSA or thrombin. LC denotes the loading control. (D) Titration curve of RCA product generation in the presence of thrombin monitored in real-time using SYBR Gold or QuantiFluor dyes. All RCA reactions conducted for 15 minutes.

Experimental Details: The protocol for (A) was similar to the “Binding Reaction in Solution Prior to RCA”, and the protocol for (B) and (C) was similar to the “RCA Reaction in Solution” described in the **Experimental Section**, however T-AP-C15 was used instead of T-AP-C9.

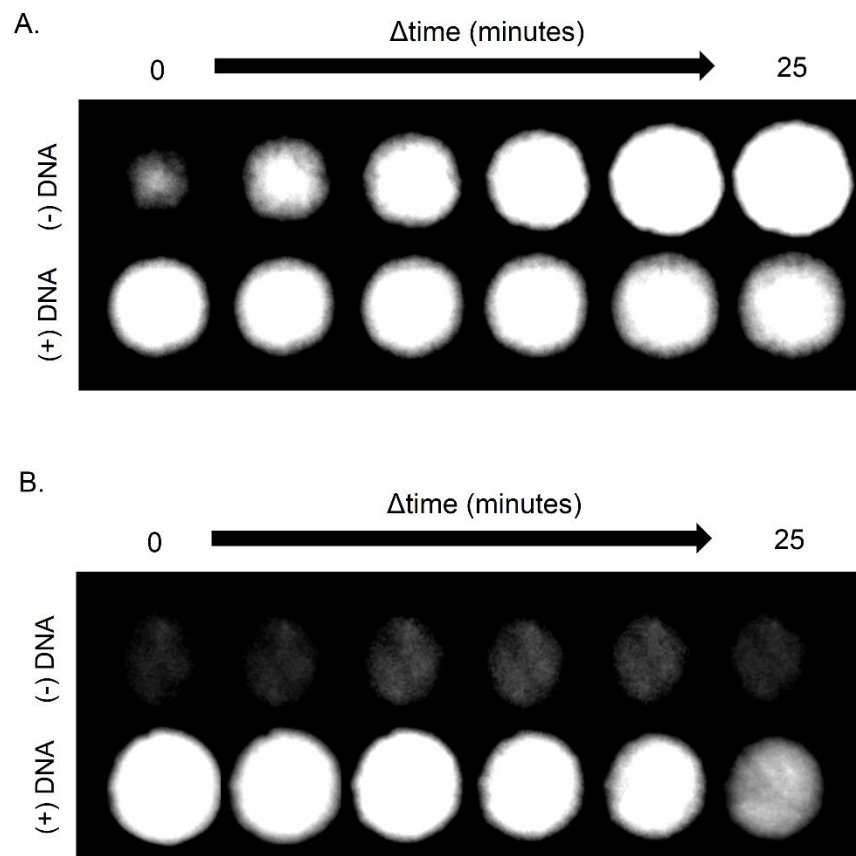


Figure S3.7. Comparison of dye performance on cellulose paper in the absence or presence of 10 pmol of a 60 nt DNA sequence (linear T-AP-C9) between: (A) SYBR Gold dye and; (B) QuantiFluor dye.

Experimental Details: The cellulose paper was prepared as described in the “Preparation of Bioactive Paper” of the **Experimental Section**. A 15 μ L solution of 1.5 μ L of 10 \times RCA buffer, 1.5 μ L of 10 \times SYBR Gold or QuantiFluor dye, and 0 or 10 pmol of linear (unligated) T-AP-C9 was spotted onto a cellulose surface. Fluorescence intensity was scanned in real-time using the ChemiDoc MP Imager over a period of 25 minutes. The image shown was obtained at 25 min.

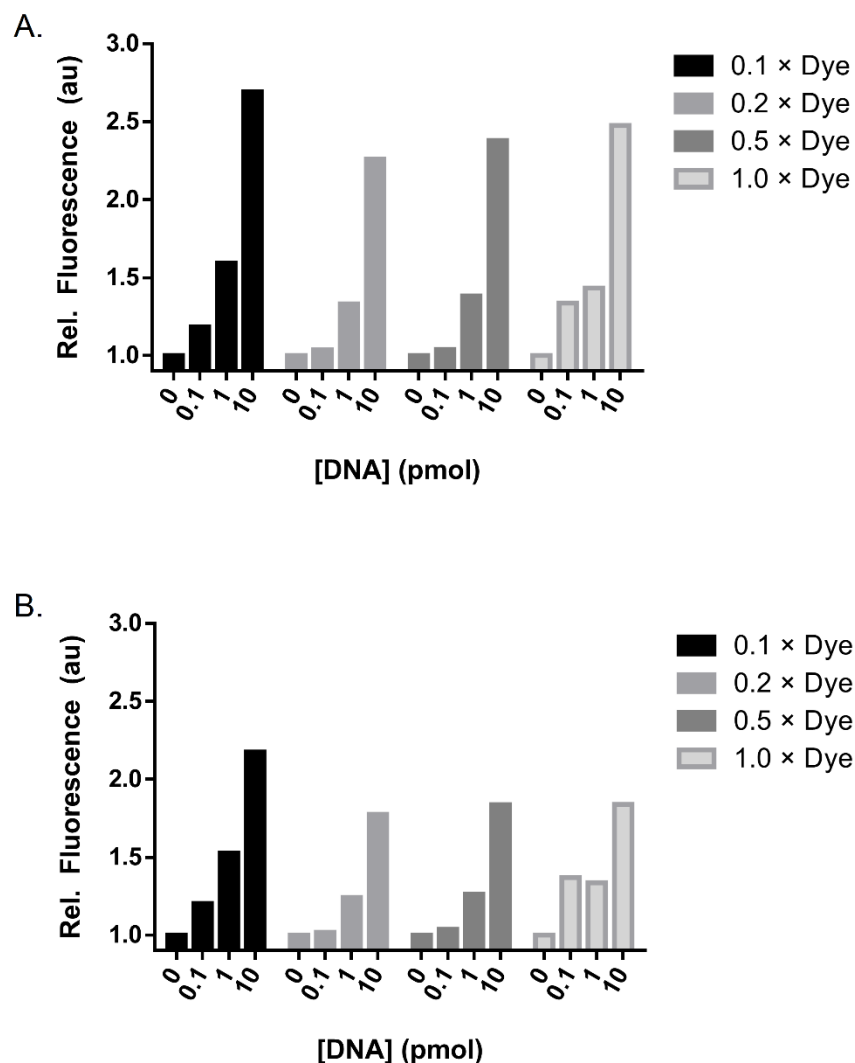


Figure S3.8. Determination of optimal QuantiFluor dye concentration for detection of varying concentrations of a 60 nt DNA sequence (linear T-AP-C9) on a cellulose surface. (A) After 15 minutes of incubation on cellulose at room temperature. (B) After 30 minutes of incubation on cellulose at room temperature.

Experimental Details: The cellulose paper was prepared as described in the “Preparation of Bioactive Paper” of the **Experimental Section**. A 15 μL solution of 1.5 μL of 10 \times RCA buffer, 1.5 μL of 1-10 \times QuantiFluor dye, and 0-10 pmol of linear (unligated) T-AP-C9 was spotted onto a cellulose surface. The fluorescence intensity was scanned in real-time using the ChemiDoc MP Imager over a period of 30 minutes. Data is shown with a reaction time of 30 minutes.

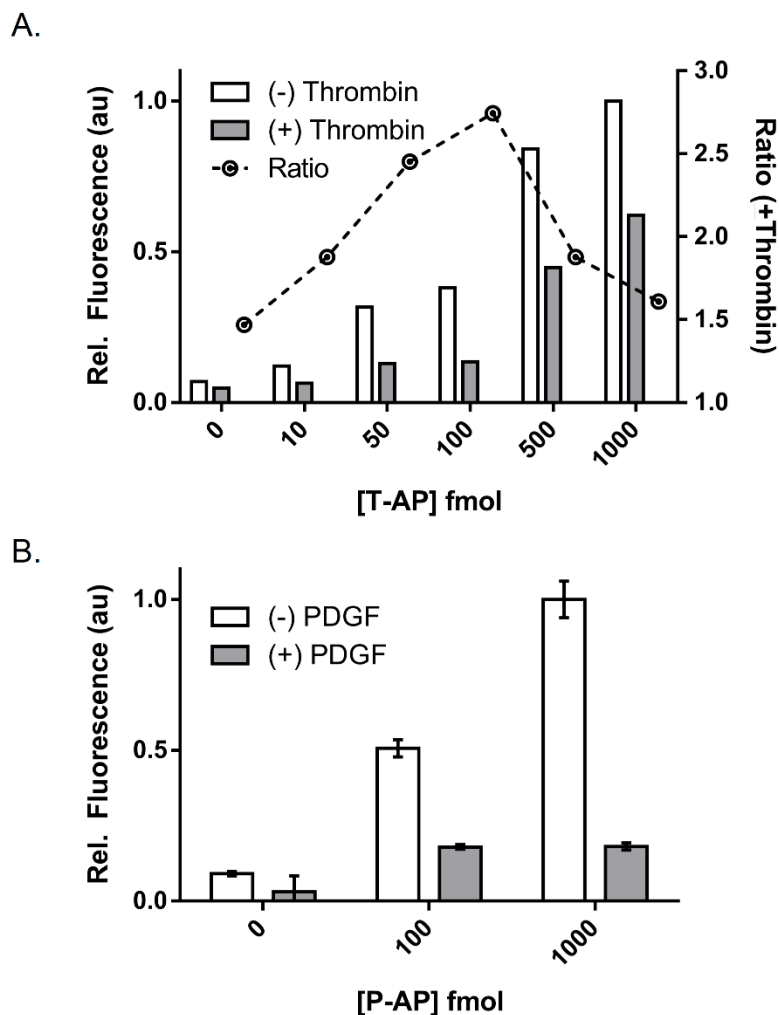


Figure S3.9. Optimization of aptamer concentration on cellulose paper using: (A) the anti-thrombin aptamer system with a 15 minute RCA reaction time; (B) the anti-PDGF aptamer system with a 30 minute RCA reaction time. The concentrations of thrombin or PDGF, respectively, was 0 μ M for (-) and 1 μ M for (+). Observed fluorescence signal of the paper wells as imaged after real-time RCA using the QuantiFluor dye.

Experimental Details: The cellulose paper and pullulan-encapsulation of RCA reagents were prepared as described in the “Preparation of Bioactive Paper” and “Preparation of Pullulan-Encapsulated RCA Reagents on Cellulose Paper” of the **Experimental Section**. The protocol was similar to the “RCA Reaction on Paper” protocol described in the **Experimental Section** however the concentrations of (A) anti-thrombin aptamer (T-AP-P) and; (B) anti-PDGF aptamer (P-AP-P) varied from 0 to 1000 fmol.

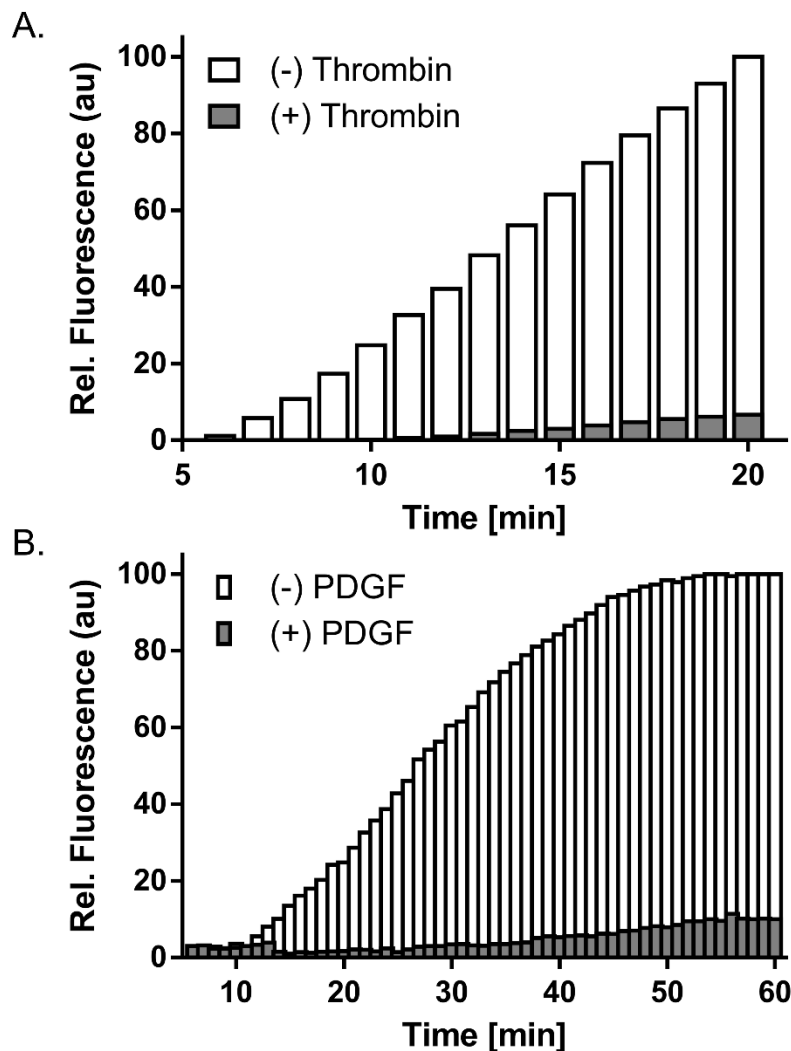


Figure S3.10. Optimization of assay reaction time on cellulose paper using: (A) the anti-thrombin aptamer system; (B) the anti-PDGF aptamer system. The concentrations of thrombin or PDGF, respectively, was 0 μM for (-) and 1 μM for (+). Observed fluorescence signal of the paper wells as imaged after real-time RCA using the QuantiFluor dye.

Experimental Details: The cellulose paper and pullulan-encapsulation of RCA reagents were prepared as described in the “Preparation of Bioactive Paper” and “Preparation of Pullulan-Encapsulated RCA Reagents on Cellulose Paper” of the **Experimental Section**. The protocol was similar to the “RCA Reaction on Paper” protocol described in the **Experimental Section** however the reaction times were extended to 20 minutes for the anti-thrombin aptamer system and 60 minutes for the anti-PDGF aptamer system.

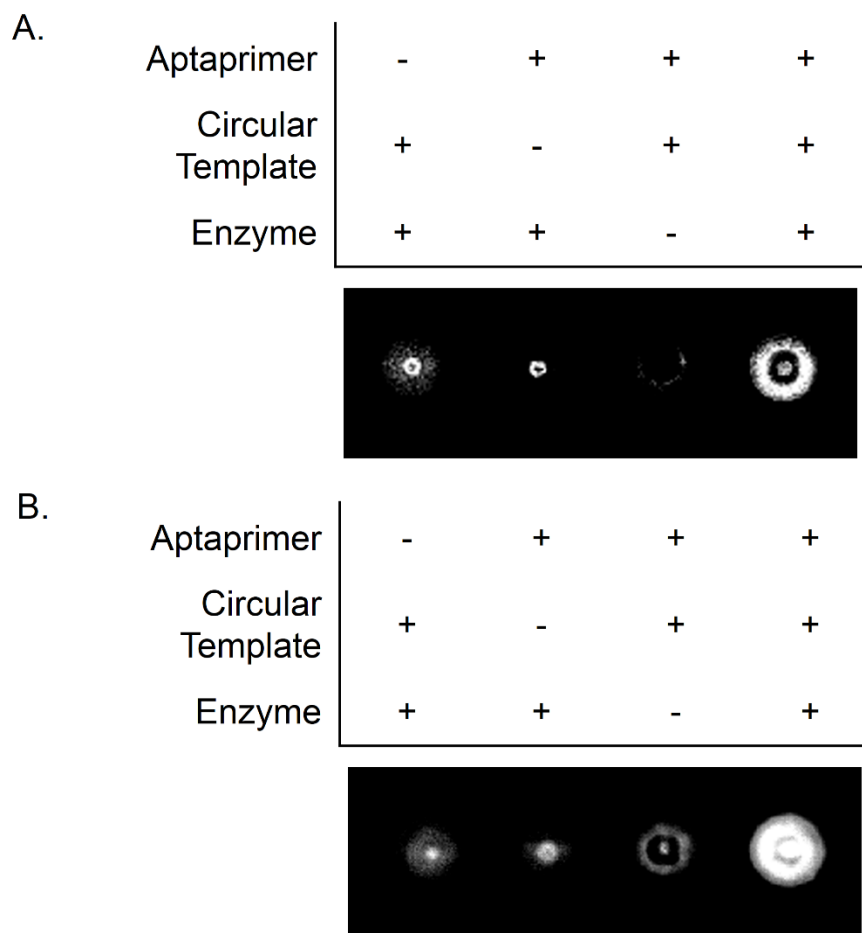


Figure S3.11. Reagent controls for the inhibition assays on cellulose paper using: (A) an anti-PDGF aptaprimer system after a 30 minute RCA reaction; (B) an anti-thrombin aptaprimer system after a 15 minute RCA reaction. Observed fluorescence signal of the paper wells as imaged after real-time RCA using QuantiFluor dye.

Experimental Details: The protocol for the Reagent controls was similar to the “RCA Reaction on Paper” protocol described in the **Experimental Section** with the exclusion of aptaprimer, circular template, or enzyme as indicated.

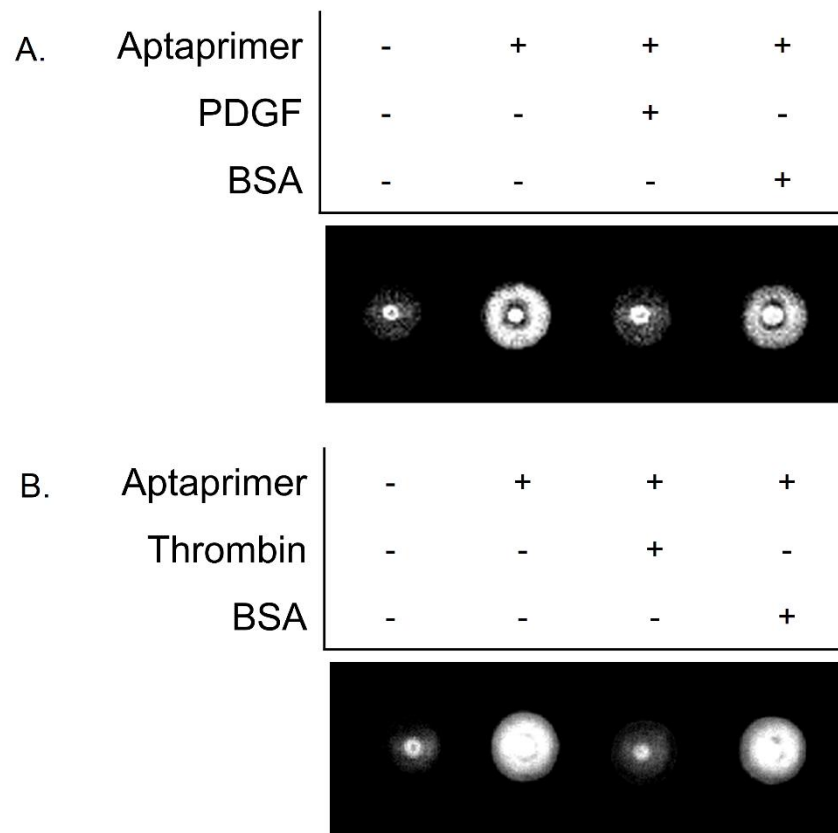


Figure S3.12. Selectivity controls for the inhibition assays on cellulose paper using: (A) an anti-PDGF aptaprimer system after a 30 minute RCA reaction; (B) an anti-thrombin aptaprimer system after a 15 minute RCA reaction. The concentrations of PDGF, thrombin and BSA were 1 μ M. Observed fluorescence signal of the paper wells as imaged after real-time RCA using QuantiFluor dye.

Experimental Details: The protocol for the Selectivity controls was similar to the “RCA Reaction on Paper” protocol described in the Experimental Section with the inclusion of PDGF, thrombin, or BSA as indicated.

CHAPTER 4.

TARGET-DEPENDENT PROTECTION OF DNA APTAMERS AGAINST NUCLEOLYTIC DIGESTION ENABLES SIGNAL-ON BIOSENSING WITH TOEHOLD-MEDIATED ROLLING CIRCLE AMPLIFICATION

4.1 Author's Preface

The following chapter was accepted in *Chemistry – A European Journal* under the citation:

Roger M. Bialy, Yingfu Li, and John D. Brennan. Target-Dependent Protection of DNA Aptamers Against Nucleolytic Digestion Enables Signal-On Biosensing with Toehold-Mediated Rolling Circle Amplification *Chem. Eur. J.* **2021** (Accepted) DOI: 10.1002/chem.202102975.

I was responsible for all experimental design, execution and analysis included in this chapter. I wrote the first draft of the manuscript. Dr. Brennan and Dr. Li provided editorial input to generate the final draft of the paper. This article has been reprinted with permission from John Wiley and Sons ©.

4.2 Abstract

We report a generalizable strategy for biosensing that takes advantage of the resistance of DNA aptamers against nuclease digestion when bound with their targets, coupled with toehold mediated strand displacement (TMSD) and rolling circle amplification (RCA). A DNA aptamer containing a toehold extension at its 5'-end protects it from 3'-exonuclease digestion by phi29 DNA polymerase (phi29 DP) in a concentration-dependent manner. The protected aptamer can participate in RCA in the presence of a circular template that is designed to free the aptamer from its target via TMSD. The absence of the target leads to aptamer digestion, and thus no RCA product is produced, resulting in a turn-on sensor. Using two different DNA aptamers, we demonstrate rapid and quantitative real-time fluorescence detection of two human proteins: platelet-derived growth factor (PDGF) and thrombin. Sensitive detection of PDGF was also achieved in human serum and human plasma, demonstrating the selectivity of the assay.

4.3 Introduction

DNA amplification is a critical component for molecular diagnostics. While many studies have utilized polymerase chain reaction (PCR),^[1] a variety of isothermal DNA amplification (ITA) techniques have emerged in the past decade to allow ultrasensitive detection of nucleic acid species without the need for expensive thermal cyclers.^[2] More recently, ITA methods have been used for detection of non-nucleic acid species, with

many assays employing creative methods to allow molecular recognition elements to modulate the degree of ITA. These include: nucleic acid modified antibodies,^[3–5] antibody-directed proximity ligation assays,^[6–8] and various methods to couple functional nucleic acids (FNAs) such as aptamers^[9–13] and DNAzymes to ITA methods.^[14–17] Common drawbacks of these strategies include the requirement for specially modified antibodies and separation steps for immuno-coupled ITA methods, optical or electrochemical labelling of nucleic acids, multiple primers or processing enzymes for most of the FNA-coupled ITA methods, or the need for elevated reaction temperatures. These barriers have made their use in simple point-of-care (POC) assays challenging.^[18]

Rolling circle amplification (RCA) is an ITA method that is well-suited for a variety of POC device outputs.^[19,20] RCA uses one linear primer which, when bound to a circular template (CT), can be elongated by phi29 DNA polymerase (phi29 DP) at room temperature to produce long concatemeric strands of DNA. Protein-binding aptamers can be used to modulate RCA activity, either by incorporation into the CT or the linear primer, allowing for sensitive protein quantification.^[21–25] In most cases, the bound target blocked DNA processing by phi29 DP, thereby inhibiting the RCA process, producing a “turn-off” sensor. However, it is also possible to produce aptamer-modulated RCA turn-on sensors, which use a structure switching aptamer bound to a primer-CT duplex to initially block the RCA process.

Target binding removes the aptamer, allowing phi29 DP to trim a pre-primer and to form a mature primer to initiate RCA.^[24,26,27] Drawbacks of this method include the need to design a tripartite structure-switching nucleic acid system and the need for costly inverted dT bases to be incorporated into both the pre-primer and aptamer to prevent non-specific digestion by phi29 DP, which would lead to activation of the RCA system without target.

In this work, we report the first example of a new generalizable strategy for amplified turn-on biosensing that takes advantage of the resistance of DNA aptamers against 3'-exonuclease digestion by phi29 DP when bound with their targets. By adding a short 5' toehold region to the aptamer, a circular template can be used to remove the bound target from the aptamer via toehold mediated strand displacement (TMSD) so that the aptamer can then act as a primer (denoted as an aptaprimer, AP) to initiate RCA (Figure 4.1). Importantly, this method does not require any other modification to the aptamer beyond the 5' toehold region, and the use of CT-mediated TMSD allows release of the protected aptamer at room temperature, which leads to room temperature RCA, making the method compatible with simple point-of-need sensing. In this approach, phi29 DP is first added to the AP, which is digested by the phi29 DP when target is absent but protected from digestion when target is bound. The CT is then added and will displace the target from the AP to allow the RCA reaction to proceed, producing a long DNA output strand (reaction product, RP) that can bind to a fluorescent

intercalating dye such as SYBR Gold to generate a fluorescence signal, resulting in a turn-on sensor. We evaluate the assay system for the detection of platelet-derived growth factor (PDGF) and thrombin and demonstrate the ability of the assay to detect proteins in diluted blood and serum.

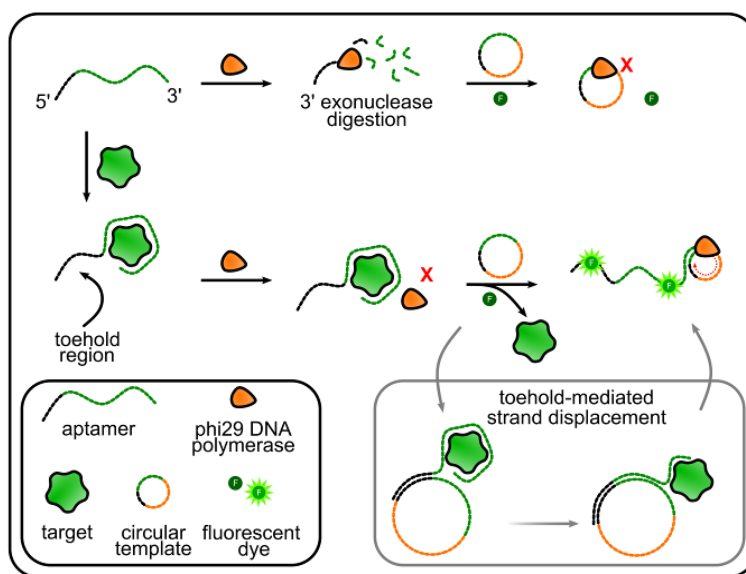


Figure 4.1. Schematic representation of the protein-mediated RCA-based assay. In the absence of a protein target, phi29 DP digests the aptaprimer prior to addition of a CT, preventing RCA. The binding of a protein protects the aptaprimer from digestion, allowing the CT to bind a 5' toehold and displace the target, resulting in RCA. The RCA product is detected using a fluorescent intercalating dye.

4.4 Results and Discussion

The turn-on RCA assay was initially developed using the 35 nt anti-PDGF-BB aptamer (P-AP).^[28,29] The first objective was to confirm that phi29 DP could successfully digest the P-AP in a target-dependent manner. P-

AP was first treated with increasing amounts of phi29 DP and the digestion of P-AP was evaluated by 10% denaturing PAGE (Figure S4.1 in the Supporting Information). As shown in Figure 4.2A, the percentage of digestion increased with phi29 concentration, with a ratio of 1.2 U of phi29 DP per 10 nM of AP leading to nearly full digestion of P-AP (>90%) using a digestion time of 10 minutes. Digestion times of 20 minutes or longer led to nearly complete digestion of the P-AP (Figure S4.2). Next, we tested whether the formation of a complex between P-AP and PDGF (AP-T) could protect P-AP from exonuclease digestion. After exposing the AP-T complex to the optimal concentration of phi29 DP for 10 minutes, the samples were heat denatured, the P-AP was recovered and the percentage of P-AP that was digested was evaluated by PAGE (Figure S4.3). As shown in Figure 4.2B, the amount of P-AP digested decreased as a function of increasing concentrations of PDGF indicating that complex formation successfully protected the P-AP from phi29 DP-mediated 3'-exonuclease digestion.

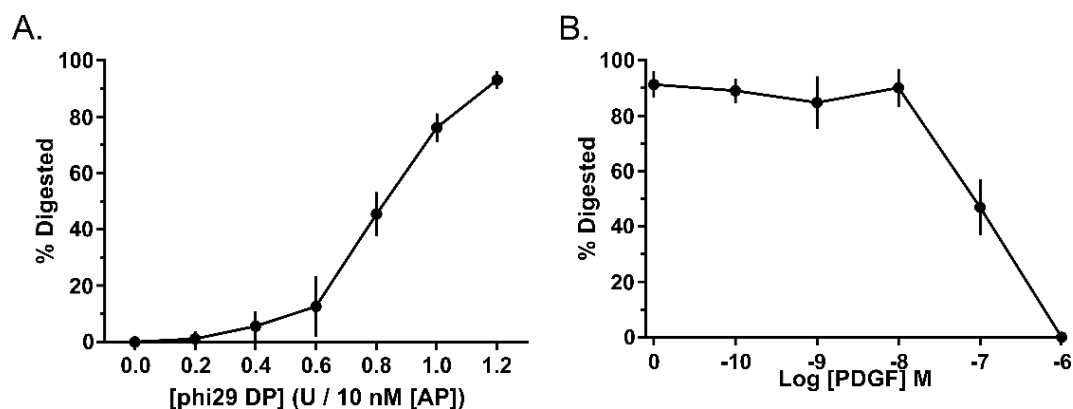


Figure 4.2. (A) Percentage of P-AP digested in 10 minutes as a function of phi29 DP concentration (U / 10 nM [AP]). (B) Percentage of P-AP digested as a function of PDGF concentration, using a digestion time of 10 minutes and 1.2 U / 10 nM [AP] of phi29 DP followed by heat denaturation at 95 °C for 5 minutes.

To avoid the need for a heat denaturation step to recover the undigested P-AP we investigated the use of toehold-mediated strand displacement, wherein the addition of a CT would lead to the release of the target and formation of an AP-CT duplex. Aptamers have very strong binding affinities for their targets, therefore, to facilitate the dissociation of PDGF from the AP via the CT, we incorporated a CT binding sequence on the 5'-end of the AP strand to act as a toehold region. Increasing the toehold length (from 0 to 5, 10, 15, or 20 nt) on the AP improved the ability of the CT to displace PDGF and bind to the AP, as demonstrated using native PAGE (Figure S4.4), with a toehold length of 15 nt showing the best performance across a range of concentrations of PDGF.

Following initial optimization using native PAGE, assay performance was further optimized by examining real-time RCA performance under different reaction conditions to ensure that a CT-liberated P-AP could initiate RCA. Figure 4.3A shows the effect of concentration of phi29 DP per 10 nM AP while Figure 4.3B shows the effect of the ratio of CT to AP on generation of the RCA product using a 3'-exonuclease digestion time of 10 minutes. These parameters were evaluated by observing the ratio between the RCA signal (based on SYBR Gold binding to the RCA reaction product) generated using an assay without PDGF and one with 10 nM of PDGF. As shown in Figure 4.3A, 0.5 U per 10 nM of AP showed the best contrast between PDGF-bound and free AP. Higher concentrations of phi29 DP showed poorer contrast, indicating that higher levels of phi29 DP could digest through the bound PDGF, reducing the protective effect. Further optimization of the digestion time (Figure S4.5) indicated that a shorter digestion time of only 6 minutes was required to completely digest the AP and inhibit RCA in the absence of target, thus suppressing background RP generation while minimizing excess digestion in the presence of low concentrations of PDGF.

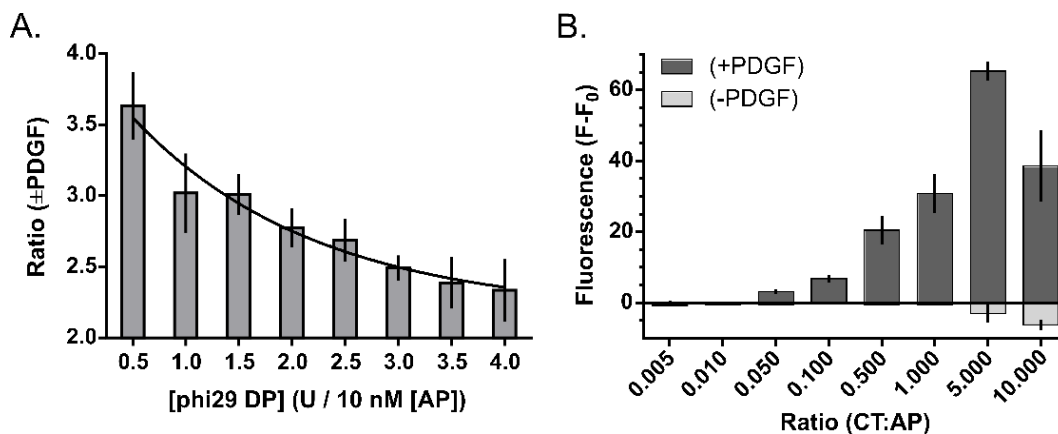


Figure 4.3. Optimization of the anti-PDGF aptamer system by the following parameters: (A) Optimal phi29 DP concentration with a digestion time of 10 minutes and a 0.1 CT:AP ratio; (B) Optimal ratio of circular template (CT) to aptamer (AP). RCA product generation monitored in real-time using SYBR Gold intercalating dye. For the optimal ratio of CT, fluorescence has been normalized by subtracting the background fluorescence at time 0. A concentration of either 0 or 10 nM PDGF was used for ratio determination. Results taken after 60 minutes of RCA.

The ratio between the concentrations of CT and AP was also optimized to balance the affinity of the aptamer for PDGF with the ability of the CT to displace PDGF through toehold binding to initiate RCA. As expected, increasing the CT:AP ratio led to an increase of the amount of RCA product, though elevated CT levels also increased the baseline fluorescence in the absence of RCA owing to the dye binding directly to the CT (Figure 4.3B). To better evaluate the optimal CT:AP ratio, the difference in fluorescence signal generated with and without PDGF was compared. A CT:AP ratio of 5:1 was optimal for achieving a large contrast in fluorescence while minimizing the background signal observed from dye binding directly to the CT. Importantly, the ratio of CT:AP changes as a function of the degree of AP digestion. When target concentration is highest, the degree of AP

digestion is lowest. Thus, at low target concentrations, the ratio between CT and AP is likely much higher than 5:1 whereas at high target concentrations the ratio approaches 5:1.

We then performed a reagent and selectivity control using the optimized assay conditions of 6 min digestion followed by 60 minutes of RCA with a 5:1 CT:AP ratio (Figure 4.4A). As expected, there was no RP generation when the CT or AP was excluded (lanes 1 and 2). In the absence of AP digestion, minimal signal contrast was observed in the presence or absence of PDGF (-Dig, lanes 3 and 4). RP was formed only when PDGF was present to protect the AP from digestion (+Dig, lane 6) but was not present when PDGF was absent or substituted with a different protein (BSA or Thrombin) (lanes 5, 7 and 8), demonstrating the selectivity of the assay. The production of RCA products also indicates that digestion of the AP does not continue during the RCA step, as addition of the CT causes the 3' end of the aptaprimer to form a duplex with the CT and then be extended by phi29 DP acting as a polymerase, preventing further digestion.

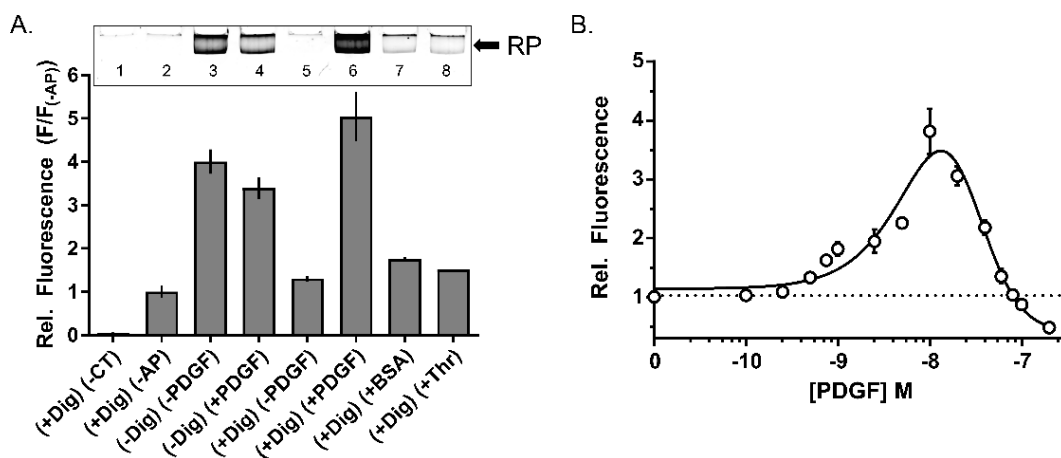


Figure 4.4. Performance of optimized anti-PDGF aptamer system with RCA product generation monitored in real-time using SYBR Gold intercalating dye. (A) Reagent and Selectivity controls, where (+Dig) denotes exonuclease digestion, and (-Dig) denotes no exonuclease digestion such that digestion time is 0 and the RCA reaction proceeds immediately following phi29 DP addition. BSA, thrombin (Thr), and PDGF concentrations were 10 nM. Inset is the denaturing PAGE of reaction products. (B) Titration curve of RCA product generation in the presence of varying amounts of PDGF. Results taken after 60 minutes of RCA.

Figure 4.4B shows the concentration dependence of the P-AP system over a range of PDGF concentrations, demonstrating a LOD of 250 pM (3σ) after a 60-minute RCA reaction time. When only minute amounts of protected AP remain, as is the case with low concentrations of target, additional reaction time is required to generate sufficient RP for detection. Compared to our previous work where target binding suppressed RCA as a signal-off method,^[25] we observed a 40-fold improvement in the LOD. This LOD could likely be further improved by using a longer RCA time or incorporating an exponential RCA method, as demonstrated for example

with the tripartite aptamer regulated RCA assay previously reported by our group (LOD of 1 fM at 120 min RCA time).^[24]

Notably, the concentration-response curve is not linear, and instead exhibited a bell-shape, where low concentrations of PDGF improved amplification while higher concentrations inhibited amplification. As shown in Figure 5, this can be explained by the ability of the CT to displace the protein target from the AP at low target concentrations, allowing RCA to proceed, while at higher protein concentrations the CT becomes unable to fully displace the target, leading to incomplete release of the AP and reduced RCA levels. To confirm this hypothesis, the AP was released from bound PDGF via heating, followed by addition of the CT, which was able to restore RP generation at higher PDGF concentrations of 100 nM (Fig S4.6), though it is possible that some rebinding of renatured PDGF occurred, preventing maximum signal from being reached. We note that the overall shape of the response curve and the concentration of peak RCA product generation (10 nM PDGF) was not affected by the length of the toehold, with 5 nt and 15 nt toehold segments showing similar curves, albeit with a higher overall signal for the 15 nt toehold (Figure S4.7).

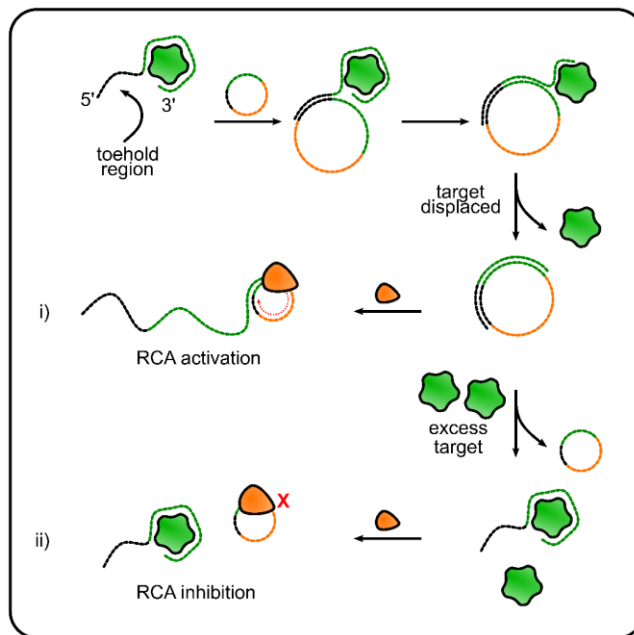


Figure 4.5. Ability of the circular template to liberate the aptamer through toehold mediated strand displacement as a function of target concentration. When target concentration is: i) low, the circular template successfully displaces the target, binds to the aptamer, and RCA is activated or; ii) high, the circular template is unable to outcompete the target for aptamer-binding, and RCA is inhibited.

PDGF in blood plasma or serum is used as a biomarker for a variety of clinical applications, with clinically relevant levels of PDGF-BB generally spanning only one order of magnitude in concentration.^[30,31] In most cases, PDGF levels range from tens to thousands of picomolar, with concentrations between cohorts differing by less than two-fold.^[32–36] As such, the narrow dynamic range afforded by the RCA activation assay should be acceptable for clinical evaluation of PDGF in whole or diluted serum samples. Access to lower PDGF concentrations should be possible by incorporating exponential amplification, such as hyperbranched RCA, as demonstrated in previous studies.^[24,37,38]

Not all nucleic acid sequences are equally susceptible to degradation by exonucleases. For example, nucleic acid sequences with G-quadruplex structures have been shown to be resistant to degradation.^[39] Therefore, we examined the activation of RCA using the 15 nt anti-thrombin aptamer as the aptamer (T-AP).^[40] T-AP forms a G-quadruplex structure in the presence of thrombin as well as in the presence of elevated levels of potassium.^[41–44] The exonuclease activity of phi29 DP requires the presence of monovalent cations such as potassium^[45] making thrombin an interesting target as this aptamer could show resistance to exonuclease activity under these conditions.

We first optimized the T-AP activation assay using the same procedures employed with the P-AP system. As expected, increasing the amount of phi29 DP increased the amount of digestion observed (Figure S4.8A), though a higher amount of phi29 DP was needed to achieve a similar degree of digestion. A significantly longer digestion time was also required relative to the P-AP system (Figure S4.8B). Together, this data suggest that the G-quadruplex structure imparted the expected exonuclease resistance, but that this could be overcome with higher concentrations of phi29 DP and longer reaction times. Importantly the thrombin-bound aptamer still showed increased resistance to exonuclease degradation in a concentration-dependent manner, with substantial recovery of undigested T-AP observed at 1000 nM thrombin (Figure S4.8C).

The ability of the CT to release thrombin-bound T-AP through the toehold displacement mechanism was also investigated (Figure S4.9). Addition of a 0 or 5 nt toehold region to the 5'-end of T-AP was insufficient to restore AP-CT duplex formation. In contrast, a 10 nt toehold region allowed for the dissociation of the AP-T complex and formation of an AP-CT duplex, which could subsequently be used for RCA. Elevated levels of unbound T-AP were observed when a 20-nt extension was used whereas the 15-nt toehold showed minimal unbound AP, thus we used a toehold region length of 15 nt for further studies.

The phi29 DP reaction buffer contains salts that encourage the aptamer to form a G-quadruplex structure even in the absence of thrombin, however they are required for optimal phi29 DP function. We investigated the effect of diluting the phi29 DP buffer, and use of different buffers that could destabilize the G-quadruplex, on assay performance (Figure S4.10). Diluting the buffer improved the contrast in signal between thrombin-bound and target-free assays. We suspect that this improvement was primarily driven by a decrease in native G-quadruplex structure owing to the decreased salt levels. A ten-fold buffer dilution was optimal as further dilution impeded the digestion reaction, likely due to decreased activity of phi29 DP. As expected, using HEPES, TRIS, or no buffer were least effective for the RCA reaction.

As was done with the P-AP system, the amount of phi29 DP was optimized with 1 U of phi29 DP per 10 nM of AP showing the best contrast between thrombin-bound and free aptamer (Figure S4.11A). Afterwards, the digestion time was investigated with an optimal contrast observed at 60 minutes of room-temperature digestion (Figure S4.11B). Where the P-AP system generated low amounts of RP and required a 5:1 ratio of CT:AP, the T-AP system showed excellent signal contrast with the best performance at a ratio of 1:2 CT:AP (Figure S4.11C). We suspect that the lower degree of intramolecular binding present in T-AP relative to P-AP allowed for the CT to bind to the AP more readily.

Reagent and selectivity testing for the T-AP system was performed using a 60 min digestion followed by 30 min of RCA using a 2:1 CT:AP ratio. As shown in Figure 4.6A, there was no RP generation when the CT or AP was excluded (lanes 1 and 2), while there was minimal signal contrast without the digestion step (-D, lanes 3 and 4). As expected, RP was formed when thrombin was present to protect the T-AP (lane 6), while no RP was produced when thrombin was absent or substituted with a different protein (BSA or PDGF) (lanes 5, 7 and 8) indicating that the T-AP system was selective for thrombin.

Once again, the concentration-response curve (Figure 4.6B) was not linear and showed the same bell-shaped curve as for the P-AP system, with a LOD of 100 pM (3σ) of thrombin after just 30 minutes of RCA and peak

RP generation at ca. 20 nM thrombin. This LOD was identical to our previous inhibition assay^[25] indicating that this approach could be generalized to include G-quadruplex or exonuclease-resistant aptamer strands. Once again, heat denaturation of thrombin prior to, and after, digestion restored RP generation at higher thrombin concentrations (Figure S4.12).

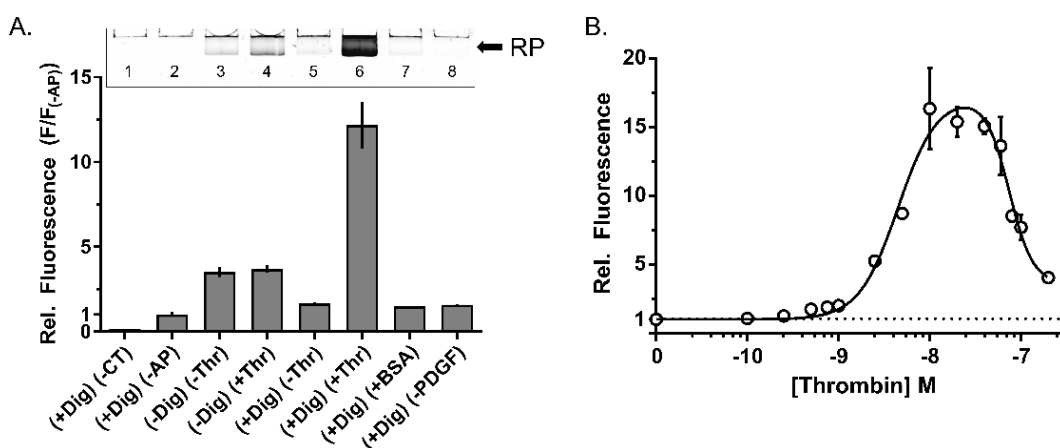


Figure 4.6. Performance of optimized anti-thrombin aptamer system with RCA product generation monitored in real-time using SYBR Gold intercalating dye. (A) Reagent and Selectivity controls, where (+Dig) denotes exonuclease digestion, and (-Dig) denotes no exonuclease digestion such that digestion time is 0 and the RCA reaction proceeds immediately following phi29 DP addition. BSA, PDGF, and thrombin (Thr) concentrations were 10 nM each. Inset is the denaturing PAGE of reaction products. (B) Titration curve of RCA product generation in the presence of varying amounts of thrombin. Results taken after 30 minutes of RCA.

Measuring thrombin in patient blood is used to determine whether patients are at risk of thrombosis. Free thrombin levels between 5 and 20 nM can be indicative of a high risk patient with concentrations above 20 nM indicating thrombosis or blood clotting.^[46] As clinically relevant thrombin concentrations fall within such a narrow range, this assay is particularly well

suiting for this application. With a detection limit of 100 pM, this allows for sample dilution of up to 50-fold while still allowing thrombin quantification at clinically relevant concentrations.

To evaluate whether the assay could be used in complex biological media, the detection of PDGF was examined in both human plasma and human serum. Biological samples often contain high levels of nucleases, which have the potential to digest DNA aptamers. Given that nucleic acid digestion is an inherent step in this assay, it was expected that additional digestion by endogenous nucleases would not pose a problem, but rather might improve assay performance.

We tested the P-AP system in 10-fold diluted serum or plasma samples spiked with varying levels of PDGF. We initially utilized the conditions that had been optimized for clean buffer. In this case, qualitative and selective detection of PDGF could be achieved in both plasma and serum, although in both cases the assay performance was compromised as elevated levels of RCA were observed even in unspiked samples (Figure S4.13), suggesting incomplete digestion of the P-AP. Increasing the digestion time from 6 min to 30 minutes for both plasma and serum restored assay performance (Figure S4.14). As shown in Figure 4.7A, the assay in serum produced an LOD of 250 pM, similar to the value in clean buffer, while in plasma the LOD was improved to 100 pM (Figure 4.7B), which represents a 100-fold improvement over the previous inhibition assay.^[25] Again, the

dynamic range of the assay fell into the clinically relevant range for PDGF detection, and as noted earlier, it is likely that further improvements in the LOD could be realized by implementing an exponential RCA step.

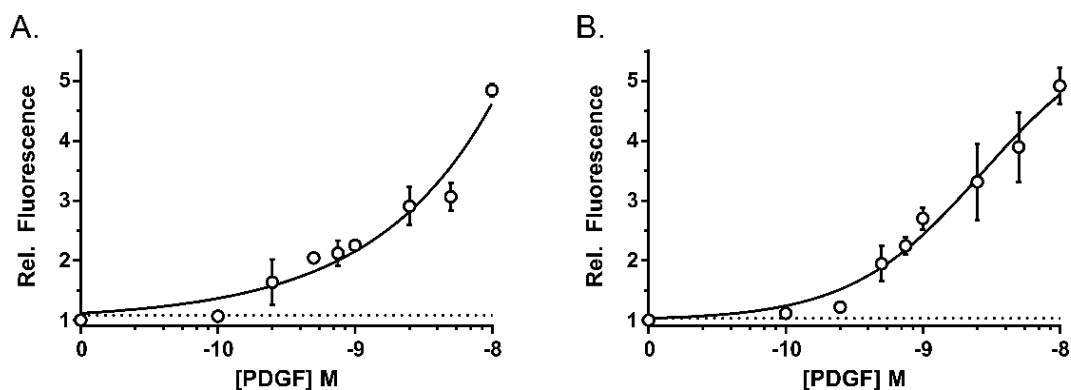


Figure 4.7. Performance of optimized anti-PDGF aptamer system in (A) 10% human serum or; (B) 10% human plasma. RCA product generation monitored in real-time using SYBR Gold intercalating dye. Results taken after 60 minutes of RCA.

Note that the T-AP system was not tested in human plasma or human serum as the 15 nt aptamer used in this work has been shown to interact non-specifically with thrombin inhibitors and serum albumin, which are present at high concentrations in blood.^[46] In contrast, the 29 nt anti-thrombin aptamer (HD22) could be a suitable alternative as this aptamer has demonstrated excellent selectivity and minimal non-specific interactions with human blood proteins.

4.5 Conclusion

In this study, we have shown that complex formation between an aptamer and a target analyte can be used to modulate the 3' exonuclease activity of phi29 DP on the aptaprimer, and that toehold-mediated strand displacement

by a complementary circular template can be used to displace the bound protein and thus liberate the aptamer and activate RCA. In our previous work,^[25] phi29 DP and CT were added simultaneously, thus exonuclease activity could not be used for regulation of primer availability. In contrast, by adding the phi29 DP to the system prior to CT addition, 3'-exonuclease digestion of the unprotected aptamer can occur, and subsequent addition of CT leads to a “turn-on” assay via the use of a toehold mechanism. This turn-on approach improved the detection limit by up to a factor of 100 relative to the inhibition assay,^[25] and unlike previous studies using phi29 DP-mediated 3'-exonuclease digestion with structure-switching aptamers,^[24,26,27] modified DNA species incorporating inverted dTs were not required and the design of a complicated tripartite system was avoided, although the structure-switching system incorporated an hyper-branched RCA method, producing a superior LOD of 1 fM.^[24] Importantly, the assay could detect picomolar concentrations of PDGF or thrombin within one hour using linear RCA, and could function in both human plasma and serum, indicating the robustness of the assay. A potential disadvantage of this approach is the non-linear concentration-response curve, which clearly shows that higher levels of target ultimately lead to the onset of RCA inhibition. This inhibition process can be eliminated by using a heating step to remove the bound protein, though this is not easily implemented in a simple POC test, making the toehold-mediated strand displacement method

preferable owing to its simplicity. We expect that the assay can be further developed into a simple solid-phase assay, for example by using a paper-based platform as was demonstrated for the previous inhibition assay,^[25] making the assay amenable to a portable POC format, which will be reported in upcoming work.

4.6 Acknowledgements

Funding for this work was provided by the Natural Sciences and Engineering Research Council of Canada (NSERC) via Discovery Grants to YL and JDB, the Canadian Foundation for Innovation (CFI) and the Ontario Ministry for Research and Innovation (ORF-RE; Grant No. RE07-045). JDB holds the Canada Research Chair in Point-of-Care Diagnostics.

4.7 References

- [1] K. B. Mullis, F. A. Faloona, in *Methods Enzymol.*, **1987**, pp. 335–350.
- [2] Y. Zhao, F. Chen, Q. Li, L. Wang, C. Fan, *Chem. Rev.* **2015**, *115*, 12491–12545.
- [3] X. Hua, W. Yin, H. Shi, M. Li, Y. Wang, H. Wang, Y. Ye, H. J. Kim, S. J. Gee, M. Wang, et al., *Anal. Chem.* **2014**, *86*, 8441–8447.
- [4] L. Zhao, H. Zhou, T. Sun, W. Liu, H. He, B. Ning, S. Li, Y. Peng, D. Han, Z. Zhao, et al., *Sci. Total Environ.* **2020**, *748*, 142330.
- [5] A. V. Ivanov, I. V. Safenkova, A. V. Zherdev, B. B. Dzantiev, *Microchim. Acta* **2019**, *186*, 549.
- [6] A. P. Frei, F. A. Bava, E. R. Zunder, E. W. Y. Y. Y. Hsieh, S. Y. Chen, G. P. Nolan, P. F. Gherardini, *Nat. Methods* **2016**, *13*, 269–275.
- [7] M. Gullberg, S. M. Gustafsdottir, E. Schallmeiner, J. Jarvius, M. Bjarnegard, C. Betsholtz, U. Landegren, S. Fredriksson, *Proc. Natl. Acad. Sci.* **2004**, *101*, 8420–8424.
- [8] E. Schallmeiner, E. Oksanen, O. Ericsson, L. Spångberg, S. Eriksson, U. H. Stenman, K. Pettersson, U. Landegren, *Nat. Methods* **2007**, *4*, 135–137.
- [9] S. Xie, Y. Chai, Y. Yuan, L. Bai, R. Yuan, *Biosens. Bioelectron.* **2014**, *55*, 324–329.

- [10] Y. Yuan, S. Wei, G. Liu, S. Xie, Y. Chai, R. Yuan, *Anal. Chim. Acta* **2014**, *811*, 70–75.
- [11] L. Xue, X. Zhou, D. Xing, *Chem. Commun.* **2010**, *46*, 7373–7375.
- [12] X. Shen, M. Zhang, S. Niu, C. Shi, *Analyst* **2015**, *140*, 6489–6492.
- [13] S. Xie, Y. Tang, D. Tang, *Biosens. Bioelectron.* **2018**, *102*, 518–524.
- [14] J. C. Achenbach, R. Nutiu, Y. Li, *Anal. Chim. Acta* **2005**, *534*, 41–51.
- [15] W. Li, Y. Yang, J. Chen, Q. Zhang, Y. Wang, F. Wang, C. Yu, *Biosens. Bioelectron.* **2014**, *53*, 245–249.
- [16] D. Wu, T. Gao, L. Lei, D. Yang, X. Mao, G. Li, *Anal. Chim. Acta* **2016**, *942*, 68–73.
- [17] T. Yu, W. Zhou, J. Liu, *ChemBioChem* **2018**, *19*, 31–36.
- [18] L. Yan, J. Zhou, Y. Zheng, A. S. Gamson, B. T. Roembke, S. Nakayama, H. O. Sintim, *Mol. Biosyst.* **2014**, *10*, 970–1003.
- [19] W. Zhao, M. M. Ali, M. A. Brook, Y. Li, *Angew. Chemie* **2008**, *47*, 6330–6337.
- [20] M. M. Ali, F. Li, Z. Zhang, K. Zhang, D.-K. Kang, J. A. Ankrum, X. C. Le, W. Zhao, *Chem. Soc. Rev.* **2014**, *43*, 3324.
- [21] W. Cheng, L. Ding, Y. Chen, F. Yan, H. Ju, Y. Yin, *Chem. Commun.* **2010**, *46*, 6720–6722.
- [22] L. Wang, K. Tram, M. M. Ali, B. J. Salena, J. Li, Y. Li, *Chem. Eur. J.* **2014**, *20*, 2420–4.
- [23] S. Wang, S. Bi, Z. Wang, J. Xia, F. Zhang, M. Yang, R. Gui, Y. Li, Y. Xia, *Chem. Commun.* **2015**, *51*, 7927–7930.
- [24] M. Liu, W. Zhang, Q. Zhang, J. D. Brennan, Y. Li, *Angew. Chemie* **2015**, *54*, 9637–9641.
- [25] R. M. Bialy, M. M. Ali, Y. Li, J. D. Brennan, *Chem. – A Eur. J.* **2020**, *26*, 5085–5092.
- [26] J. Wang, Y. Wang, S. Liu, H. Wang, X. Zhang, X. Song, J. Yu, J. Huang, *Analyst* **2019**, *144*, 3389–3397.
- [27] J. Wang, Y. Wang, S. Liu, H. Wang, X. Zhang, X. Song, J. Huang, *Anal. Chim. Acta* **2019**, *1060*, 79–87.
- [28] L. S. Green, D. Jellinek, R. Jenison, A. Östman, C. H. Heldin, N. Janjic, *Biochemistry* **1996**, *35*, 14413–14424.
- [29] W. Zhao, S. Schafer, J. Choi, Y. J. Yamanaka, M. L. Lombardi, S. Bose, A. L. Carlson, J. a. Phillips, W. Teo, I. a. Droujinine, et al., *Nat. Nanotechnol.* **2011**, *6*, 524–531.
- [30] J. Andrae, R. Gallini, C. Betsholtz, *Genes Dev.* **2008**, *22*, 1276–1312.
- [31] Y. Cao, *Trends Mol. Med.* **2013**, *19*, 460–473.
- [32] K. Leitzel, W. Bryce, J. Tomita, G. Manderino, I. Tribby, A. Thomason, A. Lipton, E. Podczaski, H. Harvey, A. Lipton, *Cancer Res.* **1991**, *51*, 4149–4154.
- [33] H. Takayama, Y. Miyake, K. Nouse, F. Ikeda, H. Shiraha, A. Takaki, H. Kobashi, K. Yamamoto, *J. Gastroenterol. Hepatol.* **2011**, *26*, 116–121.

- [34] J. Zhou, Y. Deng, L. Yan, H. Zhao, G. Wang, *Int. J. Infect. Dis.* **2016**, *49*, 94–99.
- [35] E. Fernández-Simón, A. Carrasco-Rozas, E. Gallardo, S. Figueroa-Bonaparte, I. Belmonte, I. Pedrosa, E. Montiel, X. Suárez-Calvet, J. Alonso-Pérez, S. Segovia, et al., *Sci. Rep.* **2019**, *9*, 2139.
- [36] M. Kajizuka, T. Miyachi, H. Matsuzaki, K. Iwata, C. Shinmura, K. Suzuki, S. Suda, K. J. Tsuchiya, K. Matsumoto, Y. Iwata, et al., *Prog. Neuro-Psychopharmacology Biol. Psychiatry* **2010**, *34*, 154–158.
- [37] X. Zhu, H. Xu, H. Zheng, G. Yang, Z. Lin, B. Qiu, L. Guo, Y. Chi, G. Chen, L. Guo, et al., *Chem. Commun.* **2013**, *49*, 10115–10117.
- [38] Q. Wang, H. Zheng, X. Gao, Z. Lin, G. Chen, *Chem. Commun.* **2013**, *49*, 11418–11420.
- [39] P. J. Bates, D. A. Laber, D. M. Miller, S. D. Thomas, J. O. Trent, *Exp. Mol. Pathol.* **2009**, *86*, 151–164.
- [40] L. C. Bock, L. C. Griffin, J. A. Latham, E. H. Vermaas, J. J. Toole, *Nature* **1992**, *355*, 564–566.
- [41] R. F. Macaya, P. Schultze, F. W. Smith, J. A. Roe, J. Feigon, *Proc. Natl. Acad. Sci. U. S. A.* **1993**, *90*, 3745–3749.
- [42] B. I. Kankia, L. A. Marky, *J. Am. Chem. Soc.* **2001**, *123*, 10799–10804.
- [43] X. L. Wang, F. Li, Y. H. Su, X. Sun, X. B. Li, H. J. Schluesener, F. Tang, S. Q. Xu, *Anal. Chem.* **2004**, *76*, 5605–5610.
- [44] J. W. Shim, Q. Tan, L. Q. Gu, *Nucleic Acids Res.* **2009**, *37*, 972–982.
- [45] L. Blanco, M. Salas, *Nucleic Acids Res.* **1985**, *13*, 1239–1249.
- [46] A. Trapaidze, J. P. Héroult, J. M. Herbert, A. Bancaud, A. M. Gué, *Biosens. Bioelectron.* **2016**, *78*, 58–66.

4.8 Experimental Section

Oligonucleotides and Other Materials. All DNA oligonucleotides (Table S1) were obtained from Integrated DNA Technologies (IDT), and purified by standard 10% denaturing (8 M urea) polyacrylamide gel electrophoresis (dPAGE) or high-performance liquid chromatography (HPLC). SYBR Gold, T4 DNA ligase, T4 polynucleotide kinase (PNK), phi29 DNA polymerase (phi29 DP), and the deoxyribonucleoside 5'-triphosphate mixture (dNTP) were purchased from Thermo Fisher (USA). Bovine Serum Albumin (BSA), and human plasma were purchased from Millipore Sigma (ON, Canada). Human serum was purchased from Innovative Research Inc (MI, USA) Human thrombin was purchased from Haematologic Technologies Inc (VT, USA). Recombinant Human PDGF was purchased from Cedarlane Labs (ON, Canada). Water was purified with a Milli-Q Synthesis A10 water purification system. All other chemicals and solvents were of analytical grade and were used as received.

Preparation of Circular Templates. Circular DNAs were prepared from 5'-phosphorylated linear DNA oligonucleotides through template-assisted ligation with T4 DNA ligase. Phosphorylation of linear DNA oligonucleotides was done as follows: a 50 μ L reaction mixture was prepared in 1 \times PNK buffer A (50 mM Tris-HCl, pH 7.6 at 25 $^{\circ}$ C, 10 mM MgCl₂, 5 mM DTT, 0.1 mM spermidine), containing 8 μ M linear circular template DNA (AP-C), 0.2 U PNK and 2 mM ATP. The mixture was incubated at 37 $^{\circ}$ C for 1 hour, followed by heating at 90 $^{\circ}$ C for 5 minutes. The circularization reaction was performed in a volume of 100 μ L, produced by adding 34 μ L of H₂O, 5 μ L of ligation strand DNA (AP-L) (100 μ M) and 10 μ L of 10 \times T4 DNA ligase buffer (400 mM Tris-HCl, 100 mM MgCl₂, 100 mM DTT, 5 mM ATP, pH 7.8 at 25 $^{\circ}$ C) to the 50 μ L PNK mixture. After heating at 90 $^{\circ}$ C for 2 minutes and cooling down to room temperature for 10 minutes, 1 μ L of T4 DNA ligase (10 u/ μ L) was added. The mixture was incubated at room temperature for 2 hours, followed by heating at 90 $^{\circ}$ C for 5 min. The reaction mixtures were ethanol precipitated followed by purification of the DNA circles by dPAGE and storage at -20 $^{\circ}$ C until use.

Investigation of increasing phi29 DP for 3'-exonuclease digestion for the PDGF P-AP system (Figure 4.2A). Solutions of 20 μ L were prepared in 1 \times RCA buffer (33 mM Tris acetate, pH 7.9 at 37 $^{\circ}$ C, 10 mM magnesium acetate, 66 mM potassium acetate, 0.1% (v/v) Tween 20, 1 mM DTT) containing 50 nM of aptaprimer (P-AP) and variable amounts of phi29 DP and were incubated at room temperature for 10 minutes. All solutions were subsequently mixed with an equal volume of 2 \times denaturing PAGE loading

buffer, heated to 95 °C for 5 minutes, cooled to room temperature and separated using 10% polyacrylamide gel electrophoresis (PAGE) under denaturing conditions. The gel was stained with SYBR Gold and fluorescent images of gels were obtained using a Chemidoc MP imager (Biorad), analyzed using ImageLab software (Biorad) and processed using ImageJ. Digestion as a percentage of the initial intensity obtained for undigested P-AP (no phi29) was plotted using the data obtained from ImageJ.

Investigation of increasing PDGF for 3'-exonuclease digestion for the PDGF P-AP system (Figure 4.2B). 15 μ L solutions containing 50 nM of aptaprimer (P-AP) and variable amounts of PDGF were incubated at room temperature for 15 minutes. Next, a 5 μ L solution containing 2 U of phi29 DP in RCA buffer was added and incubated at room temperature for 10 minutes. PAGE was performed as described above for Figure 4.2A and analyzed using ImageJ as noted above.

Optimization of reaction parameters for the PDGF P-AP system (Figure 4.3). The protocol was similar to the “Standard Assay for the PDGF P-AP system” described below, however the phi29 DP concentration, digestion time, and CT:AP ratio were varied as indicated in the Figure caption.

Reagent and Selectivity Controls for the PDGF P-AP system (Figure 4.4A). The protocol was similar to the “Standard Assay for the PDGF P-AP system” described below, however certain reagents were included or excluded as indicated in the Figure caption. For the (-D) cases, exonuclease digestion was avoided by adding the phi29 DP and CT simultaneously for the RCA solution. After the RCA reaction, 5 μ L aliquots were collected and used for PAGE as described above in Figure 4.2A. For selectivity studies, 10 nM of either BSA or thrombin were substituted for PDGF and the assay was run using exonuclease digestion, with assays run as in Figure 4.2A.

Standard Assay for the PDGF P-AP system (Figure 4.4B). A 5 μ L solution containing 200 fmol of P-AP15 was prepared in 1 \times RCA buffer. Next, a 10 μ L solution containing varying amounts of PDGF in 1 \times RCA buffer was added and incubated at room temperature for 15 minutes. 5 μ L of 1 \times RCA buffer containing 0.5U of phi29 DP was then added and incubated at room temperature for 6 minutes. Lastly, a 30 μ L RCA solution containing 3 μ L of 10 \times RCA buffer, 2 μ L of dNTPs (10 mM), 5 μ L of 10 \times intercalating dye (SYBR Gold) and 20 μ L of water, with a final concentration of 1 pmol of circular template (P-AP-CT), was added and the subsequent RCA reaction was monitored over 60 min using a Spark platereader (Tecan).

Reagent and Selectivity Controls for the thrombin T-AP system (Figure 4.6A). The protocol was similar to the “Standard Assay for the thrombin T-AP system” described below, however certain reagents were included or excluded as indicated in the Figure caption. For the (-D) cases, exonuclease digestion was avoided by adding the phi29 and CT simultaneously to the RCA solution. After the RCA reaction, 5 μ L aliquots were collected and used for PAGE as described above in Figure 4.2A. For selectivity studies, 10 nM of either BSA or PDGF were substituted for thrombin and the assay was run using exonuclease digestion, with assays run as in Figure 4.2A.

Standard Assay for the thrombin T-AP system (Figure 4.6B). The digestion step in the thrombin assay was run in an identical manner to the PDGF assay except that: 1) the T-AP15 aptamer was used; 2) the concentration of phi29 was two-fold higher than used in the PDGF assay and; 3) the digestion reaction was run for 60 min rather than 6 min. The RCA reaction was run identically to the PDGF assay except that a final concentration of 100 fmol of circular template (T-AP-CT) was used, and the subsequent RCA reaction was monitored over 30 minutes using a Spark platereader (Tecan).

Testing in Complex Media (Figure 4.7). The protocol for testing in complex media was similar to the “Standard Assay for the PDGF P-AP system” protocol described above except that the 10 μ L target solution contained 20% v/v human serum or human plasma such that the final serum or plasma percentage was 10% upon addition of phi29 DP for the digestion step. As well, the digestion time was 30 minutes instead of 6 minutes.

4.9 Supporting Information

Table S4.1. List of DNA Sequences Used.

Name of DNA oligonucleotide	Sequence (5'-3')
Linear precursor of PDGF system (P-AP)	
P-AP-CT (80 nt, <u>anti-aptamer region</u> , toehold region)	CGAACAAACAT <u>CAGGATCATG</u> GTGATGCTCT <u>ACGTGCCGTA</u> <u>GCCTTGCCCA</u> TACTAATCAA AGCCCATACT ACAACAACCTT
Linear precursor of thrombin system (T-AP)	
T-AP-C9 (60 nt, <u>anti-aptamer region</u> , toehold region)	CGAACAAACAT <u>CCAACCACAC</u> <u>CAACCGCCCA</u> TACTAATCAA AGCCCATACT ACAACAACCTT
DNA ligation strand	
AP-L (20 nt)	ATGTTGTTTCG AAGTTGTTGT
P-AP system aptamers	
P-AP (35 nt)	AAGGCTACGG CACGTAGAGC ATCACCATGA TCCTG
P-AP5 (40 nt, 5 nt toehold region)	TGGGC AAGGCTACGG CACGTAGAGC ATCACCATGA TCCTG
P-AP10 (45 nt, 10 nt toehold region)	TAGTATGGGC AAGGCTACGG CACGTAGAGC ATCACCATGA TCCTG
P-AP15 (50 nt, 15 nt toehold region)	TTGAT TAGTATGGGC AAGGCTACGG CACGTAGAGC ATCACCATGA TCCTG
P-AP20 (55 nt, 20 nt toehold region)	GGGCTTTGAT TAGTATGGGC AAGGCTACGG CACGTAGAGC ATCACCATGA TCCTG
P-AP with Cy5 fluorescent tag	As above but with a /5Cy5/ fluorescent tag on the 5'-end of the DNA

T-AP system aptamers

T-AP (15 nt)	GGTTGGTGTG GTTGG
T-AP5 (20 nt, 5 nt toehold region)	TGGGC GGTTGGTGTG GTTGG
T-AP10 (25 nt, 10 nt toehold region)	TAGTATGGGC GGTTGGTGTG GTTGG
T-AP15 (30 nt, 15 nt toehold region)	TTGAT TAGTATGGGC GGTTGGTGTG GTTGG
T-AP20 (35 nt, 20 nt toehold region)	GGGCTTTGAT TAGTATGGGC GGTTGGTGTG GTTGG
T-AP with Cy5 fluorescent tag	As above but with a /5Cy5/ fluorescent tag on the 5'-end of the DNA

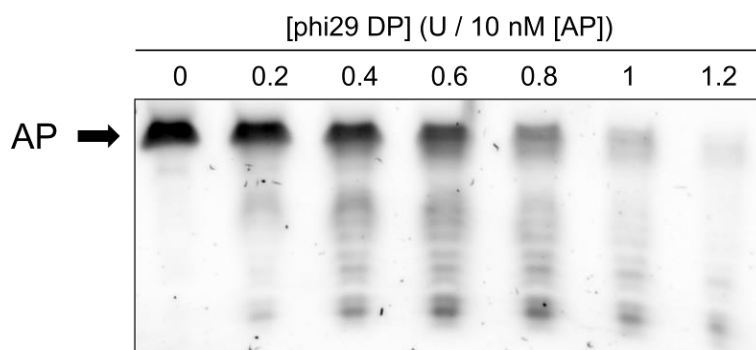


Figure S4.1. Investigation of the effect of increasing phi29 DP concentration on the 3'-exonuclease digestion of the PDGF aptamer (P-AP).

Experimental Details. See Figure 4.2A described in the **Experimental Section**.

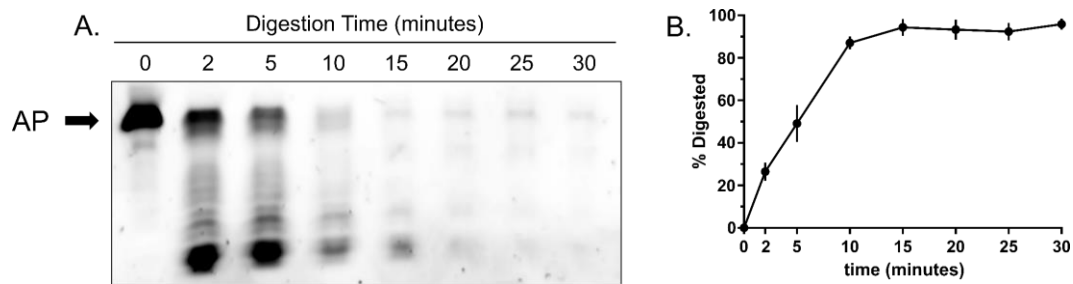


Figure S4.2. Investigation of the effect of increasing reaction time on the 3'-exonuclease digestion of the PDGF aptamer (P-AP): (A) Denaturing PAGE and; (B) Digestion as a percentage relative to the 0 minute control condition.

Experimental Details. Solutions were prepared containing 2 μL of 10 \times RCA buffer, 50 nM of aptamer (P-AP), 2 U of phi29 DP, and diluted to 20 μL with water. Next, they were incubated at room temperature for variable reaction times. PAGE was performed as described in the **Experimental Section** for Figure 4.2A. Digestion as a percentage was determined using ImageJ to analyze band intensities relative to the AP band in the control lane (0 minute).

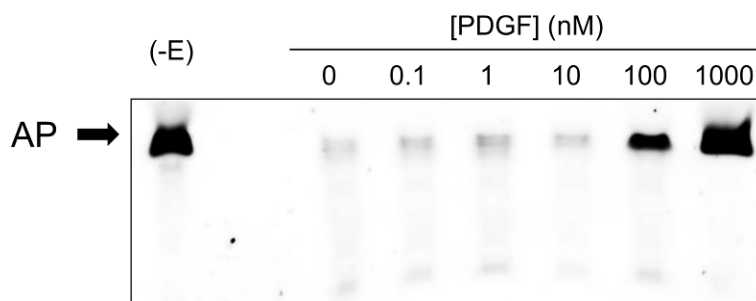


Figure S4.3. Investigation of the effect of increasing PDGF protein concentration on the 3'-exonuclease digestion of the PDGF aptamer (P-AP).

Experimental Details. See Figure 4.2B described in the **Experimental Section**.

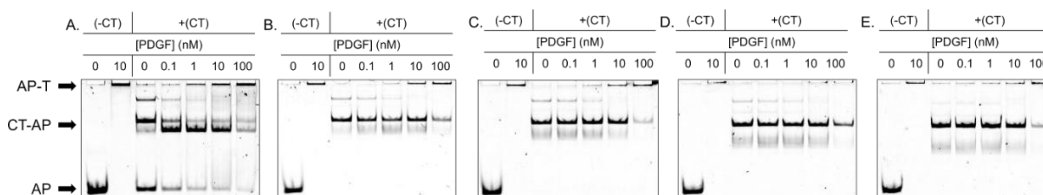


Figure S4.4. Observing the degree of liberation of AP from the AP-T complex by increasing the AP-CT binding affinity via elongation of 5'-end of the aptamer in the anti-PDGF aptamer system using native PAGE analysis: T = target (specifically PDGF). Elongation lengths of: (A) 0 nt; (B) 5 nt; (C) 10 nt; (D) 15 nt; (E) 20 nt. Note that the presence of two bands for the CT-AP complex suggests that the complex may adopt two unique conformations.

Experimental Details. A solution containing 1.5 μL of 10 \times RCA buffer, 10 nM of fluorescently-tagged aptamer ((A) P-AP-Cy5; (B) P-AP5-Cy5; (C) P-AP10-Cy5; (D) P-AP15-Cy5; (E) P-AP20-Cy5), variable amounts of PDGF, and diluted to 15 μL with water was incubated at room temperature for 30 minutes. Next, a solution containing 0.5 μL of 10 \times RCA buffer, 50 nM of circular template (P-AP-CT), and diluted to 5 μL with water was added and incubated at room temperature for 30 minutes. PAGE was performed as described in the **Experimental Section** for Figure 4.2A but non-denaturing (native) PAGE was used and without SYBR Gold staining.

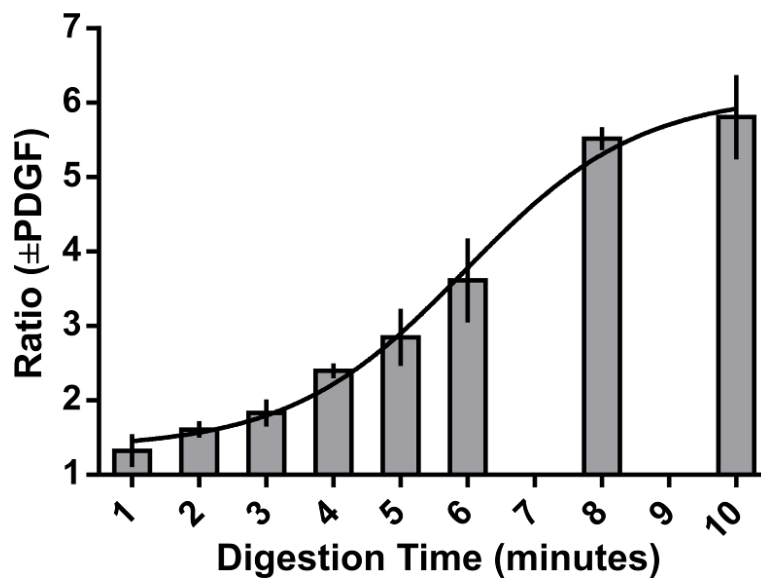


Figure S4.5. Optimization of digestion time for the anti-PDGF aptamer system using a 0.1 CT:AP ratio. RCA product generation monitored in real-time using SYBR Gold intercalating dye. A concentration of either 0 or 10 nM PDGF was used for ratio determination. Results taken after 60 minutes of RCA.

Experimental Details. The protocol was similar to the “Standard Assay for the PDGF P-AP system” described in the **Experimental Section**, however the digestion time, and CT:AP ratio were varied as indicated in the Figure 4.caption.

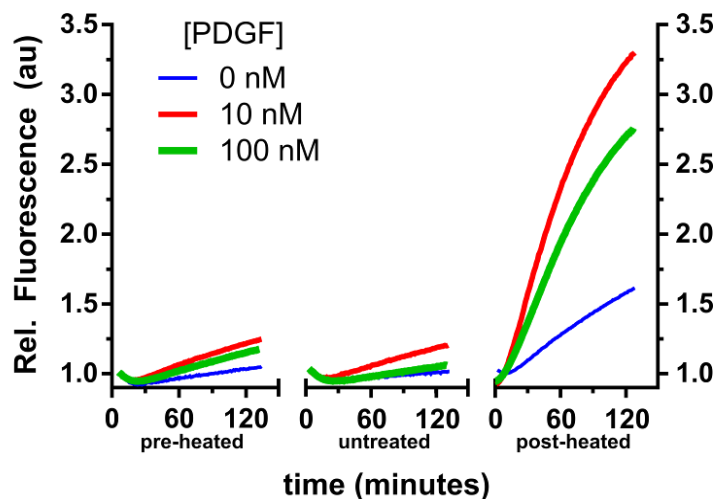


Figure S4.6. Effect of various heat treatments of protein targets on RP generation for the P-AP system. RCA product generation – monitored in real-time using SYBR Gold intercalating dye.

Experimental Details. The protocols was similar to the “Standard Assay for the PDGF P-AP system” described in the **Experimental Section**, however the target protein was either i) “pre-heated” at 95°C for 30 minutes and cooled to room temperature prior to incubation with the aptamer; ii) left unchanged or; iii) “post-heated” at 95 °C for 30 minutes and cooled to room temperature after the digestion step but prior to the addition of circular template, dNTPs, and SYBR Gold.

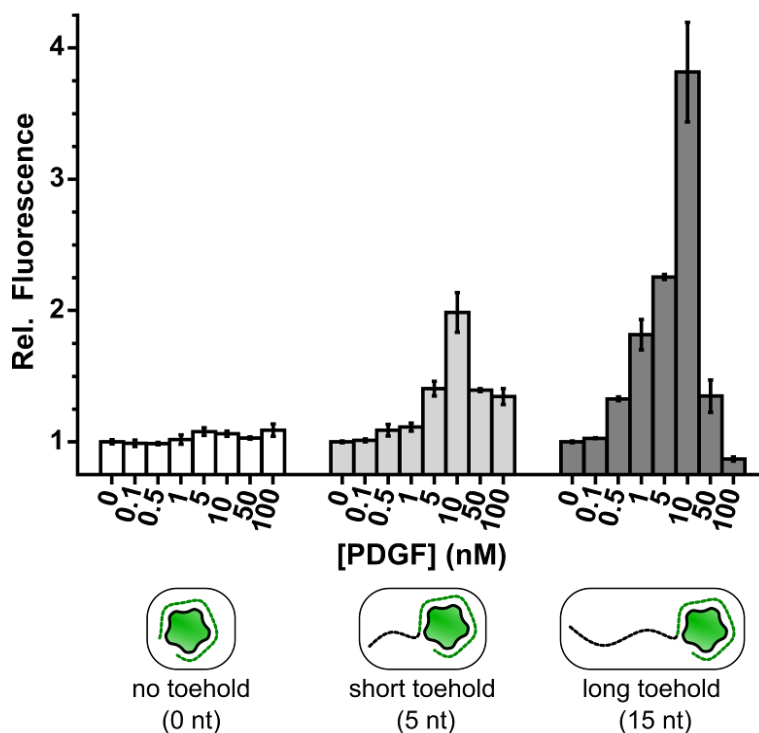


Figure S4.7. Role of toehold length on ability to activate RCA in the anti-PDGF aptamer system. The toehold length increases from left to right: i) no toehold (0 nt); ii) short toehold (5 nt) and; iii) long toehold (15 nt). RCA product generation monitored in real-time using SYBR Gold intercalating dye.

Experimental Details. The protocols was similar to the “Standard Assay for the PDGF P-AP system” described in the **Experimental Section**, however the aptaprimer used was either: i) P-AP; ii) P-AP5 or; iii) P-AP15.

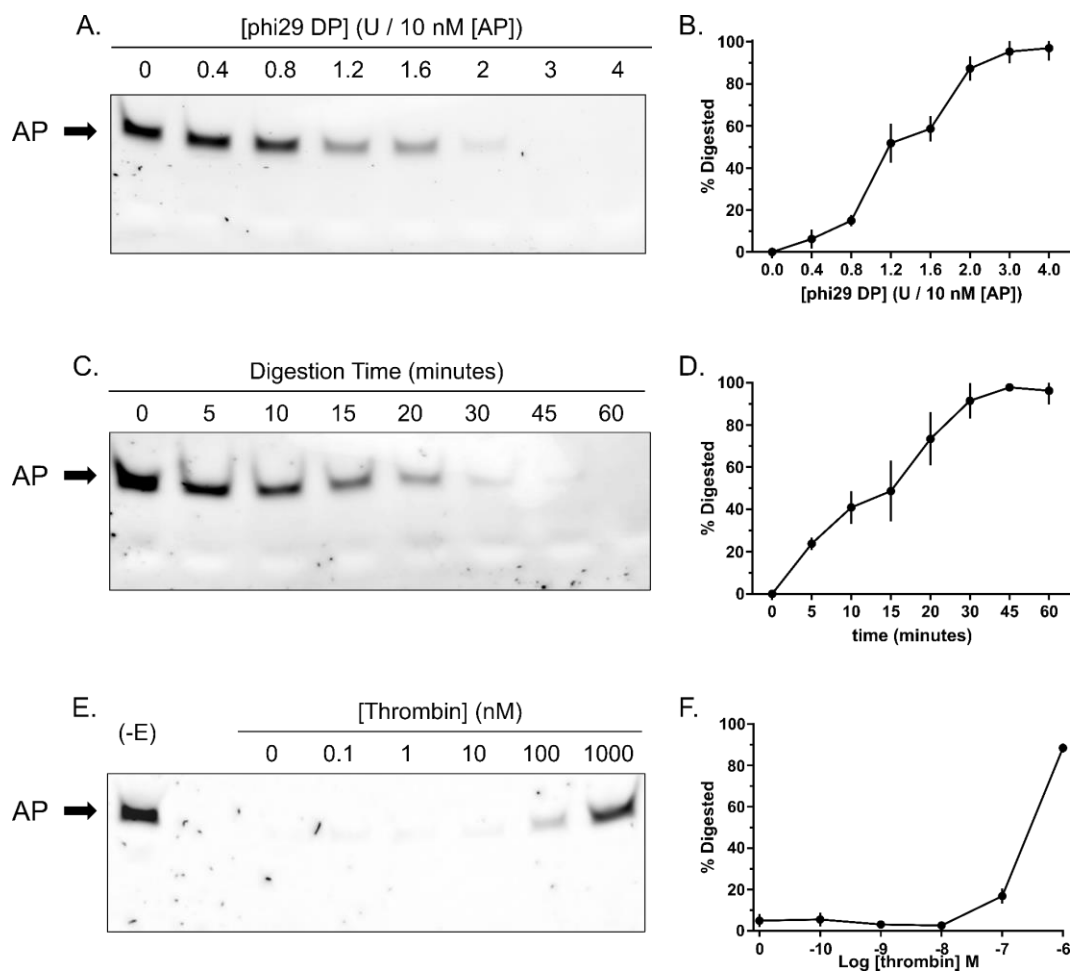


Figure S4.8. Investigation of the effect of increasing various reaction parameters for the anti-thrombin T-AP system: i) concentration of phi29 DP: (A) Denaturing PAGE and; (B) Digestion as a percentage relative to the no phi29 DP control condition. ii) digestion time: (C) Denaturing PAGE and; (D) Digestion as a percentage relative to the 0 minute control condition. iii) concentration of thrombin: (E) Denaturing PAGE and; (F) Digestion as a percentage relative to the no digestion and no target control condition.

Experimental Details. For (A), solutions were prepared containing 2 μ L of 10 \times RCA buffer, 50 nM of aptaprimer (T-AP), variable amounts of phi29 DP, and diluted to 20 μ L with water. Next, they were incubated at room temperature for 30 minutes. For (C), solutions were prepared containing 2 μ L of 10 \times RCA buffer, 50 nM of aptaprimer (T-AP), 6 U of phi29 DP, and diluted to 20 μ L with water. Next, they were incubated at room temperature for a variable number of minutes. For (E), solutions were prepared

containing 1.5 μL of 10 \times RCA buffer, 50 nM of aptaprimer (T-AP), variable amounts of thrombin, and diluted to 15 μL with water. Next, they were incubated at room temperature for 15 minutes. Next, a solution containing 0.5 μL of 10 \times RCA buffer, 6 U of phi29 DP, and diluted to 5 μL with water was added and incubated at room temperature for 60 minutes. PAGE was performed as described in the **Experimental Section** for Figure 4.2A. For (B), (D), and (F), Digestion as a percentage was determined using ImageJ to analyze band intensities relative to the AP band in the control lanes.

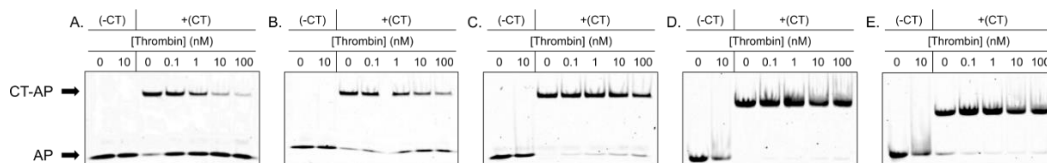


Figure S4.9. Observing the degree of liberation of AP from the AP-T complex by increasing the AP-CT binding affinity via elongation of 5'-end of the aptamer in the anti-thrombin aptamer system using native PAGE analysis: T = target (specifically thrombin). Elongation lengths of: (A) 0 nt; (B) 5 nt; (C) 10 nt; (D) 15 nt; (E) 20 nt. The top band indicates an AP-CT duplex whereas the bottom band indicates free AP. Note that the absence of a band for the AP-Target complex is likely the result of rapid on-off rates for the complex.

Experimental Details. The protocol was similar to **Figure S4.4** described above, however T-AP variations were used instead of the P-AP variations, thrombin was used instead of PDGF, and 10 nM of T-AP-CT was used instead of P-AP-CT. PAGE was performed as described in the **Experimental Section** for Figure 4.2A but non-denaturing (native) PAGE was used and without SYBR Gold staining.

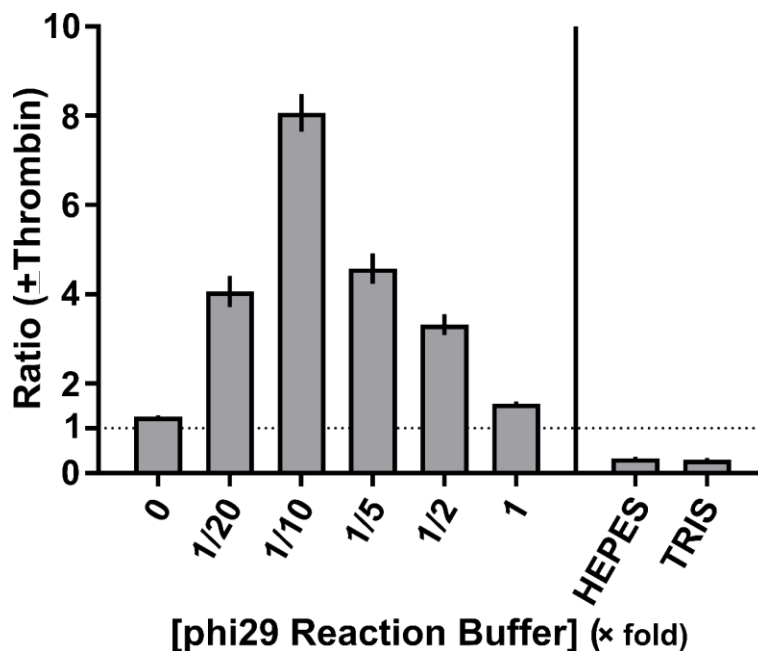


Figure S4.10. Determination of optimal buffer conditions for the T-AP system. RCA product generation monitored in real-time using SYBR Gold intercalating dye. A concentration of either 0 or 10 nM thrombin was used for ratio determination. Results taken after 30 minutes of RCA.

Experimental Details. The protocol was similar to the “Standard Assay for the thrombin T-AP system” described in the **Experimental Section**, however the buffer used during the target incubation and digestion steps was modified to either no buffer, HEPES, TRIS, or a range of 0.05-1x RCA buffer. Sufficient RCA buffer was subsequently added to achieve a 1x RCA buffer concentration for the RT-RCA step.

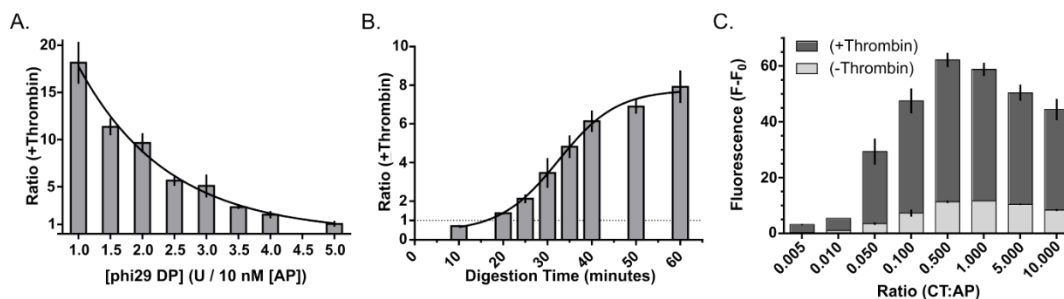


Figure S4.11. Optimization of the anti-thrombin aptamer system with by the following parameters: (A) Optimal phi29 DP concentration with a digestion time of 60 minutes and a 0.5 CT:AP ratio; (B) Optimal 3'-exonuclease digestion time with a phi29 DP concentration of 0.1 U/ μ L and a 0.5 CT:AP ratio and; (C) Optimal ratio of circular template (CT) to aptamer (AP). RCA product generation monitored in real-time using SYBR Gold intercalating dye. A concentration of either 0 or 10 nM thrombin was used for ratio determination. Results taken after 60 minutes of RCA.

Experimental Details. The protocol was similar to the “Standard Assay for the thrombin T-AP system” described in the **Experimental Section**, however the phi29 DP concentration, digestion time, and CT:AP ratio were varied as indicated in the Figure caption.

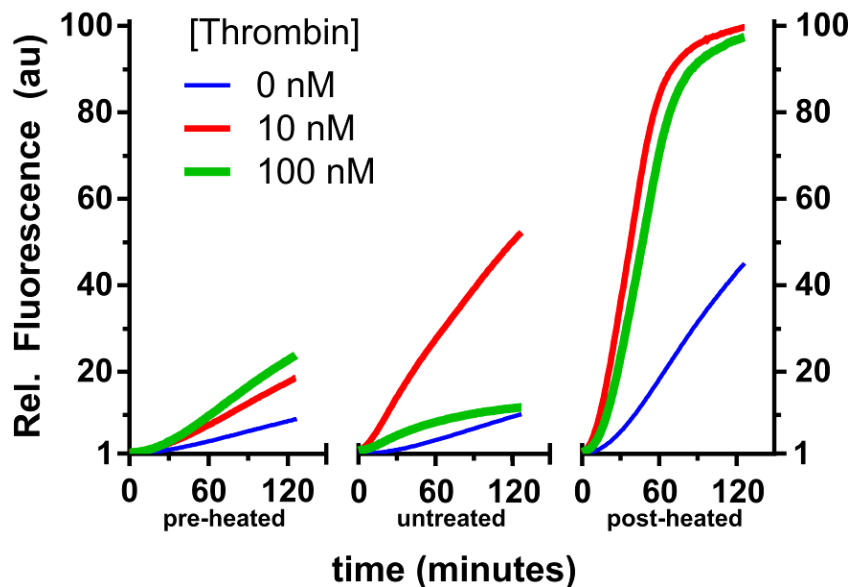


Figure S4.12. Effect of various heat treatments of protein targets on RP generation for the T-AP system. RCA product generation monitored in real-time using SYBR Gold intercalating dye.

Experimental Details. The protocols was similar to the “Standard Assay for the thrombin T-AP system” described in the **Experimental Section**, however the target protein was either i) “pre-heated” at 95°C for 30 minutes and cooled to room temperature prior to incubation with the aptamer; ii) left unchanged or; iii) “post-heated” at 95 °C for 30 minutes and cooled to room temperature after the digestion step but prior to the addition of circular template, dNTPs, and SYBR Gold.

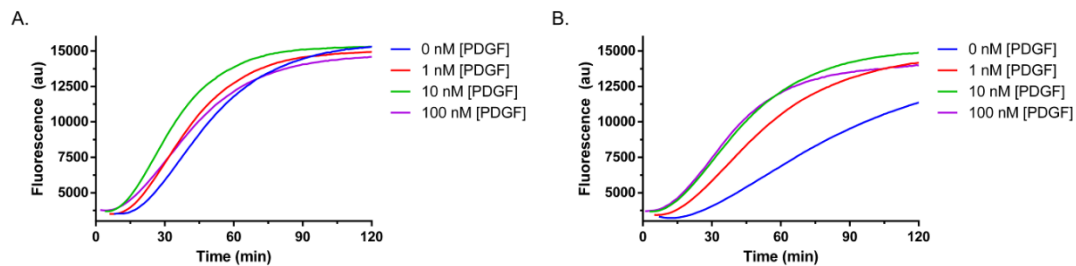


Figure S4.13. Effect of complex media on assay performance for P-AP system. (A) 10% human serum or; (B) 10% human plasma. RCA product generation monitored in real-time using SYBR Gold intercalating dye.

Experimental Details. The protocols were similar to the “Testing in Complex Media” step described in the **Experimental Section**, however the digestion time was 6 minutes instead of 30 minutes.

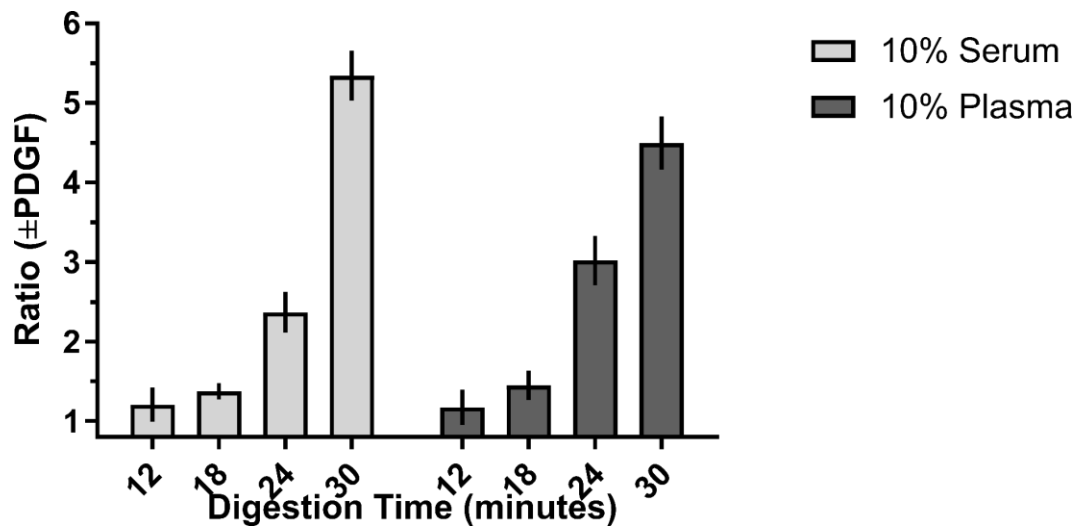


Figure S4.14. Determination of optimal digestion time for the P-AP system in either 10% human serum or 10% human plasma. RCA product generation monitored in real-time using SYBR Gold intercalating dye. A concentration of either 0 or 10 nM PDGF was used for ratio determination. Results taken after 120 minutes of RCA.

Experimental Details. The protocols were similar to the “Testing in Complex Media” step described in the **Experimental Section**, however the digestion time was either 12, 18, 24, or 30 minutes, respectively.

CHAPTER 5.

TARGET-MEDIATED 5'-EXONUCLEASE DIGESTION OF DNA APTAMERS WITH RECJ TO MODULATE ROLLING CIRCLE AMPLIFICATION FOR BIOSENSING

5.1 Author's Preface

The following chapter was submitted to *ChemBioChem* under the citation:

Roger M. Bialy, Yingfu Li, and John D. Brennan. Target-Mediated 5'-Exonuclease Digestion of DNA Aptamers with RecJ to Modulate Rolling Circle Amplification for Biosensing *ChemBioChem* **2021** (Submitted) DOI: TBD.

I was responsible for all experimental design, execution and analysis included in this chapter. I wrote the first draft of the manuscript. Dr. Brennan and Dr. Li provided editorial input to generate the final draft of the paper.

5.2 Abstract

We report a new method for biosensing based on the target-mediated resistance of DNA aptamers against 5'-exonuclease digestion, allowing them to act as primers for rolling circle amplification (RCA). A target-bound DNA strand containing an aptamer region on the 5'-end and a primer region on the 3'-end is protected from 5'-exonuclease digestion by RecJ exonuclease in a target-dependent manner. As the protected aptamer is at the 5'-end, the exposed primer on the 3'-end can participate in RCA in the presence of a circular template to generate a turn-on sensor. Without target, RecJ digests the primer and prevents RCA from occurring, allowing quantitative fluorescence detection of both thrombin, a protein, and ochratoxin A (OTA), a small molecule, at picomolar concentrations.

5.3 Introduction

A key advantage of molecular diagnostics is the ability to incorporate DNA amplification for ultrasensitive detection of nucleic acid species. While polymerase chain reaction (PCR)^[1] is a popular approach,^[2] more recent studies have focused on the development of isothermal DNA amplification (ITA) techniques, which overcome the need for expensive thermal cyclers.^[3] For the detection of non-nucleic acid species, many groups have reported on the use of functional nucleic acids (FNAs) such as aptamers^[4–8] and DNAzymes^[9–12] to regulate ITA methods, producing both turn-off and turn-on sensors.

Rolling circle amplification (RCA) is one of the most popular ITA methods for integration with FNAs, as the ability to perform RCA at room temperature makes it amenable to simple point-of-care (POC) assays.^[13,14] RCA typically uses a linear primer in conjunction with a circular template (CT) and phi29 DNA polymerase (phi29 DP) to produce long, repeating DNA reaction products (RP) complementary to the CT. Several reports have shown that protein-binding aptamers can be used for the regulation of RCA activity, allowing for sensitive protein quantification.^[15–20] The aptamers were typically present within the CT or the linear primer, in which case the bound target could inhibit processing by phi29 DP, blocking the RCA process and producing a turn-off sensor.

More recent efforts have exploited the inherent 3'-exonuclease activity of phi29 DP with aptamers to instead generate turn-on assays.^[18,21–23] Such sensors typically use structure-switching to remove a modified CT-bound aptamer that blocks the RCA reaction.^[18,21,22] However, as this method requires careful design of a tripartite structure-switching scheme, it may not be compatible with targets for which structure switching systems have not yet been developed. As an alternative, we recently reported a method that uses simple, unmodified aptamers for protein detection.^[23] This approach used the phi29 DP to digest aptamers in the absence of target, with protein-bound aptamers remaining intact. The CT was then used to initiate toehold-mediated strand displacement to remove the aptamer-

bound protein and allow for aptamer-primed RCA. However, the concentration-response curves generated using this method were non-linear and the dynamic range of the assay was relatively narrow at only two orders of magnitude.

In this work, we have investigated the potential of using digestion-mediated priming of RCA using RecJ, a 5'-exonuclease, to overcome the need for either structure-switching or toehold-mediated strand displacement, greatly simplifying initial assay design. RecJ has previously been used for 5'-exonuclease digestion of target-bound aptamers though it has not been used in the context of aptamer protection nor in conjunction with an ITA method such as RCA.^[24–27] In fact, this is the first report of the use of a 5'-exonuclease for the regulation of an RCA system for non-nucleic acid targets. Herein, we have designed a turn-on sensor that consists of a single-stranded nucleic acid (NA) sequence with a primer region on the 3' terminal end to initiate RCA, a short NA spacer, an aptamer region for target binding, and a short recognition tail on the 5' terminal end to assist in RecJ-mediated digestion (Figure 5.1A). Prior to RCA initiation, the aptaprimer (AP) is exposed to RecJ (Figure 5.1B). If no target is present, RecJ-mediated 5'-exonuclease digestion of the aptaprimer occurs, preventing RCA upon addition of a circular template (CT) and phi29 DP. However, with the target present, the aptamer region and target form a complex that shields the AP strand from digestion, and hence introduction of the CT and

phi29 DP leads to RCA, with the RP being detected by binding of an intercalating fluorescent dye. This approach was evaluated for the detection of two key targets, including thrombin, a protein target that would be expected to block digestion based on recent work that demonstrated protein-mediated modulation of aptamer digestion,^[23] and ochratoxin A (OTA), a small molecule target, that was selected to determine if smaller targets can also modulate aptamer digestion and thus control RCA.

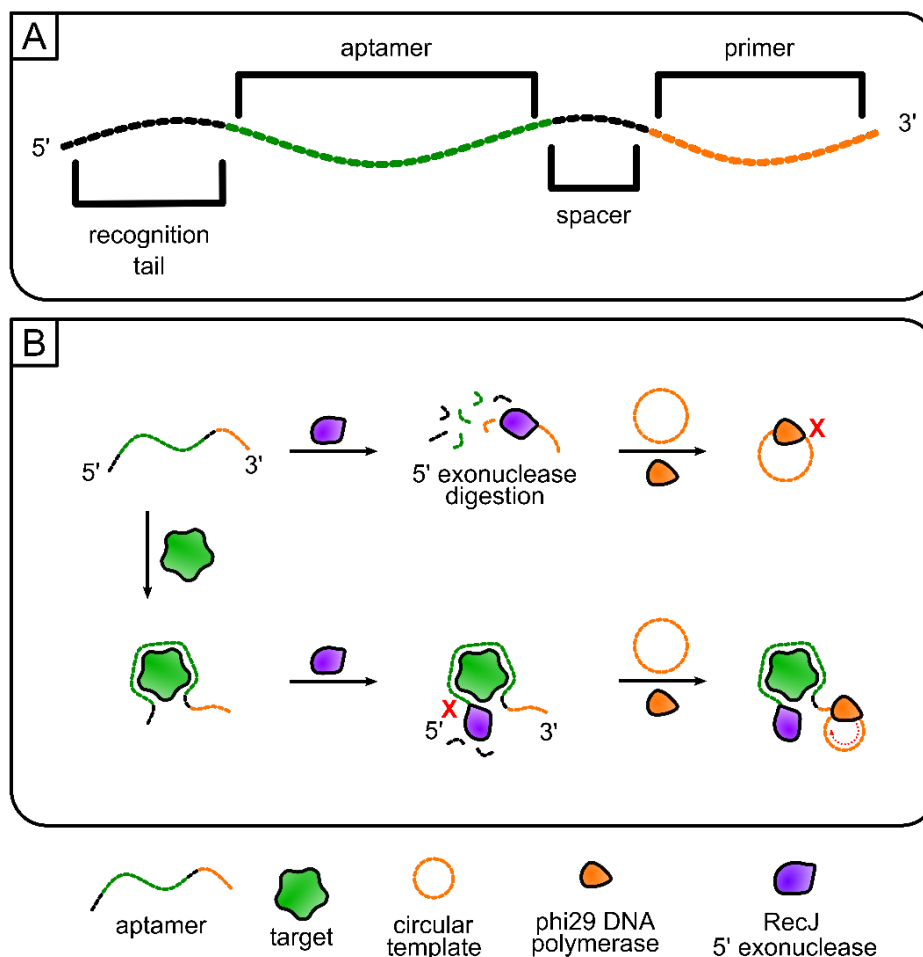


Figure 5.1. (A) The aptamer strand used for RecJ-mediated RCA. The sequence is comprised of a recognition tail on the 5'-end to promote RecJ recognition, an aptamer region for target recognition, a short spacer, and a primer region on the 3'-end for CT binding. (B) Schematic representation of the target-mediated RCA-based assay. In the absence of a target, RecJ 5'-exonuclease digests the aptamer prior to addition a CT and phi29 DP, preventing RCA. The binding of a target protects the aptamer from digestion, allowing the CT to bind to the protected primer region and permit RCA. The RCA product is detected using a fluorescent intercalating dye.

5.4 Results and Discussion

This approach was first tested using the 29 nt anti-thrombin aptamer (T-AP).^[28] To verify that RecJ could digest the T-AP, increasing amounts of RecJ were added to T-AP and the digestion of T-AP was visualized by 10% denaturing PAGE (dPAGE) (Figure S5.1A). As RecJ typically operates at 37°C and in a different buffer than phi29 DP-mediated RCA (Table S5.2), we evaluated different buffer and temperature conditions and observed that for T-AP, digestion was optimal when using phi29 DP buffer at 37°C (Figure S5.2). The use of 15 U of RecJ led to nearly complete digestion of T-AP (>95%) with the degree of digestion increasing as a function of increasing RecJ concentration (Figure 5.2A). The optimal digestion reaction time was determined to be 60 minutes (Figure 5.2B and S5.1B). The ability of thrombin to protect the T-AP from exonuclease digestion was then investigated. After incubation of T-AP with increasing amounts of thrombin, T-AP was digested using the optimized reaction conditions identified above (15 U of RecJ and 60-minute digestion time), and heat denatured to recover the protected T-AP for PAGE analysis (Figure S5.1C). Higher concentrations of thrombin led to less digestion of T-AP suggesting that RecJ-mediated digestion of T-AP could be regulated by target-binding and complex formation (Figure 5.2C).

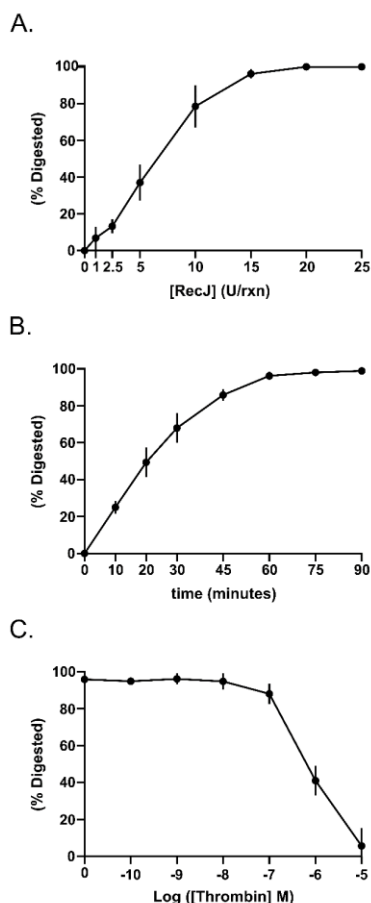


Figure 5.2. Gel-based optimization of T-AP digestion system: (A) Percentage of T-AP digested in 60 minutes as a function of RecJ 5'-exonuclease concentration (units per reaction). (B) Percentage of T-AP digested as a function of time, using 15 U of RecJ per reaction. (C) Percentage of T-AP digested as a function of thrombin concentration, using 15 U of RecJ per reaction and a digestion time of 60 minutes, followed by heat denaturation at 95 °C for 5 minutes.

Next, the ability to translate this regulation mechanism into an RCA reaction was investigated. To do so, the optimal RecJ concentration and digestion time were determined by comparing RCA performance after 30 minutes of room-temperature amplification between a thrombin-free and a thrombin-containing (10 nM) system using SYBR Gold as a fluorescent

intercalating dye. In doing so, an optimal RecJ concentration of 7.5 units per reaction was identified (Figure 5.3A) which was approximately less than half the ideal RecJ concentration identified using PAGE. This discrepancy could be attributed to using 5-fold less AP in the RT-RCA reactions relative to the gel-based reactions, or that RCA product, rather than remaining AP, is being monitored. Optimization of the digestion time showed a limited effect on the system (Figure 5.3B), likely indicating that the RecJ concentration was the more important variable. A 45-minute digestion time was used going forward as it was the minimal time needed to obtain sufficient digestion.

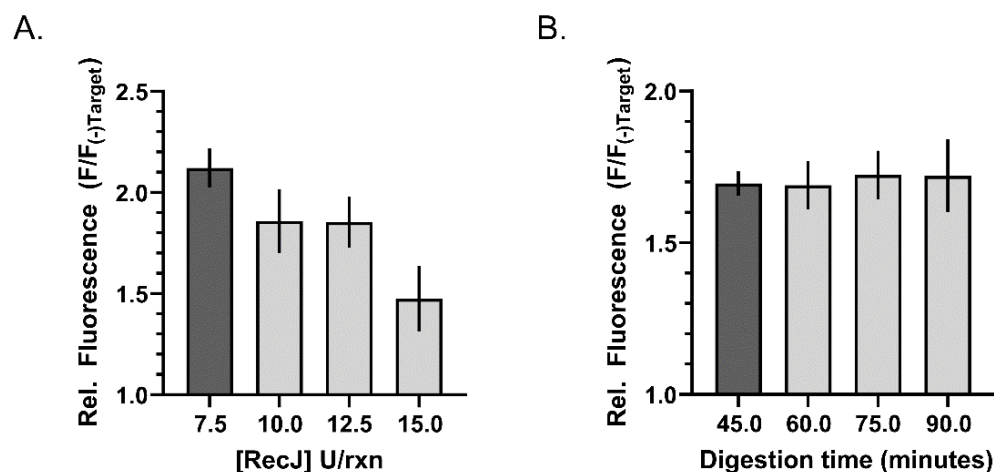


Figure 5.3. Real-time RCA-based optimization of T-AP RCA system using the following parameters: (A) Optimal RecJ concentration with a digestion time of 60 minutes; (B) Optimal digestion time with a RecJ concentration of 7.5 U. RCA product generation monitored in real-time using SYBR Gold intercalating dye. A concentration of either 0 or 10 nM thrombin was used for ratio determination. The dark grey bars indicate the selected optimal condition. Results taken after 30 minutes of RCA.

The selectivity of the optimized assay was evaluated using a 45-minute digestion by 7.5 U of RecJ per reaction in phi29 DP buffer at 37 °C, followed by performing RCA for 30 minutes at room temperature (Figure 5.4A). When the AP was excluded (lane 1), only trace amounts of RP were observed (possibly due to traces of unligated CT acting as a primer) while no RP generation was observed when the CT was excluded (lane 2). In the absence of RecJ, substantial RP was formed independent of thrombin concentration (lanes 3 and 4) as no digestion was possible. With RecJ present, elevated levels of RP was formed when thrombin was present to protect the AP from digestion (lane 6) but was reduced due to digestion of the AP when the target was absent or replaced with a different target (BSA or OTA) (lanes 5, 7, and 8).

A thrombin concentration dependence of the T-AP system was then evaluated, producing an LOD of 1 pM of thrombin (3σ) after a 30-minute RCA reaction time (Figure 5.4B). The response curve was terminated at a 1 μ M thrombin but would be expected to be sigmoidal with an upper plateau at 10 μ M based on the complete inhibition of digestion of the AP at this thrombin concentration (see Figure 5.2C). Compared to our previous 3' exonuclease digestion-based RCA assay where high concentrations of target suppressed RCA,^[23] we observed a 100-fold improvement in the detection limit and a much broader dynamic range, spanning 7 orders of magnitude, with a linear range of 5 orders of magnitude. This performance

is comparable to other linear RCA-based assays for thrombin detection, though incorporation of an exponential RCA method could potentially lower the detection limit by 2-3 orders of magnitude (Table S5.2).^[19,23,29,30]

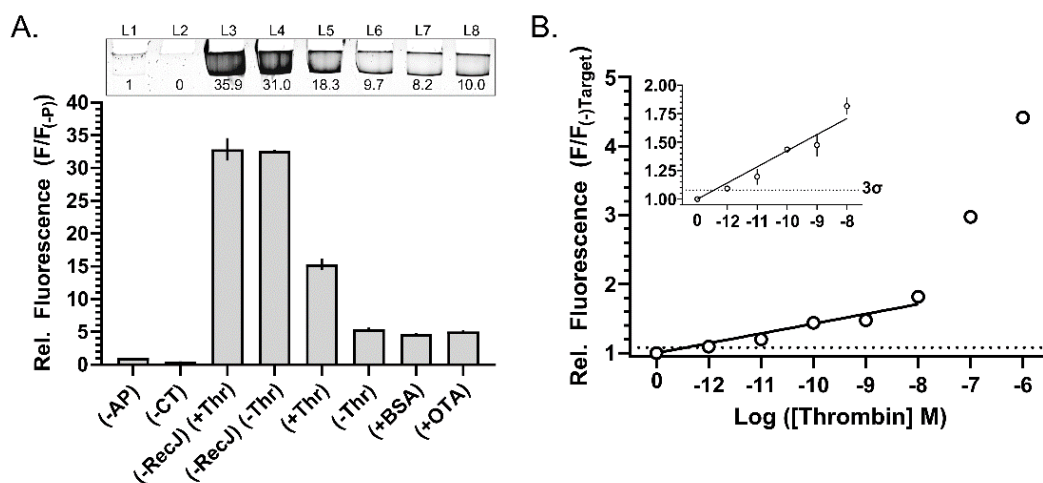


Figure 5.4. Performance of optimized anti-thrombin system with RCA product generation monitored in real-time using SYBR Gold intercalating dye. (A) Reagent and selectivity controls, where (-RecJ) denotes no RecJ-mediated exonuclease digestion. BSA, OTA, and thrombin (Thr) concentrations were 1 μM . The inset includes the denaturing PAGE gel of the reaction products as well as the intensity ratios between lanes. (B) Concentration-response curve of RCA product generation in the presence of varying amounts of thrombin. Results taken after 30 minutes of RCA.

Many of the targets for aptamers are small molecules, and hence it was important to determine whether small molecules could also protect aptamers from RecJ digestion. A well-known small molecule target with a high-affinity aptamer is ochratoxin A (OTA), with a molecular weight of 403.81 g/mol, which is a fungal-derived mycotoxin often found on foodstuffs.^[31] To test the approach with small molecules, we used the 36 nt

anti-OTA aptamer as an aptaprimer (O-AP)^[31] modified to contain the 3' primer extension and 5' RecJ recognition sequence (see Table S1). Upon optimization of the O-AP activation assay as outlined for the T-AP system, a similar dependence on RecJ was observed (Figure 5.5A, S5.3A), with 25 U of RecJ per reaction leading to nearly full digestion of O-AP (>95%). Interestingly the optimal digestion conditions were different for O-AP, with RecJ reaction buffer and 37°C reaction temperature being required for optimal digestion (Figure S5.4). When phi29 DP buffer was used, a secondary band was observed suggesting that though the 7A recognition tail was digested, RecJ could not process the OTA aptamer. It has been previously reported that RecJ digestion can terminate early when it reaches double-stranded DNA.^[32] We suspect that this early termination may be attributable to stronger intramolecular binding in phi29 DP buffer which contains elevated monovalent cation levels. As with the T-AP system, increasing the digestion time also increased the amount of digestion observed with 60 minutes or longer being optimal (Figure 5.5B, S5.3B). The addition of OTA also conferred protection onto the aptamer from RecJ-mediated digestion (Figure 5.5C, S5.3C), confirming that even a small molecule target was sufficient to block the processing of the RecJ reaction.

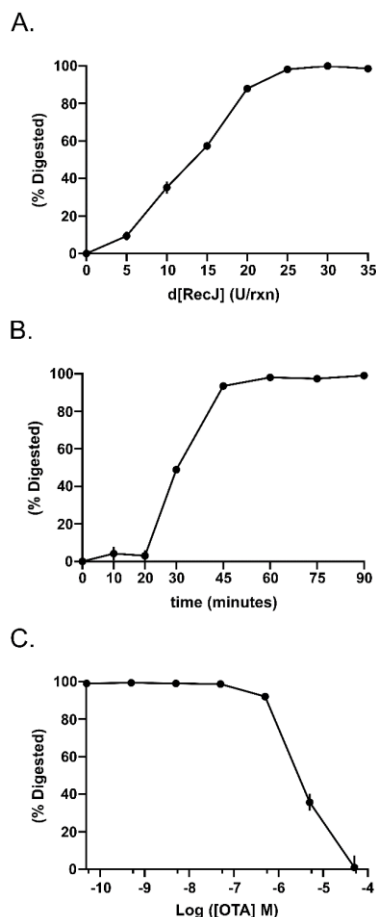


Figure 5.5. Gel-based optimization of O-AP digestion system: (A) Percentage of O-AP digested in 60 minutes as a function of RecJ 5'-exonuclease concentration (units per reaction). (B) Percentage of O-AP digested as a function of time, using 25 U of RecJ per reaction. (C) Percentage of O-AP digested as a function of OTA concentration, using 25 U of RecJ per reaction and a digestion time of 60 minutes, followed by heat denaturation at 95 °C for 5 minutes.

Optimization of the RCA reaction using real-time fluorescence monitoring indicated that 25 U of RecJ per reaction provided the best contrast between OTA-bound and free O-AP, which agreed with the gel-based optimization (Figure 5.6A). Following digestion with 25 U of RecJ for varying times (45 – 90 min), the RCA components (CT, dNTPs, SYBR Gold)

in 1× phi29 DP buffer were added to achieve a final buffer composition was two parts RecJ buffer and three parts phi29 DP buffer, and real-time RCA was run for 30 min. A digestion time of 60 min was chosen as it provided the highest and most reproducible signal levels (Figure 5.6B).

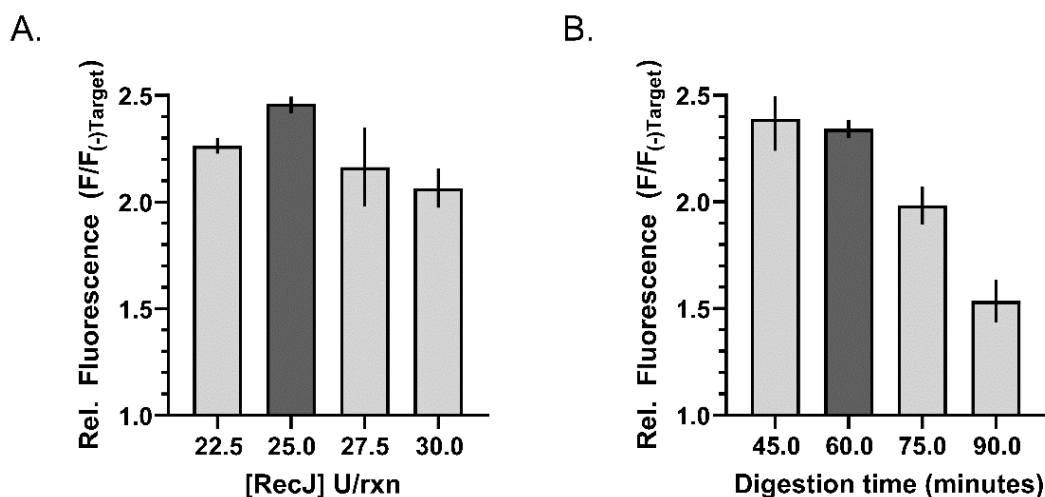


Figure 5.6. Real-time RCA-based optimization of the O-AP RCA system by varying the following parameters: (A) Optimal RecJ concentration with a digestion time of 60 minutes; (B) Optimal digestion time with a RecJ concentration of 25 U. RCA product generation was monitored in real-time using SYBR Gold intercalating dye. A concentration of either 0 or 1 μ M OTA was used for ratio determination. The dark grey bars indicate the selected optimal condition. Results were taken after 30 minutes of RCA.

These optimized conditions (60 min digestion with 25 U of RecJ followed by 30 minutes of RCA) was then used to evaluate the selectivity of the reaction (Figure 5.7A). As was observed with the T-AP system, trace amounts of RP were detected when AP was excluded (lane 1) but no RP generation was observed when the CT was excluded (lane 2). No signal contrast was observed when the digestion step was omitting indicating that digestion is critical for assay function (lanes 3 and 4). In contrast, in

samples with RecJ included (lanes 5-8) substantial RP was formed when OTA was present to protect the O-AP (lane 6), while RP generation was markedly lower when OTA was absent or substituted with a different target (BSA or thrombin) (lanes 5, 7 and 8). Notably, the relative change in signal with and without OTA (< 2-fold) was lower than was observed for the thrombin system (~3-fold), suggesting that OTA is not as efficient at preventing digestion, likely owing to the small size of the target.

The concentration-response curve for OTA (Figure 5.7B) generated an LOD of 10 pM (3σ) of target after just 30 minutes of RCA, indicating that this approach could be generalized to include non-protein targets for quantitative detection. Once again, the response curve was expected to be sigmoidal, but was terminated at 10 μ M OTA prior to reaching a plateau, which would be expected to occur at or above 10 μ M OTA based on digestion data (see Figure 5.5C). As with the T-AP system, the O-AP system exhibited a linear range of 5 orders of magnitude, which was competitive with other OTA-targeting linear RCA assays (Table S5.4).^[33–35]

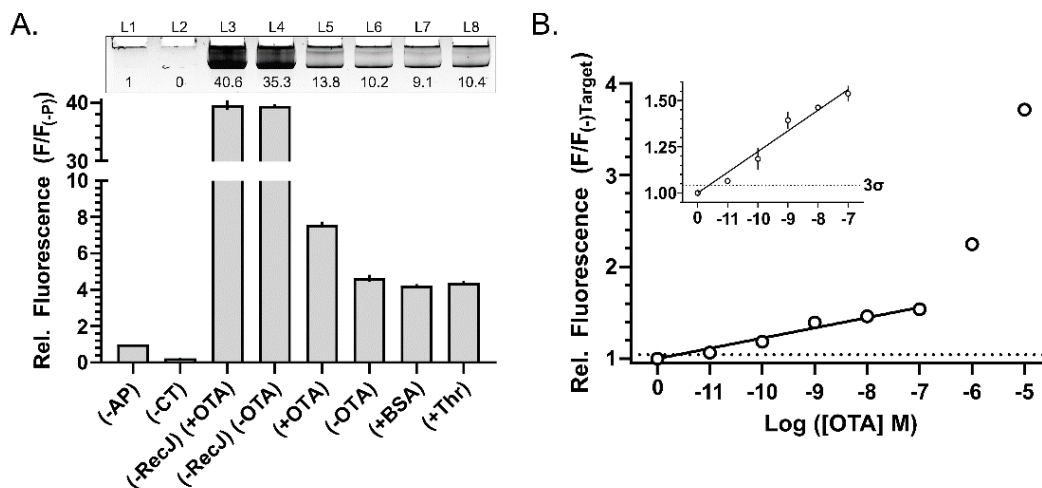


Figure 5.7. Performance of optimized anti-OTA system with RCA product generation monitored in real-time using SYBR Gold intercalating dye. (A) Reagent and selectivity controls, where (-RecJ) denotes no RecJ-mediated exonuclease digestion. BSA, thrombin (Thr), and OTA concentrations were 1 μ M. The inset includes the denaturing PAGE gel of the reaction products as well as the intensity ratios between lanes. (B) Concentration-response curve of RCA product generation in the presence of varying amounts of OTA. Results were taken after 30 minutes of RCA.

5.5 Conclusion

In this study, we have shown that target-mediated protection of aptamers from digestion by the 5'-exonuclease RecJ can be used to modulate RCA in a target concentration-dependent manner. The method does not require the use of a structure-switching aptamer system^[18,21,22,36] which may affect the native binding affinity of aptamers,^[37] or suffer from a low dynamic range observed with our previous digestion-based assay.^[23] To the best of our knowledge, this is the first report that uses a 5'-exonuclease for the regulation of RCA for the development of a real-time

fluorescence assay, and can provide excellent detection limits and a wide dynamic range for both a protein and a small molecule target in less than two hours. Potential drawbacks of this method include the need for two enzymes (RecJ and phi29 DP), in contrast to the previously reported RCA methods that utilized the inherent exonucleolytic properties of phi29 DP, and the need for a two-step process with one step occurring above room temperature (37°C). However, we have previously demonstrated that multi-step assays can be easily performed on paper-based sensors,^[38,39] while operation of assays at elevated temperatures can be achieved without the need for external power sources, allowing operation in remote or point-of-care settings.^[40] Further development of the assay toward the production of a paper-based sensor will be reported in a future manuscript.

5.6 Acknowledgements

Funding for this work was provided by the Natural Sciences and Engineering Research Council of Canada (NSERC) via Discovery Grants to YL and JDB, the Canadian Foundation for Innovation (CFI) and the Ontario Ministry for Research and Innovation (ORF-RE; Grant No. RE07-045). JDB holds the Canada Research Chair in Point-of-Care Diagnostics.

5.7 References

- [1] K. B. Mullis, F. A. Faloona, *Methods Enzymol.* **1987**, *155*, 335–350.
- [2] J. W.-F. Law, N.-S. Ab Mutalib, K.-G. Chan, L.-H. Lee, *Front. Microbiol.* **2015**, *5*, 1–19.
- [3] Y. Zhao, F. Chen, Q. Li, L. Wang, C. Fan, *Chem. Rev.* **2015**, *115*, 12491–12545.
- [4] S. Xie, Y. Chai, Y. Yuan, L. Bai, R. Yuan, *Biosens. Bioelectron.* **2014**, *55*, 324–329.
- [5] Y. Yuan, S. Wei, G. Liu, S. Xie, Y. Chai, R. Yuan, *Anal. Chim. Acta* **2014**, *811*, 70–75.
- [6] L. Xue, X. Zhou, D. Xing, *Chem. Commun.* **2010**, *46*, 7373–7375.
- [7] X. Shen, M. Zhang, S. Niu, C. Shi, *Analyst* **2015**, *140*, 6489–6492.
- [8] S. Xie, Y. Tang, D. Tang, *Biosens. Bioelectron.* **2018**, *102*, 518–524.
- [9] J. C. Achenbach, R. Nutiu, Y. Li, *Anal. Chim. Acta* **2005**, *534*, 41–51.
- [10] W. Li, Y. Yang, J. Chen, Q. Zhang, Y. Wang, F. Wang, C. Yu, *Biosens. Bioelectron.* **2014**, *53*, 245–249.
- [11] D. Wu, T. Gao, L. Lei, D. Yang, X. Mao, G. Li, *Anal. Chim. Acta* **2016**, *942*, 68–73.
- [12] T. Yu, W. Zhou, J. Liu, *ChemBioChem* **2018**, *19*, 31–36.
- [13] W. Zhao, M. M. Ali, M. A. Brook, Y. Li, *Angew. Chem. Int. Ed.* **2008**, *47*, 6330–6337.
- [14] M. M. Ali, F. Li, Z. Zhang, K. Zhang, D.-K. Kang, J. A. Ankrum, X. C. Le, W. Zhao, *Chem. Soc. Rev.* **2014**, *43*, 3324.
- [15] W. Cheng, L. Ding, Y. Chen, F. Yan, H. Ju, Y. Yin, *Chem. Commun.* **2010**, *46*, 6720–6722.
- [16] L. Wang, K. Tram, M. M. Ali, B. J. Salena, J. Li, Y. Li, *Chem. Eur. J.* **2014**, *20*, 2420–4.
- [17] S. Wang, S. Bi, Z. Wang, J. Xia, F. Zhang, M. Yang, R. Gui, Y. Li, Y. Xia, *Chem. Commun.* **2015**, *51*, 7927–7930.
- [18] M. Liu, W. Zhang, Q. Zhang, J. D. Brennan, Y. Li, *Angew. Chem. Int. Ed.* **2015**, *54*, 9637–9641.
- [19] R. M. Bialy, M. M. Ali, Y. Li, J. D. Brennan, *Chem. – A Eur. J.* **2020**, *26*, 5085–5092.
- [20] L. Yao, Y. Chen, J. Teng, W. Zheng, J. Wu, S. B. Adeloju, D. Pan, W. Chen, D. Pan, W. Chen, *Biosens. Bioelectron.* **2015**, *74*, 534–538.
- [21] J. Wang, Y. Wang, S. Liu, H. Wang, X. Zhang, X. Song, J. Yu, J. Huang, *Analyst* **2019**, *144*, 3389–3397.
- [22] J. Wang, Y. Wang, S. Liu, H. Wang, X. Zhang, X. Song, J. Huang, *Anal. Chim. Acta* **2019**, *1060*, 79–87.
- [23] R. Bialy, Y. Li, J. D. Brennan, *Chem. – A Eur. J.* **2021**, (Accepted), chem.202102975.
- [24] J. Ni, W. Yang, Q. Wang, F. Luo, L. Guo, B. Qiu, Z. Lin, H. Yang, *Biosens. Bioelectron.* **2018**, *105*, 182–187.

- [25] H. You, L. Bai, Y. Yuan, J. Zhou, Y. Bai, Z. Mu, *Biosens. Bioelectron.* **2018**, *117*, 706–712.
- [26] Y. Tan, X. Wei, Y. Zhang, P. Wang, B. Qiu, L. Guo, Z. Lin, H. H. Yang, *Anal. Chem.* **2015**, *87*, 11826–11831.
- [27] H. Zhao, D. Xiong, Y. Yan, C. Ma, *Toxins (Basel)*. **2020**, *12*, DOI 10.3390/toxins12110670.
- [28] D. M. Tasset, M. F. Kubik, W. Steiner, *J. Mol. Biol.* **1997**, *272*, 688–698.
- [29] X. Zhu, H. Xu, H. Zheng, G. Yang, Z. Lin, B. Qiu, L. Guo, Y. Chi, G. Chen, L. Guo, Y. Chi, G. Chen, *Chem. Commun.* **2013**, *49*, 10115–10117.
- [30] M. Liu, J. Song, S. Shuang, C. Dong, J. D. Brennan, Y. Li, *ACS Nano* **2014**, *8*, 5564–5573.
- [31] J. A. Cruz-Aguado, G. Penner, *J. Agric. Food Chem.* **2008**, *56*, 10456–10461.
- [32] E. S. Han, D. L. Cooper, N. S. Persky, V. A. Sutura, R. D. Whitaker, M. L. Montello, S. T. Lovett, *Nucleic Acids Res.* **2006**, *34*, 1084–1091.
- [33] Y. Zhang, L. Yang, C. Lin, L. Guo, B. Qiu, Z. Lin, G. Chen, *Anal. Methods* **2015**, *7*, 6109–6113.
- [34] R. Deng, Y. Dong, X. Xia, Y. Dai, K. Zhang, Q. He, W. C. Zeng, X. Ren, J. Li, *Anal. Chem.* **2018**, *90*, 14347–14354.
- [35] L. Hao, W. Wang, X. Shen, S. Wang, Q. Li, F. An, S. Wu, *J. Agric. Food Chem.* **2020**, *68*, 369–375.
- [36] X. Liu, F. Yang, D. Li, R. Yuan, Y. Xiang, *Sensors Actuators, B Chem.* **2020**, *305*, 127405.
- [37] R. Nutiu, Y. Li, *J. Am. Chem. Soc.* **2003**, *125*, 4771–4778.
- [38] M. M. Ali, M. Wolfe, K. Tram, J. Gu, C. D. M. Filipe, Y. Li, J. D. Brennan, *Angew. Chem. Int. Ed.* **2019**, *58*, 9907–9911.
- [39] C. Y. Hui, M. Liu, Y. Li, J. D. Brennan, *Angew. Chem. Int. Ed.* **2018**, *57*, 4549–4553.
- [40] B. Udugama, P. Kadhiresan, W. C. W. Chan, *Proc. Natl. Acad. Sci. U. S. A.* **2020**, *117*, 4632–4641.
- [41] G. Jin, C. Wang, L. Yang, X. Li, L. Guo, B. Qiu, G. Chen, Z. Lin, G. Chen, Z. Lin, G. Chen, *Biosens. Bioelectron.* **2015**, *63*, 166–171.
- [42] S. Bi, L. Li, S. Zhang, *Anal. Chem.* **2010**, *82*, 9447–9454.
- [43] J. Wang, S. Mao, H. F. Li, J. M. Lin, *Anal. Chim. Acta* **2018**, *1027*, 76–82.
- [44] X. Lin, Q. Chen, W. Liu, H. Li, J.-M. Lin, *Biosens. Bioelectron.* **2014**, *56*, 71–76.
- [45] Z. W. Wu, X. C. Xie, H. R. Guo, H. Xia, K. J. Huang, *Anal. Bioanal. Chem.* **2020**, *412*, 915–922.
- [46] T. Fan, Y. Du, Y. Yao, J. Wu, S. Meng, J. Luo, F. Gao, X. Zhang, D. Yang, C. Wang, Y. Qian, F. Gao, *Sensors Actuators, B Chem.* **2018**, *266*, 9–18.

- [47] T. Hu, Y. N. Zheng, M. J. Li, W. B. W. B. Liang, Y. Q. Chai, R. Yuan, *Anal. Chem.* **2018**, *90*, 6096–6101.
- [48] N. O. Fischer, T. M. Tarasow, J. B. H. H. Tok, *Anal. Biochem.* **2008**, *373*, 121–128.
- [49] D. A. Di Giusto, W. A. Wlassoff, J. J. Gooding, B. A. Messerle, G. C. King, *Nucleic Acids Res.* **2005**, *33*, e64.
- [50] Y. Mao, M. Liu, K. Tram, J. Gu, B. J. Salena, Y. Jiang, Y. Li, *Chem. Eur. J.* **2015**, *21*, 8069–8074.
- [51] L. Yang, Y. Zhang, R. Li, C. Lin, L. Guo, B. Qiu, Z. Lin, G. Chen, *Biosens. Bioelectron.* **2015**, *70*, 268–274.
- [52] E. Santovito, D. Greco, V. D’Ascanio, S. M. Sanzani, G. Avantiaggiato, *Anal. Chim. Acta* **2020**, *1133*, 20–29.
- [53] S. M. Taghdisi, N. M. Danesh, M. Ramezani, M. Alibolandi, M. A. Nameghi, G. Gerayelou, K. Abnous, *Talanta* **2021**, *223*, 121705.
- [54] L. Huang, J. Wu, L. Zheng, H. Qian, F. Xue, Y. Wu, D. Pan, S. B. Adeloju, W. Chen, *Anal. Chem.* **2013**, *85*, 10842–10849.
- [55] P. Tong, W.-W. W. Zhao, L. Zhang, J.-J. J. Xu, H.-Y. Y. Chen, *Biosens. Bioelectron.* **2012**, *33*, 146–151.

5.8 Experimental Section

Oligonucleotides and Other Materials. All DNA oligonucleotides (Table S1) were obtained from Integrated DNA Technologies (IDT) and purified by standard 10% denaturing (8 M urea) polyacrylamide gel electrophoresis (dPAGE) or high-performance liquid chromatography (HPLC). SYBR Gold, T4 DNA ligase, T4 polynucleotide kinase (PNK), phi29 DNA polymerase (phi29 DP), and the deoxyribonucleoside 5'-triphosphate mixture (dNTP) were purchased from Thermo Fisher (USA). RecJ 5' exonuclease (RecJ) and ochratoxin A (OTA) were purchased from New England Biolabs (USA). Bovine Serum Albumin (BSA) was purchased from Millipore Sigma (ON, Canada). Human thrombin was purchased from Haematologic Technologies Inc. (VT, USA). Water was purified with a Milli-Q Synthesis A10 water purification system. All other chemicals and solvents were of analytical grade and were used as received.

Preparation of Circular Templates. Circular DNAs were prepared from 5'-phosphorylated linear DNA oligonucleotides through template-assisted ligation with T4 DNA ligase. Phosphorylation of linear DNA oligonucleotides was done as follows: a 50 μ L reaction mixture was prepared in 1 \times PNK buffer A (50 mM Tris-HCl, pH 7.6 at 25 $^{\circ}$ C, 10 mM MgCl₂, 5 mM DTT, 0.1 mM spermidine), containing 8 μ M linear circular template DNA (CT), 0.2 U PNK and 2 mM ATP. The mixture was incubated at 37 $^{\circ}$ C for 1 hour, followed by heating at 90 $^{\circ}$ C for 5 minutes. The circularization reaction was performed in a volume of 100 μ L, produced by adding 34 μ L of H₂O, 5 μ L of ligation strand DNA (AP-L) (100 μ M) and 10 μ L of 10 \times T4 DNA ligase buffer (400 mM Tris-HCl, 100 mM MgCl₂, 100 mM DTT, 5 mM ATP, pH 7.8 at 25 $^{\circ}$ C) to the 50 μ L PNK mixture. After heating at 90 $^{\circ}$ C for 2 minutes and cooling down to room temperature for 10 minutes, 1 μ L of T4 DNA ligase (10 u/ μ L) was added. The mixture was incubated at room temperature for 2 hours, followed by heating at 90 $^{\circ}$ C for 5 min. The reaction mixtures were ethanol precipitated followed by purification of the DNA circles by dPAGE and storage at -20 $^{\circ}$ C until use.

Investigation of increasing RecJ for 5'-exonuclease digestion for the thrombin T-AP system (Figure 5.2A). Solutions of 20 μ L were prepared in 1 \times RCA buffer (66 mM K-acetate, 33 mM Tris-acetate, 10 mM Mg-acetate, 1 mM DTT, 0.1% (v/v) Tween 20, pH 7.9 @ 37 $^{\circ}$ C) containing 50 nM of aptamer (T-AP) and variable amounts of RecJ and were incubated at 37 $^{\circ}$ C for 60 minutes. All solutions were subsequently mixed with an equal volume of 2 \times denaturing PAGE loading buffer, heated to 95 $^{\circ}$ C for 5

minutes, cooled to room temperature and separated using 10% polyacrylamide gel electrophoresis (PAGE) under denaturing conditions. The gel was stained with SYBR Gold and fluorescent images of gels were obtained using a Chemidoc MP imager (Biorad), analyzed using ImageLab software (Biorad) and processed using ImageJ. Digestion as a percentage of the initial intensity obtained for undigested T-AP (no RecJ) was plotted using the data obtained from ImageJ.

Investigation of increasing reaction time 5'-exonuclease digestion for the thrombin T-AP system (Figure 5.2B). Solutions of 20 μ L were prepared in 1 \times RCA buffer (33 mM Tris acetate, pH 7.9 at 37 $^{\circ}$ C, 10 mM magnesium acetate, 66 mM potassium acetate, 0.1% (v/v) Tween 20, 1 mM DTT) containing 50 nM of aptamer (T-AP), 15 U/rxn of RecJ and were incubated at 37 $^{\circ}$ C for variable reaction times. PAGE was performed as described above for Figure 2A and analyzed using ImageJ as noted above.

Investigation of increasing thrombin for 5'-exonuclease digestion for the thrombin T-AP system (Figure 5.2C). 15 μ L solutions containing 50 nM of aptamer (T-AP) and variable amounts of thrombin were incubated at room temperature for 15 minutes. Next, a 5 μ L solution containing 15 U of RecJ in RCA buffer was added and incubated at 37 $^{\circ}$ C for 60 minutes. PAGE was performed as described above for Figure 2A and analyzed using ImageJ as noted above.

Optimization of reaction parameters for the thrombin T-AP system (Figure 5.3). The protocol was similar to the "Standard Assay for the thrombin T-AP system" described below, however the RecJ concentration, and digestion time were varied as indicated in the figure caption.

Reagent and Selectivity Controls for the thrombin T-AP system (Figure 5.4A). The protocol was similar to the "Standard Assay for the thrombin T-AP system" described below, however certain reagents were included or excluded as indicated in the figure caption. For the (-RecJ) cases, buffer instead of RecJ was added to the samples. After the RCA reaction, 5 μ L aliquots were collected and used for PAGE as described above in Figure 2A. For selectivity studies, 1 μ M of either BSA or OTA were substituted for 1 μ M of thrombin.

Standard Assay for the thrombin T-AP system (Figure 5.4B). A 5 μ L solution containing 200 fmol of O-AP was prepared in 1 \times phi29 DP buffer (66 mM K-acetate, 33 mM Tris-acetate, 10 mM Mg-acetate, 1 mM DTT,

0.1% (v/v) Tween 20, pH 7.9 @ 37 °C). Next, a 10 µL solution containing varying amounts of thrombin in 1× RecJ buffer was added and incubated at room temperature for 15 minutes. 5 µL of 1× RecJ buffer containing 7.5 U of RecJ was then added and incubated at 37 °C for 45 minutes. Lastly, a 30 µL RCA solution containing 3 µL of 10× RCA buffer (where 1× contains 66 mM K-acetate, 33 mM Tris-acetate, 10 mM Mg-acetate, 1 mM DTT, 0.1% (v/v) Tween 20, pH 7.9 @ 37 °C), 2 µL of dNTPs (10 mM), 5 µL of 10× intercalating dye (SYBR Gold), 2 U of phi29 DP, and 19.6 µL of water, with a final concentration of 1 pmol of circular template (CT), was added and the subsequent RCA reaction was monitored at room temperature over 30 min using a Spark platereader (Tecan).

Investigation of increasing RecJ for 5'-exonuclease digestion for the OTA O-AP system (Figure 5.5A). Solutions of 20 µL were prepared in 1× RecJ buffer (50 mM NaCl, 10 mM Tris-HCl, 10 mM MgCl₂, 1 mM DTT, pH 7.9 @ 25 °C) containing 50 nM of aptamer (O-AP) and variable amounts of RecJ and were incubated at 37 °C for 60 minutes. All solutions were subsequently mixed with an equal volume of 2× denaturing PAGE loading buffer, heated to 95 °C for 5 minutes, cooled to room temperature and separated using 10% polyacrylamide gel electrophoresis (PAGE) under denaturing conditions. The gel was stained with SYBR Gold and fluorescent images of gels were obtained using a Chemidoc MP imager (Biorad), analyzed using ImageLab software (Biorad) and processed using ImageJ. Digestion as a percentage of the initial intensity obtained for undigested O-AP (no RecJ) was plotted using the data obtained from ImageJ.

Investigation of increasing reaction time 5'-exonuclease digestion for the OTA O-AP system (Figure 5.5B). Solutions of 20 µL were prepared in 1× RecJ buffer containing 50 nM of aptamer (O-AP), and 25 U of RecJ and were incubated at 37 °C for variable reaction times. PAGE was performed as described above for Figure 2A and analyzed using ImageJ as noted above.

Investigation of increasing OTA for 5'-exonuclease digestion for the OTA O-AP system (Figure 5.5C). 15 µL solutions containing 1× RecJ buffer 50 nM of aptaprimer (O-AP) and variable amounts of OTA were incubated at room temperature for 15 minutes. Next, a 5 µL solution containing 25 U of RecJ in 1× RecJ buffer was added and incubated at 37 °C for 60 minutes. PAGE was performed as described above for Figure 2A and analyzed using ImageJ as noted above.

Optimization of reaction parameters for the OTA O-AP system (Figure 5.6). The protocol was similar to the “Standard Assay for the OTA O-AP system” described below, however the RecJ concentration, and digestion time were varied as indicated in the figure caption.

Reagent and Selectivity Controls for the OTA O-AP system (Figure 5.7A). The protocol was similar to the “Standard Assay for the OTA O-AP system” described below, however certain reagents were included or excluded as indicated in the figure caption. For the (-RecJ) cases, buffer instead of RecJ was added to the samples. After the RCA reaction, 10 μ L aliquots were collected and used for PAGE as described above in Figure 2A. For selectivity studies, 1 μ M of either BSA or thrombin were substituted for 100 nM of OTA.

Standard Assay for the OTA O-AP system (Figure 5.7B). A 5 μ L solution containing 200 fmol of O-AP was prepared in 1 \times RecJ buffer. Next, a 10 μ L solution containing varying amounts of OTA in 1 \times RecJ buffer was added and incubated at room temperature for 15 minutes. 5 μ L of 1 \times RecJ buffer containing 25 U of RecJ was then added and incubated at 37 $^{\circ}$ C for 60 minutes. Lastly, a 30 μ L RCA solution containing 3 μ L of 10 \times RCA buffer (where 1 \times contains 66 mM K-acetate, 33 mM Tris-acetate, 10 mM Mg-acetate, 1 mM DTT, 0.1% (v/v) Tween 20, pH 7.9 @ 37 $^{\circ}$ C), 2 μ L of dNTPs (10 mM), 5 μ L of 10 \times intercalating dye (SYBR Gold), 2 U of phi29 DP, and 19.6 μ L of water, with a final concentration of 1 pmol of circular template (CT), was added and the subsequent RCA reaction was monitored at room temperature over 30 min using a Spark platereader (Tecan).

5.9 Supporting Information

Table S5.1. List of DNA Sequences Used.

Name of DNA oligonucleotide	Sequence (5'-3')
Linear precursor for circular template (CT)	
CT (69 nt, primer-binding region)	CGAACAAACAT ATCAAAGCCC AACTACAACA ACAACATCAA ACAACATCAA ACAA ATACT ACAACAACCT
DNA ligation strand	
AP-L (20 nt)	ATGTTGTTTCG AAGTTGTTGT
T-AP system aptamer	
T-AP-P7 (61 nt, RecJ recognition region, <u>anti-thrombin aptamer region</u> , primer region , <i>spacers</i>)	AAAAAAAAGT <u>CCGTGGTAGG</u> <u>GCAGGTTGGG</u> <u>GTGACTAAAA</u> ATGTTGTAGT TGGGCTTTGA T
O-AP system aptamer	
O-AP-P7 (68 nt, RecJ recognition region, <u>anti-OTA aptamer region</u> , primer region , <i>spacers</i>)	AAAAAAGAT <u>CGGGTGTGGG</u> <u>TGGCGTAAAG</u> <u>GGAGCATCGG</u> <u>ACAAAAAATG TTGTAGTTGG GCTTTGAT</u>

Table S5.2. Comparison of other RCA-based assays for thrombin detection.

Amplification Method	Detection Method	LOD (pM)	Reference
hyperbranched RCA	electrochemical	0.0000012	[41]
hyperbranched RCA	fluorometric	0.002	[29]
linear RCA	chemiluminometric	6.6	[42]
linear RCA	chemiluminometric	0.55	[43]
linear RCA	colorimetric	15000	[16]
linear RCA	colorimetric	0.0023	[44]
linear RCA	colorimetric	0.00001	[17]
linear RCA	electrochemical	0.0353	[45]
linear RCA	electrochemical	0.035	[46]
linear RCA	electrochemical	0.0346	[47]
linear RCA	fluorometric	2000	[48]
linear RCA	fluorometric	240	[19]
linear RCA	fluorometric	100	[19]
linear RCA	fluorometric	100	[23]
linear RCA	fluorometric	30	[49]
linear RCA	fluorometric	10	[30]
linear RCA	fluorometric	1	[29]
linear RCA	fluorometric	1	[50]
linear RCA	fluorometric	1	This work.

Table S5.3. Comparison of buffer composition.

Phi29 DP Buffer (Thermo Fisher, USA)	RecJ Buffer (NEB, New England, USA)
pH 7.9 at 37 °C	pH 7.9 at 25 °C
33 mM Tris-acetate	10 mM Tris-HCl
10 mM Mg-acetate	10 mM MgCl ₂
66 mM K-acetate	50 mM NaCl
1 mM DTT	1 mM DTT
0.1% (v/v) Tween 20	No detergent

Table S5.4. Comparison of other RCA-based assays for OTA detection.

Amplification Method	Detection Method	LOD (original units)	Approximate LOD (pM)	Reference
hyperbranched RCA	electrochemical	0.02 pg/mL	0.05	[51]
hyperbranched RCA	fluorometric	1.2 fg/mL	0.003	[33]
CHA-assisted RCA	fluorometric	0.0002 ng/mL	0.5	[21]
linear RCA	colorimetric	1.09 ng/mL	2700	[52]
linear RCA	electrochemical	5 pM	5	[53]
linear RCA	electrochemical	0.065 ppt	0.16	[54]
linear RCA	fluorometric	0.01 ng/mL	24.8	[35]
linear RCA	fluorometric	18.1 pM	18.1	[34]
linear RCA	fluorometric	0.2 pg/mL	0.5	[55]
linear RCA	fluorometric	0.13 ppt	0.32	[20]
linear RCA	fluorometric	38.8 fM	0.039	[34]
linear RCA	fluorometric	10 pM	10	This work.

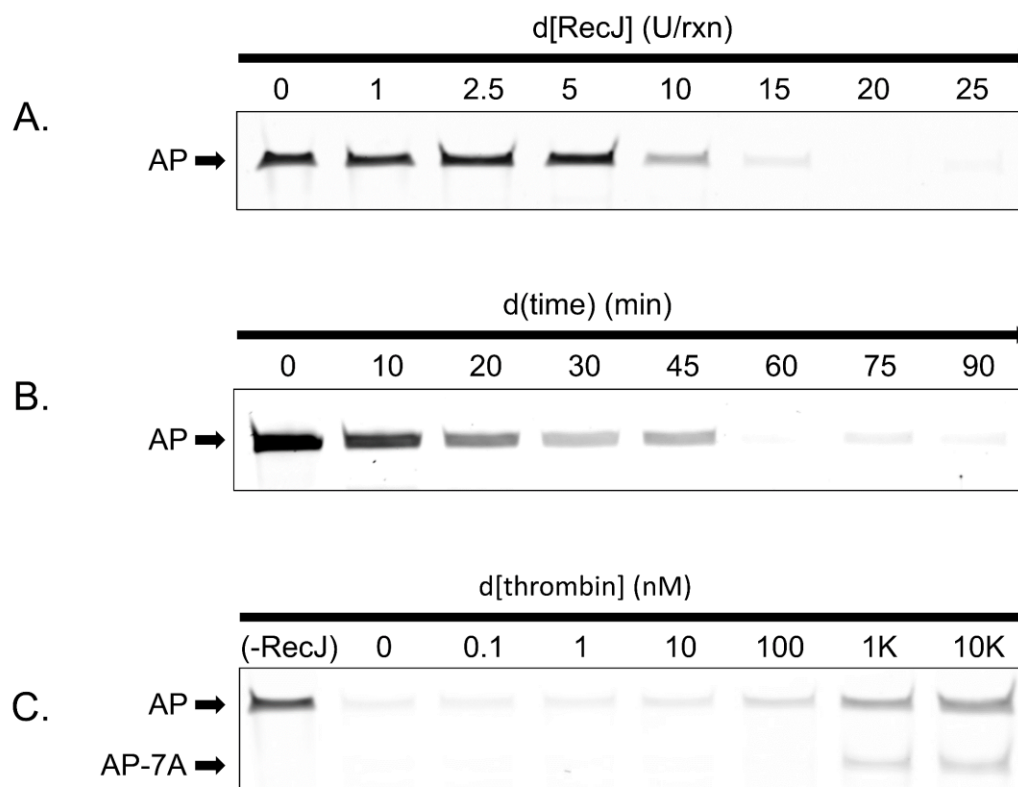


Figure S5.1. Investigation of the effect of increasing various reaction parameters for the anti-thrombin T-AP system using 10% denaturing PAGE analysis: (A) concentration of RecJ 5'-exonuclease; (B) digestion time; and, (C) concentration of thrombin.

Experimental Details. See Figures 5.2A-C described in the **Experimental Section**.

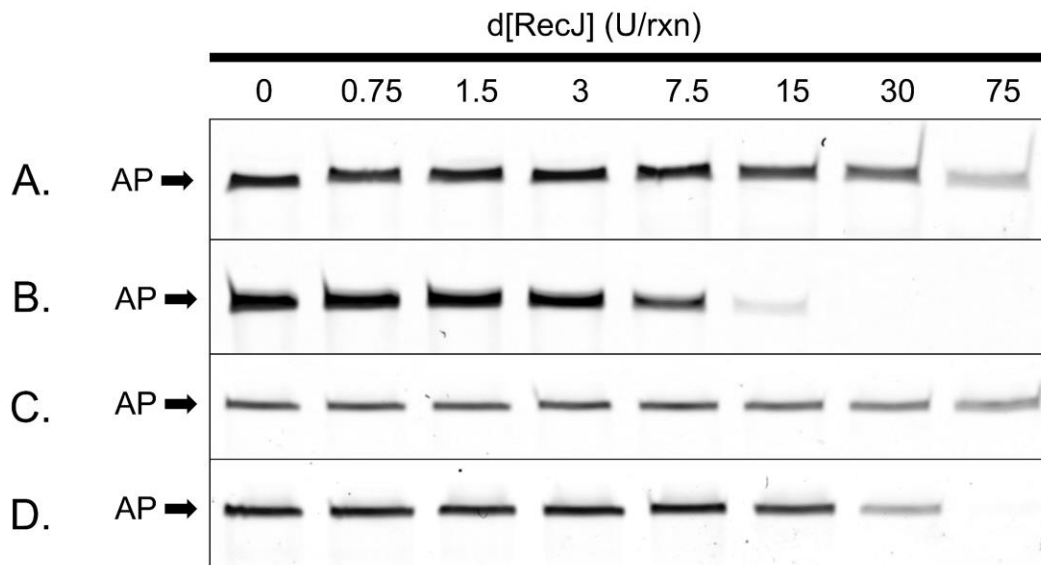


Figure S5.2. Investigation of the effect of increasing RecJ 5'-exonuclease concentration for the anti-thrombin T-AP system under different reaction conditions using 10% denaturing PAGE analysis: (A) 1x phi29 DP reaction buffer and room temperature; (B) 1x phi29 DP reaction buffer and 37°C; (C) 1x RecJ reaction buffer and room temperature and; (D) 1x RecJ reaction buffer and 37°C.

Experimental Details. The protocol was similar to Figure 5.2A described in the **Experimental Section**, however the buffer conditions and reaction temperature were varied as indicated in the figure caption.

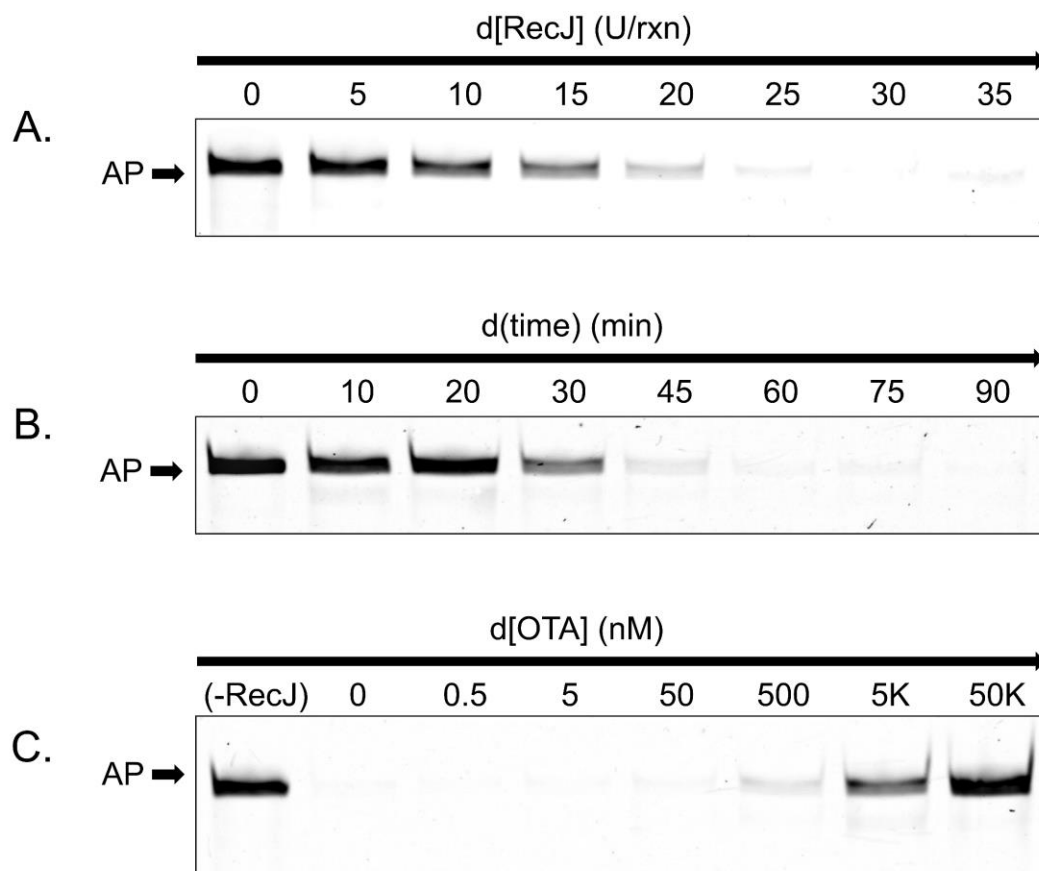


Figure S5.3. Investigation of the effect of increasing various reaction parameters for the O-AP system using 10% denaturing PAGE analysis: (A) concentration of RecJ 5'-exonuclease; (B) digestion time and; (C) concentration of ochratoxin A (OTA).

Experimental Details. See Figure 5.5A-C described in the **Experimental Section**.

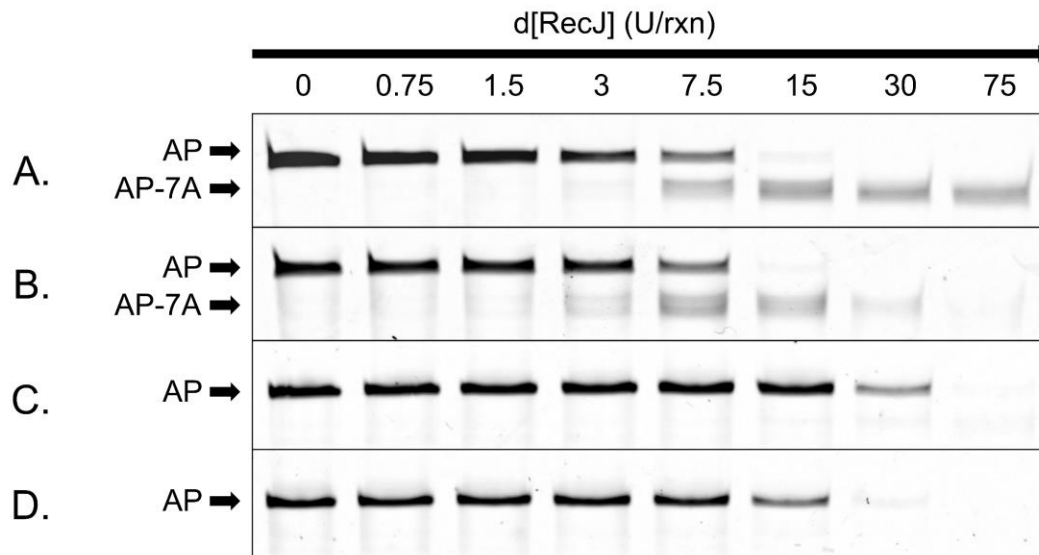


Figure S5.4. Investigation of the effect of increasing RecJ 5'-exonuclease concentration for the anti-OTA O-AP system under different reaction conditions using 10% denaturing PAGE analysis: (A) 1x phi29 DP reaction buffer and room temperature; (B) 1x phi29 DP reaction buffer and 37°C; (C) 1x RecJ reaction buffer and room temperature and; (D) 1x RecJ reaction buffer and 37°C.

Experimental Details. The protocol was similar to Figure 5.5A described in the **Experimental Section**, however the buffer conditions and reaction temperature were varied as indicated in the figure caption.

CHAPTER 6. CONCLUSIONS

6.1 Summary

The key goal of this thesis was to develop simple and generalizable strategies for sensitive detection of non-nucleic acid targets by combining: 1) linear DNA aptamers that act as primers for rolling circle amplification; 2) target mediated modulation of enzyme actions on these aptaprimers to inhibit or promote their ability to initiate the RCA reaction; and 3) real-time detection of the RCA reaction products using intercalating fluorescent dyes. The initial work described in Chapter 3 centered on the development of a simple and rapid approach for linking aptamers to RCA through target-based inhibition of the action of phi29 DP, where binding of a protein target prevented the aptamer from binding to the circular template and also prevented the ability of phi29 DP to read-through the aptamer-protein complex to initiate RCA. This resulted in a simple one-step and one-pot assay based on inhibition of RCA as target concentration was increased. This assay was also translated onto a paper-based microwell array that allowed for the assay to be utilized in a manner that could meet the ASSURED criteria.

Chapter 4 focussed on developing a target-mediated RCA assay that operated by producing an increase in signal (i.e., a turn-on assay) rather than a decrease in signal as target concentration was increased. To achieve this goal, the 3'-exonuclease activity of phi29 DP was used to digest

the aptaprimer prior to the RCA step, with increases in target leading to protection of greater amounts of aptaprimer. The use of the CT to perform a strand displacement reaction allowed the aptaprimer to release the target and initiate RCA without the need for additional processing steps. In this case, the target modulates the nuclease activity of phi29 DP, rather than modulating the aptaprimer-CT duplex formation, as in Chapter 3. However, it was observed that the latter process became dominant at high target concentrations, resulting in a non-linear (bell-shaped) concentration-response curve. Importantly, this RCA activation method produced substantially better detection limits (ca. 100-fold improvement) relative to the original RCA inhibition assay, demonstrating the advantage of the turn-on assay. The assay was also capable of operating in diluted serum and plasma, providing a step toward use of the assay for testing of clinical samples.

Chapter 5 aimed to address the non-linear response observed for the phi29 DP digestion mediated assay. To achieve this goal, a new enzyme, RecJf, which has 5'-exonuclease activity, was used to digest a modified aptaprimer with a free 3' terminus, which avoided the potential of RCA inhibition resulting from target binding, while also allowing target-mediated digestion to control the amount of aptaprimer available for RCA. The assay was demonstrated using both a protein and a small molecule target and revealed that the use of RecJf digestion was blocked by both targets. As

such, the remaining aptaprimer could be used to produce a turn-on fluorescence assay with picomolar detection limits and a wide dynamic range.

The assay methods developed in this thesis all work with linear aptamers, and as such should be widely applicable to a range of targets, so long as an aptamer exists or can be produced through in vitro selection. While all methods utilized linear RCA and intercalation of fluorescent dyes to produce a signal, it should be noted that the RCA reaction could easily be modified to be exponential in nature, and the output could be altered to produce colorimetric or electrochemical outputs, or be integrated with a variety of devices, as described in detail in the review provided in Chapter 2. Hence, the work described in this thesis should serve as a starting point for further development of a range of different solution and solid-phase assays and sensor devices.

6.2 Future Outlooks

While the work described herein has provided several new methods by which aptamers can be used to control the RCA reaction, several issues remain to be addressed. Three main points of consideration for future work are: further improvements to integration of FNAs with different RCA methods to reduce detection limits and improve overall assay performance, integration of current solution-based RCA assays with simple devices that

can meet the ASSURED criteria, and lastly, the movement toward the commercialization of RCA-based assays and devices.

Regarding the first point, Chapter 2 highlighted the already multiple examples of the integration of both aptamers and DNAzymes with linear and exponential RCA methods. The key issue to address is to find a balance between assay time and detection limit. For many targets, such as those examined in this thesis, it is possible to obtain sufficient detection limits using linear RCA with a relatively short assay time. However, detection of toxins or pathogenic bacteria often require detection of concentrations that are well below those that can be obtained with linear RCA, and in these cases exponential RCA coupled with longer assay times may be needed.¹⁻⁴ As an example, it should be relatively straightforward to couple either the phi29 DP digestion assay or the RecJ digestion assay to any of the current exponential RCA methods to improve detection limits by at least 3 orders of magnitude,⁵ and thus open the door to an expanded range of analytes that require detection at trace levels.

Regarding the second point, there has already been a substantial amount of work related to moving solution-based RCA reactions onto devices, as noted in Chapter 2. Among the devices examined thus far, paper-based sensors and electrochemical sensors are the closest to meeting the current ASSURED criteria. However, even these devices fail to meet all criteria, as many are still too expensive, require too many steps

for operation, or necessitate a reader. For example, the paper-based device described in Chapter 3, while relatively simple and affordable, required a fluorescence reader for operation, and functioned as a turn-off sensor, impacting the limit of detection. As highlighted in Chapter 2, there are paper-based RCA devices that operate by generating colorimetric outputs, but at present these still require multiple assay steps and use perishable or labile reagents, making them unsuitable for use in remote settings.

An emerging area of device design is the integration of assays with commercially available tests, such as lateral flow devices or personal glucose monitors. While several aptamer and DNAzyme-based assays have already been demonstrated using these devices, and other isothermal amplification systems including RCA have also been integrated with these devices, at present no FNA-regulated RCA assays have been coupled with either device. This is clearly an area that will require additional attention in the future.

Regarding the third point, while aptamers and DNAzymes have been used as MREs for over three decades, the commercialization of devices that use such MREs is very limited, and FNA-regulated assays incorporating ITA methods have yet to be commercialized.^{6,7} At this time, a few examples of DNAzyme-based sensors are being commercialized such as by Innovogene Biosciences Inc. (www.innovogene.com; ANDzymes and Urasensor tests), ANDalyze (www.andalyze.com; DNAzyme-based metal

ion sensors) and GlucoSentient Inc. (www.gluco sentient.com; DNAzyme-based blood glucose meter devices). Commercial devices incorporating aptamers are similarly limited,⁸ and at present there are no FNA-based devices or any devices incorporating isothermal amplification that are commercially available for clinical testing. This situation is in part due to the complex nature of biological media, which often contain nucleases and DNA binding proteins that can interfere with the FNAs.⁹ In addition, many examples of FNA-based devices have only been demonstrated using clean buffers or artificial biological samples, and have not yet been validated using patient samples, which is a critical step in the commercialization pathway.¹⁰ Increased collaboration between scientists, engineers, clinicians and industry partners will be needed to help address this issue.

6.3 References

- (1) Craw, P.; Balachandran, W. *Lab Chip* **2012**, *12*, 2469–2486.
- (2) Park, K. S. *Biosens. Bioelectron.* **2018**, *102*, 179–188.
- (3) Tian, T.; Bi, Y.; Xu, X.; Zhu, Z.; Yang, C. *Anal. Methods* **2018**, *10*, 3567–3581.
- (4) Ali, M. M.; Li, F.; Zhang, Z.; Zhang, K.; Kang, D.-K.; Ankrum, J. A.; Le, X. C.; Zhao, W. *Chem. Soc. Rev.* **2014**, *43*, 3324.
- (5) Liu, M.; Zhang, W.; Zhang, Q.; Brennan, J. D.; Li, Y. *Angew. Chem. Int. Ed.* **2015**, *54*, 9637–9641.
- (6) Dhiman, A.; Kalra, P.; Bansal, V.; Bruno, J. G.; Sharma, T. K. *Sensors Actuators, B Chem.* **2017**, *246*, 535–553.
- (7) Chen, A.; Yang, S. *Biosens. Bioelectron.* **2015**, *71*, 230–242.
- (8) Zhang, J. J.; Lan, T.; Lu, Y. *Adv. Healthc. Mater.* **2019**, *8*, 1–24.
- (9) Röthlisberger, P.; Hollenstein, M. *Adv. Drug Deliv. Rev.* **2018**, *134*, 3–21.
- (10) Liu, M.; Yin, Q.; Chang, Y.; Zhang, Q.; Brennan, J. D.; Li, Y. *Angew. Chem. Int. Ed.* **2019**, *58*, 8013–8017.